

Westinghouse Non-Proprietary Class 3



Westinghouse Energy Systems



9405090160 940420
PDR ADCK 05200003
A PDR

WCAP-13389
Revision 1

WESTINGHOUSE PROPRIETARY CLASS 3

WESTINGHOUSE CLASS 2 VERSION
EXISTS AS WCAP-13388

AP600 PHENOMOLOGICAL
EVALUATION SUMMARIES

Westinghouse Electric Corporation
Energy Systems Business Unit
Nuclear and Advanced Technology Division
P.O. Box 355
Pittsburgh, Pennsylvania 15230

©1994 Westinghouse Electric Corporation
All Rights Reserved

TABLE OF CONTENTS

<u>Section</u>	<u>Title</u>
iv	Summary
1	A Phenomenological Evaluation Summary on Steam Explosions in Support of the AP600 Risk Analysis
2	A Phenomenological Evaluation Summary on External Cooling of the RPV in Support of the AP600 Risk Analysis
3	A Phenomenological Evaluation Summary on High Pressure Melt Ejection and Direct Containment Heating in Support of the AP600 Risk Analysis
4	A Phenomenological Evaluation Summary on Molten Core-Concrete Interaction in Support of the AP600 Risk Analysis
5	A Phenomenological Evaluation Summary on the Probability and Consequences of Deflagration and Detonation of Hydrogen in Support of the AP600 Risk Analysis
6	A Phenomenological Evaluation Summary on Fission Product Retention Capability in Support of the AP600 Risk Analysis

SUMMARY

This document is prepared in support of the AP600 probabilistic risk assessment (PRA). It contains six individual reports that examine the potential challenges to the AP600 containment integrity from key severe accident phenomena.

Modular Accident Analysis Program Version 4.0 (MAAP 4.0) is used in the AP600 PRA to examine the core damage progression and to predict fission product source term. The MAAP 4.0 code performs a realistic simulation of severe accident progression and yields best estimate source terms. The impact of phenomenological uncertainties on the source terms are also examined as an integral part of the AP600 PRA. This is accomplished by performing AP600-specific phenomenological evaluations and sensitivity studies with the MAAP 4.0 code. This report documents the phenomenological evaluations carried out. These evaluations provide the basis for the treatment of severe accident phenomena in the containment event trees utilized in the AP600 PRA.

The evaluations presented here address a range of phenomenological issues and provide an in-depth review of the AP600 plant-specific features which influence the uncertainty, or act to mitigate, the consequences of such phenomena. They investigate both the likelihood of occurrence and the probable consequences of key severe accident phenomena.

Section 1 describes an evaluation carried out to examine the potential for AP600 containment failure from either an in-vessel or an ex-vessel steam explosion. It concludes that a steam explosion of magnitude sufficient to challenge the AP600 containment integrity does not occur in any credible core damage events.

Section 2 contains an evaluation to ascertain if sufficient heat can be removed from the outside surface of the reactor vessel when submerged in water, so that the reactor vessel failure can be prevented by flooding the reactor cavity in events involving core damage. The evaluation concludes that cavity flooding can prevent the reactor vessel failure.

An evaluation of the likelihood of and the consequences from a high pressure melt ejection event is presented in Section 3. It concludes that the AP600 containment failure due to high pressure melt ejection is not a credible event.

Section 4 examines phenomenological issues pertaining to core-concrete interaction. A bounding analysis performed assuming a dry core debris bed in the reactor cavity with no overlying water pool shows that the basemat penetration does not occur for at least 172 hours. However, containment failure may occur sooner from pressurization due to noncondensable gas generation, but not before 48 hours into the accident. The analysis supporting the latter statement is documented in the AP600 PRA.

The challenge to the AP600 containment integrity from hydrogen deflagrations and detonations during core damage events is examined in Section 5. The evaluation concludes that containment failure from a deflagration or a detonation is not a credible event for AP600.

Section 6 examines the fission product source term and the retention capabilities of the AP600 primary system and passive containment. It is concluded that the low containment design leakage rate and the design configuration with significant in-containment water sources limit the fission product releases to the environment.

Based on the phenomenological evaluations presented here, it is concluded that the AP600 containment is not expected to fail from an energetic event during severe accidents. Therefore, severe accident phenomena are not explicitly modelled in the containment event trees developed for the AP600 PRA.

FAI/92-14

A PHENOMENOLOGICAL EVALUATION SUMMARY ON
STEAM EXPLOSIONS
IN SUPPORT OF THE AP600 RISK ANALYSIS

Submitted To:

Westinghouse Electric Corporation
Pittsburgh, Pennsylvania

Prepared By:

Fauske & Associates, Inc.
16W070 West 83rd Street
Burr Ridge, Illinois 60521
(708) 323-8750

February 1992

ABSTRACT

Previous studies evaluating risk from severe accident sequences have considered steam explosions as a potential mechanism for violating both the primary system and the containment. Steam explosions have been postulated to occur both in-vessel and ex-vessel. This paper examines the potential for containment failure in the AP600 design due to in-vessel and ex-vessel steam explosions. The controlling physical processes for steam explosions are described in terms of industry experience, experimental programs, and analytical results. This body of knowledge is applied to the AP600 design to evaluate the challenge offered to containment by steam explosions. Results demonstrate that steam explosions present no credible threat to the AP600 containment design. In-vessel steam explosions prove not to be a credible scenario for the AP600 design, based on the experimental and analytical results presented herein. The conditions required for an in-vessel steam explosion are extremely unlikely for the AP600 design. Steam explosions ex-vessel can be postulated for the AP600 design. [

](a.c)

TABLE OF CONTENTS

	<u>Page</u>
ABSTRACT	i
TABLE OF CONTENTS	ii
LIST OF FIGURES	iv
LIST OF TABLES	v
1.0 PURPOSE	1-1
2.0 PHENOMENA	2-1
2.1 Description	2-1
2.1.1 Controlling Physical Processes	2-1
2.1.2 Relationship to Containment Failure Mechanisms and Modes	2-4
2.1.3 Relationship to Source Term	2-5
2.2 Industry Experience With Steam Explosions	2-6
2.2.1 Nuclear Incidents	2-6
2.2.2 Non-Nuclear Explosion Boiling Studies	2-7
2.3 Experiments	2-9
2.3.1 Early Sandia Thermite and Corium Experiments	2-9
2.3.2 Aluminum-Water Experiments	2-13
2.3.3 Liquefied Natural Gas and Water Experiments	2-15
2.3.4 FAI Thermite Experiments	2-15
2.3.5 Sandia FITSB Tests	2-19
2.3.6 Summary	2-27
2.4 Analysis	2-27
2.4.1 Effect of System Pressure on Steam Explosions	2-27
2.4.2 Steam Explosion Models	2-29

TABLE OF CONTENTS

(Continued)

	<u>Page</u>
2.4.3 Possible Mechanism for Maximum Steam Generator Rate	2-30
2.4.4 Shock Waves	2-32
3.0 METHODOLOGY	3-1
3.1 In-Vessel Steam Explosions	3-1
3.2 Ex-Vessel Steam Explosions	3-2
3.2.1 Pressure Rise Due to Rapid Steam Generation	3-2
3.2.2 Shock Waves	3-3
4.0 PLANT SPECIFIC APPLICATION	4-1
4.1 Issues	4-1
4.1.1 In-Vessel Steam Explosions	4-1
4.1.2 Ex-Vessel Steam Explosions	4-2
4.1.3 Uncertainty Considerations	4-5
4.2 Conclusions	4-6
5.0 ACCIDENT MANAGEMENT INSIGHTS AND CONSIDERATIONS	5-1
6.0 SUMMARY	6-1
7.0 REFERENCES	7-1

LIST OF FIGURES

<u>Figure No.</u>		<u>Page</u>
2-1	Behavior modeled in WASH-1400	2-2
2-2	Comparison of predicted pressure-time behavior from WASH-1400 (400 μ m particle size) and available experimental results for steam explosions	2-3
2-3	Measured debris-water energy transfer rates from EPRI sponsored Mark I liner tests	2-17
2-4	FITS containment chamber	2-20
2-5	FITS2B chamber air pressure	2-23
2-6	FITS3B chamber air pressure	2-24
2-7	FITS7B chamber air pressure (no camera data)	2-25
2-8	FITS6B chamber air pressure (saturated water)	2-26
2-9	Debris dispersion configuration	2-31
2-10	Comparison of shock wave pressures for TNT and point source explosions	2-33

LIST OF TABLES

<u>Table No.</u>		<u>Page</u>
2-1	Effective Heat Flux Measurements for Debris-Water Interactions	2-18
2-2	FITSB Initial Conditions and Observations	2-21
2-3	Chamber Air Pressure Data From FITSB (Times From Melt Entry)	2-35

1.0 PURPOSE

A steam or vapor explosion refers to a boiling process in which steam or vapor production occurs at a rate larger than the surrounding media can acoustically relieve the resulting pressure increase, leading to the formation of a shock wave. In previous studies evaluating the public risk associated with severe accident sequences, such as the Reactor Safety Study [NRC, 1975], steam explosions within the primary system have been considered as a potential mechanism for violating both the primary system and the containment, thereby generating a direct release path for fission products. The in-vessel steam explosion considered was theorized to result from the following chain of events:

1. loss of water from the core resulting in fuel overheating and melting,
2. the catastrophic collapse of the core debris into the water remaining in the lower plenum,
3. an instantaneous fine scale intermixing of the core debris and water,
4. rapid heat removal from the core material and expansion of the steam against an assumed continuous, overlying liquid slug,
5. impact of this liquid slug on the reactor vessel head with sufficient energy to rupture the head, and
6. ejection of this missile with sufficient velocity to fail the containment wall upon impact.

In NUREG-1116 [NRC, 1985], the NRC sponsored Steam Explosion Review Group (SERG) provided recommendations regarding the likelihood that an in-vessel steam explosion could cause containment failure. The main conclusion of the group report was: "Based upon the probability estimates summarized above, the consensus of the SERG is that the occurrence of a steam explosion of sufficient energetics which could lead to alpha-mode containment failure has a low probability. This conclusion is reached despite the expansion of differing opinions on modeling of basic steam explosion sequence phenomenology."

Ex-vessel steam explosions may also potentially occur in the progression of a severe accident should debris be discharged from the reactor vessel into a pool of water. Within a containment, the occurrence of a steam explosion would impose shock waves on submerged surfaces and subcompartment walls. These must be evaluated to determine if the resulting loads could challenge the integrity of interior walls and the containment boundary.

In Generic Letter 88-20 [NRC, 1988], the NRC identified steam explosions as a potential containment failure mechanism that should be assessed as part of an IPE. Both in-vessel and ex-vessel steam explosions have been postulated as a potential mechanism for early containment failure, possibly with an elevated release location. Either of these characteristics could have substantial effects on the consequence evaluation for hypothetical accident sequences. The objective of this report is to evaluate the potential for in-vessel and ex-vessel steam explosions to threaten containment integrity in the AP600 design.

2.0 PHENOMENA

2.1 Description

Explosive interactions between higher and lower temperature liquids have been encountered for decades in metal foundries as well as the pulp and paper industries. Experience has shown that these accidents can result in significant damage to typical industrial components (furnaces, casting pits, recovery boilers, etc.) as well as to light industrial buildings. Human casualties have also occurred as a result of these events, but the major hazard to operating personnel from these events has generally been burns resulting from hot molten material dispersed by the explosive interaction. In addition to such non-nuclear experiences, destructive steam explosions have been observed in the BORAX [Deitrich, 1965] and SPERT [Miller, 1964] test reactors as well as in the SL-1 accident [SL-1]. In all of these three test reactor configurations, the destructive explosion followed a rapid (~ 30 ms) reactivity insertion that was sufficient to melt both uranium-aluminum alloy fuel and aluminum cladding. Figures 2-1 and 2-2 provide some visualization of the physical processes considered for an in-vessel steam explosion in [NRC, 1975].

2.1.1 Controlling Physical Processes

For large scale steam explosions to occur inside or outside a reactor vessel, large fractions of hot molten material must be very finely fragmented and intermixed with the water on the time scale of the explosion. Such processes were envisioned in [NRC, 1975], but, in addition, rapid heat transfer was calculated in the supercritical and superheated steam regions, and the resulting energy transfer was delivered to a postulated overlying liquid slug that covered the interaction zone. Without the slug transmission mechanism, the pressure-time curves shown in the Reactor Safety Study [NRC, 1975] would have been insufficient to rupture the reactor pressure vessel, which was the mechanism envisioned as causing containment failure (α mode failure).

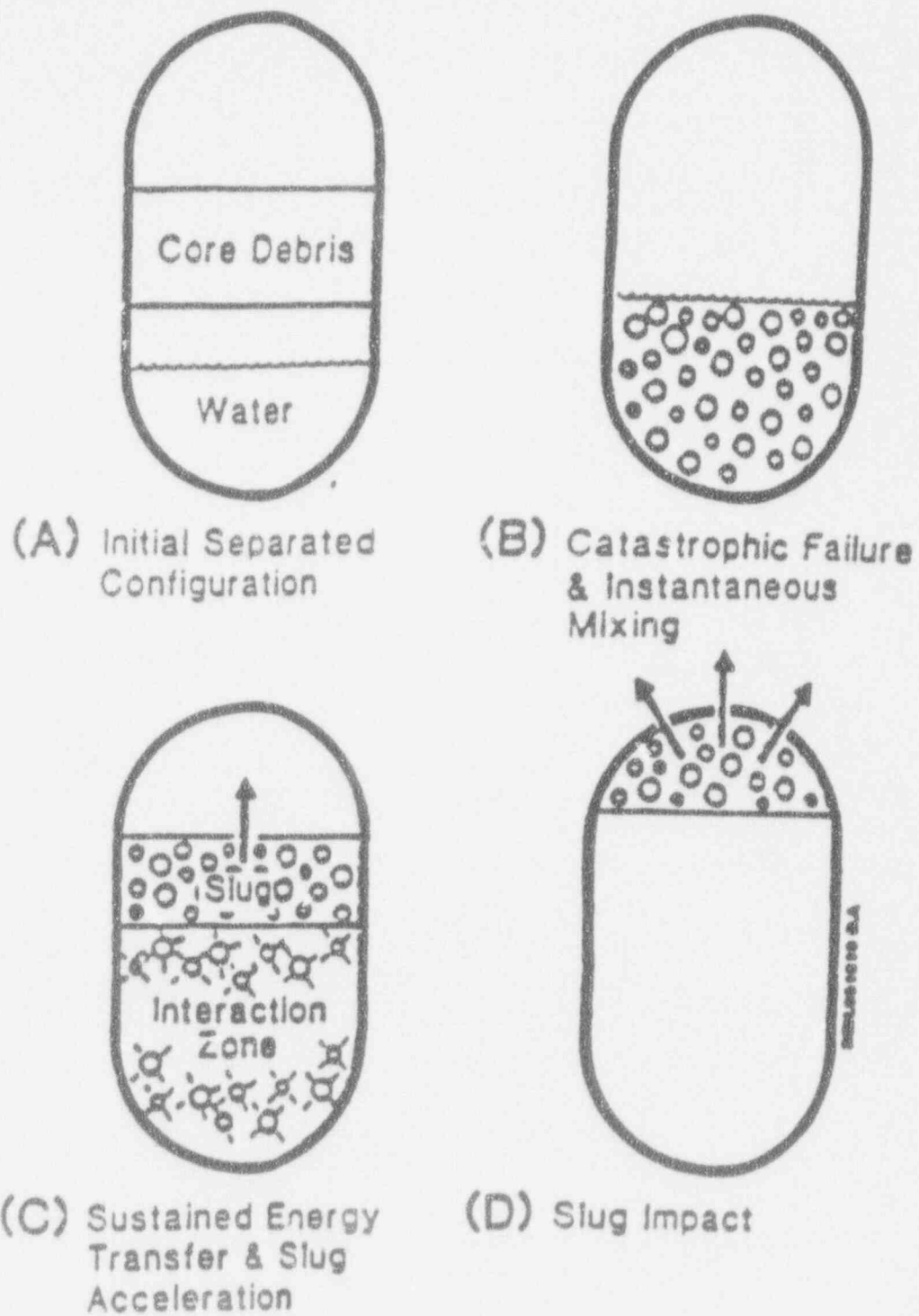


Figure 2-1 Behavior modeled in WASH-1400.

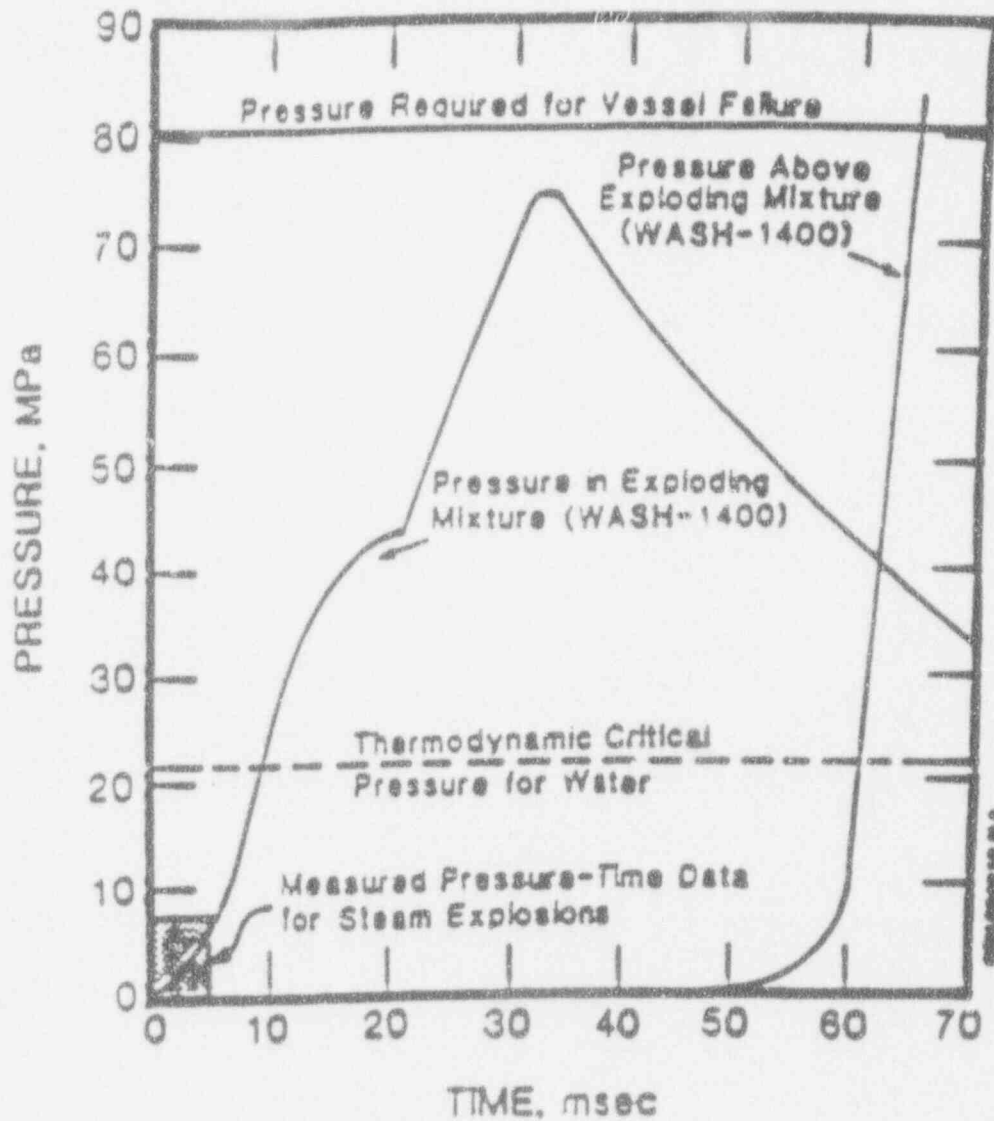


Figure 2-2 Comparison of predicted pressure-time behavior from WASH-1400 (400 μ m particle size) and available experimental results for steam explosions.

The key physical factors which determine the magnitude of steam explosions within BWRs and PWRs include the energy required to rupture a reactor pressure vessel, the amount of core material needed to provide such an energy release, the fragmentation of the hot material in the water, the mixing energy requirements when the material is finely fragmented and rapidly intermixed during the explosion, the size of an external trigger to initiate the explosion, the propagation characteristics for the coarsely fragmented system, the likelihood of having a water slug over the reaction zone to transmit the energy in a coherent fashion, and the ability of this slug to be transmitted through upper core structures within the reactor pressure vessel. Each of these factors must be sufficient to create an event of enough magnitude to rupture a reactor pressure vessel; the failure of a single factor to achieve the proper conditions will preclude an event of such magnitude.

2.1.2 Relationship to Containment Failure Mechanisms and Modes

Both in-vessel and ex-vessel steam explosions have been postulated to be early containment failure mechanisms that would occur following slumping of the core material into the reactor vessel lower head. The largest potential for the occurrence of an in-vessel steam explosion would exist during a core melt sequence with a low primary system pressure. The largest threat to containment integrity as the result of an ex-vessel steam explosion would exist for a core melt sequence with a relatively coherent pour of molten material at vessel failure into a water pool.

Three actual containment failure mechanisms are considered to be encompassed by containment failures induced by steam explosions. For in-vessel steam explosions, a missile (e.g., the reactor vessel upper head) would have to be created with sufficient energy to pierce the containment. For ex-vessel steam explosions two possibilities are considered: the blast could weaken the cavity walls sufficiently that the vessel moves and tears out one or more containment penetrations, or the generated steam could overpressurize the containment. For the first mechanism the failure area has been assumed as a large break in the containment wall (i.e., on

the order of several square feet). If containment penetrations are torn, it is expected that the area would be small, more like a "leak before break" condition. A failure resulting from containment overpressure would be dictated by the rate of pressure rise and the total mass of steam generated. Typically this would be a "leak before break" response, but, as will be discussed, the anticipated rate of pressure increase from a steam explosion is less than that associated with a design basis large break LOCA.

2.1.3 Relationship to Source Term

Containment failure resulting from a steam explosion would influence the expected fission product source term for a sequence by providing a large gas flow path out of the containment shortly after vessel failure. The effect on the source term would strongly depend on the availability of water in the containment during a sequence. However, such an early containment failure would generally increase the source term for accident sequences, since the airborne fission product concentration at the time of containment failure would be much greater than for a case with a late containment failure. Also, the relatively large expected failure area would cause a rapid blowdown of the initially available airborne fission products to the auxiliary building or environment, thereby reducing the fission product retention effectiveness of the containment. On the other hand, fission products entering the containment atmosphere after the blowdown would experience little driving force from the containment to the auxiliary building or the environment. Thus, fission products evolved by long term revaporization within the reactor vessel would be subject to the naturally occurring deposition mechanisms in the containment.

2.2 Industry Experience With Steam Explosions

2.2.1 Nuclear Incidents

The explosion model used in the Reactor Safety Study [NRC, 1975] resulted principally from concerns generated by the low pressure BORAX and SPERT destructive experiments and the SL-1 accident. Reactor conditions leading to the SL-1 accident [SL-1] and the destructive transients in BORAX [Deitrich, 1965] and SPERT [Miller, 1964] were produced in a fundamentally different system than that representative of a postulated severe accident in a commercial LWR. It is not only important to realize these differences, but it is essential to understand the resulting implications for the phenomenon as well. These basic differences are delineated below.

1. All three destructive events were produced by power excursions in which the core was driven to molten conditions in 30 msec or less. Such strong reactivity transients are not possible in commercial power reactors.
2. The specific core designs of these reactors could be brought to supercritical conditions by the withdrawal of a single control rod. In these transients, a control rod was rapidly withdrawn which caused a nuclear excursion with sufficient energy deposition to melt the fuel-clad plates.
3. Each of these three reactors was fueled with thin uranium-aluminum alloy fuel plates clad in aluminum. Thus, the fuel and water were uniformly premixed on a fine scale in the as-fabricated geometry. No additional melt fragmentation was required to accomplish the explosive energy release.
4. Since the reactors were essentially at room temperature prior to the excursion, the vessels were filled with cold water except for a small freeboard volume at the top, i.e. a long, coherent overlying liquid slug was in place prior to the reactivity insertion.
5. The vessel internal geometry was very simple and open, which provided little attenuation or dispersion of any slug movement.

With these initial conditions, the configuration established was essentially an inertial layer of water above an expanding layer of water, as assumed in the Reactor Safety Study. The essential feature of the strong reactivity transient is that it brought the fuel and clad to melting before this configuration could substantially change. Given these particular characteristics, a slug impact following a steam explosion within the core would indeed be the expected chain of events. However, this is fundamentally different than an initially separated state of high temperature molten core material and saturated water existing at an elevated pressure with substantial internal structure to prevent catastrophic collapse, intimate mixing, and slug formation.

2.2.2 Non-Nuclear Explosion Boiling Studies

In a number of industrial operations the possibility exists of contacting two liquids -- one hot and relatively nonvolatile and the other cold and volatile. Should such an event occur, boiling would occur in a sufficiently short time scale that the surrounding medium cannot relieve the expansion acoustically and a shock wave, i.e., an explosion, forms. Accidents of this nature have been given various names, e.g., explosive boiling, rapid-phase transitions (RPTs), vapor explosions, thermal explosions, fuel-coolant interactions (FCI), etc. They have been observed in a number of industrial operations, e.g., when water contacts molten aluminum (or other metals), molten salts or paper mill smelt, or when cryogenic liquids such as LNG (liquefied natural gas) are spilled into water. In the first two examples noted above, water is the volatile liquid which explosively boils whereas in the last example the cryogenic liquid plays the role of the volatile, boiling liquid and water is then the "hot" fluid.

2.2.2.1 Smelt-Water Explosions

Studies of molten salt-water explosions were carried out because industrial accidents involving these reactants have taken place. Emphasis has been placed on events occurring in the paper industry where molten smelt is produced in the recovery boilers. This smelt is a mixture of, primarily, sodium chloride, sodium carbonate, and sodium sulfide. The smelt temperature is much higher than the critical point of water (~ 1520°F (1100°K) compared to 750°F (647°K)). Severe explosions have taken place when water inadvertently contacted molten smelt.

Laboratory investigations [Krause, et al., 1973], [Shick, 1980] into the mechanism of smelt-water explosive boiling events have been primarily useful in delineating the effect of smelt composition on the sensitivity of the salt in producing explosive boiling. For example, pure molten sodium carbonate has never led to explosive boiling. Addition of either sodium chloride or sodium sulfide, or both, leads to smelts which are more prone to explosive boiling. Investigators experimented with many additives both to the smelt and to the water in an attempt to obtain less sensitivity. Most had little or no effect.

2.2.2.2 Melt-Water Interactions

The metals processing industries, particularly those producing aluminum, have also been plagued by explosive boiling incidents. Alcoa has carried out several test programs [Lemmon, 1980], [Hess, et al., 1980] directed primarily at effecting means to prevent such accidents in casting plants. In most tests, molten aluminum was dropped into water and the subsequent events recorded. Many variables were studied such as water temperature, drop height, nozzle diameter, etc. The principal result of these investigations was to show that water containers, suitably coated with an organic-based paint, would not lead to explosions when molten aluminum was spilled into the container. Use of such paints in aluminum plants has indeed reduced the frequency of explosions, but many still occur. In a large number of accidents, the quantity of water was quite small, e.g., when "wet" aluminum ingots were loaded into melting furnaces

containing molten aluminum. In contrast to this fact, few, if any, serious events have occurred when small quantities of aluminum were contacted with a large mass of water. Since laboratory tests were often carried out in the latter fashion, most of these have not resulted in explosive interactions.

2.2.2.3 Other

In industries dealing with "reactive" metals, such as titanium, zirconium, etc, only a few serious explosive boiling events have been documented. In most of these, a significant quantity of molten metal has contacted water and, simultaneously, there has been some external shock such as an electrode falling into the metal-water mixture. In the few known incidents, damage has been severe, but quite localized. Due to the reactive nature of the metal, however, subsequent hydrogen fires have often compounded the problem and led to extensive damage.

2.3 Experiments

A wide range of laboratory scale and large scale experiments relating to vapor explosions have been performed over the past thirty-five years. The laboratory scale experiments constitute an extensive literature base and are reviewed in detail in [FAI, 1982] and [IDCOR, 1983].

2.3.1 Early Sandia Thermite and Corium Experiments

Large scale steam explosion experiments have been carried out at the Sandia Laboratories in three different test series, two using an iron-thermite mixture [Buxton, et al., 1979], [Mitchell, et al., 1981] to simulate the degraded core material and the other using both an iron-thermite and a corium-thermite [Buxton, et al., 1980] which has a higher melting temperature and is a more realistic simulant of the anticipated debris character. In both of these experimental series, artificial triggers (explosive detonators) were used to initiate the interaction in some tests.

In the first set of experiments [Buxton, et al., 1979], the iron-thermite melt was discharged directly into a 2.95 ft (0.9 meter) diameter vessel filled with water. For all those experiments carried out with an artificial trigger, the water was at the ambient temperature, assumed to be 70°F (295 K). (In these experiments the ambient pressure was always slightly less than 14.7 psi (0.1 MPa).) The melt temperature resulting from the thermite reaction is approximately 4400°F (2700 K) and results in reaction products of metallic iron (Fe) and aluminum trioxide (Al_2O_3). The melting temperature for the aluminum trioxide is approximately 3680°F (2300 K) and is about 2780°F (1800 K) for metallic iron. Consequently, solidification of either of these constituents requires a substantial decrease in temperature and the resulting fragmentation process could continue as the melt cools, i.e., lower temperatures reduce the film boiling steam generation rate and allow finer particulation. To externally trigger an explosive interaction, a 1.41×10^{-3} lbm (0.64 g) charge of high explosives was used. Some of the experiments had a considerable delay before the explosion was initiated, i.e. over 2 sec. Many tests in this experimental series observed the presence of spontaneous trigger events as well.

A second test series was performed at Sandia [Buxton, et al., 1980] with a different test vessel (3.94 ft (1.2 m) internal diameter) and molten material generated from both iron-aluminum oxide thermite and a corium-A+R thermite. This latter reaction had products of uranium dioxide, zirconium dioxide, nickel oxide, stainless steel, and molybdenum. The minimum liquidus temperature for this mixture is reported to be 4526°F (2770 K), which is considerably greater than the 3680°F (2300 K) temperature for aluminum oxide. Boiling steel would limit the maximum temperature for the corium reaction to 5066°F (3070 K).

In this second test series, external triggering was also induced by explosive detonators, but two different sizes were used. One was the same as that employed in the first iron-thermite test, i.e. 1.41×10^{-3} lbm (0.64 g) of PETN, and the other was a detonator plus a lead-covered explosive cord 2.49 ft (0.76 m) in length and containing 1.32×10^{-2} lbm (6 g) of PETN. This second method represented a much more energetic trigger than that used in the thermite tests. In fact, the pulse duration for the corium A+R event in Run 59, which used this larger trigger,

was not much different than that represented by the trigger alone. Also the measured work (~ 33 Btu (30 kJ)) was less than the work released by the high explosive (~ 39 Btu (35 kJ)). Explosions were observed with the iron-thermite as initiated by both spontaneous and artificial triggers. However, with the corium A+R melt only one mild explosion is reported and this was triggered by the 1.32×10^{-2} lbm (6 g) PETN external trigger. The time delay before the trigger is fired (~ 1.3 sec) is longer than the time required to cool the coarsely fragmented particles to the liquidus temperature. The fact that the trigger was needed to mix a considerable fraction of the melt down to an explosive size scale is indicative of the difficulty encountered in making such materials undergo a thermal explosion. A major part of this difficulty is due to the rapid cooling and freezing of the corium particles as described above.

The results of 17 tests were reported [Mitchell, et al., 1981] for both ambient and high pressure initial conditions and also with and without an external trigger. The two experimental series were designated as Melt Delivery and FITS (Fully Instrumented Test Series). The Melt Delivery experiment consisted of 12 tests all performed at atmospheric initial pressure without an external trigger. These resulted in eight self-triggered explosions -- two in the water coolant before the melt impacted the reservoir bottom and six when the melt contacted the reservoir base. The initial FITS experimental matrix consisted of five runs -- three at atmospheric and two at an elevated pressure. Two explosions resulted -- one at atmospheric pressure and in the free stream before the melt hit the reservoir bottom, and one at elevated pressure (~ 1 MPa/150 psi) which was initiated by an external trigger when the melt was lying on the reservoir base.

The purpose of the Melt Delivery test series was to develop an efficient means of delivering the melt into the coolant and that of the FITS experiment was to determine the mechanical work output from such explosions. The melt used in both these experiments was iron-thermite ($\text{Fe-Al}_2\text{O}_3$) which had an initial temperature of ~ 4400°F (2700 K). Melt masses of 1.32 - 11.8 lbm (0.6-5.38 kg) were employed which resulted in coolant-melt mass ratios of 366-37 respectively, and the conversion ratio of mechanical work to melt initial thermal energy

was reported to be about 1-3%. These tests resulted in eight self-triggered explosions, but explosions were not observed for water-melt mass ratios of 83-113.

The explosivity and initiation site were apparently sensitive to melt mass and shape in the 15 non-externally triggered tests at ambient pressure. There were no self-triggered explosions when the initial melt mass was less than approximately 4.0 lbm (1.8 kg), and there were nine such explosions for the initial melt mass greater than ~ 6.6 lbm (3 kg). This was interpreted as a threshold for an appropriate melt-water mixture to produce a thermal explosion.

Five different phases were observed in these experiments: (1) melt entry, (2) pre-mixing, (3) triggering, (4) propagation, and (5) expansion of the interaction products. The melt was observed to start coarse fragmentation and pre-mixing virtually upon entry into the water. The triggering and propagation phases of the thermal explosions were observed to start at the leading edge of the melt, both when the melt was still in the free stream and also upon impact with the coolant reservoir base. Propagation of the event was observed to start at the base of the melt and propagate through the mixture at ~ 656 - 1969 ft/s (200-600 m/s). This phase was considered to be complete at the start of the expansion of the melt-water mixture.

The FITS-A experiment was conducted in a closed vessel to assess the influence of an external trigger (1.4×10^{-3} lbm (635 mg PETN, 3.6 Btu (3.8 KJ)) on high pressure cut-off of thermal explosions. In this test series, the Fe-Al₂O₃ melt (4.3 - 11.8 lbm, 5072°F (1.94-5.38 kg, 3073K)) was poured from ~ 3.9 ft (1.2 m) into tap water (198 ~ 498 lbm, 50 - 77°F (90-226 kg, 10-25°C)) producing a 1 - 1.5 ft (0.3-0.45 m) long melt mass at entry and coolant-melt mass ratios of 41-80. Five tests were performed -- three at ambient pressure (12 psi (0.083 MPa)) and two at an elevated pressure (148 and 158 psi (1.02 and 1.09 MPa)). Two explosions resulted -- one at ambient pressure which was self-triggered in the free stream and one at 1.09 MPa which was externally triggered.

Tests FITS-4A and 5A are of particular interest because they were designed to investigate the effect of high pressure cut-off on steam explosions. In the FITS-4A test, 9.5 lbm (4.29 kg) of melt was delivered to 498 lbm (226 kg) of water at 77°F (25°C) in an ambient pressure of 148 psi (1.02 MPa) without an external trigger and did not produce an explosion. This benign result was explained on the basis of a dispersed and cooled melt at entry into the coolant. The FITS-5A test was performed at a system pressure of 158 psi (1.09 MPa) and was essentially a rerun of FITS-4A but with an external trigger. The FITS-5A run did produce a thermal interaction after being initiated with the detonator (3.6 Btu (3.8 KJ)), but the mixture had not self-triggered after 0.44 sec at which time all the melt was on the bottom of the coolant reservoir.

2.3.2 Aluminum-Water Experiments

Large scale tests have also been carried out for an aluminum-water system where either external triggers [Long, 1957], [Hess, et al., 1980], [Lemmon, 1980], [Higgins, 1955], [Higgins, 1956] or a shock tube configuration [Wright, et al., 1966] have been employed.

In [Long, 1957], large scale molten aluminum-water experiments were performed to investigate the manner in which steam explosions could be triggered. The reference test, which repeatedly produced explosions, involved the discharge of 22.8 kg (50 lbm) of commercially pure molten aluminum into a clean, mild steel container partially filled with water at temperatures of 59.5 - 78.1°F (12.8-25.6°C). In contrast to chemical explosions, no flash or fire could be detected either during or after the explosions. The following parameters were varied:

1. discharge rate and mass,
2. drop height,
3. water depth, and
4. aluminum and water temperature

Also, different water additives, solid surfaces, and surface coatings were employed in the experiment. It was concluded that three requirements must be met to produce an aluminum-water explosion:

1. Molten metal in considerable quantities must penetrate to the bottom surface of the water container.
2. A triggering action must occur on the container bottom surface when it is covered by the molten metal.
3. The water depth and temperature must lie within certain ranges.

In [Hess, et al., 1980], tests were performed to study the level of external stimulus (a hammer impact) required to initiate explosive interactions in aluminum-water systems. For these experiments, ~ 48.5 lbm (22 kg) of molten aluminum was poured into a square container 0.98 ft (0.3 m) on a side. The molten aluminum temperatures varied between 1346°F (780°C) with the water temperature variation being from 37.4°F (3°C) to 89.6°F (32°C). In the experiments, 4 seconds elapsed between the entry of melt into the water and the hammer impact, thereby allowing much of the material to be accumulated on the bottom of the container instead of as individual particles in the water. The impact level determined in the experiments of [Hess, et al., 1980] was 0.176 Btu (186 J) and the authors suggested that perhaps only half of this was actually transmitted to the mixture due to inherent losses within the impact on the wall and the transmission of the energy to the coolant.

Other aluminum-water experiments have been carried out by Lemmon [Lemmon, 1980] and Higgins [Higgins, 1955], [Higgins, 1956] where molten material has been poured or injected into water and an explosive interaction was initiated by a strong external trigger. For those experiments reported in [Lemmon, 1980], triggers up to 1.1×10^{-2} lbm (5 g) of primacord were used. A No. 6 blasting cap was employed by Higgins in his experiments. Scoping calculations for the specific experimental configurations used in these references result in an assessment that

the external stimulus was orders of magnitude greater than that required to rapidly mix the materials on an explosive time scale.

Another type of aluminum-water experiment of note is the shock tube experiment described in [Wright, et al., 1966]. In these tests, a long column of water was separated from a molten aluminum surface by a diaphragm and a cover gas. To carry out these tests, the recovery gas was evacuated and the diaphragm was ruptured allowing the atmospheric pressure to accelerate a water slug resulting in a strong, direct impact of the cold water column on a molten aluminum surface. Large interaction pressures for these events were measured in the water column.

2.3.3 Liquefied Natural Gas and Water Experiments

Large scale tests [Koopman, et al., 1981] have been performed with Liquefied Natural Gas (LNG) and water using material volumes approaching those of interest for the reactor accident case. In these tests, water is the hot fluid and LNG (mostly methane) is the cold liquid which undergoes the explosive vaporization. This fluid pair is similar to the corium-water system in that the interface contact temperature is far greater than the thermodynamic critical temperature of the LNG, making explosions difficult to initiate. Long delay times were provided in an attempt to accumulate substantial quantities of LNG below the water surface. The magnitudes of the explosions obtained represented the interaction of only a small fraction of the LNG injected.

2.3.4 FAI Thermite Experiments

Two sets of experiments have been performed at FAI in which 44 lbm (20 kg) of molten iron-thermite was injected into water. The first [Malinovic, et al., 1989] was performed to study the role of water in protecting the Mark I containment liner under severe accident conditions while the second [FAI, 1990] addressed the influence of water during a high pressure melt

ejection. Both of these represent conditions which could cause ex-vessel steam explosions and both facilities were instrumented sufficiently to evaluate the steam generation rates resulting from these interactions.

Interpretation of the rate, in terms of a heat flux based upon the projected floor area where the interaction occurs, provide a means of applying the results to a reactor/containment system. Figure 2-3 illustrates the measured heat flux to the overlying water pool in the Mark I experiments when the test apparatus was instrumented to detect the energy transfer to the test box walls. All tests show a very high energy transfer rate within the first few seconds, the value being between 6.3×10^6 and 9.5×10^6 Btu/h-ft² (20 and 30 MW/m²), which subsequently decreased to about 0.28×10^6 Btu/h-ft² (0.9 MW/m²) after the debris is frozen. In this set of experiments, 11 tests were performed, 10 of which had water available in the simulated containment prior to the discharge of the molten iron thermite. In all 10 experiments, rapid energy transfer rates (6.3×10^6 - 9.5×10^6 Btu/h-ft² (20-30 MW/m²)) were observed when the debris was discharged into the water.

FAI direct containment heating experiments [FAI, 1990] also had sufficient instrumentation to estimate the steam generation rates when debris was discharged from the simulated RCS into the reactor cavity and subsequently up onto the containment floor. Table 2-1 summarizes the information for these experiments in terms of the energy transfer rate in the cavity for the three experiments in which water was available (DCH-1, DCH-2, and DCH-4) and also for the energy transfer rates from the debris to the water as the debris was discharged onto the containment floor. Values are also given for estimated additional energy transfer due to the transfer into the steel structural heat sinks in the simulated containment lower compartment. These additional energy transfer rates should be summed with those determined from the containment compartment pressurization rates. As illustrated by this table, the energy transfer rates are large and comparable to those observed in the MARK I tests. These rates are an order of magnitude greater than those typical of the critical heat flux (CHF) for a horizontal upward facing surface.

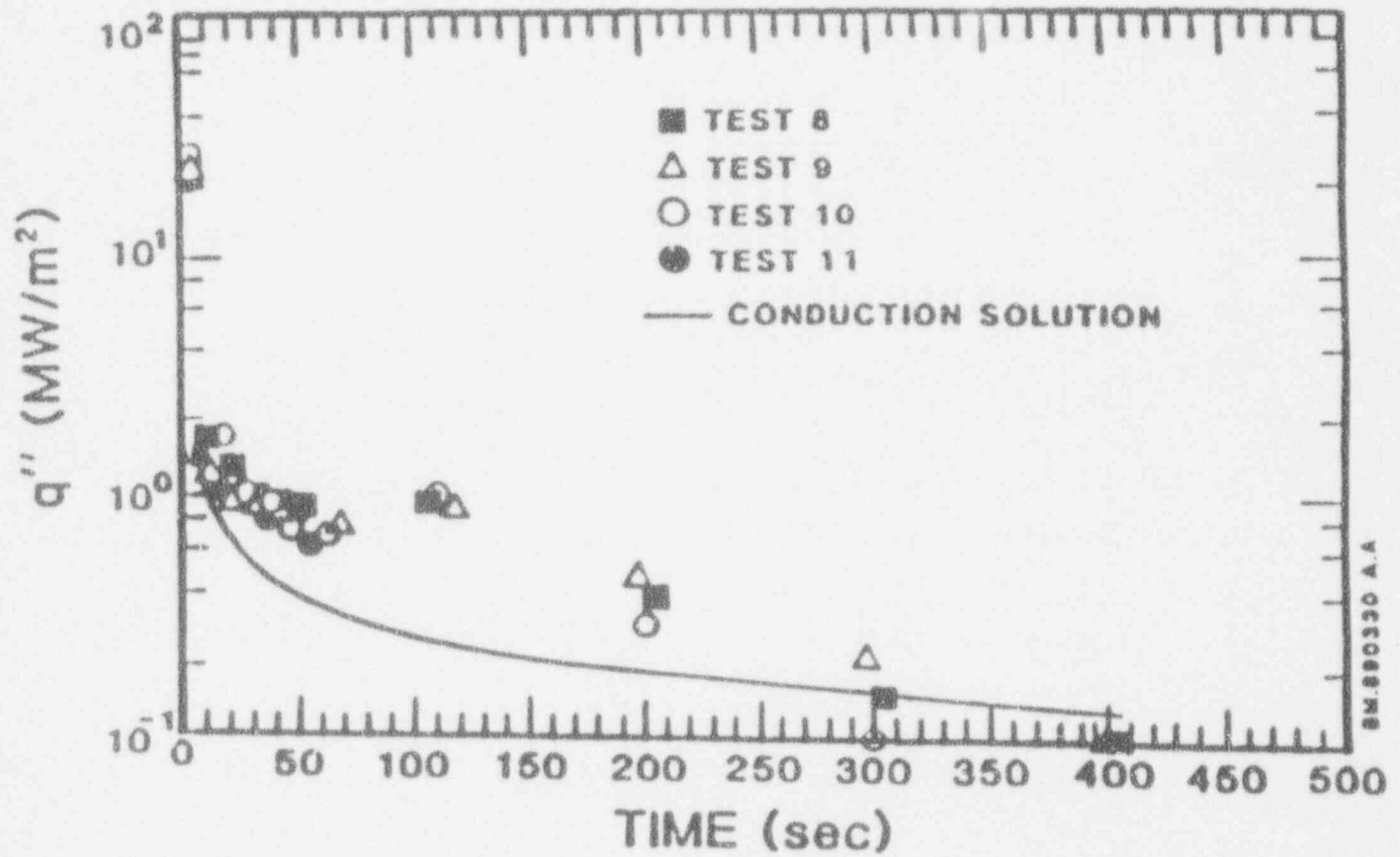


Figure 2-3 Measured debris-water energy transfer rates from EPRI sponsored Mark I liner tests.

Table 2-1

EFFECTIVE HEAT FLUX MEASUREMENTS FOR DEBRIS-WATER INTERACTIONS

Test	Initial Pressurization		Intermediate Period		Long Term Quenching	
	M Btu/b-ft ²	MW/m ²	M Btu/b-ft ²	MW/m ²	M Btu/b-ft ²	MW/m ²
DCH-1	4.75/13.3*	15/42*	3.49/6.02*	11/19*	2.75/5.5*	8.5/17.5*
DCH-2	2.22/10.78*	7/34*	4.12/6.66*	13/21*	2.31/5.17*	7.3/16.3*
DCH-3	N/A	N/A	N/A	N/A	1.27/4.12*	4/13*
DCH-4	1.27/9.83*	4/31*	3.49/6.02*	11/19*	N/A/2.85*	N/A/9*

*Contribution from the heat sinks added to the vaporization calculation.

2.3.5 Sandia FITSB Tests

Later Sandia FITS tests provided sufficient pressure transient information to evaluate the average steam generation rate resulting from explosive interactions. Steam generation rates can then be divided by the cross-sectional area of the FITS vessel to determine the effective heat fluxes. Figure 2-4 taken from [Mitchell, et al., 1986] shows a cross-section of the FITS facility. In this test series, about 18.6 kg (41 lbm) of molten thermite was poured into water test containers located in the FITS chamber and the resultant pressure history in the chamber gas space was recorded. Table 2-2, which was also taken from [Mitchell, et al., 1986], summarizes the test conditions and observations made with respect to explosive interactions. Figures 2-5 through 2-8 illustrate the pressurization of the gas space, the first three with initially subcooled water and the last with saturated water.

While only some of the experiments had explosive interactions, the principal focus is on the net steam generation rate created by the explosive interaction. The large steel vessel is considered to be pressurized with steam with the realization that this also increases the potential for condensation on the vessel walls. The results shown in Figures 2-5 through 2-8 are those with the largest vessel pressurization. A comparison of these figures also shows that the time to the peak pressure is approximately 1 sec for these tests, even though the path to this pressure may differ somewhat. (Test FITS 7B experienced about 90% of the pressure increase in the first second with the remainder occurring over the next 3 secs.)

The average steam generation rate can be estimated by using the ideal gas equation.

$$\frac{dP}{dt} = \frac{RT}{V} \frac{dN}{dt}$$

WESTINGHOUSE CLASS 3

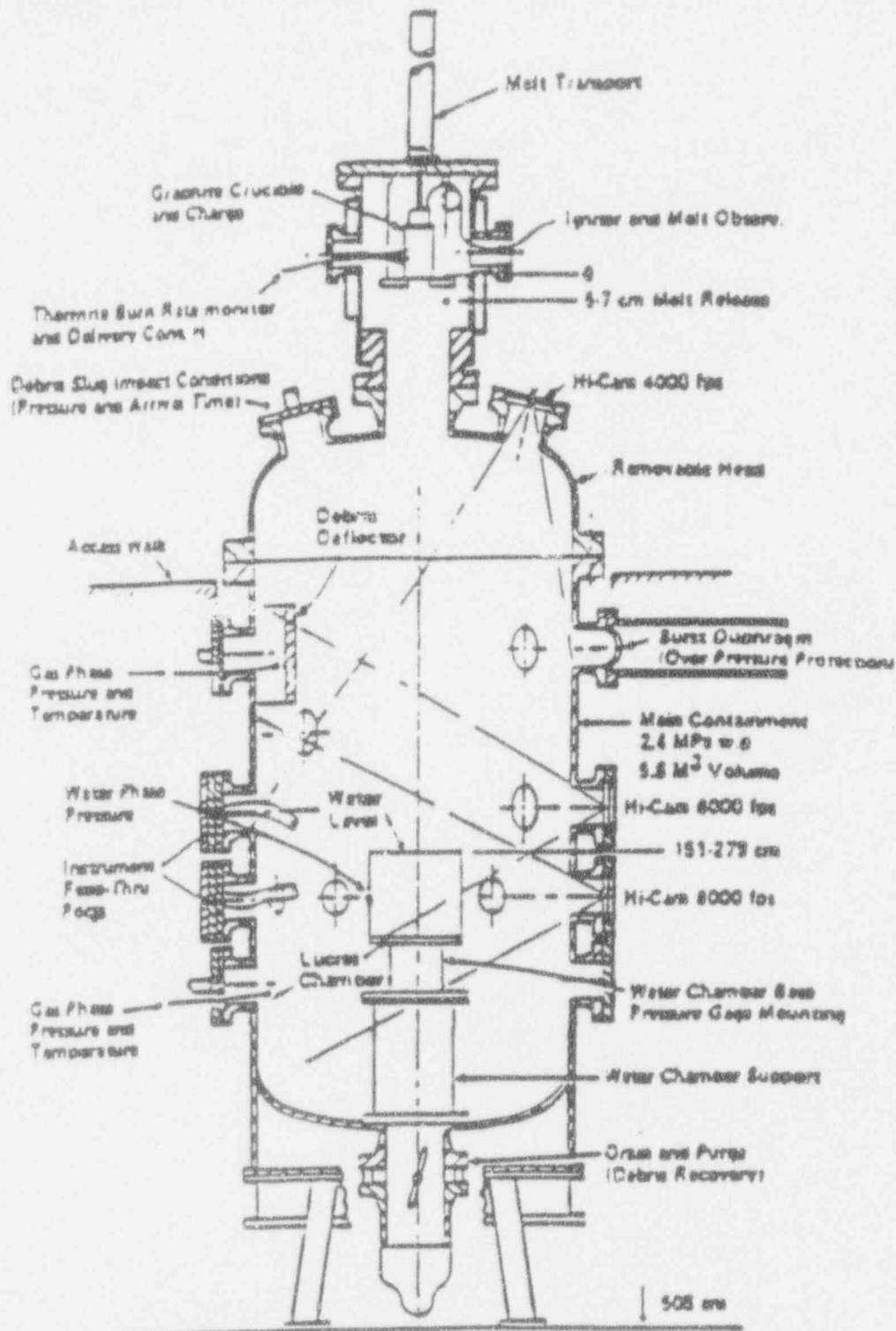


Figure 2-4 FITS containment chamber.

WESTINGHOUSE CLASS 3

Table 2-2

FITSB INITIAL CONDITIONS AND OBSERVATIONS

Expt.	Melt			Water			Initial Ratio Water/Melt		Other Observations		Other Observations
	Mass (kg)	Entry ol. (m/s)	Avg. dia. at Entry ¹ (cm)	Geometry (cm) Sq x Deep	Mass (kg)	Temp (K)	Mass	Vol. ²	Location	Time After Melt Entry (ms)	
1B	18.7	5.4	4.1	61 x 61	226.0	298	12.0	46.0	Surface Unknown	142 275	First explosion. Second explosion.
2B	18.6	6.0	6.0	61 x 30	113.0	298	6.0	23.0	Surface	84	Single explosion.
3B	18.6	6.0	24.0	43 x 30	57.0	295	3.0	11.5	Base	77	Single explosion weak interaction at surface at 70 ms after entry that did not propagate.
4B	18.7	6.8	5.8	61 x 61	226.0	299	12.0	46.0	Surface Base	29 146	First explosion. Second explosion.
6B	18.7	7.2	6.5	46 x 30	63.4	367	3.4	12.9	None	—	Multiple interactions at 40, 57 82, and 153 ms after melt entry, no propagation of steam explosion.
7B	18.7	7.4	n.o. ³	43 x 15.2	28.1	291	1.5	5.7	n.o.	80	No camera data, time estimated from water phase gauges.
8B	18.7	6.5	29.0	61 x 76.5	283.5	288	15.0	57.4	Surface Base	27 146	First explosion. Second explosion.
9B	18.7	7.0	5.6	61 x 45.7	170.0	289	9.0	34.6	Base	98	Single explosion.

¹Optical measurement.

²Melt density 3.8 g/cm³.

³Not observed.

WESTINGHOUSE CLASS 3

Table 2-2 (cont.)

FITSB INITIAL CONDITIONS AND OBSERVATIONS
(English Units)

Expt.	Melt			Water			Initial Ratio Water/Melt		Other Observations		Other Observations
	Mass (kg)	Entry vel. (m/s)	Avg. dia. at Entry ¹ (cm)	Geometry (cm) Sq x Deep	Mass (kg)	Temp (K)	Mass	Vol. ²	Location	Time After Melt Entry (ms)	
1B	41.2	17.71	1.61	24 x 24	498.0	77	12.0	46.0	Surface Unknown	142 275	First explosion. Second explosion.
2B	41.0	19.68	2.36	24 x 11.8	249.0	77	6.0	23.0	Surface	84	Single explosion.
3B	41.0	19.68	2.45	17 x 11.8	125.7	71.6	3.0	11.5	Base	77	Single explosion weak interaction at surface at 70 ms after entry that did not propagate.
4B	41.2	22.31	2.28	24 x 24	498.0	78.8	12.0	46.0	Surface Base	29 146	First explosion. Second explosion.
6B	41.2	23.62	2.56	18 x 11.8	139.8	201.2	3.4	12.9	None	--	Multiple intractions at 40, 57, 82 and 153 ms after melt entry, no propagation of steam explosion.
7B	41.2	24.28	n.o. ³	17 x 6	61.95	64.4	1.5	5.7	n.o.	80	No camera data, time estimated from water phase gauges.
8B	41.2	21.33	11.42	24 x 30	625.0	59.0	15.0	57.4	Surface Base	27 146	First explosion. Second explosion.
9B	41.2	22.97	2.2	24 x 18	374.79	60.8	9.0	34.6	Base	98	Single explosion.

¹Optical measurement.
²Melt density 3.8 g/cm³.
³Not observed.

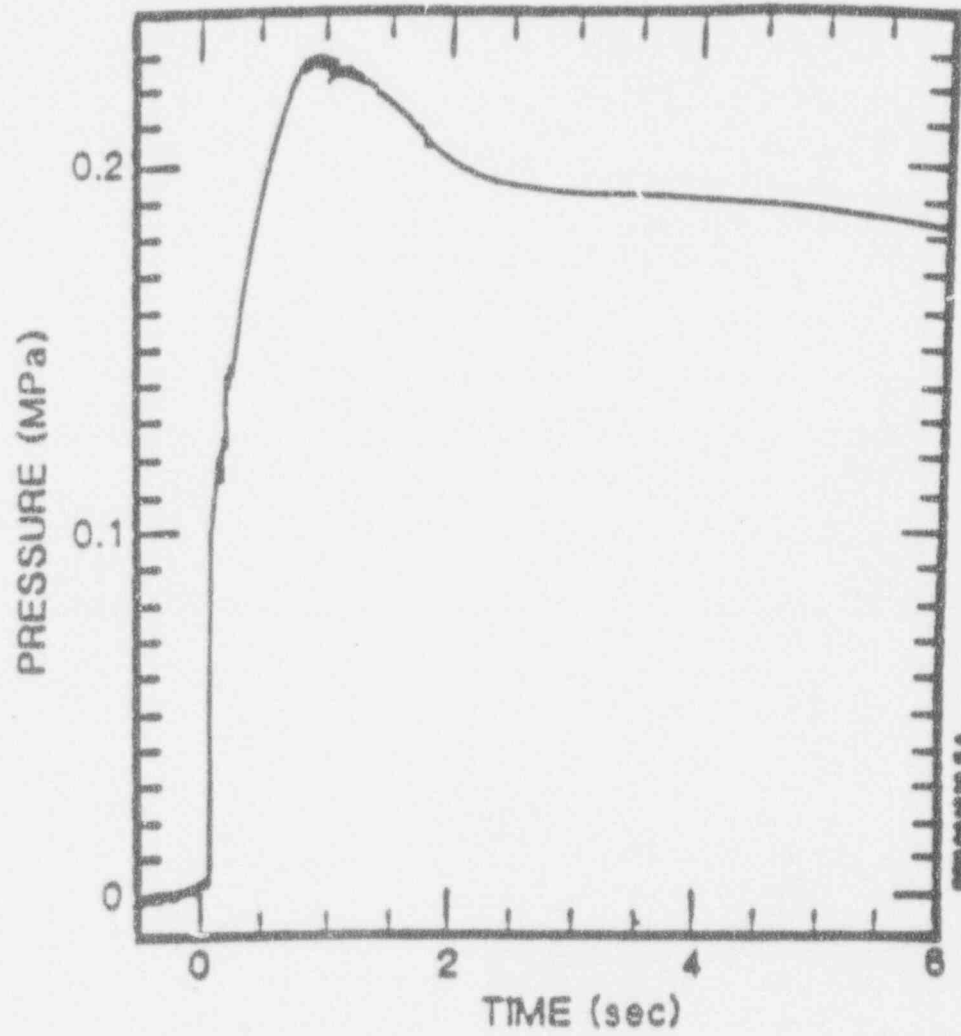


Figure 2-5 FITS2B chamber air pressure.

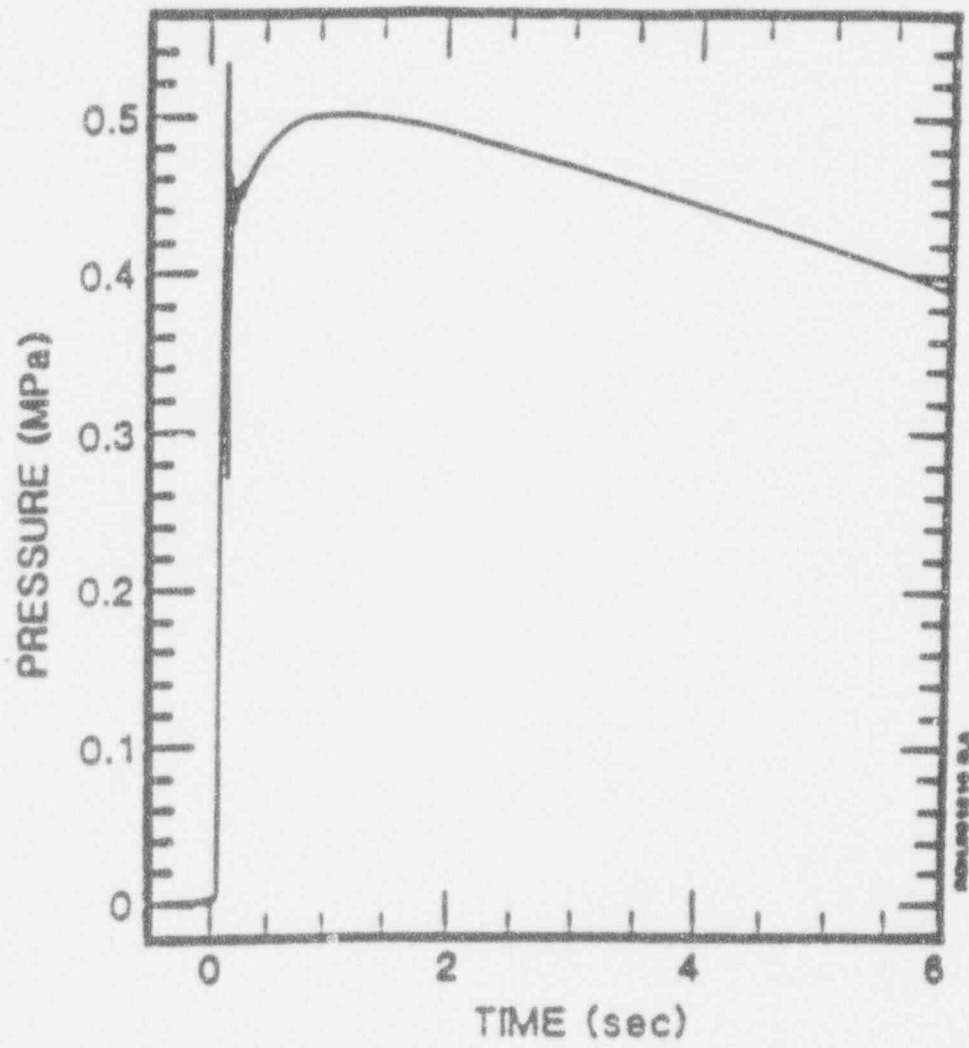


Figure 2-6 FITS3B chamber air pressure.

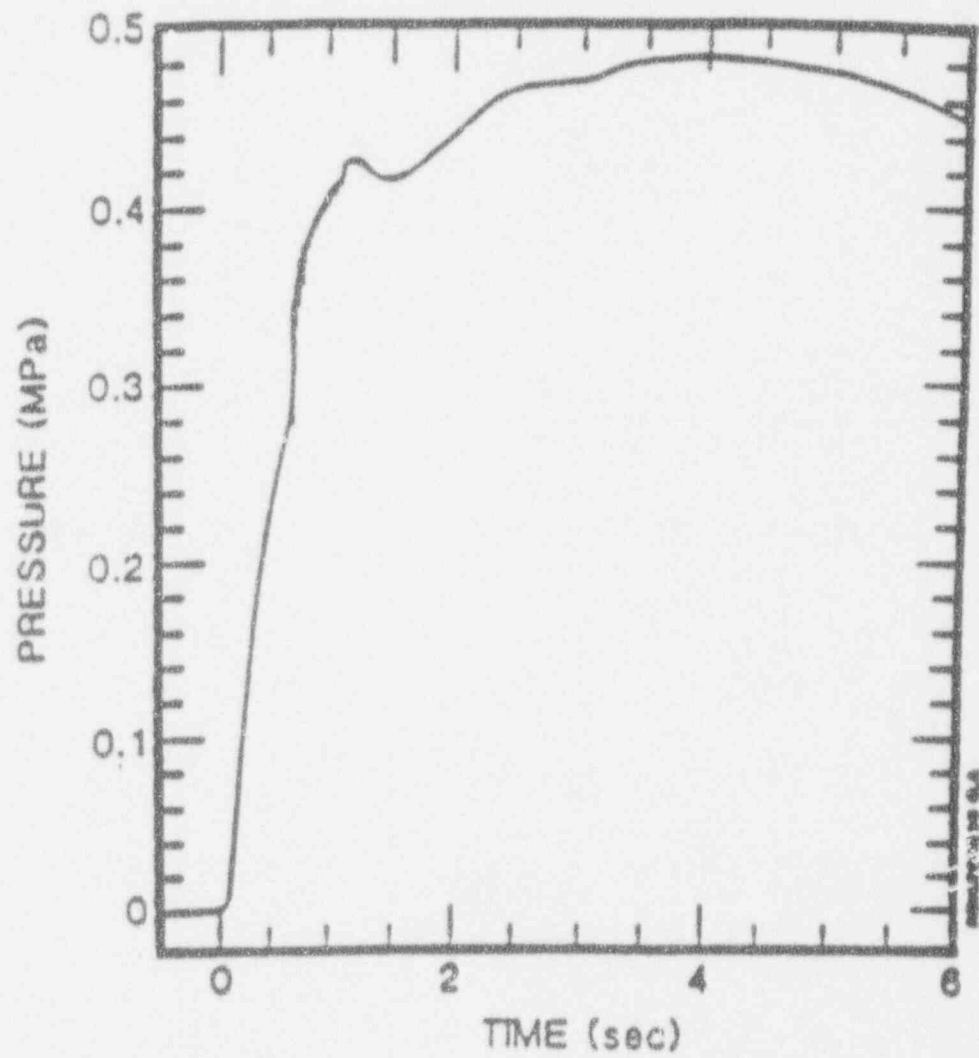


Figure 2-7 FITS7B chamber air pressure.

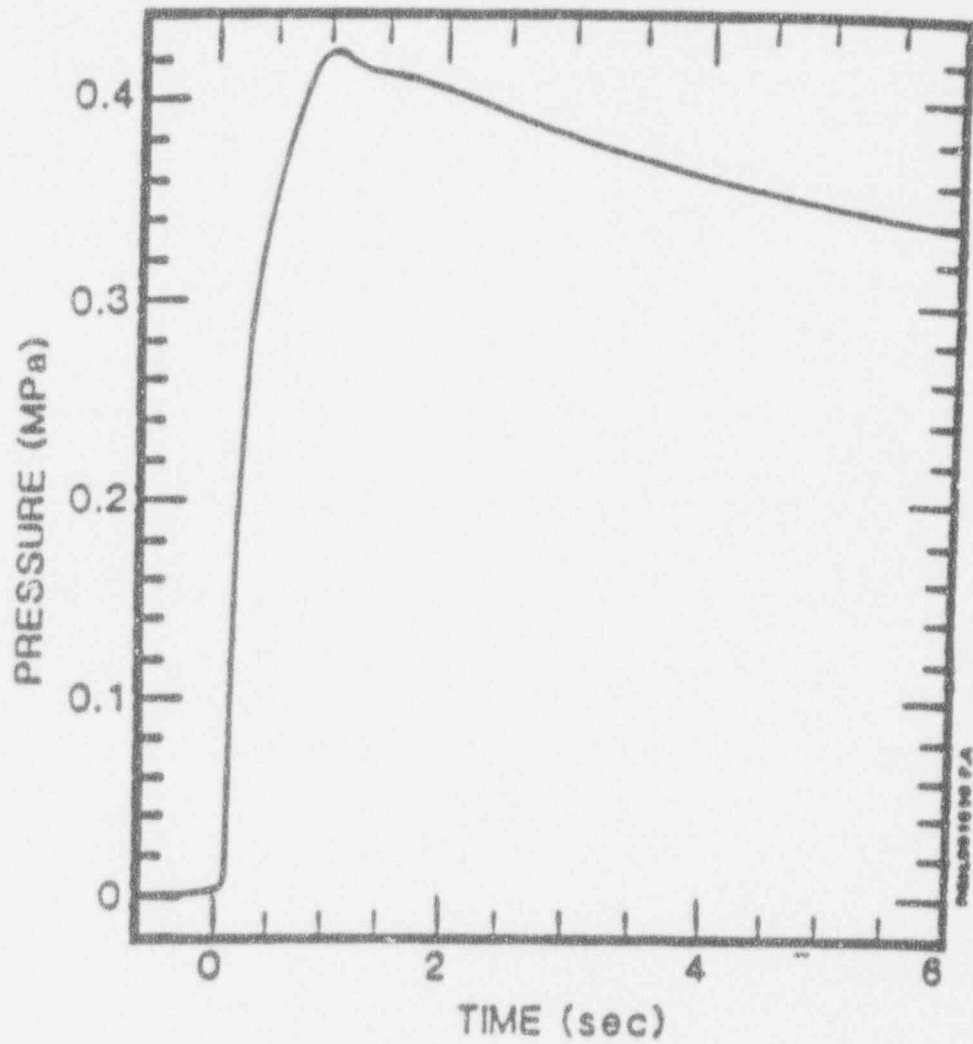


Figure 2-8 FITS6B chamber air pressure (saturated water).

where each variable has the standard meaning. As an average representation, assume that the gas space pressure increases 0.35 MPa (51 psi) in 0.5 sec. The volume of the FITS vessel is 198 ft³ (5.6 m³) [Marshall, 1986] and, if an average gas temperature of 260°F (400°K) is assumed, the steam generation rate is 2.65 lbm-moles/sec (1.2 kg-moles/sec), which is a mass addition rate of 47.5 lbm/sec (21.6 kg/sec). As the melt enters the vessel, the dynamic interactions (either explosive or non-explosive) would expel melt and water from the lucite test vessel. To provide an equivalent basis for comparison with the FAI/EPRI Mark I tests, the steaming rate should be represented as a heat flux using the cross-sectional area of the FITS vessel (~ 19.4 ft² (1.8 m²)). Using this area, the average heat flux from the melt to the water is about 8.6×10^6 Btu/h-ft² (27 MW/m²), i.e. a value in close agreement with that observed in the Mark I experiments.

2.3.6 Summary

In summary, the results from significant scale experiments with greatly different geometries can be compiled to develop a basis on which to provide interpretation for the containment response due to rapid steam generation by dynamic interactions. Specifically, dynamic interactions should be considered with steam generation rates from 3.2×10^6 to 9.5×10^6 Btu/h-ft² (10 to 30 MW/m²). The projected area of the compartment floor should be used as the pertinent value for determining the total energy production rate. This can then be used to determine if the uncertainties in this range provide for any substantial change in the overall accident progression or in the accident management decisions that would be exercised in such events.

2.4 Analysis

2.4.1 Effect of System Pressure on Steam Explosions

Several experimental investigations have focused on the effect of elevated pressures. These include studies using Freon-22 as the working (exploding) fluid [Henry-Fauske, 1979] as

well as water [Hohman, et al., 1979] and [Hohman, et al., 1982]. These test series employed fluid pairs which had been demonstrated to explode in a reproducible manner, such that a single parameter (pressure variation) would be meaningful. Increasing the system pressure was observed to prevent explosions in all three studies. Those performed without external triggers found that a reduced pressure (ratio of the pressure and the thermodynamic critical pressure for the working fluid) of 0.05 was sufficient to prevent explosions. This corresponds to a pressure of 150 psi (1 MPa) for water. It was also observed that the explosions became somewhat less efficient as the ambient pressure increased. In fact, in the water experiments, no explosions were observed for system pressures of ~ 75 psi (0.5 MPa).

Experiments performed with external triggers found that explosive interactions could be induced at somewhat higher pressures, but a reduced pressure of 0.10 was found to suppress explosions even with very strong external triggers. For water this is a pressure of ~ 300 psi (2 MPa). Therefore, this single experimental observation is sufficient to address the issue of in-vessel steam explosions. Explosive triggers do not exist in a reactor system. Hence, the set of experiments most relevant for the AP600 PRA analyses are those without explosive external triggers. These will be used in the application to the reactor system, which would reduce the limiting pressure even further.

For those primary system conditions where explosions could be initiated, the assessment of the threat to the RCS integrity needs to evaluate the magnitude of the explosive interactions and the capability of the interaction to transfer an impact loading to the RPV walls and upper head. This was treated in the IDCOR Program [IDCOR, 1983] in terms of (1) the maximum molten mass and water which could be intimately mixed, (2) the efficiency of the explosion and (3) the capability of transferring an impact load to the RPV upper head. Through these evaluations it was concluded that a sufficient melt-water mixture could not be established to approach the energy yield necessary for challenging the vessel integrity. In addition, no efficient energy transfer mechanism could be found which could transmit the necessary impact load to cause failure of the RPV upper head.

2.4.2 Steam Explosion Models

Numerous models have been proposed to explain the primary steps in the occurrence of a steam explosion. However, no consensus on modeling of steam explosions has emerged to date. The wide variation in views exhibited by the members of the SERG underscores this fact. Since the NRC states that no truly predictive mechanistic model exists [NRC, 1988], this section is limited to a short overview of two types of models that exist. These basically address the mechanisms for fragmentation of the lower volatility material and the mechanisms for providing the intimate liquid-liquid contact; the former is required to obtain the characteristic larger heat transfer area, while the latter is required for the characteristic rapid heat transfer rate.

Since fragmentation of the hot material is considered to be a necessary (but not sufficient) condition for a large scale explosive interaction, a rather extensive experimental and theoretical effort has been devoted to the understanding of this process. The fragmentation models may be grouped into the following four general categories:

1. hydrodynamics models: which treat effects between the molten material and coolant independent of thermal conditions;
2. violent boiling models: fragmentation induced in the molten material via the disruptive forces and associated with bubble growth and collapse including spontaneous nucleation;
3. thermal stresses theories: molten material breakup as a consequence of surface quenching and solidification; and
4. entrapment/gas release theories: rapid phase change of an entrapped species resulting in sudden expansion and fragmentation of the molten material.

From metal-water experiments it appears that an essential precursor to a vigorous interaction is the establishment of a stable vapor film between the fuel and coolant. The interaction is triggered by the destabilization of the vapor film, allowing extensive liquid-liquid

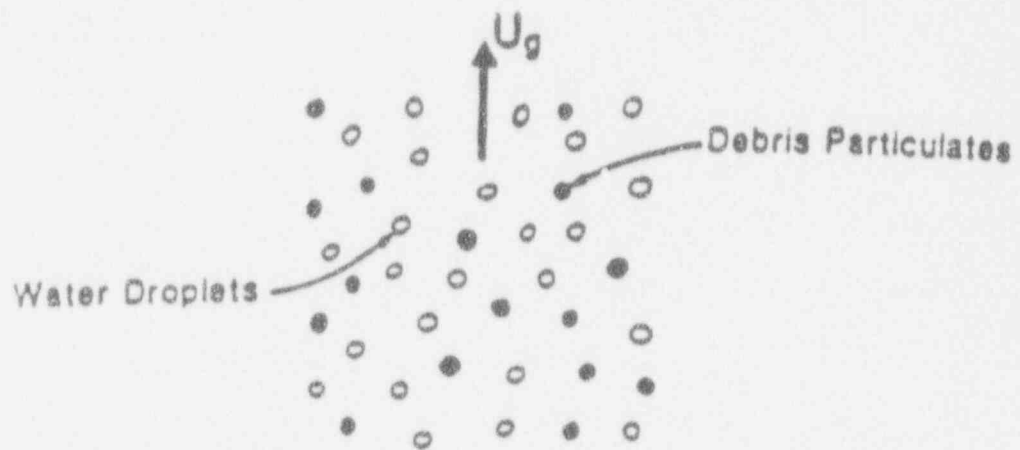
contact. In general, the models developed to explain the mechanism allowing liquid-liquid contact can be roughly classified into two broad types: (1) boiling models, which depend upon the rapid production of vapor after liquid-liquid contact is established, and (2) hydrodynamic models, which depend on the breakup of high temperature material due to the large relative velocity between fuel and coolant after collapse of the vapor layers due to arrival of a pressure wave. Some recent models consider that both types may be present at the same time. There are also purely parametric models which are concerned with the consequences, but not the mixing process physics, once a set of initial conditions is assumed.

2.4.3 Possible Mechanism for Maximum Steam Generation Rate

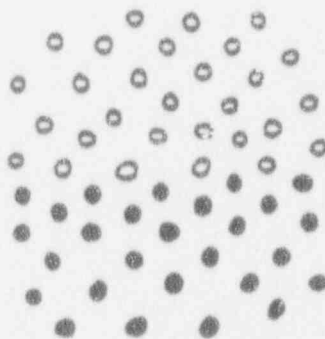
The information presented in Section 2.4.2 was taken from a wide variety of experimental information and provides a substantial data base for describing the maximum melt-water steam generation rate in containments. One can provide a theoretical basis for heat fluxes in the range of 10.4×10^6 Btu/h-ft² (30 MW/m²) for a system with co-dispersed debris and water as depicted in Figure 2-9. A steam velocity sufficient to levitate and separate the water droplets from the high temperature dense debris is given by

$$U_g = \frac{3.7 \sqrt[4]{g\sigma(\rho_f - \rho_g)}}{\sqrt{\rho_g}}$$

where g is the acceleration of gravity, σ is the steam-water surface tension and ρ_f and ρ_g represent the saturated water and steam densities respectively. If this is considered to be the maximum steam production rate which could exist without separation of the water droplets from



(a) Co-Dispersed Configuration



(b) Configuration if the Droplets are Fluidized

Figure 2-9 Debris dispersion configuration.

the co-disperse configuration, then the heat flux associated with the vapor production rate is given by

$$q/A = 3.7 h_{fg} \sqrt{\rho_g} \sqrt[4]{g\sigma(\rho_f - \rho_g)}$$

where h_{fg} is the latent heat of vaporization. Substituting the appropriate values for steam and water at 1 atm into this expression results in a value of 10.4×10^6 Btu/h-ft² (30 MW/m²); a value in agreement with those observed in the various experiments. Hence, the major ramification of an explosive interaction could be the co-dispersion of melt and water which then continues to transfer energy and vaporize water into the containment atmosphere at a rate limited by the ability of the water droplets to remain as part of the co-dispersed medium.

2.4.4 Shock Waves

Modeling of the shock waves induced by steam explosions is only necessary if it is conceived that these would challenge the containment integrity. Figure 2-10 taken from [Glass, 1974] illustrates the decay of substantial shock waves in air as the shock wave expands. A slope corresponding to a pressure amplitude decay proportional to $1/r^2$ is also included for reference and provides a reasonable assessment of the decay characteristic for strong waves. If anything, the higher amplitude portion of the curve decays faster than this simplified representation. If an interaction zone size is postulated along with a maximum pressure for the interaction, this type of decay can be applied to the Sandia FITS experiments to compare the measured shock wave pressures in these tests with this decay characteristic. Table 2-2 summarizes the experimental conditions for the FITSB series, including the size of the test chamber in which the thermite and water were mixed. As an interaction zone, half of the square dimension is used as the radius for

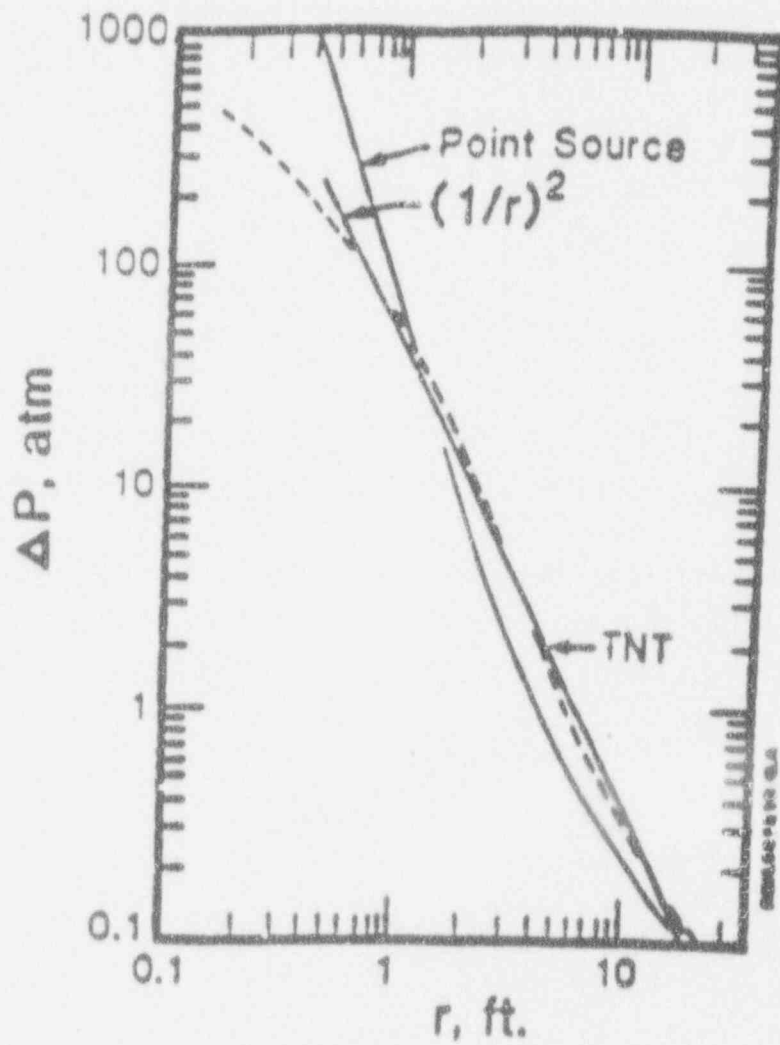


Figure 2-10 Comparison of shock wave pressures for TNT and point source explosions.

the initial calculation. Also, for the peak pressure achieved in the interaction zone one half the critical pressure (~ 1450 psi or 10 MPa) is used since this corresponds to a condition in which the critical size bubble embryos equal the size for thermally dominated bubble growth [Henry, et al., 1979]. For pressures greater than this value, the vapor cannot be produced. Other experiments have shown this value to be an upper bound of the pressure that can be achieved when the system is not tightly constrained.

The expansion from the interaction zone out to the diameter of the FITS vessel, 2.5 ft (0.76 m) radius, is performed following the approximation shown in Figure 2-10. Since only three different size vessels were used in the eight experiments, only three different shock wave pressures incident on the FITS vessel wall are calculated by this approximate method. These are illustrated in Table 2-3 for the different experiments. As illustrated, this technique substantially overestimates the measured pressure at the FITS vessel boundary. This is not surprising since the curve shown in Figure 2-10 is compared to a chemical explosion which is typically more energetic and has a stronger shock wave than those generated by steam explosions.

Table 2-3
CHAMBER AIR PRESSURE DATA FROM FITSB
(Times From Melt Entry)

Expt.	Steam Explosion Phase				Calculated Pressure Peak (MPa/psig)
	Explosion (s)		Pressure Peaks (MPa/psig)		
	1st ¹	2nd	1st	2nd	
1B	0.144	0.282	0.095/12.78	0.197/28.6	1.6/218
4B	0.029	0.146	0.020/2.9	0.500/72.5	1.6/218
8B	0.017	0.144	0.01/1.45	0.373/54.1	1.6/218
2B	0.087	n.o. ²	0.220/31.9	n.o.	1.6/218
3B	0.081	n.o.	0.440/63.8	n.o.	0.7/87
6B	n.o.	n.o.	n.o.	n.o.	0.9/116
7B	±0.20	n.o.	0.01/1.45	n.o.	0.7/87
9B	0.102	n.o.	0.210/30.45	n.o.	1.6/218

¹ Time taken from start to pressure rise. Zero time taken from average of two active melt position sensors 2.5 cm above water surface.

² Not observed.

3.0 METHODOLOGY

The disposition of containment failure due to steam explosions relative to plant response involves separate approaches for in-vessel and ex-vessel steam explosions, respectively. The IDCOR work, which is consistent with the recommendation of the SERG in [NRC, 1985], forms the basis for the treatment of in-vessel steam explosions. Results of analyses performed in accordance with significant scale experiments and expansion characteristics of shock waves form the basis for the treatment of ex-vessel steam explosions. This section describes the methodology for addressing steam explosions.

3.1 In-Vessel Steam Explosions

Fundamental experiments (see Section 2.4.1) show that the initiation of steam explosions is very sensitive to pressure levels and is prevented at system pressures beyond 10% of the primary system normal operating pressure. As a result, there is no threat to the RPV integrity by this phenomenon in accident sequences that do not meet this criterion.

For sequences which result in a depressurized (< 1 MPa/150 psia) primary system at the time molten core debris would be expected to flow into the lower plenum, the approach utilizes the IDCOR analysis [IDCOR, 1983]. With the mechanistic evaluations for the melt-water masses which could interact and the assessment of the energy transmission capability, there is no set of credible conditions which could approach conditions sufficient to challenge the vessel head integrity. This is consistent with the conclusions of the NRC sponsored Steam Explosion Review Group. Further details are presented in Section 4.1.

3.2 Ex-Vessel Steam Explosions

As discussed in Section 2, ex-vessel steam explosions could occur and may be a major mechanism for quenching of core debris should it be discharged from the reactor vessel. There are two aspects to be addressed:

- (1) the overpressure in the containment due to rapid steam generation and
- (2) the shock waves which could be created by the interactions.

3.2.1 Pressure Rise Due to Rapid Steam Generation

Based on the possible mechanism for maximum steam generation rate postulated in Section 2.4.3, the steam generation rate due to the explosive interaction of debris and water can be written as

$$\dot{m}_s = \frac{q_{ex}'' A_{pool}}{h_{fg}} \quad (3-1)$$

where in SI units,

\dot{m}_s = steam generation rate (kg/s)

q_{ex} = heat flux due to explosive interaction and based on pool area
= 30 MW/m²

A_{pool} = water pool cross sectional area where explosive interaction occurs (m²)

h_{fg} = latent heat of vaporization of water
= 2.25 MJ/kg

The pressure increase (ΔP) due to this rapid steam generation, using the ideal gas law, is given by

$$\Delta P = \frac{RT}{M_{H_2O} V} \dot{m}_s \Delta t \quad (3-2)$$

where

T = containment temperature ($^{\circ}\text{K}$)

R = universal gas constant = 8314 J/kg-mol $^{\circ}\text{K}$

V = total containment free volume (m^3)

M_{H_2O} = molecular weight of water = 18 kg/kg-mol

Δt = explosive interaction time (s)

3.2.2 Shock Waves

The $1/r^2$ decay of shock waves from the interaction zone, through air to the containment boundary was described in Section 2.4.4. The two basic parameters are (1) the 10 MPa maximum attainable pressure (P_{IZ}) in the interaction zone, and (2) the dimensions of the interaction zone. Assuming the interaction zone to be a sphere, we can find the radius of the sphere that contains steam equivalent to the amount generated at the rate \dot{m}_s during the interaction time period Δt (typically on the order of milliseconds) as

$$\frac{4}{3} \pi R_{IZ}^3 = \frac{\dot{m}_s \Delta t}{M_{H_2O}} \frac{RT}{P_{IZ}} \quad (3-3)$$

or

$$R_{IZ} = \left[\frac{3}{4\pi} \frac{\dot{m}_s \Delta t RT}{M_{H_2O} P_{IZ}} \right]^{1/3} \quad (3-4)$$

The $1/r^2$ decay law, then, gives the impact pressure at the containment wall as

$$P_{cw} = \left(\frac{R_{IZ}}{X_{cw}} \right)^2 P_{IZ} \quad (3-5)$$

where

P_{cw} = impact pressure at containment wall

X_{cw} = distance from center of interaction zone to containment wall.

4.0 PLANT SPECIFIC APPLICATION

4.1 Issues

4.1.1 In-Vessel Steam Explosions

As discussed in Section 3.1, in-vessel steam explosions are prevented at system pressures beyond about 10% of normal operating pressure. There is no threat to RPV integrity for accident sequences that meet this condition. With the AP600 design, however, the automatic depressurization system (ADS) will depressurize the reactor coolant system during transient and small LOCA sequences so that the IRWST can inject to the vessel. The vast majority of accident sequences postulated for the AP600 will be at low pressure, so in-vessel steam explosions cannot be dismissed on the basis of high RPV pressure.

The potential for containment failure by in-vessel steam explosion is still extremely low, in spite of the fact that the RPV will be depressurized in nearly all accident sequences. Reasons for this conclusion are listed in [DOE, 1991] and summarized here. Various estimates for the probability of this containment failure mode have all resulted in extremely low probabilities, even though a variety of modeling techniques and assumptions were employed by the investigators. These results are summarized as follows:

REFERENCE	RESULTS	COMMENTS
SERG	0 to $10E-2$	Six of ten estimates less than $10E-4$
APS	Much less than Reactor Safety Study	Some investigators thought the probability was zero
SANDIA	$10E-4$	Based on steam explosion experiments
IDCOR		Cannot occur because limited amount of fuel can react
NUREG-1150	0 - $10E-3$ $4 \times 10E-5$	For Mark I BWR For PWRs: median
BNL	$10E-4$	Best estimate value

(a,c)

4.1.2 Ex-Vessel Steam Explosions

(a,c)

4.1.2.1 Pressure Rise Due to Rapid Steam Generation

In order to evaluate the pressure rise from Equation (3-2), the interaction pool area (A_{pool}) and the interaction time (Δt) must be determined. However, even when conservative values for A_{pool} and Δt are used, this still results in an insignificant pressure rise that will not threaten containment integrity. Due to the design of the AP600 containment, the cavity for almost every sequence will contain a substantial amount of water, so the cavity floor area is appropriate for

A_{pool} . [

(a,c)

4.1.2.2 Shock Wave Impact

If the vessel fails, corium will exit the vessel and potentially cause a steam explosion in the cavity. The impact of a steam explosion in the cavity can be assessed using the equations and methodology described in Section 3.2.2. [

(a,c)

(a,c)

4.1.3 Uncertainty Considerations

As discussed in this document, in [NRC, 1985] and in [IDCOR, 1983], a specific chain of events must occur before an in-vessel explosive interaction could challenge the RPV integrity. The failure of any link in this chain would prevent interactions which could challenge RPV integrity. Evaluations of each link in the chain conclude that the only link which could be achieved is an explosive event, but then only when the RPV pressure is very low, i.e. typically less than 300 psia (2 MPa). Even if an explosion would occur, the mass of material, the efficiency, the slug formation and the slug transmission could not be realized to any significant degree. Given (1) the extent of individual analyses performed on each link in the chain of events, (2) the extent to which each is not satisfied in a realistic analysis and (3) the importance that each be satisfied before the RPV integrity could be challenged, it is concluded that there is no realistic combination of uncertainties which could make such an event credible.

Ex-vessel explosive interactions could occur for sequences which would progress to vessel failure. Here again, the extent of the interaction (and damage potential) is determined by the mass of molten material involved, the efficiency of the interaction and the decay of the shock waves as they propagate from the source. In this evaluation we have assumed:

- an efficient interaction since the shock waves are calculated to decay as for TNT, and
- an unimpeded expansion of the shock waves to the containment boundary

These global representations are sufficient to determine if ex-vessel explosions could challenge containment integrity. However, best estimate analyses would consider:

- a much smaller interaction zone,
- much weaker shock waves for steam explosions than for chemical explosions, and
- the breakup of shock waves by the structures in the annular containment compartment, in particular the concrete shield walls and various equipment structures located in the area of the steam explosion.

With the conservative assessments used for these individual evaluations, it is concluded there is no realistic combination of uncertainties which could result in a credible threat to containment integrity.

4.2 Conclusions

There is no credible set of circumstances in which steam explosions could challenge the AP600 design containment integrity.

5.0 ACCIDENT MANAGEMENT INSIGHTS AND CONSIDERATIONS

The AP600 plant design precludes containment failure by steam explosions due to a variety of features. As noted in Section 4.0, in-vessel steam explosions cannot generate sufficient energy, in a short time scale, to generate a missile which could fail containment. With respect to in-vessel steam explosions, the same arguments made for the current generation of LWRs apply to the AP600 design. With regard to ex-vessel steam explosions, the AP600 design assures that steam explosions in containment could occur only in the cavity, if they could occur at all.

(a,c)

Although steam explosions cannot fail the AP600 containment, they can have an effect on containment response and severe accident progression. Severe accident progression is partially dictated by the conditions in the cavity. If the cavity is completely flooded when the debris reaches the lower plenum, the lower head will not fail and steam explosions ex-vessel cannot occur [Fauske & Associates, 1992]. Conversely, if the cavity remains dry throughout the accident progression, the lower head could fail, although steam explosions would be precluded because of a lack of water. The only credible scenario for a steam explosion is when the cavity is partially filled with water. If the operator attempts to flood the cavity in response to core damage, it is conceivable that vessel failure could occur before the entire cavity is flooded and lower head coolability is established. In this instance, melt ejection would occur into a water pool and steam explosions might result. As demonstrated by the calculations of Section 4.0, a steam explosion would cause a rapid, transient pressure rise in the cavity. This transient might last a few seconds, until the debris is quenched and dynamic interactions (and/or steam

explosions) cease. The global pressure rise in containment might be noticeable, but certainly not threatening. Therefore, the results of Section 4.0 suggest that cavity flooding should always be established, regardless of the potential for steam explosions in the cavity.

6.0 SUMMARY

The influence of in-vessel and ex-vessel steam explosion events on the potential for containment failure has been addressed for the accident conditions of interest.

The evaluations for in-vessel events closely parallel those performed as part of the IDCOR program and result in a conclusion that the slumping of molten debris into the RPV lower plenum could not result in sufficient energy release to threaten the vessel integrity. Hence, such interactions could not lead directly to containment failure (alpha mode) and a consequential release of fission products to the environment. This is in concert with the conclusion of the NRC sponsored Steam Explosion Review Group.

Evaluations of both steam generation rate and shock waves induced by ex-vessel explosive interactions show that these would not be of sufficient strength to threaten the containment integrity. While such explosions could occur, the principal result of these events would be to rapidly cool debris and slightly pressurize the containment. Neither of these would be sufficient to challenge the containment integrity for any realistic accident conditions.

As a result of the evaluations performed for both in-vessel and ex-vessel events and the conclusion that these would not lead to challenges of the containment integrity, steam explosions are not included as a potential failure mode for the AP600 design.

7.0 REFERENCES

- Buxton, L. D. and Benedick, W. B., 1979, "Steam Explosion Efficiency Studies," NUREG/CR-0947, SAND 79-1399.
- Buxton, L. D., Benedick, W. B. and Corradini, M. L., 1980, "Steam Explosion Efficiency Studies: Part II Corium Experiments," NUREG/CR-1746, SAND 80-1324.
- Deitrich, J. R., 1965, "Experimental Investigation of the Self-Limitation of Power During Reactivity Transients in a Subcooled Water-Moderated Reactor-BORAX-1 Experiments, 1954," AECD-3668.
- DOE, "Passive ALWR Requirements to Prevent Containment Failure," 1991.
- FAI, 1982, "Assessment of Steam Explosion Potential in Hypothetical LWR Core Meltdown Accidents," Draft Report Submitted to the Nuclear Safety Analysis Center, Electric Power Research Institute.
- FAI, 1990, "FAI/CECo Direct Containment Heating Experiments for a Zion-Like Geometry," Fauske & Associates, Inc. Report, FAI/90-60.
- FAI, 1992, "Westinghouse AP600 Phenomenological Evaluation on External Cooling of the RPV in Support of the ALWR Risk Analysis", FAI/92-13.
- Glass, I. I., (1974), Shock Waves and Man, The University of Toronto Press.
- Henry, R. E. and Fauske, H. K., (1979), "Nucleation Processes in Large Scale Vapor Explosions," Trans. ASME, Jr. of Heat Transfer, Vol. 101, pp. 280-287.
- Hess, P. D., Miller, R. E., Wahnsiedler, W. E. and Cochran, C. N., 1980, "Molten Aluminum/Water Explosions," Light Metals, (E. McMinn, Ed.), p. 287. (Proc. of Technical Sessions Sponsored by TMS Light Metals Committee at 190th AIME Annual Mtg.).
- Higgins, H. M., 1955, "A Study of the Reaction of Metals and Water," AECD-3664.
- Higgins, H. M., 1956, "The Reaction of Molten Uranium and Zirconium Alloys with Water," Aerojet Report No. 2914-2, Metallurgy & Ceramics, Aerojet-General Corporation, Azusa, CA.
- Hohmann, H., Henry, R. E. and Kottowski, H. M., 1979, "The Effect of Pressure on NaCl-H₂O Explosions," 4th CSNI Specialist Mtg. on Fuel-Coolant Interactions in Nucl. Reactor Safety, Bournemouth, United Kingdom, CSNI Report No. 37, pp. 308-323.

- Hohmann, H., Kottowski, H. M., Schins, H. and Henry, R. E., 1982, "Experimental Investigations of Spontaneous and Triggered Vapour Explosions in the Molten Salt/Water System," Intl. Mtg. on Thermal Reactor Safety, Chicago, IL.
- IDCOR, 1983, "Key Phenomenological Models for Assessing Explosive Steam Generation Rates," Technical Report 14.1A.
- Koopman, R. P., et al., 1981, "Description and Analysis of Burro Series 40 m³ LNG Spill Experiments," UCRL-53186.
- Krause, H. H., et al., 1973, "Smelt-Water Explosions," Final Reports to Fourfrinier Kraft Board Institute, Inc., Batelle Columbus Laboratories, Columbus, OH.
- Lemmon, A. W., 1980, "Explosions of Molten Aluminum and Water," Light Metals, (E. McMinn, Ed.), p. 817. (Proc. of Technical Sessions Sponsored by TMS Light Metals Committee at 190th AIME Annular Mtg.).
- Long, G., 1957, "Explosions of Molten Aluminum and Water," Metal Progress, Vol. 71, p. 107.
- MacGregor, J. G., Simmonds, S. H. and Rixkalla, S. H., 1980, "Test of a Pre-Stressed Concrete Secondary Containment Structure," University of Alberta, Department of Civil Engineering Report.
- Malinovic, B., Henry, R. E. and Sehgal, B. R., 1989, "Experiments Relating to Drywell Shell-Core Debris Interactions," Natl. Heat Transfer Conf., Philadelphia, PA, AIChE Symposium Series, Vol. 85, No. 269, pp. 217-222.
- Marshall, Jr., B. W., 1986, "Hydrogen:Air:Steam Flammability Limits and Combustion Characteristics in the FITS Vessel," NUREG/CR-3468, SAND 84-0383.
- Miller, R. W., Sola, A. and McCardell, R. K., 1964, "Report of the SPERT-1 Destructive Test Program on an Aluminum, Plate-Type, Water Moderated Reactor," IDO-16883.
- Mitchell, D. E., Corradini, M. L. and Tarbell, W. W., 1981, "Intermediate Scale Steam Explosion Phenomena: Experiments and Analysis," Sandia National Laboratory, SAND/81-0124, NUREG/CR-2145.
- Mitchell, D. E. and Evans N. A., (1986), "Steam Explosion Experiments at Intermediate Scale: FITSB Series," NUREG/CR-3983, SAND 83-1057.
- NRC, 1975, "Reactor Safety Study," WASH-1400, NUREG/75-0114.

WESTINGHOUSE CLASS 3

NRC, 1985, "A Review of the Current Understanding of the Potential for Containment Failure from In-Vessel Steam Explosions," NUREG-1116.

NRC, 1989, "An Assessment of Steam Explosion Induced Containment Failure," NUREG/CR-5030.

Shick, P. E., 1980, "Concentration-Gradient Trigger Mechanism for Smelt-Water Explosions. Paper presented at the American Paper Institute Annual Recovery Boiler Committee Mtg., Chicago, IL, 30-31.

SL-1 Project, "Final Report of SL-1 Recovery Operations," IDO-19311.

Westinghouse Electric Corporation, AP600 MAAP 4.0 Parameter File, November, 1991.

Wright, R. W., Firstenberg, A. F., Humberstone, G. H., Neal, L. G., Wentz, L. G. and Zivi, S. M., 1966, "Kinetic Studies of Heterogeneous Water Reactors - Annual Summary Report - 1966," STL-372-50, Space Technology Laboratories, Canoga Park, CA.

FAI/92-12

A PHENOMENOLOGICAL EVALUATION SUMMARY ON
EXTERNAL COOLING OF THE RPV
IN SUPPORT OF THE AP600 RISK ANALYSIS

Revision 1

Prepared By:

Fauske & Associates, Inc.
16W070 West 83rd Street
Burr Ridge, Illinois 60521

March 1994

ABSTRACT

The Westinghouse AP600 design features result in substantial water accumulation within the containment during numerous, postulated accident sequences. Based on the AP600 containment configuration and the several, passively injected safety systems, during accident conditions the containment water level would not only be sufficient to submerge the reactor pressure vessel (RPV) lower head but also a substantial fraction of the vessel cylinder. Under these conditions, should the accident progress to slumping of core debris into the vessel lower plenum, significant energy could be removed through the vessel wall with nucleate boiling on the vessel outer surface. Assessments of internal circulation within the debris and the energy transferred to the wall show that the heat flux from the melt to vessel wall would be of the order of 10^5 W/m^2 . If these could be removed by nucleate boiling on the vessel outer surface the reactor vessel may be sufficiently cooled to prevent downward failure of the reactor vessel and release of the core debris into containment. This would eliminate considerations of ex-vessel events such as:

- direct containment heating,
- core-concrete attack,
- ex-vessel debris coolability, and
- ex-vessel fission product release.

Because of the importance of this external cooling mechanism, the Commonwealth Edison Company (CECo) has sponsored significant scale experiments to evaluate the external cooling mechanisms. These were performed with a simulated reactor vessel insulated by reactor grade reflective insulation with sufficient instrumentation to evaluate the surface boiling regime for heat fluxes far above those that would be anticipated for the reactor system. These results demonstrate that there is no limitation to the boiling regime, even if there is insulation on the reactor vessel. Since the AP600 design incorporates standoff insulation which encapsulates the reactor vessel below the hot leg nozzle elevation creating a minimum 9" gap around the

cylindrical section of the vessel, results obtained by the CECe experiments are applicable in the current analysis as well.

With these analytical and experimental insights with respect to the potential for external cooling and prevention of downward failure of the RPV, a best estimate evaluation of the AP600 design indicates that the presence of sufficient water to submerge the RPV lower head on a continual basis would prevent downward vessel failure.

TABLE OF CONTENTS

	<u>Page</u>
ABSTRACT	i
LIST OF FIGURES	v
LIST OF TABLES	vi
NOMENCLATURE	vii
1.0 PURPOSE	1-1
2.0 PHENOMENA	2-1
2.1 Description	2-1
2.1.1 Controlling Physical Processes	2-1
2.1.2 Relationship to Containment Failure Mechanisms and Modes	2-2
2.1.3 Relationship to Source Term	2-4
2.2 Experiments	2-5
2.3 Relevant Analyses	2-11
3.0 METHODOLOGY	3-1
3.1 Analysis	3-1
3.2 Approach	3-4
4.0 PLANT SPECIFIC APPLICATION	4-1
4.1 AP600 Design Considerations	4-1
4.2 AP600 RPV Cooling Analysis	4-14
5.0 UNCERTAINTIES	5-1

TABLE OF CONTENTS (continued)

	<u>Page</u>
6.0 ACCIDENT MANAGEMENT IMPLICATIONS	6-1
7.0 SUMMARY	7-1
8.0 REFERENCES	8-1

APPENDIX A: MAAP 4 Analysis of External Cooling of the RPV
for the AP6000 Design

LIST OF FIGURES

<u>Figure No.</u>		<u>Page</u>
2-1	Heat transfer from the molten debris to the RPV wall	2-3
2-2	Schematic of the CECO experimental apparatus	2-6
2-3	Description of the reflective insulation used in CECO tests	2-7
2-4	AP600 design reactor vessel insulations	2-10
3-1	Heat transfer from the molten debris to the RPV wall	3-2
4-1a	AP600 containment isometric view	4-3
4-1b	AP600 containment isometric view	4-4
4-1c	AP600 containment isometric view	4-5
4-2	AP600 reactor cavity flooding from refueling canal	4-7
4-3	AP600 containment flooding	4-9
4-4	AP600 cavity flooding based on IRWST discharge through 10" and 4" drain lines	4-13

LIST OF TABLES

<u>Table No.</u>		<u>Page</u>
2-1	CECo Lower Head Cooling Experimental Matrix	2-8
4-1	AP600 Passive Core Cooling System Water Inventories	4-2
4-2	AP600 Non-LOCA Cavity Flood Height Without IRWST Thermal Expansion	4-10

NOMENCLATURE

<u>Symbol</u>	<u>Definition</u>
g	acceleration of gravity
h	heat transfer coefficient
h_{fg}	latent heat of vaporization
κ	thermal conductivity
ℓ	debris pool depth in vessel lower head
\dot{m}_g	steam production rate
q''	heat flux from debris pool
q_d	average downward and horizontal heat flux
$q_{d,max}$	maximum downward and horizontal heat flux
q_{min}	minimum downward and horizontal heat flux
q_u	average upward heat flux
Q	volumetric heat generation rate
\dot{Q}_d	total downward heat transfer rate
R	debris pool or reactor vessel radius
R_s	Rayleigh number for a heat generating fluid
ΔT	debris pool temperature above its melting temperature
Z	height of lower head hemispherical cap
α	debris pool thermal diffusivity
β	debris pool coefficient of volumetric expansion
ν	debris pool kinematic viscosity

FAI/92-13

PHENOMENOLOGICAL EVALUATION SUMMARY ON
HIGH PRESSURE MELT EJECTION AND
DIRECT CONTAINMENT HEATING

IN SUPPORT OF THE
AP600 RISK ANALYSIS

Revision 1

Prepared By:

Fauske & Associates, Inc.
16W070 West 83rd Street
Burr Ridge, Illinois 60521

March 1994

ABSTRACT

This phenomenological evaluation summary assesses the susceptibility of the AP600 containment to failure as a result of High Pressure Melt Ejection (HPME) following vessel failure. In particular, the possibility of an early containment failure due to Direct Containment Heating (DCH) is addressed.

For the AP600 design, HPME occurs if (1) RPV failure occurs at locations that allow a large mass of molten core debris in the lower head to be discharged into the reactor cavity (i.e., below the debris pool surface) and (2) the RPV fails at high pressure. Should either of these phenomena not occur to a sufficient degree, HPME would be prevented.

The AP600 design features include the automatic depressurization system (ADS), low core power density, an RPV lower head without penetrations mounted on it, and the capability to flood the reactor cavity with water from IRWST to remove decay heat from the external surface of the RPV. The ADS would ensure that the RCS remains at low pressure during any accident sequences. If the RPV is assumed to fail at high pressure due to the failure of the ADS and external RPV cooling capability, the RPV would fail due to creep rupture from a location above the molten debris pool. This failure location would result in passive depressurization of the RCS without significantly discharging the molten debris out of the RPV lower head. The low core power density of the AP600 would lead to a stable crust formation on the top of the debris pool by the time of the RPV creep rupture failure. The presence of the solid crust layer would be sufficient to prevent the direct contact between the gaseous phase and the liquid phase of the core debris during blowdown, thereby preventing any entrainment of molten core debris from inside the vessel during RCS depressurization.

Since HPME/DCH is a postulated containment failure phenomenon for current PWRs with penetrations mounted on the RPV lower head, the AP600 design which does not include lower head penetrations precludes this potential RPV failure location and potential mechanism for HPME initiation through its design. Hence, it is sufficient to show that prevention of significant HPME would eliminate the issue of DCH from the AP600 risk analysis. Furthermore, a bounding DCH calculation which conservatively assumes HPME shows the resulting pressurization to be much less than a value that would challenge the containment integrity for the AP600 design.

TABLE OF CONTENTS

	<u>Page</u>
ABSTRACT	i
TABLE OF CONTENTS	ii
LIST OF FIGURES	v
LIST OF TABLES	vii
1.0 PURPOSE	1-1
2.0 PHENOMENA	2-1
2.1 Description	2-1
2.1.1 Controlling Physical Processes	2-1
2.1.2 Relationship to Containment Failure Mechanisms and Modes	2-3
2.1.3 Relationship to Source Term	2-4
2.2 Experiments	2-4
2.2.1 Sandia HIPS Experiments	2-4
2.2.2 Argonne Wood's Metal Tests	2-7
2.2.3 Argonne CWTI Experiments	2-13
2.2.4 SNL-DCH (Surtsey) Experiments	2-17
2.2.5 BNL Simulant Fluid Test	2-22
2.2.6 IDCOR/FAI Wood's Metal Tests	2-22
2.2.7 FAI-DCH Experiments	2-24
2.2.8 Scaling Effects	2-36
2.3 Analyses	2-41
2.3.1 Zion Probabilistic Safety Study	2-41
2.3.2 Sandia's Preliminary Calculation	2-42
2.3.3 HARDCORE	2-43
2.3.4 PARSEC	2-44
2.3.5 Kiva-DCH	2-44
2.3.6 CONTAIN	2-45
2.3.7 Simplified Model for Representing Comparable Debris Dispersal Processes	2-46

TABLE OF CONTENTS - Continued

	<u>Page</u>
2.3.8 Jet Breakup Model	2-48
3.0 METHODOLOGY	3-1
3.1 Mass of Debris Distributed Into the Containment Atmosphere	3-1
3.1.1 Extent of Entrainment	3-2
3.1.2 De-Entrainment	3-3
3.2 DCH Pressure Rise	3-3
3.3 Likelihood of Hydrogen Combustion	3-4
3.4 The Influence of Uncertainties	3-4
3.4.1 Core Melt Progression	3-5
3.4.2 RPV Failure Mechanism	3-5
3.4.3 Extent of Debris Particulation	3-6
3.4.4 Influence of Structures	3-7
3.4.5 Potential for Hydrogen Combustion	3-7
4.0 PLANT SPECIFIC APPLICATION	4-1
4.1 Automatic Depressurization System (ADS)	4-1
4.2 Reactor Vessel Failure Location	4-3
4.3 Crust Formation at RPV Creep Rupture	4-6
4.4 HPME/DCH Bounding Calculation	4-8
5.0 ACCIDENT MANAGEMENT IMPLICATIONS	5-1
6.0 SUMMARY	6-1
7.0 REFERENCES	7-1

TABLE OF CONTENTS - Continued

	<u>Page</u>
APPENDIX A FORMULATIONS OF DEBRIS ENTRAINMENT PROCESSES	A-1
APPENDIX B CALCULATIONS OF DCH TEMPERATURE AND PRESSURE RISE	B-1
APPENDIX C HYDROGEN COMBUSTION LIMITS	C-1
APPENDIX D SCALING OF ENTRAINMENT AND DISPLACEMENT RATES	D-1

LIST OF FIGURES

<u>Figure No.</u>		<u>Page</u>
2-1	Plan view of the experimental apparatus for the ANL Wood's metal tests, taken from [Spencer, 1983].	2-8
2-2	Location of simulated core debris dispersal in the ANL Wood's metal experiment, taken from [Spencer, 1983a]. In the legend, U_g - gas velocity m/sec, h/D_i - dimensionless height of water in the reactor cavity.	2-10
2-3	ANL thermite apparatus for the CWTI tests, taken from [Spencer, 1987].	2-14
2-4	Schematic of the Surtsey Direct Heating Test Facility, taken from [Marx, 1989]. The apparatus used in both the DCH-2 and DCH-3 experiments is shown.	2-19
2-5a	1 % linear scale building block experiments/reactor cavity.	2-25
2-5b	1 % linear scale building block experiments/reactor cavity and seal table.	2-26
2-5c	1 % linear scale building block experiments/2D representation of the lower compartment.	2-27
2-5d	1 % linear scale building block experiments/elevation view of 3D lower compartment.	2-28
2-5e	1 % linear scale building block experiments/plan view of 3D lower compartment.	2-29
2-6	Elevation view of the vessel interconnection to simulate the containment configuration.	2-30
2-7	Cross-section of the melt generator, reactor cavity, instrument tunnel and the simulated lower compartment with structures.	2-31
2-8	Relationship of the test configuration to the Zion containment buildings.	2-32

LIST OF FIGURES

<u>Figure No.</u>		<u>Page</u>
2-9	De-entrainment modeling of particles making a 90° turn (adapted from [Walker, 1987]).	2-39
2-10	Characteristic debris length and displacement length for debris movement.	2-47
4-1	Master creep rupture curve for 316 stainless steel.	4-4
4-2	AP600 cavity layout at EL 60'-6" (adapted from [Westinghouse, 1991c]).	4-10
4-3	AP600 cavity layout at EL 81'-6" (adapted from [Westinghouse, 1991d]).	4-11
4-4	AP600 containment isometric view of cavity loop compartment.	4-12
C-1	Normalized peak pressure (P_{max}/P_o) for hydrogen:air:oil:gas mixtures, comparing CO ₂ and steam (AICC = adiabatic isochoric complete combustion, Rh = relative humidity).	C-2
C-2	Experimental data for combustion limits with fans on and off shown with the exponential curve fit.	C-3

LIST OF TABLES

<u>Table No.</u>		<u>Page</u>
2-1	Selected HIPS Experiments	2-6
2-2	Summary of Wood's Metal Injection/Dispersal Tests	2-11
2-3	Summary of Characteristic Dispersal Times	2-12
2-4	ANL CWTI DCH-Related Experiments	2-16
2-5	SNL-DCH Experiments	2-21
2-6	Model Comparisons for DCH Test	2-23
2-7	Zion Cavity Building Block	2-33
2-8	CECo/FAI-DCH Experiments	2-35
2-9	DCH-1 Final Debris Distribution	2-49
2-10	DCH-2 Final Debris Distribution	2-50
B-1	Heat of Oxidation	B-7
B-2	Properties of Core Debris Constituents	B-8
B-3	Primary System and Core Debris Conditions for DCH Assessment	B-9

1.0 PURPOSE

Analyses of core damage events which could progress to slumping of molten core material into the reactor pressure vessel (RPV) lower plenum must consider the dynamic processes that could occur following debris relocation and possible vessel failure. Vessel failure could lead to dispersal of high temperature debris from the reactor vessel and possibly from the reactor cavity. The process of hydrodynamically forcing melt out of the reactor vessel due to primary system blowdown is termed High Pressure Melt Ejection. A potential consequence of HPME is direct containment heating (DCH).

DCH is the process of directly heating the containment atmosphere by molten core debris. Potential early failure of a PWR containment due to DCH has been the subject of numerous technical exchange meetings between the NRC, NRC contractors, and the nuclear industry. Discussions have been motivated by the concern that a large fraction of molten core debris exiting a failed reactor vessel following a high-pressure blowdown could be finely fragmented and distributed into the containment atmosphere.

The timing of the postulated containment failure resulting from the above mechanism (i.e., shortly after vessel failure) has potentially important ramifications regarding the radiological source term. Containment functions would be compromised and natural fission product deposition mechanisms would not have sufficient time to significantly reduce the masses of fission products that could be released through the failure location. In addition, the process of high pressure melt ejection has the potential to increase the fission product inventory released to the containment atmosphere.

The objective of this paper is to evaluate, with due concern for realistic uncertainties in the physical processes, whether there is a significant likelihood of containment failure due to HPME for the AP600 design. This evaluation provides best estimate conclusions which will help form the basis for the probabilistic assessment of plant performance for the AP600.

2.0 PHENOMENA

2.1 Description

Direct containment heating is a postulated event of rapid heat transfer between finely fragmented core debris and the containment atmosphere assuming (1) the occurrence of post core-melt reactor pressure vessel failure at a high pressure and (2) the HPME causes extensive debris dispersal. DCH has been hypothesized as a means of early containment failure because the stored energy of the debris, including potential energy release through debris oxidation and hydrogen burning, is enough to cause high containment pressure if a large quantity of the core inventory participates. The extent of pressurization thus depends upon:

- the amount of debris which would be discharged at vessel failure,
- the containment geometry which could be conducive to or an impediment to dispersal beyond the reactor cavity, and
- the fraction of the debris which could be finely fragmented and dispersed into the containment atmosphere.

2.1.1 Controlling Physical Processes

The fundamental issue for DCH is whether a massive dispersion of particulated core debris (tens of tonnes) into the containment atmosphere would be possible. Five steps can be identified which would be necessary for such an outcome.

- First, the reactor vessel must fail at high pressure, and in such a way that a majority of the core debris is ejected from the RPV (e.g., HPME occurs).
- Second, the plant geometry must be such that debris dispersal could occur from the reactor cavity.
- Third, fine fragmentation of debris must occur and be sustained.
- Fourth, the debris particles must remain dispersed in the flow stream and be distributed throughout the containment gas atmosphere.

- Fifth, the particles must remain airborne long enough to transfer energy and react chemically if in contact with steam or oxygen.

As will be discussed, some bounding analyses have considered that hydrogen combustion would occur and contribute a pressure rise which would be in addition to that created by the thermal energy transfer. For this to occur, the atmosphere must be such that hydrogen combustion could be sustained.

Major impediments to these processes are the inherent inability to entrain and finely particulate debris, the number of directional changes which particles must endure, the presence of structure in the flow path, stagnation of the flow at corners or around obstacles, expansion of the flow path into the compartment, and the presence of water in the cavity and in the loop compartment. Each of these is briefly characterized below. Also, the steam partial pressure in the containment would have a significant influence on the likelihood of hydrogen combustion.

It would be difficult to maintain an entrained flow of finely particulated, high density debris. Changes in flow direction, stagnation points, and structure all tend to provide for impaction of the particulate on walls, i.e. de-entrainment. Each change in flow direction tends to separate the heavier debris from the gas stream since the debris would move to the outside of the flow curvature as a result of the large density difference. Only the smaller particles, which could respond to the gas flow more quickly, could avoid separation from the high velocity gas stream. The particulate captured on the structure walls would form a liquid layer or film and would have to be re-entrained to form particulate. In experiments simulating the reactor cavity at Zion Nuclear Plant (which is not necessarily prototypic for the industry) most debris is ejected from the cavity. For these experiments, the materials dispersed in the flow have a wide range of size from 10 micron to several millimeters. Larger sizes result in a very inefficient heat transfer process between the hot debris and the containment gases, as demonstrated by the relevant experiments.

Expansion (deceleration) of the flow and the presence of structure allows for significant de-entrainment and deposition of most particle sizes. As the flow area increases, flow velocities decrease and large particles no longer remain airborne. Also, impaction on structures would

serve to remove particles of all sizes. Only that fraction of the debris which could persist as fine particulate could substantially contribute to direct containment heating.

Water would have substantial mitigating capacity in direct containment heating scenarios. Because of the AP600 design provision to flood the reactor cavity with IRWST water through an operator action, the RPV lower head would be submerged in water in many core melt scenarios. CECO sponsored experiments performed at FAI indicate that failure of the vessel wall would not occur [Henry, et al., 1991]. Hence, the RPV lower head would not be breached and debris would not be discharged to the containment. Obviously, water would have a major influence on these sequences.

For those very low probability sequences with limited water in the reactor cavity which could progress to RPV failure, debris discharged from the vessel breach would undergo dynamic interactions and rapid heat transfer to the water upon contact. Subsequent removal of debris from the cavity would occur simultaneously with removal of the water, and quenching would continue in this multiphase stream. Experiments involving water in the simulated cavities and on the containment floor have consistently verified the efficacy of water as a mitigator.

2.1.2 Relationship to Containment Failure Mechanisms and Modes

Direct containment heating is a postulated mechanism for containment failure immediately after reactor vessel failure. If such a mechanism could occur, the largest potential for the occurrence would be expected during core melt accident scenarios that would maintain a high reactor vessel pressure until the time of vessel failure. Furthermore, vessel failure must occur in such a way that a majority of the core debris would be ejected from the RPV (HPME). The containment failure mechanism would be overpressurization due to a rapid increase in gas temperature as the core debris thermal and chemical energy is transferred to the gas.

2.1.3 Relationship to Source Term

Prior to the core debris slump into the lower plenum which could lead to vessel failure and high pressure melt ejection, fission products such as the noble gases, iodine, cesium and perhaps tellurium would have been released from the fuel matrix and into the primary system. For such conditions, significant quantities would likely be released to the containment through openings in the RPV pressure boundary such as PORV operation or a break in the reactor coolant system (RCS). In addition, the fine particulation of core debris in the reactor cavity, if high pressure melt ejection occurred, could liberate additional fission products to the containment atmosphere. Therefore, any postulated process which would fail the containment shortly after RPV failure would also likely occur when the airborne fission product inventory in containment would be at, or near, the maximum. Hence, the potential release would also be at a maximum. After this point in time, the concentration of airborne fission products would decrease due to natural deposition mechanisms such as sedimentation, impaction, condensation, etc.

2.2 Experiments

Several investigations have been performed and documented which provide a data base for understanding and modeling direct containment heating phenomena. These experiments have been carried out at Argonne National Laboratory, Sandia National Laboratory, Brookhaven National Laboratory and Fauske & Associates, Inc. The tests demonstrate that, given the conditions for a high-pressure melt ejection, DCH can occur, but that containment structures have a first-order influence on the mitigation of the DCH process.

2.2.1 Sandia HIPS Experiments

The Sandia HIPS experiments (High Pressure Melt Streaming) [Tarbell, 1984] were conducted following the SPIT series to confirm the dispersal of debris from a simulated cavity geometry and to assess the phenomena of jet geometry, gas solubility, and aerosol generation [Tarbell, 1986a]. In those tests which have been reported [Tarbell, 1986b and Pilch, 1986], a

1:10 linearly scaled model of the Zion cavity was used. This cavity was either open to the desert or placed within an expansion chamber with one end open to the desert. No attempts were made to maintain the geometric similarity of containment internal structures of Zion for these experiments. Iron-alumina thermite charges with masses of about 176 lb (80 kg) were used. A table of reported tests, presented in Reference [Pilch, 1986] is reproduced here at Table 2-1.

In experiments (HIPS-3C, -7C, and -8C) carbon dioxide was used as the cover gas, at pressures between about 3 MPa (435 psia) and 5.6 MPa (812 psia). Pressures as high as 11.7 MPa (1697 psia) were used in two other tests (HIPS-2C and -4W). In two reported experiments (HIPS-4W and -6W), a water-filled cavity was used, and destroyed by overpressure during the blowdown. As will be discussed later, it is doubtful that the RPV could be failed if the reactor cavity were filled with water. Consequently, these tests are not relevant to the response of the RCS and containment. One experiment (HIPS-8C) featured an annular gap around the thermite generator, simulating the gap around the RPV if the insulation were assumed to be removed. Such tests which ignore the insulation do not represent the response of the RCS and containment and are not used in our assessment.

For all the HIPS tests, dense aerosol clouds surrounded the debris jet, and sweepout from the cavities was nearly complete in all cases, above 95%. After tests in which the cavity was placed inside the confinement room, this debris was found either within the room or on the concrete pad just outside its open end. This test series demonstrated the substantial influence of structures to capture the debris outside of the reactor cavity/instrument tunnel.

In the HIPS-7C tests, over 30 percent of the debris was found in the rear of the confinement chamber, much of it against the rear wall. Observations with high speed films show that debris exiting the cavity splashed off the ceiling and rained down in that location.

Table 2-1
SELECTED HIPS EXPERIMENTS

Test Name	Scale	Thermite Mass		Initial Vessel Pressure		Extent Dispersal (%)	Water In Cavity
		(kg)	(lbm)	(MPa)	(psia)		
SPIT-19	1:20	10.3	22.7	12.6	1827	95	No
HIPS-2C	1:20	80.0	176	11.7	1697	99	No
HIPS-4W	1:10	80.0	176	11.7	1697	~95*	Yes
HIPS-5C	1:10	80.0	176	6.7	972	99	No
HIPS-6W	1:10	80.0	176	3.8	551	~95*	Yes
HIPS-7C	1:10	81.5	179	5.5	798	98	No
HIPS-8C	1:10	80.0	176	3.7	537	98	No

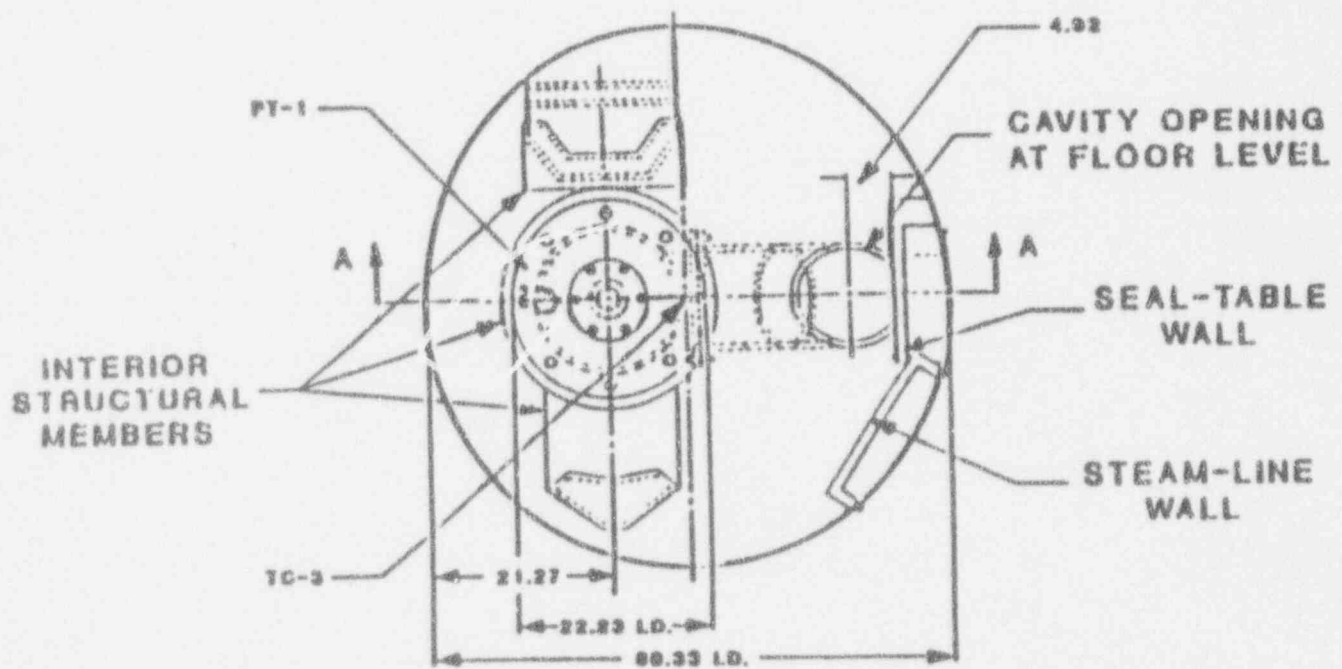
*Cavity destroyed during test.

Over 97 percent of the original melt mass was recovered from the chamber and concrete pad, and the rest either landed on the ground beyond the pad or was in the aerosol cloud which billowed out. Thus, the confinement chamber does not model the containment lower compartment structures. On the other hand, it does illustrate that a minimal representation of the structure results in substantial removal of the debris from the gas stream.

In the HIPS-8C tests, aluminum collection pans were placed on the chamber floor to determine the spatial distribution of debris exiting the cavity, and deduce which fraction exited through the keyway outlet, and which fraction exited through the angular gap around the melt generator. About 25% of the debris was concluded to have been released through this gap, deflected off the ceiling, and fallen into pans around the melt generator. This corresponds to the area fraction taken up by the annular opening assuming the insulation had been removed. As mentioned above, this is not representative for the RCS because the reflective insulation around the reactor vessel was not represented in any manner.

2.2.2 Argonne Wood's Metal Tests

The influence of the containment configuration outside the reactor cavity and instrument tunnel was demonstrated by the isothermal Wood's metal experiments [Spencer, 1983a]. In these tests, the Zion reactor cavity-instrument tunnel configuration was mocked-up along with the seal table and biological shield inside the crane wall (missile barrier). Wood's metal, which has a melting temperature of 73°C (163°F) and a density of about 9500 kg/m³ (593 lbm/ft³), was used to simulate the debris. The experimental configuration is illustrated in Figure 2-1, and the experimental conditions are summarized in Tables 2-2 and 2-3. As shown in these tables, the parameters investigated included various masses of water initially accumulated within the reactor cavity as well as different gas velocities through the cavity following molten metal discharge from the simulated reactor vessel. The results of these experiments are shown in the bar graphs of Figure 2-2, which is taken from Reference [Spencer, 1983a]. The final debris configuration is reported in terms of (1) the material left within the reactor cavity, (2) that which was



NOTE: ALL DIMENSIONS IN CENTIMETERS

Figure 2-1 Plan view of the experimental apparatus for the ANL Wood's metal tests, taken from [Spencer, 1983].

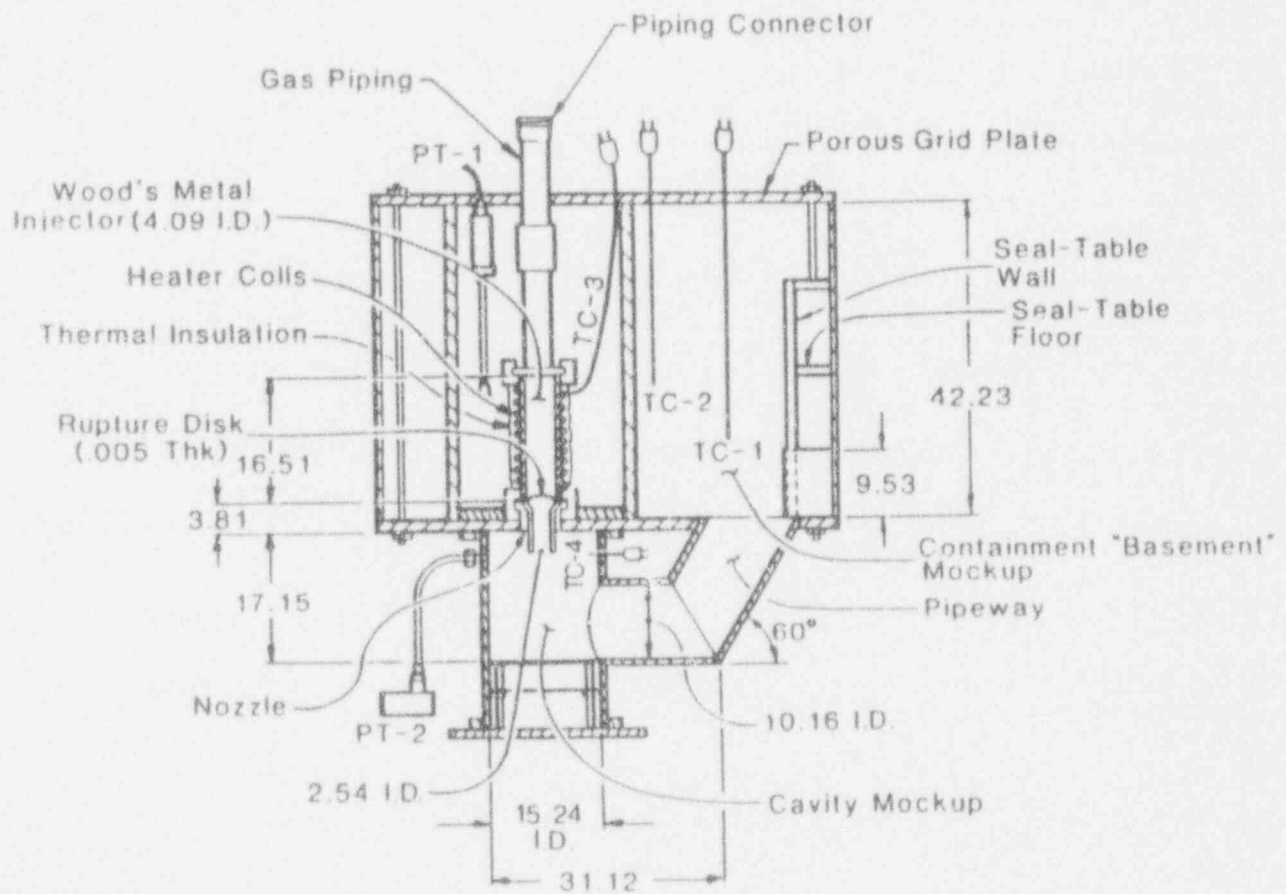


Figure 2-1 (Cont'd) Sectional view of the experimental apparatus for the ANL Wood's metal tests, taken from [Spencer, 1983].

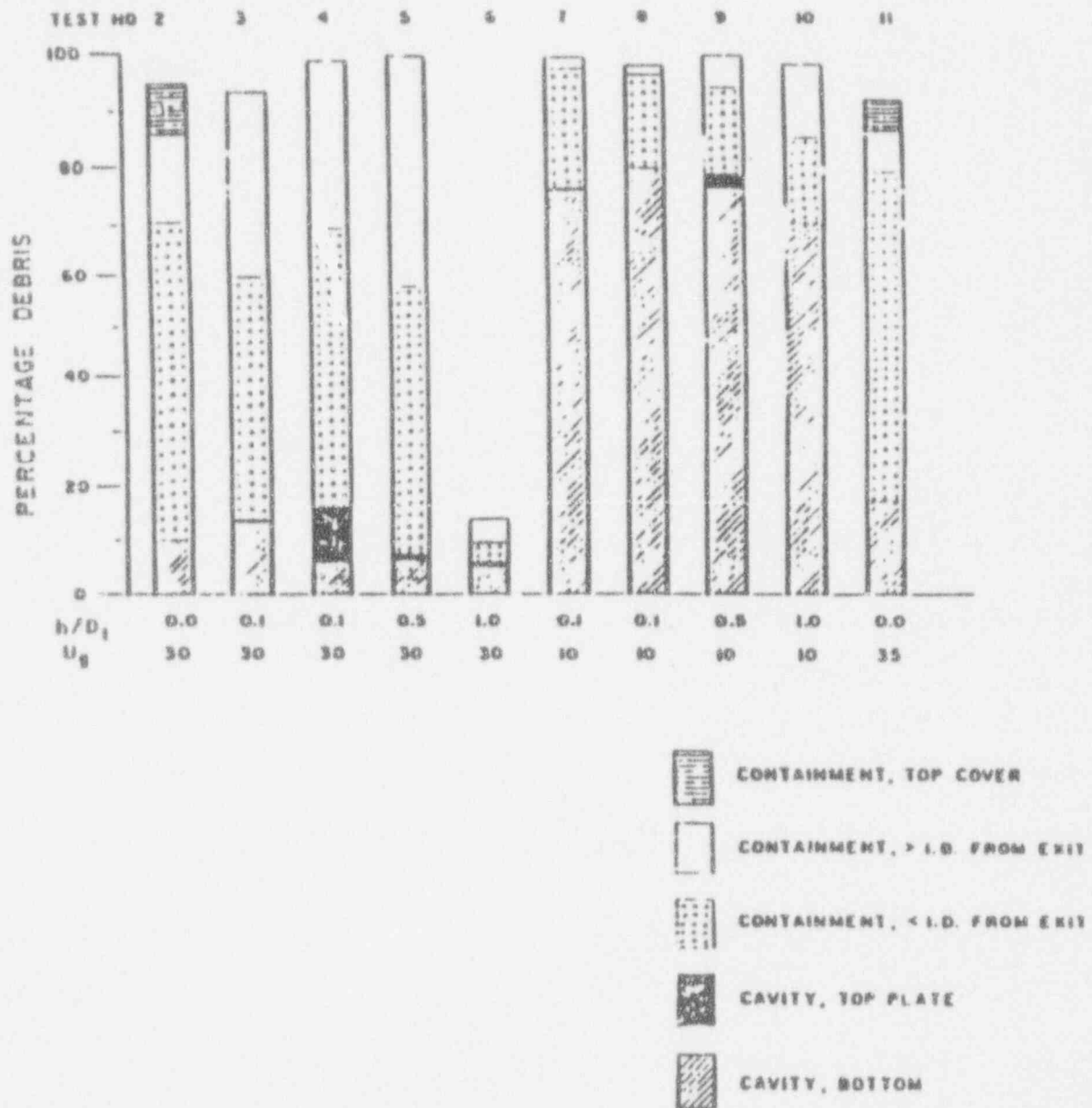


Figure 2-2 Location of simulated core debris dispersal in the ANL Wood's metal experiment, taken from [Spencer, 1983a]. In the legend, U_g - gas velocity m/sec, h/D_t - dimensionless height of water in the reactor cavity.

Table 2-2

SUMMARY OF WOOD'S METAL INJECTION/DISPERSAL TESTS

Test Number (Old Ref.)	1 (17)	2 (18)	3 (19)	4 (20)	5 (21)	6 (22)	7 (24)	8 (25)	9 (26)	10 (27)	11 (28)
Injected Material (1)	Gas Only	WM	WM	WM	WM	WM	WM	WM	WM	WM	WM
Cavity Water Level, h/D _i (2)	0.5	Dry	0.1	0.1	0.3	1.0	0.1	0.1	0.5	1.0	Dry
Injector Temperature, °C/°F	---	89/192.2	91/195.8	75/192.2	89/192.2	90/194	89/192.2	88/190.4	87/188.6	88/190.4	89/192.2
Injection Pressure, MPa/psia	0.65/94.25	0.70/101.5	0.68/98.6	(3)	0.55/79.75	0.68/98.6	0.68/98.6	0.30/43.5	0.25/36.25	0.25/36.25	1.40/203
WM Injection Velocity, m/s/ft/s	7.8/25.57	7.8/25.57	7.8/25.57	7.8/25.57	7.8/25.27	7.8/25.57	7.8/25.57	5.4/17.70	5.4/17.70	5.4/17.70	11.7/17.70
Gas Velocity (4" pipe), m/s/ft/s	28/91.80	29/95.08	27/88.52	28/91.80	27/88.52	29/95.08	9.7/31.80	9.3/30.49	9.3/30.49	9.4/30.82	35/114.75
Maximum Cavity Pressurization, kPa	---	10	35	20	80	190	33 (4)	10	60	120	50

NOTES: (1) WM = Woods Metal ($T_{\text{melt}} = 73^{\circ}\text{C}$).

(2) D_i = pipeway diameter, 10.2 cm.

(3) WM frozen in PT standoff line.

(4) High pressure caused cavity apparatus to rupture at 60° pipe elbow.

Table 2-3

SUMMARY OF CHARACTERISTIC DISPERSAL TIMES

Test Number (Old Reference Number)	1 (17)	2 (18)	3 (19)	4 (20)	5 (21)	6 ⁽⁴⁾ (22)	7 (24)	8 (25)	9 (26)	10 (27)	11 (28)
Emergence of WM at cavity top, ms	(1)	0	0	0	0	0	0	0	0	0	0
WM contacts water/base ms	---	23	26	25	22	13	26	37	26	18	15
Water crater contacts base, ms	6	---	(2)	(2)	32	32	(2)	48	42	45	---
Crater rim grows radially to R _m , ms	---	---	38	36	36	38	32	---	64	---	---
Gas breaks through at WM trailing edge, ms	---	46	47	39	45	45	43	64	61	58	23
Crater rim/splash grows in amplitude to occlude pipeway, ms	10	---	49	41	47	(3)	46	65	63	(3)	30
Start of water slug dispersal, ms	21	---	76	61	68	66	68	93	88	80	---
End of water slug dispersal, ms	48	---	99	83	108	---	87	110	117	117	---
Horizontal water jet at seal table recess, ms	36	---	(6)	101	103	95	97	---	122	124	---
Start of WM dispersal, ms	---	84	(2)	(2)	(2)	~ 90 est	106	150	(2)	(2)	41
End of water dispersal, ms	290	---	~ 200	~ 200	~ 500	---	~ 300	~ 300	~ 1500	~ 1500	---
End of WM dispersal, ms	---	650	950	800	~ 1200	860(5)	~ 300	~ 300	---	---	350

NOTES: (1) Time of gas release by rupture disk breach = 0. ms.

(2) Not discernable.

(3) Water occludes pipeway as an initial condition.

(4) Bend in pipeway failed at 104 ms while water slug ejection was still in progress.

(5) Dispersal took place out horizontal pipeway stub only.

(6) Upper camera did not function.

dispersed within one equivalent diameter of the instrument tunnel exit, and (3) that fraction of debris dispersed beyond one equivalent diameter of the instrument tunnel. High speed movies showed that a large fraction of the debris is initially transported as a large wave moving along the outer sloping surface of the instrument tunnel which impacts upon the bottom surface of the seal table. The results demonstrate that the structure in the lower compartment is very effective in separating the debris from the high velocity gas stream and depositing the debris on the containment floor in close proximity to the instrument tunnel. More specifically, the structure has a first order effect on the debris distribution in the simulated containment.

2.2.3 Argonne CWTI Experiments

EPRI sponsored a series of reactor material experiments at Argonne National Laboratory known as the CWTI tests (Corium/Water Thermal Interaction [Spencer, et al., 1983b, Spencer, et al., 1987 and Spencer, et al., 1988]). The experimental configuration represented some major features of the Zion reactor lower containment compartment cavity, and the upper compartment at a 1:30 linear scale. Reactor materials (principally UO_2 and stainless steel) were used and were created by an exothermic thermite reaction. Molten debris was injected downward into a simulated cavity and keyway, see Figure 2-3, which was connected to an expansion volume that was partitioned like the lower and upper compartments of a containment. In some tests, water was present either in the cavity or the expansion volume or both. The objectives of these tests were to examine heat transfer between core debris and water, sweepout of water and core debris from the cavity, steam generation, hydrogen generation, and to characterize the spatial distribution of dispersed debris.

The test apparatus included the thermite reaction vessel (which is the source of the molten core debris), an interaction vessel (which represents the reactor cavity), a pipe simulating the instrument tunnel, an expansion vessel representing the containment, a "trap" above the pipe discharge to simulate a seal table and a baffle plate to separate the expansion vessel into upper and lower compartments. It is noted that the geometric similarity of the simulated cavity was

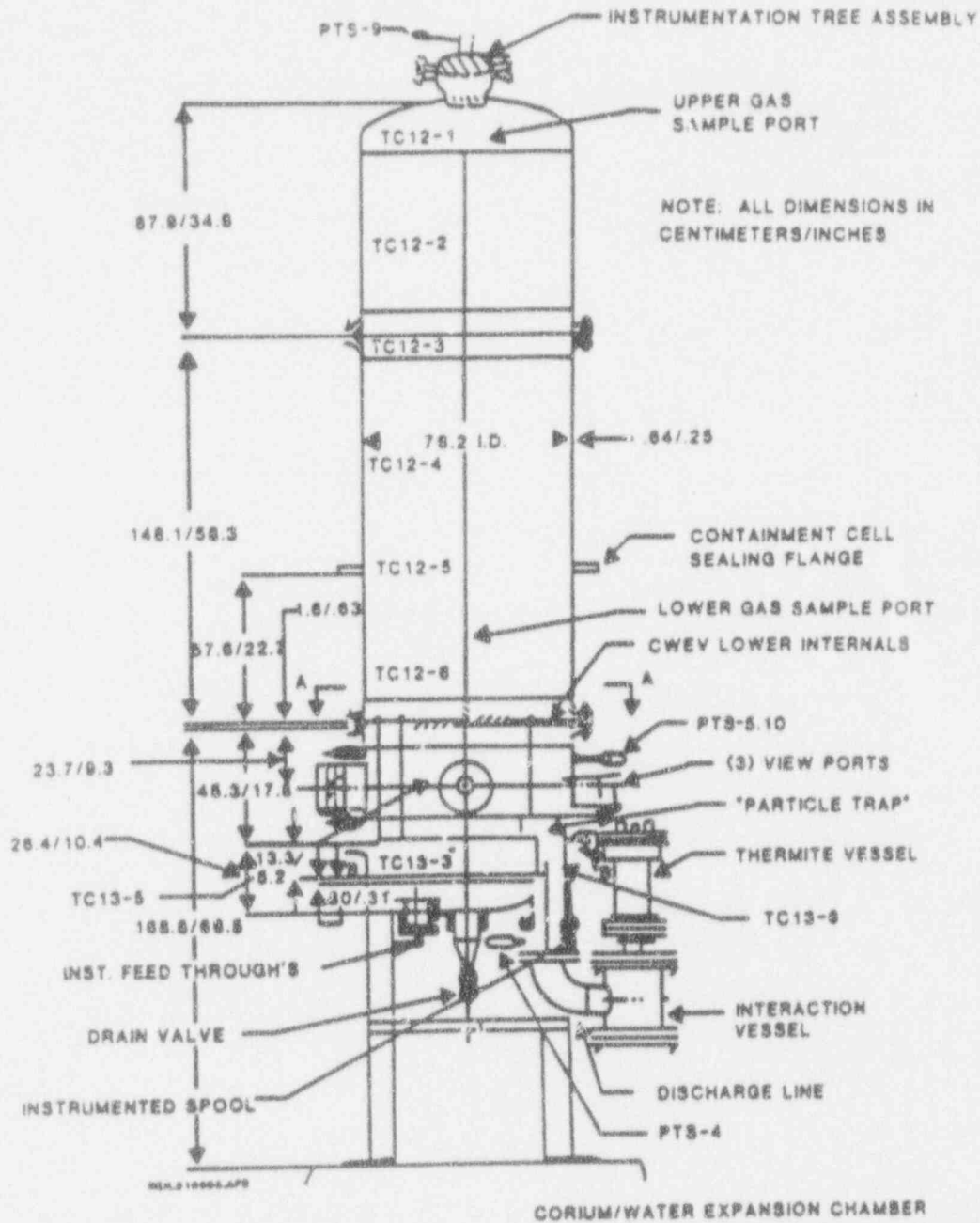


Figure 2-3 ANL thermite apparatus for the CWTI tests, taken from [Spencer, 1987].

somewhat distorted (from the Zion cavity design) because of the use of a 90°-bend circular pipe as a keyway instead of a 64°-bend rectangular duct. The simulated core debris produced by the thermite reaction was composed of 60% UO_2 , 16% ZrO_2 , 24% stainless steel (67% Fe, 21% Cr, 12% Ni) and had a temperature of about 3100 K (5120°F).

Tests were performed with low (less than 0.5 MPa or 75 psia) and high (~ 5 MPa or 725 psia) pressure blowdowns as well as with inert and oxidizing atmospheres. Several different initial water level conditions were tested in the interaction vessel ranging from completely empty to essentially full of water before the melt was released from the thermite furnace. Initial conditions and results for DCH-related CWTI tests are listed in Table 2-4 (adapted from [Spencer, 1988]). The corium masses used in the CWTI tests corresponded to a range of about 36%-60% of the corium inventory for Zion.

The DCH-related tests were conducted by starting thermite reaction at nominally atmospheric pressure. The melt was subsequently pressurized (by gas from external high pressure gas cylinders) to burst a bottom diaphragm and initiate melt ejection. The duration of the gas blowdown was sufficiently long to assure sweepout of all available melt. Debris that was not swept out remained as a 1 ~ 3 mm thick crust uniformly deposited on the wall of the interaction vessel and the entire pipe surface (for CWTI-5 and -6).

Various mass fractions of debris were observed to be dispersed from the reactor cavity into the simulated containment volume. Debris was collected at various locations in the apparatus including (1) the interaction vessel and pipe, (2) the "particle trap reflector" at the top of the pipeway as it exited into the bottom of the expansion vessel, (3) on the floor of the simulated containment, and (4) on the top of the simulated lower compartment which represented the operating deck. Characteristic particle sizes for the swept out into the air atmosphere ranged from 64 to 700 microns for tests CWTI-11 and -13, which had no water in the cavity. Most particles were in the range 100 ~ 300 microns [Spencer, 1988]. The experiments with water in the interaction vessel or expansion volume prior to melt ejection demonstrated the

Table 2-4

ANL CWTI DCH-RELATED EXPERIMENTS¹

Test No.	5	6	11	12	13
Driving Pressure, MPa/psia	5.0/725	4.7/681.5	5.1/739.5	2.8/406	4.0/580
Atmosphere	AR	AR	air	air	air
Corium Mass Injected, kg/lbm	3.94/8.67	3.75/8.25	2.93/6.45	2.69/5.92	2.27/4.99
Corium Mass Swept Out, kg/lbm	2.44/5.37	1.21/2.66	0.88/1.94	1.31/2.77	0.20/.44
Corium Mass Remained, kg/lbm	1.5/3.3	2.54/5.59	2.05/4.51	1.38/3.04	2.07/4.55
Water in Cavity, kg/lbm	5.6/12.32	dry	dry	4.6/10.12	dry
Dispersal Impediments	s/b ²	s/b	s/b	none	none
Atmosphere Initial Temp, K/°F	419/294.2	408/274.4	411/279.8	422/299.6	298/76.4
Atmosphere Peak Temp, K/°F	417/290.6	461/369.8	435/323	407/272.6	621/657.8
Atmosphere Initial pressure, MPa/psia	0.52/75.4	0.22/31.9	0.22/31.9	0.37/53.65	0.32/46.4
DCH Efficiency ³ , %	0	5	1	0	62

¹3.33% linear scale model of Zion.²s/b = shroud/baffle.

$$^3 \text{ DCH Efficiency} = \frac{\text{Measured Atm. Heatup}}{\text{Max. Equilibration Atm. Heatup}} \times 100.$$

effectiveness of water for removing heat from dispersed debris, including the energy released due to oxidation. These tests exhibited little or no direct containment heating. Results for test CWTI-12 show no significant contribution to DCH with the co-dispersal of debris and water into the containment atmosphere. Test CWTI-12 was performed without the presence of the impeding structure and clearly demonstrates the influence of co-dispersed water. Modest direct containment heating was observed in tests CWTI-6 and -11 which had water only in the pan of the expansion vessel (containment floor). The largest atmospheric heating occurred in test CWTI-13 where no structures and no water were present in either the interaction vessel (cavity) or expansion vessel (containment). This heatup was caused by a sweepout mass of only 0.2 kg. Hydrogen generation and/or oxygen depletion that occurred during these tests were also measured to determine the extent of oxidation and its contribution to the overall energy input to the system.

The most important observation from the ANL experiments concerns the influence of structure on debris dispersal. The "particle reflector" in this experiment was a simulation of the in-core instrument tube seal table configuration in a Zion-like containment. The horizontal baffle plate above the "particle reflector" represented the floor separating the Zion containment into upper and lower compartments. Comparison of results from CWTI Tests 6, 11, and 13 reveals the effect of structure on direct containment heating. All three of these tests were performed with a dry interaction vessel (reactor cavity), but Tests 6 and 11 included structure in the expansion vessel (containment) while test 13 had no structure. The DCH efficiencies (whose definition is given in Table 2-4 and calculated in [Spencer, 1988]) for Tests 6 and 11 were 5% and 1%, while the DCH efficiency for Test 13 was reported at 62%. Thus, the substantial effect of the seal table structure was to prevent a significant fraction of the debris from entering the containment atmosphere directly. Because of the structure, a major fraction of the entrained debris was deposited on the lower containment floor.

2.2.4 SNL-DCH (Surtsey) Experiments

Sandia has also conducted a series of experiments designated as Surtsey [Tarbell, 1987a; Tarbell, 1987b; Tarbell, 1988a; Tarbell, 1988b; Allen, 1991]. Experiments DCH-1, 2, 3 and

4 used cavity configurations similar to those of the HIPS 1:10 linear-scale Zion mockups. These cavities have been completely enclosed in a large expansion vessel, i.e., 3637 cubic feet (103 m³) capacity and a 145 psia (1.0 MPa) design pressure. No attempts were made to represent the geometry of the Zion containment internal structures such as the seal table, the lower compartment, the operating deck, etc. Four tests have been performed, and results have been presented in detailed reports [Tarbell, 1987; Tarbell, 1988a; Allen, 1991].

DCH-1 involved 44 lb (20 kg) of molten iron-alumina thermite injected into a 1:10 linear scale model of the Zion cavity only, with a nonprototypic exit guide box added to the instrument tunnel exit to direct debris vertically upward along the centerline of the vessel. Figure 2-4 illustrates the Surtsey facility. The thermite was propelled with nitrogen gas initially at 2.55 MPa (370 psia). Peak pressures ranged from 0.09 MPa (13 psia) to 0.13 MPa (18.9 psia) and were achieved less than one second after debris dispersal. High speed film shows that debris shooting upward at 40 m/s (131 ft/s) expanded laterally and filled the entire chamber cross-section within a few meters of the cavity exit.

About 11.6 kg (25.5 lb) were dispersed from the cavity, which includes the correction for estimated oxidation. Melt retained within the cavity and chute was in the form of a thin crust, and a 1.2 kg (2.64 lb) mass was found at the base of the keyway inclination. Aerosol measurements indicated that much material was fragmented to a size under 10 microns, but the measurements may be inaccurate and a large uncertainty is present in the actual amount of such material. The calculated range of aerosolized debris was 5 to 25 percent of the dispersed mass. Mechanical sieving of debris collected in the chamber showed a log-normal size distribution with a mass mean size of 0.55 mm. Thus the bulk of the debris ejected from the cavity was of millimeter size. This test was analyzed using the methodology described in [Henry, 1989] and good agreement was obtained when the specific configuration without structure was considered.

DCH-2 involved 80 kg (176 lb) of molten iron-alumina thermite injected into a 1:10 linear scale model of the Zion cavity and instrument tunnel only, with a nonprototypic exit guide box added to the exit to direct debris vertically upward along the centerline of the vessel. The

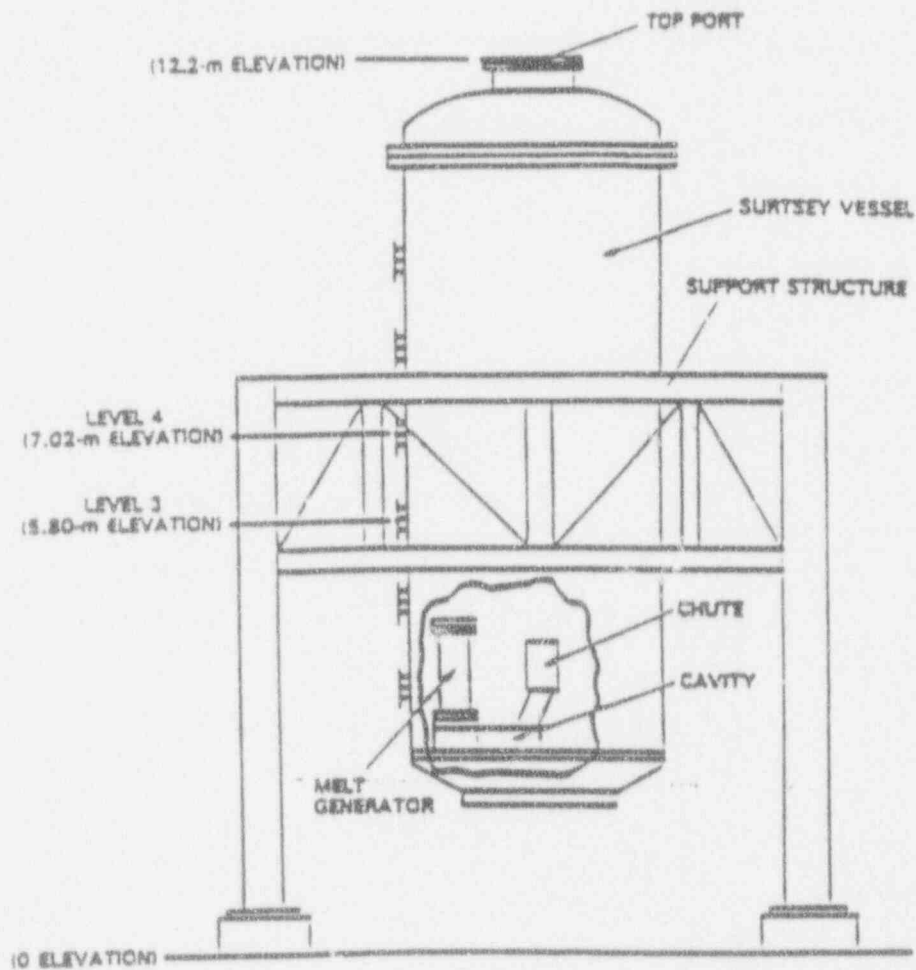


Figure 2-4 Schematic of the Surtsey Direct Heating Test Facility, taken from [Marx, 1989]. The apparatus used in both the DCH-2 and DCH-3 experiments is shown.

thermite was propelled with nitrogen gas initially at 982 psia (6.77 MPa) and peak pressures ranged from 0.22 MPa (32 psia) to 0.31 MPa (45 psia), and were achieved less than one second after debris dispersal. High speed film shows that debris leaving the guide box expanded laterally and filled the entire chamber cross-section within a fraction of a second, likely indicating that the debris-gas two-phase mixture was "choked" at the exit of the guide box.

The total mass recovered from the test chamber, cavity, and melt generator was about 99.5 kg (219 lb), which represents an increase in mass of 24%. This attributed to several potential sources related to the construction of the apparatus and test conduct as well as oxygen uptake by oxidation of the iron in the thermite. The latter source was considered to be the most dominant mechanism. About 91.3 kg (201 lb) were dispersed from the cavity. Five types of debris were identified, with each type being generally associated with a particular area of the apparatus. On the upper third of the vessel in line with the cavity exit, 1-2 mm thick sheets of brittle debris were tightly bonded to the wall. Debris stuck to lower portions of the vessel wall was loosely bonded and formed sheets of 2-4 mm thickness. On horizontal surfaces, debris was found to be approximately 1 - mm diameter spheres, and agglomerations of such spheres with irregularly-shaped masses of previously molten debris. Melt retained within the cavity and chute was in the form of a thin crust, and a 4.4 lb (2 kg) mass was found directly underneath the melt generator. This test was also analyzed using the methodology described in Appendix A [Henry, 1989] and found to be consistent with the proposed methodology considering the simplified geometry used in the experiment.

DCH-3 and DCH-4 recently have been fully reported [Allen, 1991]. The overall results are summarized in Table 2-5 [Tarbell, 1987a]. Test DCH-1 as reported in [Tarbell, 1987b], had the largest efficiency of energy transfer from the debris to the atmosphere with > 90%, while the DCH-4 test was lowest with nominally 35%. The latter was affected strongly by the absence of chemical energy release because of the lack of oxygen in the chamber atmosphere. For consumption of oxygen in the chamber, the degree of oxidation in the DCH-1 test was the greatest, while the DCH-3 debris was the least oxidized. As discussed previously, the

Table 2-5

SNL-DCH EXPERIMENTS^{1,2}

Test	Driving Pressure MPa/psia	Driving Gas	Thermite Mass (kg/lbm)			Atmosphere	
			Initial	Swept-Out	Remained	Peak Temp °C/°F	Peak Press MPa/psia
DCH-1	2.4/348	N ₂	20/44	~ 10/22	~ 10/22	260/500	0.18/26.1
DCH-2	6.8/986	N ₂	80/176	~ 76/167.2	~ 4/8.8	880/1616	0.33/47.9
DCH-3	6.0/870	N ₂	80/176	~ 75/165	~ 5/11.0	860/1580	0.28/40.6
DCH-4 ³	6.9/1000.5	N ₂	80/176	~ 74/162.8	~ 6/13.2	860/1580	0.27/39.2

¹10% linear scale model of Zion cavity only, no representation of the containment structures outside of the reactor cavity/instrument tunnel.

²Dry cavity and containment.

³Inert atmosphere.

methodology presented in Appendix A [Henry, 1989] constitutes part of this paper assessment. Table 2-6 compares the methodology with the SNL DCH tests. There is good agreement with the measured results when the simplified geometry of the experiments is considered. Therefore, the difference between the SNL experiments and the evaluation of the reactor system is dominated by the absence of structure and not by the experimental scale, the materials used, or the driving medium (nitrogen or steam).

2.2.5 BNL Simulant Fluid Test

Brookhaven National Laboratory has performed a series of simulant fluid tests to investigate the extent of entrainment in the reactor cavity and the influence of reactor cavity geometry [Tutu, 1988]. Scaled (1/42) models were constructed of the Zion, Surry and Watts Bar reactor cavity and instrument tunnel configurations. Of particular note for this application is that models of the Zion containment [Ginsberg, 1988] "suggest that the structures exert a strong influence on the flow which issues from the cavity, redirecting the flow and, very likely, changing its droplet size characteristics." These observations clearly point to the inclusion of containment structures in both experimental studies and probabilistic risk studies.

2.2.6 IDCOR/FAI Wood's Metal Tests

During the IDCOR Program, a set of "building block" experiments were performed with the single purpose of demonstrating the extensive influence of structures in the lower compartment. These 1% linear scale models began with the reactor cavity and instrument tunnel, added the seal table, expanded this to a two-dimensional representation of the lower

Table 2-6

MODEL COMPARISONS FOR DCH TEST

Test Parameters/ Predictions Measurements	DCH-1	DCH-2	DCH-3	DCH-4
1. Geometrical Parameters and Vessel Pressure				
A_v (m^2/ft^2)	0.002/0.21	0.002/0.21	0.002/0.21	0.002/0.21
A_h (m^2/ft^2)	0.5/5.37	0.5/5.37	0.5/5.37	0.5/5.37
L_v (m/ft)	2.8/9.18	2.3/9.18	2.8/9.18	2.8/9.18
L (m/ft)	1.45/4.75	1.45/4.75	1.45/4.75	1.45/4.75
A_c (m^2/ft^2)	0.06/645	0.06/645	0.06/645	0.06/645
P_c (MPa/psia)	2.5/362.5	6.0/870	6.0/870	6.9/1000.5
2. Debris Size				
Predicted ($\mu m/ft$)	240/00079	65/00021	40/00013	30/000094
Measured Mass Mean ($\mu m/ft$)	550/0018	Not Available	Not Available	Not Available
3. Mass Dispersed as Fine Particulates				
Predicted (kg/lbm)	20/44	27/59.4	31/68.2	33/72.6
Measured (kg/lbm)	11.6/25.52	33/72.6 [Mass Deposited on] [the Lower Head]	18.4/40.48 [Mass deposited on] [the Lower Head]	30/66 [Mass deposited on] [the Lower Head]
4. Peak Temperature				
Predicted	681/765.8 [Using Measured] [Mass Dispersed]	1032/1397.6	1104/1527.2	1138/1588.4
Measured (K/°F)	501/441.0	~1150/1610	1193/1687.4	1193/1687.4
5. Peak Pressure				
Predicted (MPa/psi)	0.19/27.55 [Using Measured] [Mass Dispersed]	0.30/43.5	0.32/46.4	0.33/47.85
Measured (MPa/psia)	0.18/26.1	0.33/47.85	0.28/40.6	0.27/39.15

compartment and completed the test series with a three-dimensional representation of the lower compartment. The same driving pressure of nitrogen gas (2 MPa/300 psia) mass of Wood's metal (0.3 kg/10.66 lbm) was used in all tests and the principal measurement was the fraction of the Wood's metal retained in the test section. Figures 2-5a through 2-5e illustrate the various test sections used to sequentially add the influential structure. Table 2-7 lists the Wood's metal retained in the test apparatus and shows that, with only the seal table, virtually no material remains; yet with the 3-D lower compartment essentially all of the simulated core material remains in the lower compartment, most of it close to the instrument tunnel. (If we assume that the debris which is not retained in the lower compartment could cause direct heating, these results suggest the process would have an efficiency of only about 2.5%). The observations with respect to structures agree completely with those from the ANL Wood's metal experiments and clearly show the first order influence of structure. Hence, experiments used to represent the reactors response must include the structures (geometry) of the containment lower compartment.

2.2.7 FAI-DCH Experiments

A jointly funded Commonwealth Edison and Fauske & Associates, Inc. experimental program was established and carried out at Fauske & Associates, Inc. [FAI, 1990a]. The program addressed the issue of direct containment heating in support of the Zion IPE. In keeping with lessons learned from smaller scaled tests, these experiments were conceived and designed to have a 5% linear scale simulation of the reactor cavity, instrument tunnel, lower compartment (including two steam generators, two reactor coolant pumps and the refueling canal wall) and upper compartment of the Zion containment building. Figures 2-6 and 2-7 show the experimental apparatus and Figure 2-8 describes how the experiment represents the reactor containment. Iron-aluminum thermite was used to simulate the molten core material, with the 20 kg (44 lbm) thermite mass representing about twice the scaled debris mass and energy content. This was done to compensate for the greater propensity of freezing on the reactor cavity walls in small scale experiments. The experiments can also be viewed as a study of the effect of lower containment structures on the dispersal of iron-aluminum debris when compared with SNL-DCH tests, which also used iron-aluminum as a core material simulant, but had no

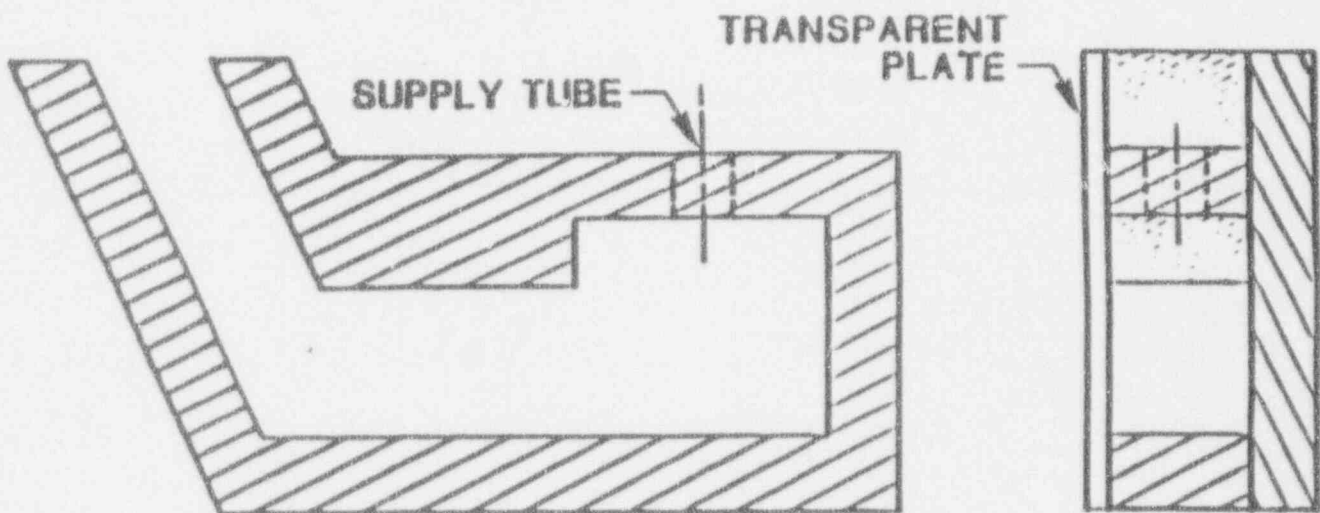


Figure 2-5a 1% linear scale building block experiments/reactor cavity.

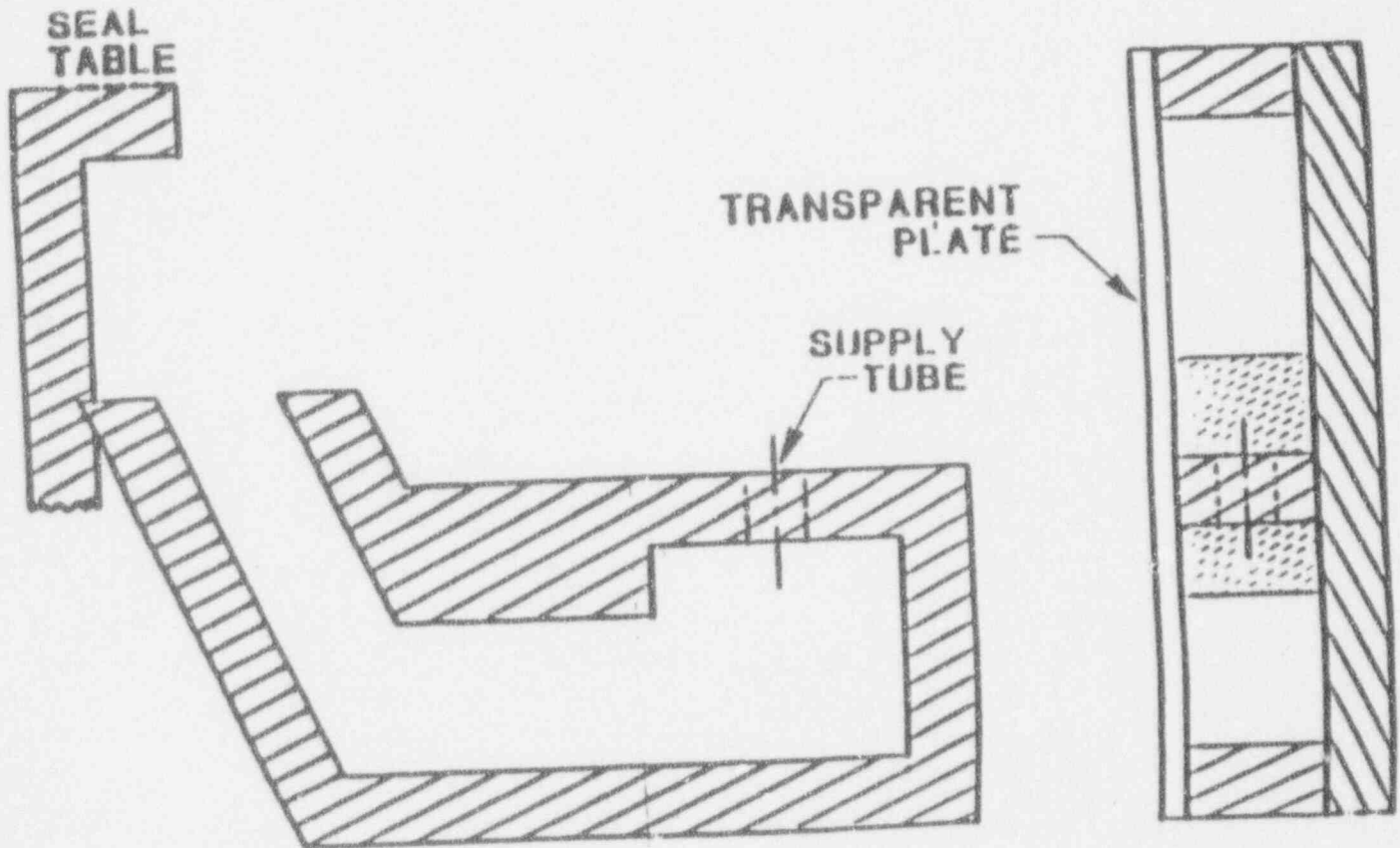


Figure 2-5b 1% linear scale building block experiments/reactor cavity and seal table.

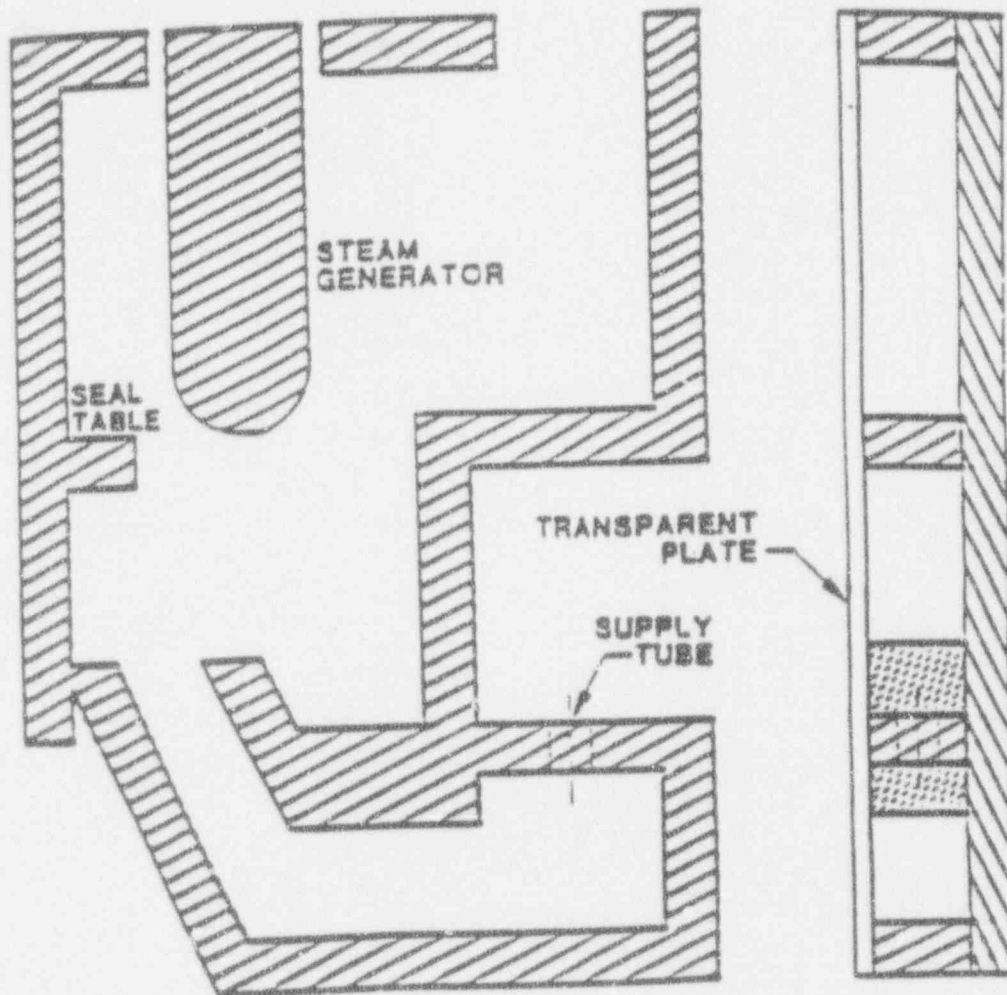


Figure 2-5c 1% linear scale building block experiments/2D representation of the lower compartment.

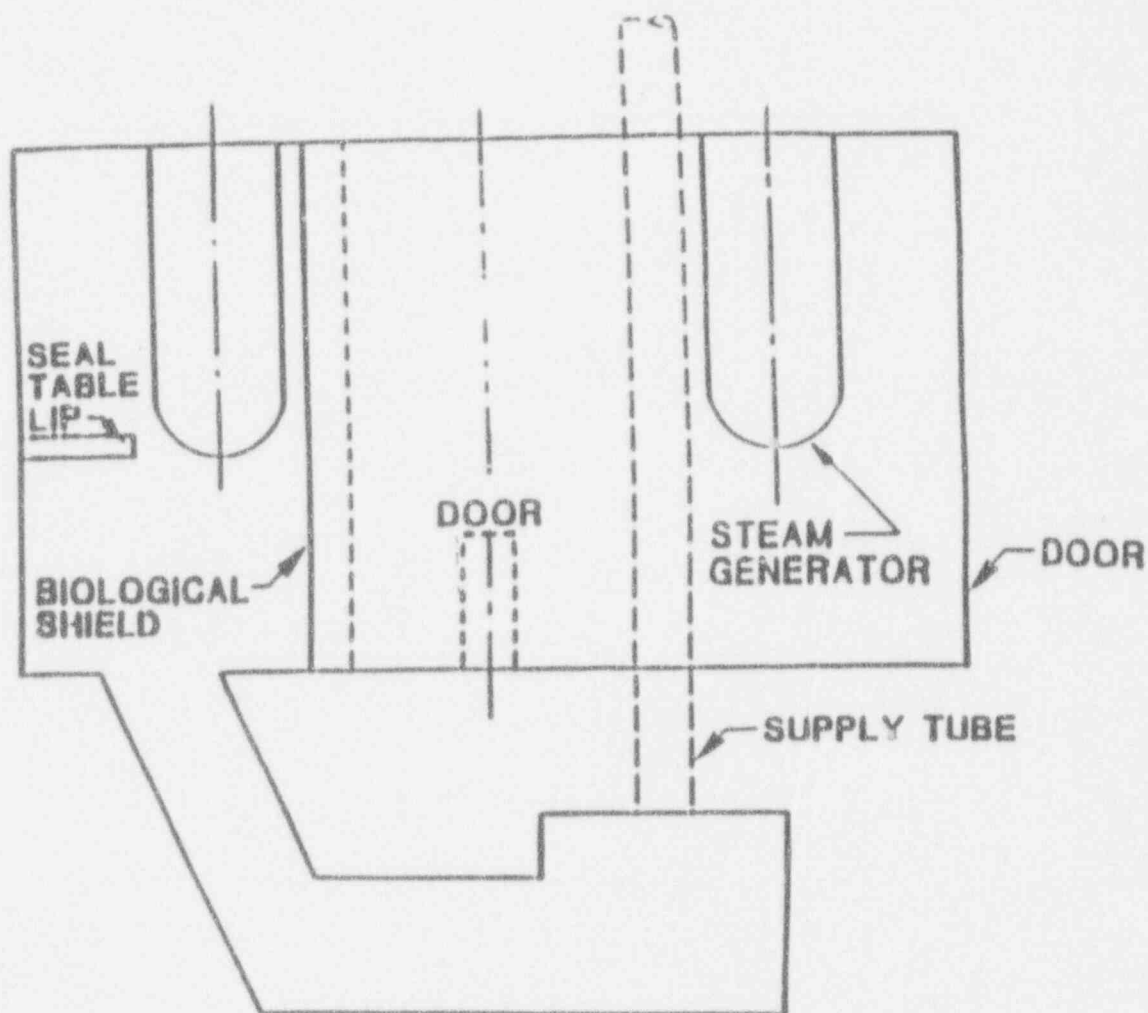


Figure 2-5d 1% linear scale building block experiments/elevation view of 3D lower compartment.

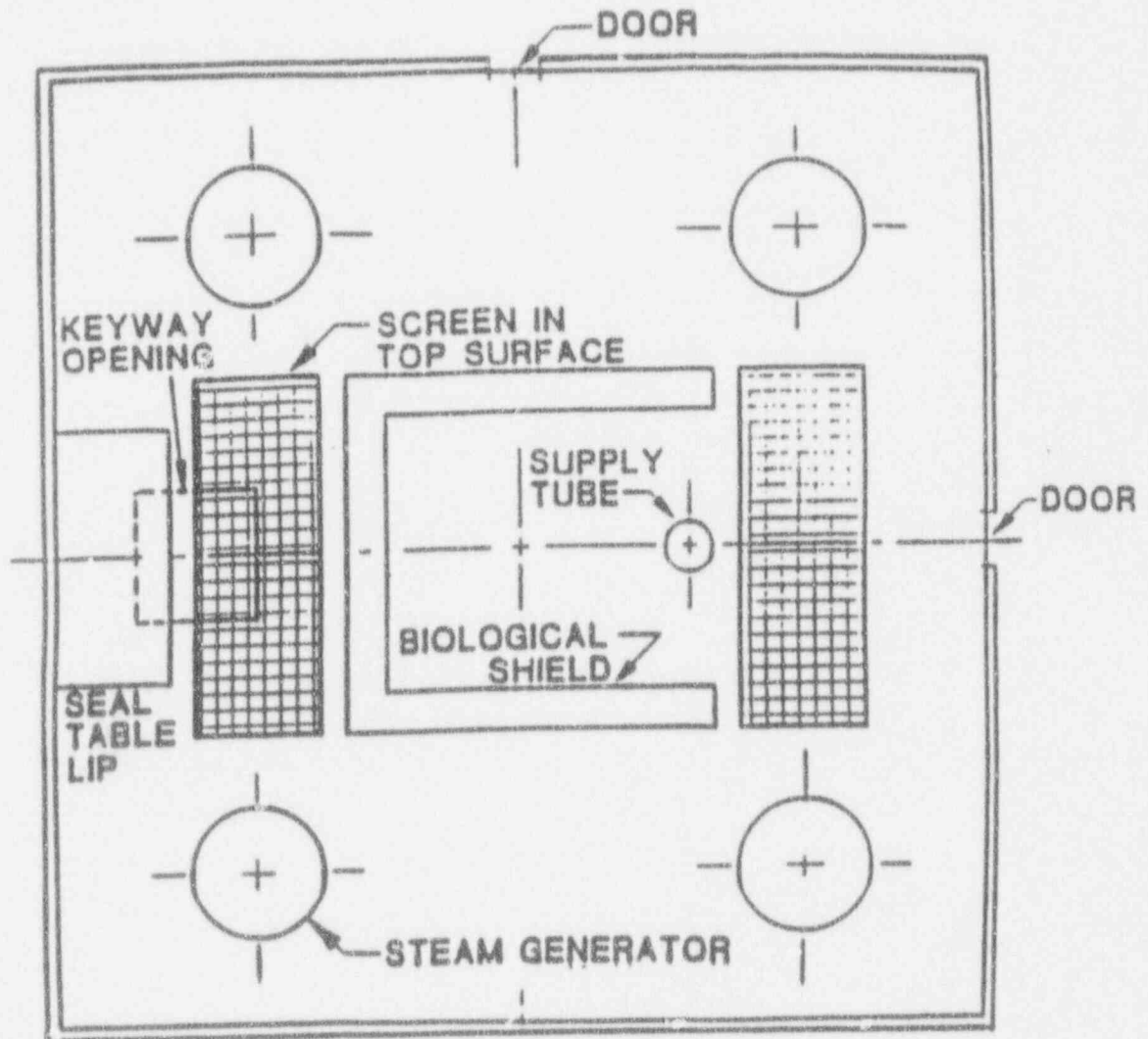


Figure 2-5e 1% linear scale building block experiments/plan view of 3D lower compartment.

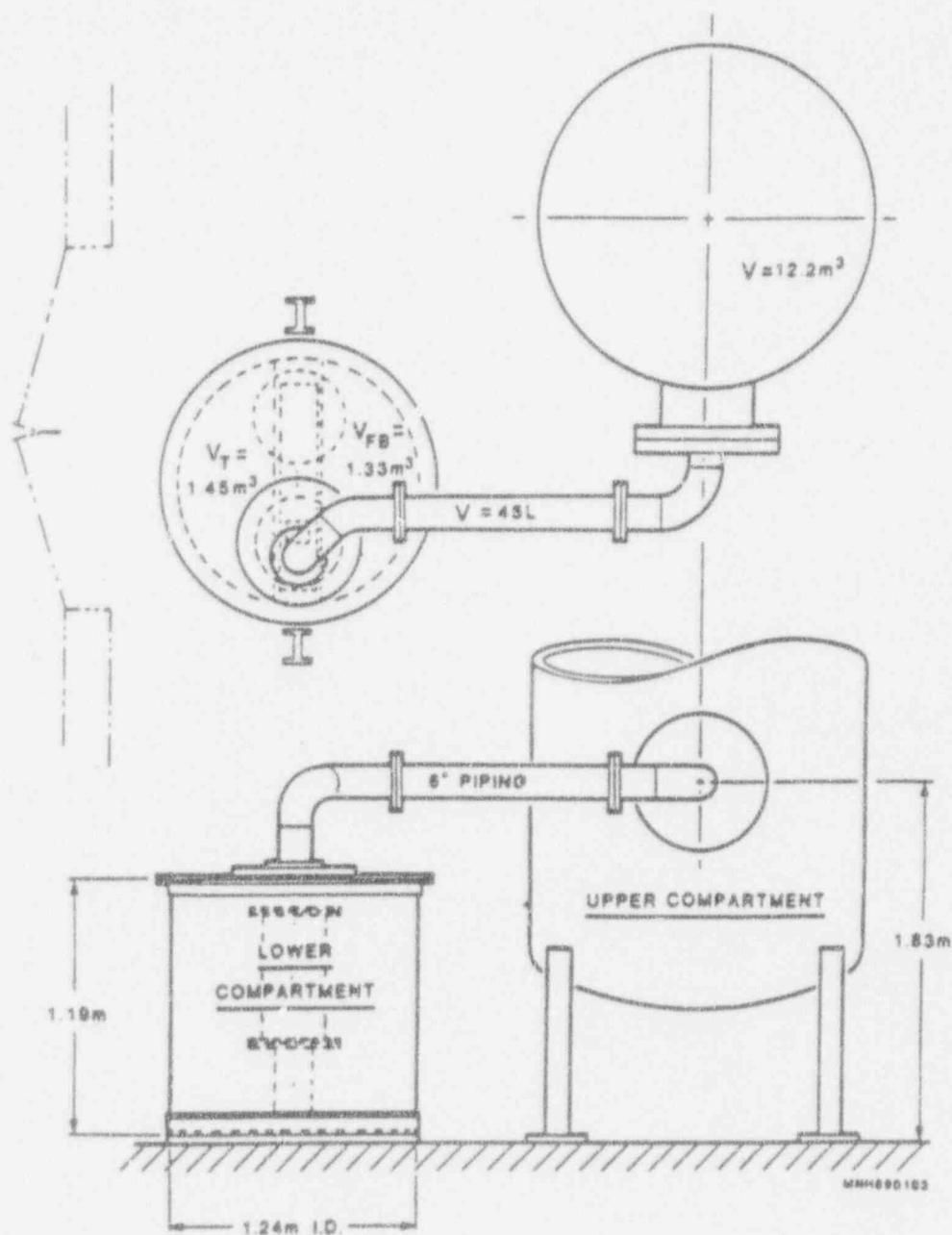


Figure 2-6 Elevation view of the vessel interconnection to simulate the containment configuration.

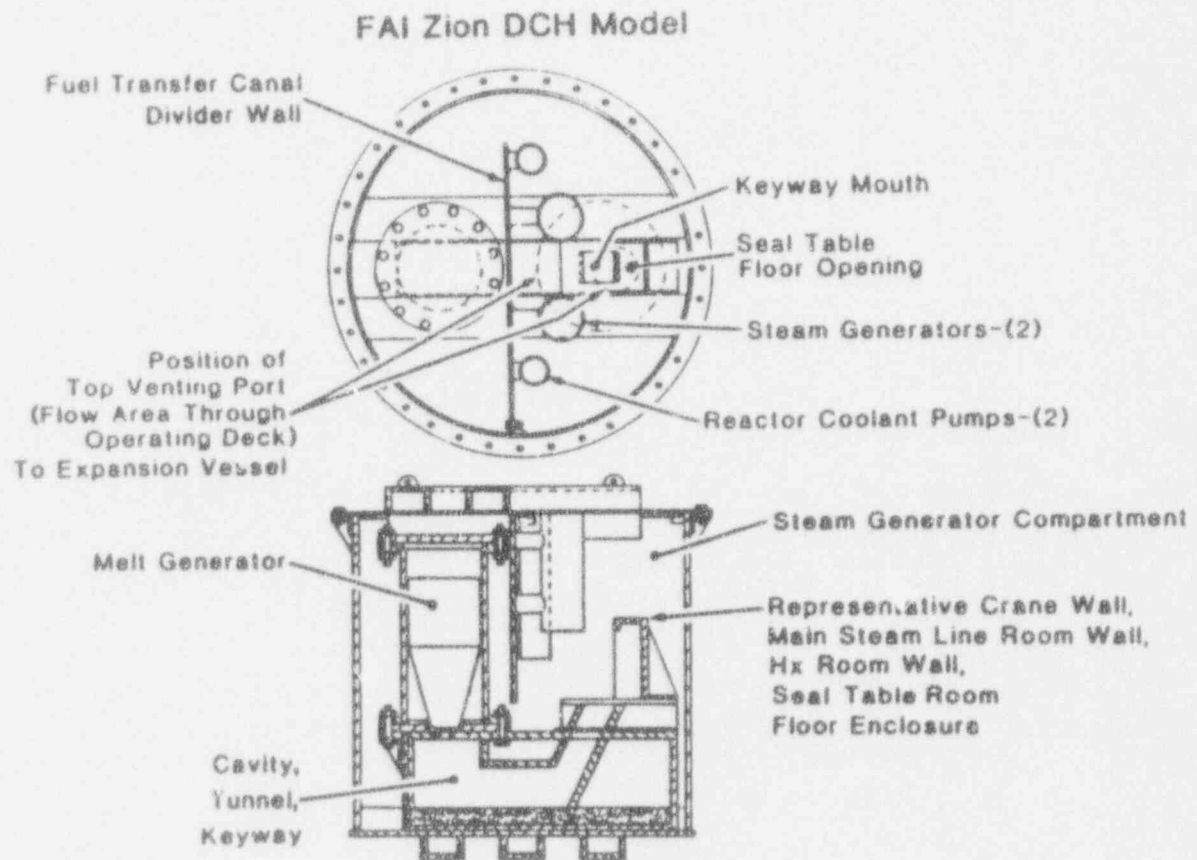


Figure 2-7 Cross-section of the melt generator, reactor cavity, instrument tunnel and the simulated lower compartment with structures.

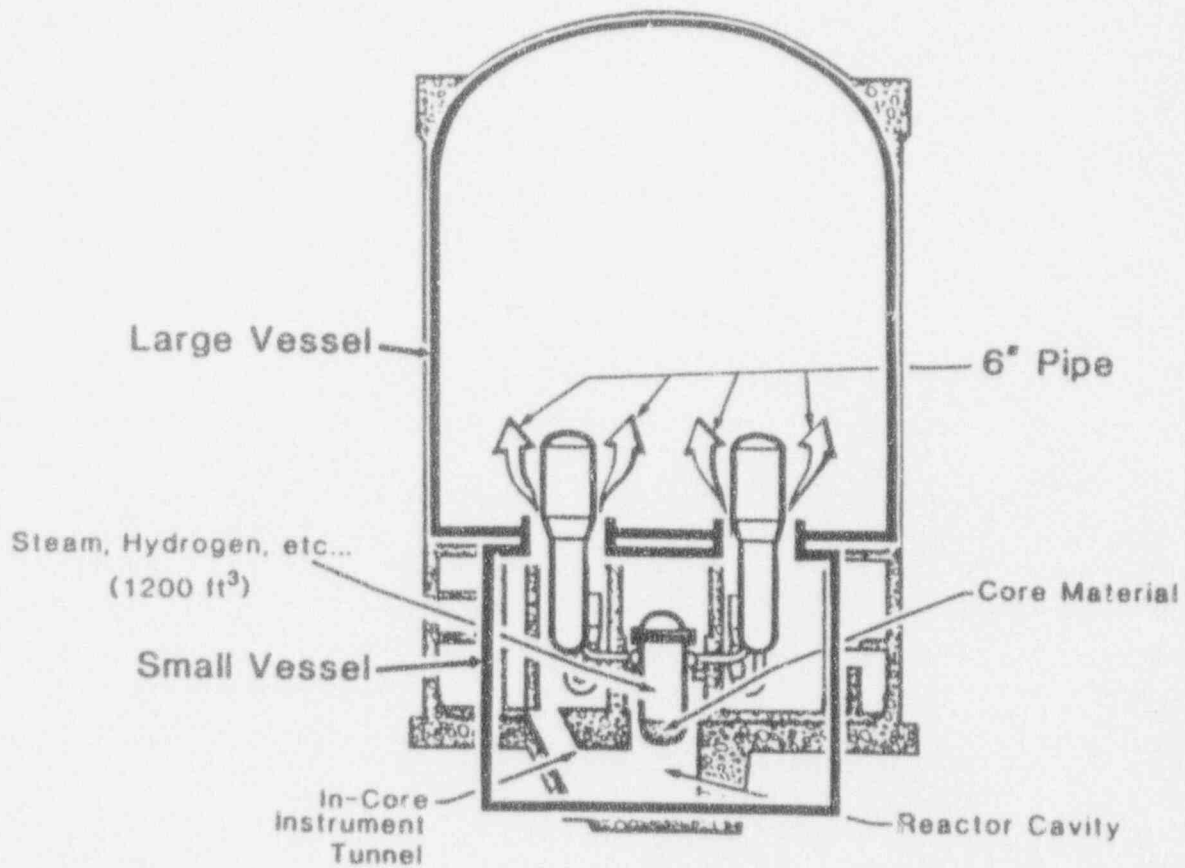


Figure 2-8 Relationship of the test configuration to the Zion containment buildings.

Table 2-7

ZION CAVITY BUILDING BLOCK

	Percent of Debris Retained in the Test Section
Reactor Cavity and Seal Table	6.07
2D Lower Compartment	48.0
2D Lower Compartment Within Reduction Flow Area to the Upper Compartment	76.6
3D Lower Compartment	97.4

containment internal structures. This work represents the most complete geometric similarity of the cavity and containment internal structures for the scaled DCH experiments performed to date.

The experimental matrix included four tests, all with 20 kg of thermite, three driven by nitrogen and one by steam. Water was available on the containment floor in all tests and was also available, to different extents, in the various tests; two having about 1 cm ($\sim 1/2$ ") of water on the cavity floor, one test had 8 cm (~ 3 in) and the other was performed with a dry reactor cavity. Steam was used to test apparatus to pressure the RCS with steam after the thermite reaction was initiated. Table 2-8 presents the test conditions for the experimental matrix.

Table 2-8 also summarizes the test results and clearly demonstrates that (1) the tests are very similar in their response and (2) caused very little pressurization in the upper containment compartment. Measurements of the containment pressurization showed very little, if any, contribution to direct heating even though 90% of the material was dispersed. Pressurization in the reactor cavity and instrument tunnel, as well as the lower compartment, was essentially due to debris-water thermal interactions in the reactor cavity, the flowdown of the melt generator and steam generated in the debris quenching process on the lower compartment floor. The measured peak temperatures of the lower compartment atmosphere were mostly the results of rapid steam generation due to quenching followed by slow heating of the gas due to debris frozen on structures. This latter energy transfer did not contribute to the pressurization because of the cooling provided by other heat sinks.

Maximum local DCH efficiency of about 2%, based on the peak pressure, was measured in FAI-DCH-1 where only a limited water mass was present in the reactor cavity before the blowdown. This is an upper-bound estimate of DCH efficiency because the steam partial pressure was conservatively estimated (underestimated). The temperature increase in the lower compartment was about 5-6 times as high as in the upper compartment but was dominated by the rapid steam generation since the measured peak temperature was only slightly superheated.

WESTINGHOUSE CLASS 3

Table 2-8

CECo/FAI-DCH EXPERIMENTS

Test	Driving Pressure (MPa/psia)	Driving Gas	Thermite Mass (Kg/lbm)		Measured Peak Containment Pressure		Water (kg/lbm)	
			Initial	Swept-Out	Pa	Psia	Cavity	Compartment Floor
DCH-1	3.3/478	N ₂	20/44	~ 18/ ~ 39.6	165	23.9	1.1/2.4	90/198
DCH-2	2.9/420	N ₂	20/44	~ 18/ ~ 39.6	170	24.7	5.3/11.7	47/103
DCH-3	3.2/464	N ₂	20/44	~ 18/ ~ 39.6	155	22.5	Dry	47/103
DCH-4	2.3/333	Steam	20/44	~ 18/ ~ 39.6	172	25.0	1.1/2.4	47/103

The results for all four tests were very consistent with respect to the extent of debris dispersed, the peak temperature in the lower compartment and the pressurization transient in the containment. The only differences are the response caused by dynamic interactions in the reactor cavity (determined by the water mass in the cavity) and the hydrogen generated which is a function of the water in the cavity and the driving medium. Given the similarity of the global response for all four tests, these differences have a second order influence on the containment response.

The results were consistent with CWTI-DCH tests in that significant heatup of the containment atmosphere was not observed in any runs that included the important structural barriers of a seal table and the lower containment compartment. In fact, the capacity of structures to mitigate DCH can be seen by comparing these results to SNL-DCH results which did not represent these structures. It is to be noted that the use of steam to eject the debris simulant yielded a containment temperature and pressure response virtually identical to the nitrogen blowdown tests, even though more hydrogen was generated, i.e., from 7% to 15% of the metal reacted.

2.2.8 Scaling Effects

Experimental observations in scaled experiments must be related to the full scale conditions (reactor system) with similar initial conditions. For complex phenomena like DCH, the scaling effects may distort the time scale of the processes and analyses must be performed to see if such distortion occurs and, if so, whether it is important in the overall conclusion.

As discussed, DCH experiments at FAI and ANL were performed, respectively, using 5% and 3-1/3% linear scale mockups of the Zion containment building. Contrast these with the SNL-DCH experiments, which included only a 10% linear scale mockup of the Zion cavity without modeling the geometry of the containment compartments. Consequently, only the FAI and ANL tests can be related directly to determine if there is any experimental indication of a scale dependency.

Using the two different scaled experiments available which incorporated all of the major influential features of a reactor system, we find a maximum of 2% contribution to direct heating of the atmosphere and this is reproducible for tests within a given experimental matrix, and between different tests. We also find for experimental scales varying from 1% to 10%, that when the structures are not represented, the dispersion of debris is virtually complete and that significant heating of the gas occurs. Hence, the applicability of the results to the reactor system should focus primarily on the influence of structures. Another feature of the reactor system is the availability of water in the containment which can substantially mitigate the gas temperature rise. This is also discussed below in terms of its influence on scaling.

2.2.8.1 Sweepout and Extent of Entrainment Scaling

The phenomenological discussions in the Zion Study [CECo, 1981] described several mechanisms whereby debris could be swept out of a Zion reactor cavity given the conditions of core melt, failure of the RPV lower head, debris discharge into the reactor cavity and substantial pressure in the RCS. Sweepout mechanisms included (1) roll wave formation and displacement by the follow-on gas flow, (2) wave formation by the impact of high velocity gas with subsequent breakup in the gas stream, and (3) entrainment off the debris surface by the high velocity gas stream. Subsequent experiments at different facilities (ANL, BNL, FAI and SNL) and different scale (1% and 10%) have demonstrated that sweepout would occur given the necessary conditions. Therefore, debris sweepout is not an issue for scaling considerations. However, the extent of debris particulation (entrainment) is an issue to be considered for scaling.

As discussed in Appendix A, the issue for entrainment is not which mechanism applies for debris removal; rather the issue is how much entrainment could occur while other processes are also occurring. Specifically, as debris would be entrained, what would be the feedback on other mechanisms such as displacement of the debris by an imposed pressure difference. Considerations of the simultaneously occurring processes resulted in the model for the extent of debris which could be entrained and accelerated into the gas stream while the remainder was being displaced (driven) from the cavity, as a more contiguous mass, by the imposed pressure difference. Comparisons of this model with the Sandia Surtsey experiments show good

agreement with the measured results. Given the co-existence of these processes and the agreement with experiments, what is the influence of experimental scale?

If two processes are occurring simultaneously, the experimental scale should not distort one process with respect to the other. To accomplish this, the ratio of the rates of debris transport should be preserved in scaled tests. This is discussed in Appendix D.

2.2.8.2 De-Entrainment Scaling (Due to the Change in Flow Direction)

Sandia National Laboratory [Walker, 1987] developed a model for estimating the likelihood of debris particles not deflecting with the flow due to a 90 degree change in flow direction. Thus impacting structural boundaries of the flow path. The model was developed for the Zion-type seal table structure overhanging the instrument chase entrance into the lower containment space (see Figure 2-9), and was benchmarked against HIPS test results mentioned in Section 2.2.2. The model can be applied to the AP600 cavity compartment design that results in a 90° turn of flow from a cavity. The model was presented in the following dimensionless form

$$\alpha = \frac{1}{\lambda W} \ln \left[1 + \lambda W \left[\frac{W}{L'} - \left[\frac{W}{L'} - 1 \right] \alpha \right] \right] \quad (2-1)$$

where

$$\lambda = \frac{3}{4} \left[\frac{1}{d} \right] \frac{\rho_g}{\rho_d} C_d,$$

α = fraction of particles failing to make the turn [dimensionless],

W = equivalent width of aperture through which the particles travel as they turn to leave the instrumentation tunnel [m or ft] = $\sqrt{\text{aperture flow area}}$

L' = equivalent instrumentation tunnel width [m or ft] = $\sqrt{\text{tunnel flow area}}$,

C_d = drag coefficient [dimensionless],

d = debris particle diameter [m or ft].

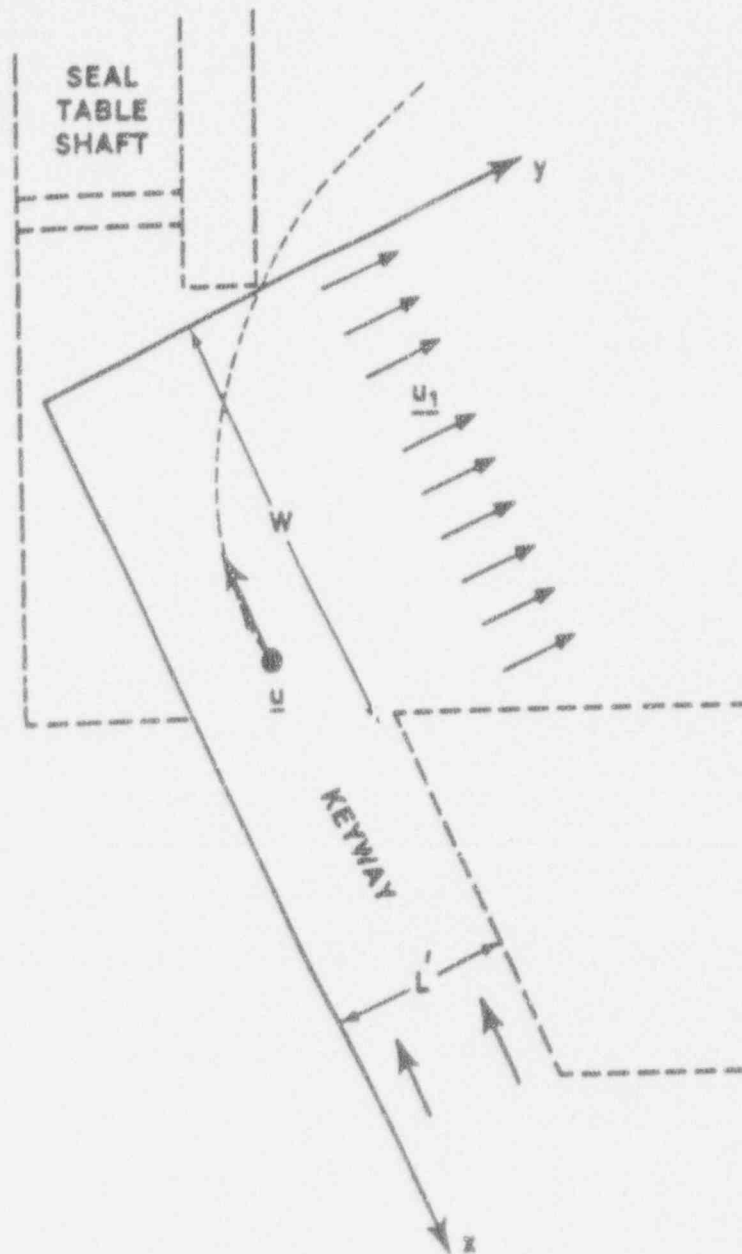


Figure 2-9 De-entrainment modeling of particles making a 90° turn (adapted from [Walker, 1987]).

The ratio W/L' in Equation (2-1) does not change with the linear scale. However, because λ does not necessarily vary with the scale, the term λW will, therefore, change with the scale. The effects of the scale in the Zion-mockup experiments can be examined by the following calculation. For the following actual Zion dimensions and assumed conditions: $W = 6$ m (19.7 ft), $L' = 3$ m (9.8 ft), $\rho_g = 1$ kg/m³, $\rho_d = 7000$ kg/m³ (0.06 lb m/ft³), $C_d = 0.44$ and $d = 1.9$ mm (0.075 in), the α value is calculated to be 96.4%. On the other hand, a 5% linear scale with $W = 0.3$ m (1 ft), $L' = 0.15$ m (6 in) and same λ would yield a value of 99.8%. Therefore, the small scale mockup tends to overpredict the de-entrainment compared to the full scale. However, the overprediction is only a few percent. It is noted that the 99.8% α value in the 5% linear scale corresponds to $\sim 0.2\%$ entrainment which is close to the low DCH efficiency measured in the FAI-DCH experiments.

Although, a large-fraction sweepout (as mentioned in Section 2.2.6) can be expected in full scale, most of the swept-out mass will fail to make the turn at the entrance into the lower compartment, and will most likely be de-entrained onto the floor of the lower compartment. This model is combined with the entrainment fraction model to develop a methodology for relating scaled experiments to the plant. This is discussed in Section 3.

2.2.8.3 Time of Flight Scaling

One of the issues to be addressed for scaled experiments is the influence of the "time of flight" for airborne debris which could be exchanging heat with the local atmosphere or oxidizing. Fractional scaled experiments have shorter lengths, which means that the airborne debris is in flight for a shorter time in the tests than would be the case in the reactor accident sequence. This is an inherent shortcoming of scaled experiments and must be addressed when evaluating the likely plant response.

As discussed previously, the issues of particular note are that all debris cannot be entrained and that all the entrained material cannot remain entrained because of the influence of structure in de-entraining particulate. Therefore, for the AP600 design, the entrained fraction may only encounter a small fraction of the containment gases as the debris particles traverse

from the cavity compartment, where several equipments and structures are located, to the loop compartment. To address this for the AP600 design, we will evaluate the energy transfer from the fraction of debris dispersed into the atmosphere by assuming that the debris equilibrates with the containment atmosphere. This eliminates any consideration with respect to the time of flight. This conservatism is adopted in the methodology of Section 3.0.

2.3 Analyses

The direct containment heating issue was first discussed as sensitivity calculations in the Zion Study [CECo, 1981]. Since then a number of efforts, from simple modeling to complex computer codes, have been directed at quantifying the magnitude of direct containment heating. These works include Sandia's DCH preliminary calculations, FAI's DCH model and computer codes such as HARDCORE, PARSEC, Kiva-DCH, and CONTAIN.

2.3.1 Zion Probabilistic Safety Study

The Zion Study [CECo, 1981] considered a wide variety of ex-vessel interaction scenarios, of which the high pressure melt ejection was notable because of the conclusions regarding debris dispersal. Three phenomena were identified which could eject debris from the cavity should core slump and vessel failure occur. The mechanisms include (1) hydraulic jump at the keyway slope, (2) wave formation during the steam/hydrogen blowdown, and (3) entrainment of the debris by high velocity gases. The first two phenomena provide for a debris configuration which could directly impede the progress of the gas mixture exiting the vessel, resulting in debris sweepout of the cavity. The third phenomenon recognizes the fact that the relatively high gas velocities could entrain, levitate and accelerate large particles to the cavity exit. Since the adjacent lower containment compartment had substantial structure to capture and redirect debris and water to the containment floor, debris ejected from the cavity was anticipated to be deposited and quenched thereafter. Aerosol formation and direct heat transfer to the lower compartment atmosphere were not considered, although sensitivity calculations included in the study did consider the effect of direct heating. The best estimate evaluation attributed the

containment pressurization to be dominated by the primary system blowdown and steam formation from debris quenching.

2.3.2 Sandia's Preliminary Calculation

Sandia National Laboratory has performed parametric scoping calculations for the effects of direct containment heating in a sample problem [Pilch, 1986]. These calculations were taken up in two parts, steady-state calculations of pressurization by simple energy balances, and rate-dependent energy release assessments.

The parametric steady-state predictions are energy balances, and rate-dependent energy release assessments.

The parametric steady-state predictions are energy balance calculations in which an energy inventory is determined for assumed debris constituents at a given temperature, including contributions from oxidation of zirconium, iron, and uranium dioxide (to U_3O_8). The fraction of debris required to participate in direct heating (as aerosol) to cause containment failure by overpressure was presented as a function of mass expelled from the cavity. The calculations show that at least 101,200 lb (46,000 kg) would be required for containment failure assuming 100% DCH efficiency.

The rate-dependent calculations only evaluated the correlations for the Nusselt and Sherwood numbers to predict heat and mass transfer from particles of given diameters. Such calculations presume the processes to generate and maintain a finely divided aerosol and neglect issues related to rate of entrainment and de-entrainment due to structural barriers. Because of the substantial limitations in the parametric calculations, these can only be used to assess the minimum debris quantities required to challenge containment integrity. Hence, these will only be used to compare the minimum mass to that which could be realistically anticipated.

2.3.3 HARDCORE

In parallel to the conduct of the DCH experiments as part of the CWTI program, the HARDCORE and PARSEC codes were developed at Argonne National Laboratory. HARDCORE analyzes debris sweepout, while PARSEC determines the extent of direct containment heating by dispersed debris. HARDCORE is formulated using one-dimensional, Eulerian, three-fluid equations and two-phase flow and heat transfer correlations. The code includes mechanistic modeling of the entrainment rate of liquid droplets from films or layers, crust formation, correlations for forced convective heat and mass transfer for spherical particles, debris cloud thermal radiation, droplet size, and drag coefficients. Particle-gas interactions assume the debris particulate is a single particle in the gas stream and does not consider the influence of a dense particulate layer separating the gas flow stream and the debris which has not been entrained. The model also does not include the dispersal of debris out of the reactor cavity by any means except entrainment. The code does account for steam oxidation of corium metallic constituents such as zirconium, iron, and chromium and accompanying hydrogen generation. Oxidation rates are set by whichever of the following processes is limiting: transport of steam molecules to the droplet surface or diffusion of ions through the oxide shell assumed to form on each core debris droplet.

Given these assumptions, HARDCORE [Sienicki, 1986] calculates the size of the dispersed corium droplets and the swept-out debris mass. The calculations require the total core debris mass ejected from the reactor vessel, the time-dependent flowrate of blowdown gas, and temperature data as inputs. HARDCORE satisfactorily reproduced the measured values for debris sweepout and debris particle size for Tests CWTI-13 and SNL DCH-1. However, no comparisons with other data have been reported to date. HARDCORE does not treat particle de-entrainment due to structural barriers at the tunnel exit. Given the substantial experimental evidence for other removal processes and de-entrainment, these processes must be incorporated into the calculation before the model can be used to assess the plant response to severe accident conditions.

2.3.4 PARSEC

PARSEC [Sienicki, 1987] is a one-dimensional, coupled Eulerian-Lagrangian code for solving particle-laden fluid flow problems with heat transfer and oxidation reactions. PARSEC calculates the heatup of a gas atmosphere in a closed containment resulting from (1) dispersal of high temperature debris droplets/particles, (2) heat transfer, (3) oxidation of reactive debris constituents with oxygen or steam to produce hydrogen. PARSEC accounts for the formation of aerosols by the oxidation-enhanced vaporization of metal from the surfaces of the core debris droplets but neglects the decrease in the mass of an individual droplet. A debris cloud, thermal radiation model accounts for back scattering by debris particles into the cloud and has been shown to be significant. Otherwise, radiation heat loss to the structures could be overpredicted resulting in less atmospheric heatup. Outputs from HARDCORE such as swept-out mass, dispersed debris size distribution, entering debris temperature, entering gas pressure and temperature are used as inputs to PARSEC. Hence, the resulting model is limited due to the limitations to HARDCORE discussed above. PARSEC calculations reportedly showed good agreement with CWTI-13 and SNL DCH-1 tests where impeding structures were not present, however, no other comparisons with data have been reported to date. Due to its one-dimensional nature, PARSEC cannot account for internal structural effects mechanistically. Until models representing other modes of debris dispersal and the influence of de-entrainment are included, the model cannot be used to evaluate the response of the plant to severe accident conditions.

2.3.5 Kiva-DCH

Kiva-DCH [Marx, 1989], which is similar to PARSEC, calculates atmospheric heatup due to the release of molten debris into a container. However, in contrast to the one-dimensional PARSEC code, Kiva-DCH simulates the processes in two or three dimensional geometry. Kiva-DCH is a modification of the Kiva computer code which was developed at Los Alamos National Laboratory to simulate spray transport and combustion processes in internal combustion engines. The similarity between the spray and debris droplets allows a straightforward modification for direct containment heating applications. Kiva-DCH utilizes a

three-dimensional finite difference scheme for gas flow calculations, coupled with a Lagrangian particle transport algorithm. The debris-wall interaction is treated by assigning a probability for trapping particles on the walls, and for particles dripping off the walls.

Kiva-DCH simulates the transport of the debris through the gas and evaluates radiative and convective heat transfer effects, and chemical reaction of the debris. Theoretically, due to its multidimensional features, Kiva-DCH could be used to simulate internal structure effects on debris transport of any containment design. However, since Kiva-DCH represents an effort to simulate virtually every individual DCH process, using the most sophisticated turbulent flow model in multi-dimensions, it requires extensive computational resources. Kiva-DCH simulations of SNL DCH-1 and DCH-3 tests showed modest differences between calculations and experimental observations. However, like PARSEC, until the code includes models for processes which compete with entrainment for debris removal from the reactor cavity, and until it includes a representation for de-entrainment, the model can not be used to evaluate the response of the plant.

2.3.6 CONTAIN

CONTAIN [Bergeron, 1986], developed at Sandia National Laboratory, is a lumped-parameter code for studies of the full scale reactor containment. Many of the models in CONTAIN have been imported directly from other codes. The DCH model implemented in CONTAIN assumed the mass particulated and the debris size (user specified) and assesses the transport of finely dispersed debris with the blowdown gas, heat transfer among the gas, debris, walls, removal or trapping of the debris as it is transported, and chemical reactions between unoxidized metals and oxygen or steam. The DCH model implemented in CONTAIN is less mechanistic than the one-dimensional HARDCORE and PARSEC codes and suffers from the same limitation as these codes with respect to assessing the response of the plant to postulated severe accident conditions.

2.3.7 Simplified Model for Representing Comparable Debris Dispersal Processes

A closed form model has been developed [Henry, 1989] for estimating the character of the debris mass dispersed out of the cavity/tunnel by the combination of entrainment and displacement (Appendix A). The thesis for this model is that the entrainment of the debris and its transport into the gas stream (where it would be accelerated), would cause the gas to be decelerated due to conservation of momentum. With a decreased gas velocity and a constant delivery rate (choked flow) from the RPV, the reactor cavity would begin to pressurize which would enhance debris removal due to the pressure difference. Entrainment rates are represented by the Ricou-Spalding correlation [Ricou-Spalding, 1961] and the entrained debris is assumed to equilibrate with the gas thereby decreasing the gas velocity. Debris displacement is evaluated by imposing the calculated pressure difference on a debris layer with a characteristic length equal to that of the reactor cavity floor. This is shown as dimension L in Figure 2-10. To escape the reactor cavity/instrument tunnel, the debris layer must be displaced over the distance L_p shown in Figure 2-10. The time required for this displacement determines the interval for debris entrainment and the ratio of the entrained mass to the total mass represents the fraction of the debris which could be finely particulated. An estimate of the debris size for the particulated fraction is obtained through a Weber number stability criterion based upon the initial (highest) gas velocity through the reactor cavity. For the condition of interest, this results in particle sizes in the range of $100\ \mu\text{m}$.

The model, which was originally formulated to evaluate fission product releases for HPME and does therefore not include a de-entrainment assessment, was compared to the SNL Surtsey tests which did not represent the containment structures outside of the reactor cavity. Table 2-6 illustrates the comparison of the predicted and measured behavior, and the predictions are in good agreement with the observations for the tests using 80 kg (DCH-2, 3 and 4). Test DCH-1 only used 20 kg and more than half of the debris froze as a thin film on the cavity walls. Freezing was not included in the closed form model, but if we assume that the first 11 kg freezes on the cold walls and insulates the walls for the remaining 9 kg, which could then be

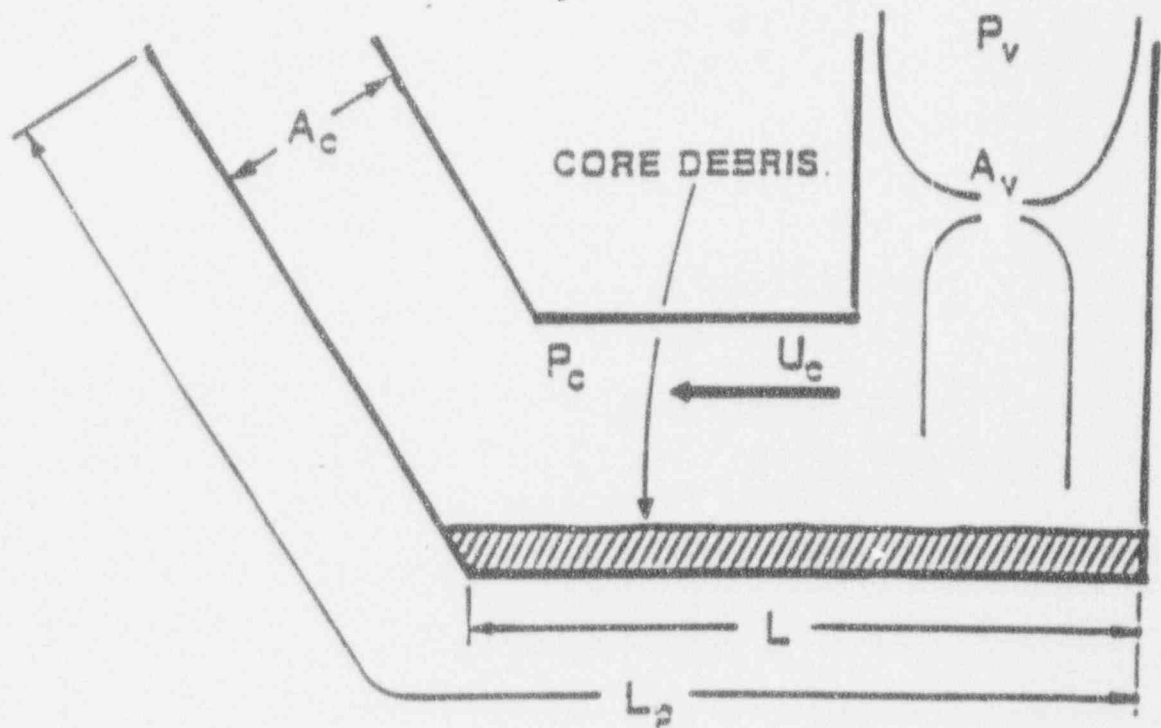


Figure 2-10 Characteristic debris length and displacement length for debris movement.

entrained, the model predicts that all of the 9 kg would be entrained due to the blowdown. This is consistent with experimental observation.

Application of the model for the mass entrained to the 5 % linearly scaled experiments results in a prediction of 5.5 kg entrained. Tables 2-9 and 2-10 illustrate the debris disposition in CECo/FAI tests DCH-1 and DCH-2. The debris locations are very similar for the tests and were virtually identical for the other two tests. If we assume that the sum of the masses frozen on the steam generators, refueling canal wall, reactor coolant pumps and the under side of the operating deck (lid) is the debris mass which escaped as particulated debris, we calculate masses of 2.1 kg (4.6 lbm) and 3.6 kg (7.9 lbm) respectively. This is in agreement with the prediction from the model in that only a limited fraction of the melt could be particulated.

Another facet of the model is that substantial pressurization of the reactor cavity could occur as a result of the debris entrainment. This could lead to a critical (choked) discharge of the debris-gas mixture, which would cause the mixture to expand rapidly and fill the cross-section of the Surtsey vessel. While a qualitative argument, it is consistent with the experimental observations. As mentioned above, this model focused on assessing the fraction of melt which could be particulated in the reactor cavity and hence did not include a de-entrainment model. To assess the behavior of the plant, this model for the fraction particulated must be combined with the de-entrainment due to the seal table as proposed by [Walker, 1987] in Equation (2-1).

2.3.8 Jet Breakup Model

A model has been presented for initial jet breakup between the vessel exit and impact with the cavity floor [Frid, 1986]. This model quantifies the effect of effervescence of dissolved gases from the debris through an assumed bubble nucleation density in the jet. Bubble growth at these nucleation sites is tracked, and the jet is assumed to break up when a void fraction of 50% is attained. It is concluded that jet breakup could occur within a few diameters of the reactor vessel, generating particles in the 30-150 micron range. However, when the debris-gas

Table 2-9

DCH-1 Final Debris Distribution

Location	Mass (kg/lbm)
1. Compartment Floor South Half North Half	6.77/14.89 7.64/16.81
2. Frozen on Steam Generators, Reactor Coolant Pumps and Refueling Canal Wall	1.26/2.77
3. Frozen on the Reactor Cavity Walls	2.02/4.44
4. Laying on the Top of the Reactor Cavity Box	1.25/2.75
5. Frozen on the Lid of the Lower Compartment	0.58/1.28
6. Inside the C Channel Reinforcement on the Lower Compartment Lid	0.16/.35
7. First Elbow in 6" Pipe	0.04/.008
8. Second Elbow in 6" Pipe	0.06/.132
9. 6" Line	0.06/.132
10. Melt Generator	0.0/0
TOTAL RECOVERED	19.78/43.52

Table 2-10

DCH-2 Final Debris Distribution

Location	Mass (kg/lbm)
1. Compartment Floor South Half North Half	5.65/12.43
2. Frozen on Steam Generators, Reactor Coolant Pumps and Refueling Canal Wall	2.06/4.53
3. Frozen on the Reactor Cavity Walls	1.96/4.31
4. Laying on the Top of the Reactor Cavity Box	2.11/4.64
5. Frozen on the Lid of the Lower Compartment	0.78/1.72
6. Inside the C Channel Reinforcement on the Lower Compartment Lid	---
7. First Elbow in 6" Pipe	0.43/.95
8. Second Elbow in 6" Pipe	0.24/.53
9. 6" Line	0.10/.22
10. Melt Generator	0.30/.66
TOTAL RECOVERED	19.14/42.11

flow encounters the cavity floor and changes direction by 90° , the debris would be expected to be redeposited as a molten layer. Therefore, this aspect was not included in the methodology of Section 3.0.

3.0 METHODOLOGY

Much like design basis analyses, if reactor vessel failure were to occur at high pressure, which is a very low probability event for the AP600 design, the most important consequence would be the increase in containment pressure. However, direct containment heating by core debris expelled at vessel failure has been postulated to be a significant contributor to the containment pressure increase for plants without depressurization capability. This section provides a method for estimating the energy released to the containment by the core debris which could be discharged immediately after vessel failure. The resulting pressure increase should then be part of the assessment for the likelihood of containment failure by overpressurization immediately following vessel failure. The methodology described below is somewhat conservative (i.e., it overestimates the containment pressurization). If the calculated pressure loadings that result from the application of this methodology for the AP600 design (see Section 4) are far less than those which would challenge the containment capability, containment failure by this means should be assessed as essentially impossible.

First, the extent of debris entrainment which could occur in the reactor cavity is determined. Next, the fraction of entrained debris which would be deentrained at the cavity exit is assessed. Then, the effect of hydrogen combustion that could possibly accompany DCH is assessed. Finally, the potential for containment pressurization is assessed and compared to the containment capability to characterize the likelihood of containment failure due to overpressurization.

3.1 Mass of Debris Distributed Into the Containment Atmosphere

The methodology focuses on (1) the debris mass that could potentially be particulated in the reactor cavity and (2) that fraction of the entrained (particulated) debris which could escape the change in flow direction caused by complex containment layout such as the cavity exit to the loop compartment (manway). (The cavity exit does not represent all of the debris-structure interactions which include blow-out panel, reactor coolant drain tank (RCDT), HVAC fan, removable grating, etc. Hence, the analysis is inherently conservative.) That fraction of the

debris which is not particulated would have such a large characteristic dimension that the manway would collect all of the debris and prevent it from entering the containment atmosphere.

A limitation exists on the extent of entrainment which could be affected by the RCS blowdown. The entrainment mass is not dependent upon the mass discharged from the RCS, except to the extent that the discharged mass should equal, or exceed, the entrained mass. The assessment of the particle size utilizes the conservative assessment described in Appendix A based on the maximum gas velocity in the reactor cavity and a single droplet Weber number criterion.

3.1.1 Extent of Entrainment

The mass of debris which could be entrained, according to Equation 20 of Appendix A, is proportional to the product of the square root of RCS pressure and the size of the breach in the RPV, i.e., the larger this product, the greater the mass which could be entrained. To evaluate the maximum mass which could be particulated, we may consider the pressure to be the pressurizer safety valve lowest set point of approximately 17 MPa (2475 psia). If we consider the initial vessel failure to be an instrument tube, the methodology presented in [CECo, 1981 and IDCOR, 1983] would suggest a vessel breach of about 0.3 m (12 in) in diameter at the time of gaseous blowdown. If the vessel fails by creep rupture at the vessel wall, the failure size should be smaller than this. Using the combination of the failure size and the RCS pressure, the calculated entrained mass in the reactor cavity can be obtained from Equation (20) of Appendix A. Gas density required in Equation (20) is determined from Equation (24) of Appendix A. Particulation of the melt by the RCS gaseous blowdown would result in a nominal debris size determined by Equation (25) of Appendix A with a critical Weber number equal to 12. For the small LOCA sequences with ADS failure, the RCS pressure would be less, resulting in a small RPV failure size (for the same debris mass). Both of these would reduce the mass of debris which could be entrained. In addition, gas velocity in the cavity would be reduced causing the average debris particulate size to be larger. Therefore, the conditions typical of a station blackout like scenario with ADS failure (RCS pressure at the safety valve set point at the time of RPV failure) bound the parameters of interest.

This evaluation of the mass of particulated debris is determined by the gas kinetic energy. As such, it is not a function of the debris mass discharged from the RPV, except for the trivial point that the entrained mass is the minimum of the calculated value and the mass discharged from the vessel. Assessing the particle size based on a single particle in the gas free stream underestimates the particle size. Hence, the following section will overestimate the fraction of particulate melt which could remain in the gas stream despite the directional change at the cavity exit. Since the melt is assumed to equilibrate with the containment gases, this results in an overestimate of the pressurization due to DCH.

3.1.2 De-Entrainment

Application of Equation (2-1) with a debris size calculated in a previous step will result in a prediction that a fraction of the particulated melt would be captured by the structure. Comparing this to the total debris mass results in a melt fraction discharged to the atmosphere.

The methodology conservatively calculates a particle size which is less than the observed value in the available experiments. Hence, the impact of the assumption that the droplet size is determined by the Weber number criterion based on the free stream velocity may also be evaluated for a larger particle size as a sensitivity study.

3.2 DCH Pressure Rise

Debris of sufficiently small size to be swept past the structures at the cavity exit and remain airborne in the containment atmosphere is assumed to thermally equilibrate with the containment atmosphere. With this assumption, issues with respect to "time of flight" (extent of energy transfer) are included in the methodology in a conservative (overestimated) manner. This is an accepted conservatism in the model.

The method for calculating the containment pressure due to DCH is illustrated in Appendix B.

3.3 Likelihood of Hydrogen Combustion

Most of the hydrogen generated by cladding oxidation would still be in the RCS prior to vessel failure and would enter the containment during the gaseous blowdown; i.e., after the debris discharge has occurred. The anticipated blowdown would be a few tens of seconds long. This is important since the initial debris discharged from the RPV would contact and vaporize the small water mass accumulated due to condensation on the reactor cavity walls. All of these would immediately displace oxygen from the lower compartment and add to the steam inventory in the containment atmosphere at a greater rate than hydrogen would be discharged from the RPV. More importantly, the steam concentration in the region of debris dispersal would be very high. Consequently, it is doubtful that the hydrogen-steam-air environment would be combustible for this sequence. Hydrogen combustion limits are discussed in Appendix C.

3.4 The Influence of Uncertainties

For the containment integrity to be threatened by a DCH event, all of the following phenomena must occur.

1. Core melt progression must occur in a manner where most of the core is molten and slumps to the lower plenum such that it could be discharged immediately following RPV failure.
2. RPV failure must occur in a manner that would allow a large mass of core debris to be discharged into the reactor cavity before RPV blowdown would be completed.
3. Once the melt is discharged from the RPV to the reactor cavity, the RCS blowdown must be sufficient to particulate and entrain most, or all, of the melt.
4. If sufficient melt is finely particulated, it must remain in this state as it flows out of the reactor cavity and into the loop compartment.
5. Burning of the hydrogen in the containment following debris particulation and dispersal must occur before containment integrity can be challenged.

Should any one of these phenomena not occur to a sufficient degree, the containment would not be threatened. Each will be discussed below with respect to the "best estimate" behavior and realistic uncertainties.

3.4.1 Core Melt Progression

Should the core melt progression also result in a substantial amount of solid material being discharged to the lower plenum the material discharge rate could be substantially limited as a result of "clogging" by the solid debris. For the analyses presented in this document, this uncertainty has been set aside by assuming that the solid material would not be available for limiting the melt discharge. Another limitation caused by solidified debris would be a reduction in the melt velocity and therefore a reduction in the rate of ablation for the vessel wall. Hence, the failure size associated with a given melt mass would be decreased thereby reducing the potential for dispersion of the melt from the reactor cavity by the RCS blowdown. Deviations from the core melt progression processes represented in this analysis would decrease the potential for DCH.

3.4.2 RPV Failure Mechanism

Several mechanisms have been identified as having the potential to cause reactor vessel lower head failure [Rempe, 1990]:

- *Penetration Tube Heating and Failure.* Corium melt attack on lower head penetrations may result in melt entering a penetration channel and refreezing causing tube blockage and/or failure.
- *Penetration Tube Ejection and Rupture.* Corium melt attack and sustained heating from accumulated debris may lead to tube penetration weld failure and subsequent penetration failure via tube ejection or rupture under system pressure.

- *Lower Head Global Rupture.* Stress induced by elevated system pressure and/or the core and structure weight, in conjunction with sustained heating from accumulated debris, may lead to lower head global failure.
- *Localized Effects/Jet Impingement.* Non-uniform heat sources within the debris bed can cause localized thermal and mechanical loads on the lower head. Impingement by a coherent jet of corium is one example of such a localized effect. In addition to lower head failure from the thermal and mechanical loads, there is also concern that a coherent jet can ablate the vessel head.

Since the AP600 design eliminates penetrations from the RPV lower head, the first two mechanisms can be excluded from AP600 considerations. The likely RPV failure mechanism for the AP600 design (as will be discussed in Section 4) would be near to top of the debris pool and would be due to creep rupture. Given the strong temperature dependence of the creep rupture phenomenon, the anticipated failure mechanism would be a localized failure (blowout of the vessel wall) followed by RCS depressurization. In this type of failure, most of the debris would not be discharged from the RPV and there would be no potential for a DCH type behavior. However, because of the uncertainties in the mixing of metallic and oxide phases in the molten debris, phase separation may occur resulting in the RPV failure from the location in contact with the metallic layer. In this analysis, uncertainties of this nature are considered by bounding calculations that assume localized failure from the location that would lead to total expulsion of the metallic layer.

3.4.3 Extent of Debris Particulation

Once debris is discharged from the reactor vessel and accumulated in the reactor cavity, the RCS blowdown represents the potential for debris particulation. The action of particulation would also impact the ability of the gas flow to sustain the entrainment process, as discussed in Appendix A. This debris-gas interaction is used in this assessment to determine the response of the reactor cavity under worst case conditions, i.e., full RCS pressure vessel failure at the bottom of the RPV and substantial melt accumulation within the reactor cavity. Application of

this methodology to available experiments shows agreement with the extent of debris particulation and, if anything, tends to overestimate the mass of material which could be finely particulated.

3.4.4 Influence of Structures

Numerous experiments have demonstrated the extensive role of structures in limiting the mass of material which could remain airborne during the debris dispersal. The approach taken uses published results for the structures which require an assessment of the debris particle size. In carrying out this part of the evaluation, the particle size was determined by the Weber number stability criteria based on the maximum gas velocity in the reactor cavity. A comparison of this particle size to the data in the Sandia SURTSEY DCH tests show that such a characterization tends to underestimate the average particle size. As a result, the influence of the structure is underestimated, i.e., the mass of material "trapped" by the structure is understated which therefore overestimates the mass of finely particulated debris which could be distributed into the containment atmosphere. Hence, the major uncertainty associated with this behavior is that of the particle size and these analyses used a size which would overestimate the mass distributed into the containment atmosphere.

In addition, there are other structures in the cavity and loop compartment which would be effective in removing particulated debris from the containment atmosphere. None of these were credited in the analysis. Neglecting these structures also tends to overestimate the heat transfer to the gas atmosphere and the pressurization that could result by directly heating the containment atmosphere.

3.4.5 Potential for Hydrogen Combustion

The potential for hydrogen combustion is greatly influenced by steam in the containment atmosphere. Calculation results that assume complete hydrogen combustion in addition to direct heating of the atmosphere by the airborne debris mass should be performed to see whether this

will result in a pressure sufficient to challenge the containment integrity. This is an additional conservatism with respect to the uncertainties of these physical processes.

In summary, each of the major elements that must be available for a DCH event have been represented in this discussion in a manner which overstates the potential for debris fragmentation, dispersal, and heating of the atmosphere. This conservative methodology will therefore result in containment pressures higher than would actually be encountered if a DCH event would occur.

4.0 PLANT SPECIFIC APPLICATION

The AP600 designs incorporate features that prevent high pressure melt ejection (HPME) in the event of RPV failure. These features include the automatic depressurization system (ADS), low core power density, and the RPV lower head without penetrations [Westinghouse, 1992]. The ADS is a key feature that will depressurize the RCS if any abnormalities would occur regardless of accident initiators. The design of the RPV lower head without penetrations would not allow a large mass of core debris to be discharged into the reactor cavity in the event of the RPV failure. The low core power density would ensure that the RCS blowdown from the failure location above the top of the debris pool would not entrain the molten debris from inside the vessel due to the crust formation on top of the debris pool inside the lower head.

4.1 Automatic Depressurization System (ADS)

(a,c)

(a,c)

4.2 Reactor Vessel Failure Location

The analysis in this section will examine the RPV failure mechanism while the RCS remains at its maximum elevated pressure typical of the pressurizer safety valve setpoint (17 MPa or 2500 psi). This postulated condition represents the worst case scenario with the highest possibility of HPME/DCH.

For the AP600, a postulation of RPV failure at high pressure requires assumptions including (1) the unlikely failure of the ADS and (2) the failure to drain the IRWST inventory to submerge the RPV. If either of the above assumptions is not met, the postulated scenario would no longer exist. For example, if the ADS does not fail, the RCS will definitely be at low pressure. If the RPV is sufficiently submerged by water from the IRWST, the RPV would be cooled and would not fail as discussed thoroughly in the AP600 evaluation summary on RPV external cooling [Fauske & Associates, 1992].

For those potential accident conditions in which core debris could relocate to the reactor vessel lower head without the benefit of external cooling, overheating of the vessel wall could induce creep rupture failure of the RPV. The potential for strain induced rupture by extensive creep has been characterized by Larson and Miller [Larson and Miller, 1952]. The information can be represented by Figure 4-1 and the Larson-Miller parameter which is defined as

$$LM = T(20 + \log t_r) \cdot 10^{-3} \quad (4-1)$$

where LM is the Larson-Miller parameter, T is the absolute temperature in °R, t is the time to rupture in hours and "log" indicates the base 10 logarithm. Figure 4-1 illustrates creep rupture data where the Larson-Miller parameter (LM) is shown on the abscissa with the stress in the affected member being the ordinate. This information is used here to provide a best-estimate evaluation of the expected reactor vessel response under elevated temperature conditions and in the absence of external vessel cooling.

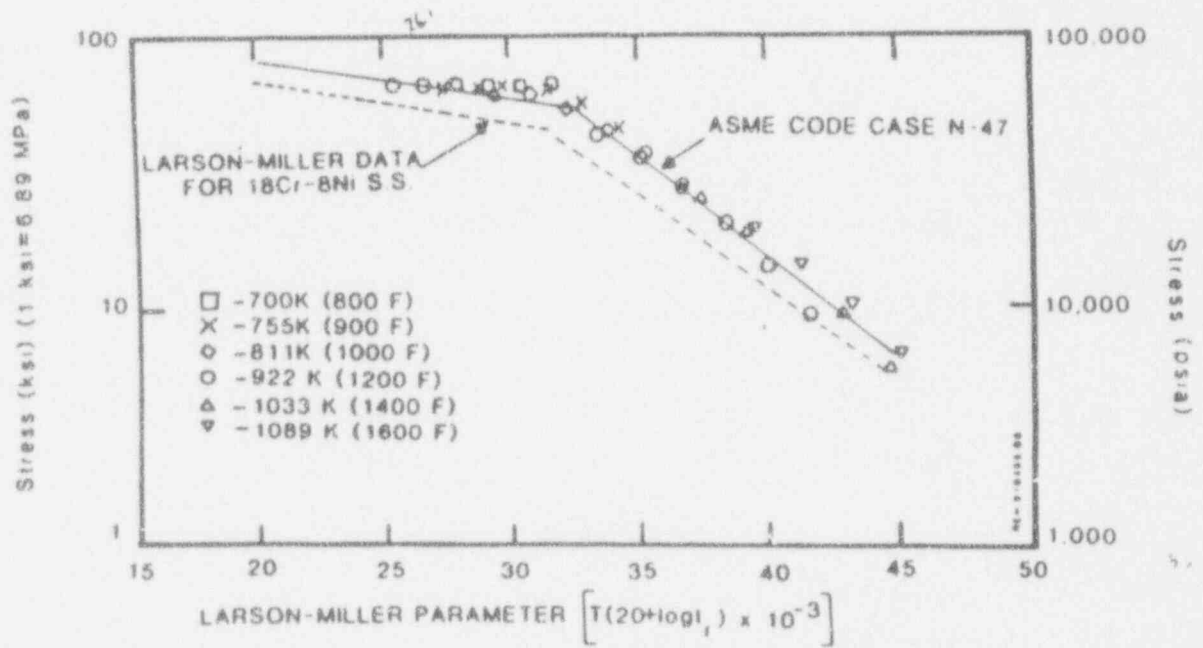


Figure 4-1 Master creep rupture curve for 316 stainless steel.

(a,c)

(a,c)

4.3 Crust Formation at RPV Creep Rupture

In Section 4.2, it has been calculated that once the RPV wall temperatures reach the neighborhood of [](a,c), the vessel would fail by creep rupture at the highest heat flux zone on the RPV wall typically near the debris pool surface. Depressurization of the RCS through the RPV rupture located near the debris surface yields a possibility of entrainment of

the molten debris directly from inside the vessel. However, if a crust could be formed near or on top of the debris pool, entrainment would be highly limited or even eliminated.

(a,c)

(a,c)

4.4 HPME/DCH Bounding Calculations

(a,c)

(a,c)

With the molten metal layer on top of the UO_2 pool, the highest heat flux zone would be the RPV portion which is in contact with the molten metal layer. The RPV failure location would be at the level of the molten metal layer which is above the crust. Therefore, before RCS blowdown begins from the creep rupture location, the molten metal would be pushed out through the hole first leaving the UO_2 pool within the lower head.

(a,c)

(a,c)

Figure 4-2 AP600 cavity layout at EL 60'-6" (adapted from [Westinghouse, 1991c]).

(a,c)

Figure 4-3 AP600 cavity layout at EL 82'-6" (adapted from [Westinghouse, 1991d]).

(a,c)

Figure 4-4 AP600 containment isometric view of cavity and loop compartment.

(a,c)

(a,c)

(a,c)

(a,c)

(a,c)

1. hydrogen combustion is not considered feasible in the best estimate analysis, and
2. even if a burn is postulated, containment integrity would not be challenged.

The fact that the assessment is tolerant of this conservatism adds to the robustness of the conclusion.

5.0 ACCIDENT MANAGEMENT IMPLICATIONS

The insights from these evaluations with respect to accident management are straightforward and important. They are, in their order of importance:

1. If a high pressure melt ejection were to occur as the result of a severe accident, the containment structures would limit the extent of debris particulation and transport into the containment atmosphere. The pressurization would be dominated by the RCS blowdown and the steam generated by quenching the debris, with the peak pressure being much less than that required to challenge the containment integrity. As a result, no accident management actions are recommended to specifically eliminate or mitigate DCH phenomena.
2. Water accumulation in containment has been demonstrated to be very effective in mitigating the consequences of a HPME. Water accumulation sufficient to submerge the lower head of the RPV would likely prevent failure of the vessel lower head. This would eliminate considerations of direct containment heating and all other ex-vessel debris considerations. Obviously this would be a most important accident management insight. A provision has been made in the AP600 design to flood the reactor cavity with IRWST water.
3. External cooling of the lower head can be generalized to be one of the recommended accident management actions any time that substantial core damage would be detected (high radiation in containment or high (> 1200°F) core exit thermocouple readings) regardless of the water level in the vessel. Even with the vessel completely filled with water, the TMI-2 vessel reached elevated temperatures when the high temperature

molten debris flowed into the lower plenum. [

]

(a,c)

6.1 SUMMARY

If external vessel cooling is not available during a core damage accident in which core debris relocates to the lower head, then creep rupture failure of the RPV may eventually occur. Best-estimate evaluations presented here for the AP600 (with no lower head penetrations) indicate that in this case vessel failure would most likely occur near the surface of the debris pool in the lower head.

Vessel failure in this manner would rapidly blow down and depressurize the RCS gas space, but would retain the majority of core debris in-vessel. Eventually, the lower head may detach and dump the core debris into the cavity, but this would occur after the primary system was already depressurized. High pressure melt ejection would not occur.

As a result of these evaluations, it is concluded that HPME/DCH related behavior would not challenge the AP600 containment design. Given the occurrence of HPME, a conservative bounding DCH calculation using mechanistic models for debris dispersal, which take into account entrainment from within the cavity and de-entrainment at the cavity exit, to evaluate the containment response to a postulated high pressure melt ejection shows the resulting pressurization to be much less than a value that would challenge the containment integrity.

The potential for hydrogen combustion ignited by high temperature debris during high pressure melt ejection is not likely due to steam inerting. Steam inerting would occur in the cavity and loop compartment. Steam generation in the cavity as debris is discharged into the water pool would create locally high steam mass fraction close to unity. Furthermore, the AP600 igniter system would continuously burn a substantial amount of hydrogen released prior to RPV failure. Hence, the amount of hydrogen available at RPV failure time would be much less than that assumed in the bounding calculation. Bounding calculations, neglecting the availability of igniters, show that even if a burn of conservatively large amount of hydrogen is assumed to occur in a steam inerted environment, the pressure increase would be much less than that required to challenge the AP600 containment design. This adds to the robustness of the conclusion.

7.1 REFERENCES

- Allen, M. D., et al, 1991, "Experimental Results of Direct Containment Heating by High-Pressure Melt Ejection Into the Surtsey Vessel: The DCH-3 and DCH-4 Tests," SAND90-2138, Sandia National Laboratory.
- Bendick, W. B., et al, 1984, "Combustion of Hydrogen: Air Mixtures in the VGES Cylindrical Tank," NUREG/CR-3273, SAND83-1022.
- Bergeron, K., et al., 1986, "Development and Applications of the Interim Direct Containment Heating Model for the CONTAIN Computer Code," Transactions of the Fourteenth Water Reactor Safety Information Meeting, NUREG/C:-0081, Gaithersburg, MD.
- Commonwealth Edison Company (CECo), 1981, Zion Probabilistic Safety Study, Chicago, Illinois.
- Consolidated Edison (Con.Ed.) and the Power Authority of the State of New York (PASNY), 1982, Indian Point Probabilistic Safety Study, New York, NY.
- Fauske & Associates, Inc., 1990a, "FAI/CECo Direct Containment Heating Experiments for a Zion-like Geometry," FAI/90-60, report submitted to Commonwealth Edison Company.
- Fauske & Associates, Inc., 1990b, MAAP 3.0B User's Manual, Vol. 1.
- Fauske & Associates, Inc., 1992, "Phenomenological Evaluation Summary on Cooling of the RPV in Support of the AP600 Risk Analysis," FAI/92-12, report submitted to Westinghouse Electric Corporation.
- Frid, W. E., 1986, "Behavior of a Corium Jet in High Pressure Melt Ejection from a Reactor Pressure Vessel," Proc. of the International ANS/ENS Topical Meeting on Thermal Reactor Safety, San Diego, CA.
- Ginsberg, T., and Tutu, N. K., 1988, "Progress in Understanding of Direct Containment Heating Phenomena in Pressurized Light Water Reactors," Invited Paper Presented at the Third International Topical Mtg. on Nuclear Power Plant Thermal Hydraulics and Operations, South Korea.
- Henry, R. E. 1989, "An Evaluation of Fission Product Release Rates During Debris Dispersal," Proc. of the ANS/ENS Intl. Topical Mtg. on Probability, Reliability and Safety Assessment, Vol. 1, pp. 375-383.
- Henry, R. E., et al, 1991, "Cooling of Debris Within the Reactor Vessel Lower Head," Invited paper presented at the ANS Annual Mtg., Orlando, FL.

REFERENCES - Continued

- IDCOR Technical Report 15.2, 1983, "Debris Coolability, Vessel Penetration, and Debris Dispersal."
- Larson, F. R. and Miller, J., 1952, "A Time-dependent Relationship for Rupture and Creep Stress," Trans. ASME, pp. 765-775.
- Marshall, B. W., 1986, "Hydrogen: Air:Steam Flammability Limits and combustion Characteristics in the FITS Vessel," NUREG/CR-3468, SAND84-0383.
- Marx, K. D., 1989, "A Computer Model for the Transport and Chemical Reaction of Debris in Direct Containment Heating Experiments," Nuclear Sci. & Eng., 102, 391-407.
- NRC (1988) letter to All Licensees Holding Operating Licenses and Construction Permits for Nuclear Power Facilities, "Individual Plant Examination for Severe Accident Vulnerabilities - 10 CFR 50.54(f)," Generic Letter No. 88-20.
- Pilch, M. and Tarbell, W. W., 1986, "Preliminary Calculations on Direct Heating of a Containment Atmosphere by Airborne Core Debris," SAND85-2439, NUREG/CR-4455, Sandia National Laboratories.
- Rempe, J. L., et al, 1990, "Light Water Reactor Lower Head Failure Analysis (Draft)," NUREG/CR-5642, EGG-2618 (Draft), Idaho National Engineering Laboratory.
- Ricou, F. B. and Spalding, D. B., 1961, "Measurements of Entrainment by Axisymmetrical Turbulent Jets," Journal of Fluid Mechanics, 11, pp. 21-32.
- Sienicki, J. J. and Spencer, B. W., 1986, "Corium Droplet Size in Direct Containment Heating," ANS Trans., V.53, pp. 557-558.
- Sienicki, J. J. and Spencer, B. W., 1987, "The PARSEC Computer Code for Analysis of Direct Containment Heating By Dispersed Debris," AIChE Symp. Series, 257, V. 83, pp. 355-362.
- Spencer, B. W., et al, 1983a, "Corium/water Dispersal Phenomena in Ex-Vessel Cavity Interactions," Paper TS-15.5, proc. Int'l. Mtg. on LWR Severe Accident Evaluation, Vol. 2, Cambridge, MA.
- Spencer, B. W., et al., 1983b, "Overview and Recent Results of ANL/EPRI Corium/Water Thermal Interaction Investigations," Paper TS-15.2, Proc. Int'l. Mtg. on LWR Severe Accident Evaluation, Vol. 2, Cambridge, MA.
- Spencer, B. W., et al., 1987, "Hydrodynamics and Heat Transfer Aspects of Corium-water Interactions," EPRI NP-5127, Argonne National Laboratory.

REFERENCES - Continued

- Spencer, B. W., et al., 1988, "Results of EPRI/ANL DCH Investigations and Model Development," ANS/ENS Conference on Thermal Reactor Safety, Avignon, France.
- Tarbell, W. W., et al., 1984, "High-Pressure Melt Streaming (H PS) Program Plan," SAND82-2477, NUREG/CR-3025, Sandia National Laboratories.
- Tarbell, W. W., et al., 1986a, "Melt Expulsion and Direct Containment Heating in Realistic Plant Geometries," Proc. of the International ANS/ENS Topical Meeting on Thermal Reactor Safety, San Diego, California.
- Tarbell, W. W., et al., 1986b, "Pressurized Melt Ejection into Scaled Reactor Cavities," SAND86-0153, NUREG/CR-4512, Sandia National Laboratories.
- Tarbell, W. W., et al., 1987a, "DCH Experiments and Analyses at Sandia National Laboratories," Containment Loads and Molten Core Containment Expert Opinion Meeting, Albuquerque, New Mexico.
- Tarbell, W. W., et al., 1987b, "Results from the DCH-1 Experiment," SAND86-2483, NUREG/CR-4817, Sandia National Laboratory.
- Tarbell, W. W., et al., 1988a, "DCH-2: Results from the Second Experiment Performed in the Surtsey Direct Heating Test Facility," SAND87-0976, NUREG/CR-4917, Sandia National Laboratory.
- Tarbell, W. W., et al., 1988b, "Direct Containment Heating and Aerosol Generation During High-Pressure-Melt Expulsion Experiments," Trans. Am. Nucl. Soc., 57, 361.
- Thinnes, G. L., and Moore, R. L., 1989, "Comparison of Thermal and Mechanical Responses of the Three Mile Island Unit 2 Reactor Vessel," Nuclear Technology, Vol. 87, pp. 1036-1049.
- Tutu, N. K., et al., 1988, "Debris Dispersed from Reactor Cavities During High-Pressure Melt Ejection Accident Scenarios," NUREG/CR-5146, BNL-NUREG-52147.
- Walker, J. V., 1987, "Reactor Safety Research Semi-Annual Report," NUREG/CR-5039, SAND87-2411.
- Westinghouse Electric Corporation, 1991a, AP600 Passive Core Cooling System, System Specification Document.
- Westinghouse Electric Corporation, 1991b, AP600 Core Makeup Tanks System Document.

REFERENCES - Continued

Westinghouse Electric Corporation, 1991c, AP600 General Arrangement Plan at EL 60'-6",
DWG. No. 1010 P2 001.

Westinghouse Electric Corporation, 1991d, AP600 General Arrangement Plan at EL 82'-6",
DWG. No. 1020 P2 001.

Westinghouse Electric Corporation, 1992, Seena Srinivas' letter to W. Luangdilok (January 30,
1992).

APPENDIX A
FORMULATIONS OF DEBRIS ENTRAINMENT PROCESSES

Proceedings of the ANS/ENS International Topical Meeting on
Probability, Reliability and Safety Assessment

Pittsburgh, Pennsylvania

(April, 1989)

AN EVALUATION OF FISSION PRODUCT RELEASE RATES DURING DEBRIS DISPERSAL

ROBERT E. HENRY
Fauske & Associates, Inc.
16W070 West 83rd Street
Burr Ridge, Illinois 60521
(312) 323-8750

ABSTRACT

Failure of a reactor pressure vessel under severe accident conditions could result in debris dispersal into the containment if the vessel were at an elevated pressure. This process could influence both containment loading and fission product release from the core debris. Recent modeling approaches have focused on the potential for debris entrainment by high velocity gases resulting from the primary system blowdown. This paper considers both the potential for entrainment, which also results in deceleration of the gas flow as the entrained debris is accelerated, and the simultaneous potential for displacing debris from the reactor cavity without fine scale particulation. If substantial amounts of the debris would be expelled from the cavity region as a relatively continuous mass, limited amounts would be dispersed into the containment atmosphere, and the interfacial area available for heating of the containment atmosphere and for release of fission products from the melt would be minimal. The resulting model is compared with the recent direct containment heating experiments, including those incorporating fission product simulants.

INTRODUCTION

The spectrum of severe accidents involves conditions wherein water is depleted from the reactor core for tens of minutes, thereby causing the core materials to overheat, oxidize, melt, and slump into the lower head of the reactor vessel. At this point, core debris could fail the reactor vessel through either thermal attack of instrument penetrations in the reactor vessel wall, or through attack of the vessel wall itself. If the vessel wall were penetrated, debris would be discharged into the reactor cavity, followed by blowdown of the primary system gaseous inventory. If the blowdown is sufficient to cause entrainment of the accumulated debris within the reactor cavity, this material could be dispersed into the lower containment compartment. Finely particulated debris from the entrainment process, could be distributed into the containment atmosphere, potentially resulting in a rapid heating and

pressurization. Debris dispersal was first addressed in the Zion¹ and Indian Point² Probabilistic Safety studies and has been further considered in the Industry Degraded Core Rulemaking (IDCOR and RRC programs^{3,4} and in recent probabilistic risk assessments such as Millstone-3⁵ and Seabrook.⁶ It has also been the subject of several experimental studies using both simulant fluids and prototypic materials.⁷⁻¹¹ A major question for application to reactor systems is whether all the debris would be finely particulated, or would it be displaced from the reactor cavity as a comparatively continuous mass with limited particulation?

Particulation would also increase the fission product release rate from the debris. This would be accelerated due to the area amplification and could result in a significant addition of nonvolatile fission products to the containment atmosphere at the time of reactor vessel failure.

MODELING APPROACH

Consider the condition shown in Figure 1, i.e., the RPV at a pressure P_v with a failure site area A_v in the lower vessel head. For elevated primary system pressures the gas flow through the breach would be choked. Gases undergoing rapid depressurization expand isentropically unless sufficient energy is transferred to the gas. Generally, this energy transfer is a comparatively slow process. However, in the situation being modeled the expanding gases would receive heat from both deposited and entrained high temperature core debris. This additional energy transfer could occur within the reactor vessel during the expulsion process as well as in the reactor cavity/instrument tunnel. As an approximation to this process, one can assume that the gas expands isothermally, in which case the gas would receive sufficient energy to remain at a constant temperature. Under this condition, the gas mass flow rate is given by

$$\dot{m}_g = P_v A_v \left(\frac{M}{RT} \right)^{0.5} = 0.6 P_v A_v \left(\frac{M}{RT} \right)^{0.5} \quad (1)$$

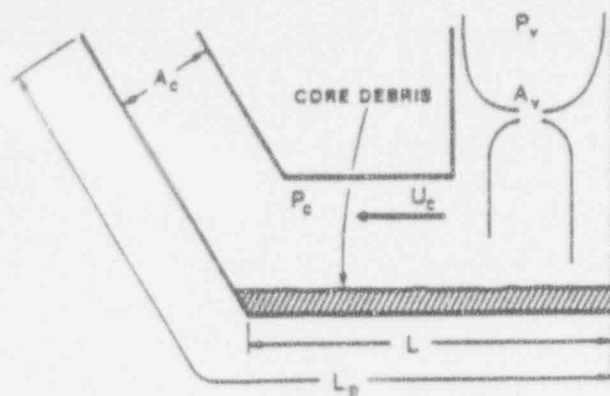


FIGURE 1 SCHEMATIC OF THE MAJOR VARIABLES IN THE MODEL

In a choked isothermal expansion, the ratio of the throat pressure (P_t) and the vessel pressure is approximately 0.6.

Given a sufficient gas velocity, entrainment would occur as long as the molten debris resides in the cavity. This minimum entrainment velocity is given by Kutateladze¹²

$$U_e = \frac{3.7 [g \sigma (\rho_D - \rho_g)]^{0.25}}{(\rho_g)^{0.5}} \quad (2)$$

As an example, let $\rho_D = 7000 \text{ kg/m}^3$, $\sigma = 1 \text{ N/m}$ and $\rho_g = 3 \text{ kg/m}^3$. For these conditions the entrainment velocity would be about 35 m/sec, which is the minimum gas velocity for entrainment. As illustrated in Figure 2, movement (displacement) of the debris would also be anticipated due to the imposed pressure differential ($P_o - P_c$) created by stagnation of the gas flow discharged from the primary system. The acceleration of debris along the reactor cavity and instrument tunnel (neglecting friction) wall can be represented by

$$a = \frac{F}{m} = \frac{(P_o - P_c) b \delta}{\rho_D b \delta L} = \frac{P_o - P_c}{\rho_D L} \quad (3)$$

Assuming the acceleration to remain constant, the time required for the core material to traverse the length of the flow path (L_p) is

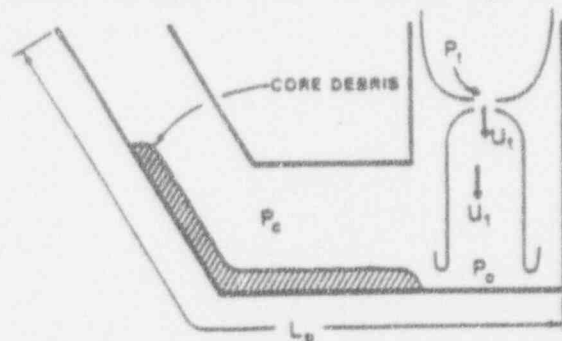


FIGURE 2 SCHEMATIC REPRESENTATION OF DEBRIS DISPLACEMENT

$$t = \left(\frac{2 L_p}{a} \right)^{0.5} = \left(\frac{2 L_p L \rho_D}{P_o - P_c} \right)^{0.5} \quad (4)$$

While wall friction is neglected, this is compensated by the assumption that the debris has a long characteristic length (L) which is assumed to remain constant. In actuality, the molten debris would deform into "roll-up waves" which would shorten the effective debris length.

The stagnation pressure imposed by the gas stream on the molten debris can be evaluated by considering the unbounded expansion shown in Figure 2. Given a choked flow condition at the RPV failure location, the one-dimensional momentum equation relating the gas flow rate and the pressure difference between the throat and the point where the expansion is complete is given by:

$$(P_t - P_c) A_v = \dot{m}_g (U_1 - U_t) \quad (5)$$

Generally, $P_t \gg P_c$, hence, this can be approximated by

$$U_1 = \frac{P_t A_v}{\dot{m}_g} + U_t \quad (6)$$

Furthermore, assuming an isothermal process as represented in Equation (1), this can be reduced to:

$$U_1 = \left(\frac{RT}{M_v} \right)^{0.5} + U_t = 2U_t \quad (7)$$

where the first term in Equation (7) is the flow velocity (choked) at the throat for isothermal expansion. Stagnation of this high velocity gas stream would cause a pressure difference to support flow along the lower surface of the reactor cavity/instrument tunnel configuration. Pressurization due to the stagnation can be evaluated by integration of the compressible Bernoulli equation, again assuming the path to be isothermal, i.e.,

$$\int_{P_c}^{P_o} \frac{dP}{\rho_g} = \int_{U_t}^0 d \left(\frac{U^2}{2} \right) \quad (8)$$

This yields a prediction for the pressure ratio (stagnation pressure to the cavity pressure):

$$\frac{P_o}{P_c} = \exp \left[\frac{\rho_g U_t^2}{P_c} \right] = \exp \left[\frac{U_t^2 M_v}{2 RT} \right] \quad (9)$$

Since

$$U_1 = 2U_t = 2 \left(\frac{RT}{M_v} \right)^{0.5} \quad (10)$$

the above equation reduces to

$$P_o = 7.4 P_c \quad (11)$$

This is the pressure which is imposed on the debris and should be used in Equation (3), hence

$$\tau = \frac{P_c - P_g}{\rho_D L} = \frac{6.4 P_g}{\rho_D L} \quad (12)$$

As a result, the time for available entrainment, Equation (4) becomes

$$\tau = \left(\frac{2 L_p L \rho_D}{6.4 P_g} \right)^{0.5} \quad (13)$$

This development shows that the debris displacement along the channel can be related to the reactor cavity pressure. Therefore, if the cavity pressure is estimated, the time available for entrainment before the debris is displaced out of the reactor cavity and instrument tunnel can be evaluated.

The rate of entrainment between a dense two-phase mixture and the surrounding gas has been addressed by Epstein and Fauske¹² utilizing an entrainment rate relationship developed by Ricou and Spalding.¹⁴ In this approach, the entrainment rate per unit surface area of the debris can be related to the gas velocity by

$$\frac{\dot{m}_D}{A_D} = E_D \left(\frac{\rho_D}{\rho_g} \right)^{0.5} U_c \rho_g \quad (14)$$

Equation (14) can be related to the gas flow rate as

$$\dot{m}_D = 0.1 \left(\frac{\rho_D}{\rho_g} \right)^{0.5} \frac{A_D}{A_C} \dot{m}_g \quad (15)$$

By using the minimum cross-sectional flow area, the model evaluates the minimum sizes which could be developed by hydrodynamic fragmentation. Also, since the minimum area usually occurs at the exit of the instrument tunnel, the model accounts for the potential to entrain debris on the reactor cavity floor, deposit the entrained material on the inclined instrument tunnel wall (due to curvature effects), and reentrainment of the molten material by the gas stream. This approach may overstate the potential for debris particulation. As such, this will provide a conservative estimate of the containment load potential. As the debris is entrained, the acceleration of the dense material toward the gas velocity will also cause the gas velocity to decrease. Considering the momentum of the flowing stream to be conserved, the increased momentum of the entrained debris is obtained at the expense of the gas momentum. Assuming that the gas behaves reversibly after the unbounded expansion when it leaves the reactor vessel, conservation of momentum between the gas and debris can be written as

$$\dot{m}_g U_1 = (\dot{m}_g + \dot{m}_D) U \quad (16)$$

(The speed of the entrained debris is assumed to equilibrate with the gas velocity.) The velocity U_1 is equal to twice the throat velocity as developed in Equations (1), (6), and (7). Further assuming that the entrained debris does not occupy a substantial fraction of the cross-sectional flow area, Equation (16) can be written as

$$\frac{1}{A_C P_g} = \frac{2}{1 + 0.1 \frac{A_D}{A_C} \left(\frac{\rho_D}{\rho_g} \right)^{0.5}} \left(\frac{1}{0.6 A_V P_V} \right) \quad (17)$$

In general $0.1 A_D/A_C (\rho_D/\rho_g)^{0.5} \gg 1$ so Equation (17) this can be further approximated by

$$P_g = 0.03 \frac{A_D}{A_C^2} \left(\frac{\rho_D}{\rho_g} \right)^{0.5} P_V A_V \quad (18)$$

Due to the approximations involved, this pressure should be limited to the throat pressure for choked flow, or $0.6 P_V$. When applied to typical test geometries, this results in substantial pressurization because entrainment slows the gas velocity dramatically. This pressurization requires on the order of 100 msec and debris dispersal may be finished before the pressure increases to this level. However, this quasi-steady value provides some measure of the cavity pressurization which influences both the gas jet dynamics as it exits the vessel and the potential for moving debris along the cavity floor.

The gas density, which is a function of the cavity pressure, appears on the right-hand side of the above equation. However, since the value on the right-hand side only varies as the square root of the cavity pressure, it will be assumed that this can be adequately represented by an average value of twice the pressure in the reactor cavity immediately prior to ejection of the core debris. With this expression, the value of the reactor cavity pressure can then be substituted into the expression for the material ejection time from the reactor cavity configuration, Equation (13), to yield

$$\tau = \left(\frac{10.4 L_p L A_C^2}{P_V A_D A_V} \right)^{0.5} (\rho_D \rho_g)^{0.25} \quad (19)$$

Multiplying the entrainment rate given in Equation (15) by this interval results in an expression for the total mass entrained by the gas stream before the remainder of the debris is "pushed" out of the reactor cavity as a comparatively coherent liquid mass as

$$\dot{m}_D = 0.19 A_V \left[P_V L_p L \rho_D \left(\frac{A_D}{A_V} \right) \left(\frac{P_V}{RT} \right) \left(\frac{\rho_D}{\rho_g} \right)^{0.5} \right]^{0.5} \quad (20)$$

This is the mass which could interact with the gas atmosphere to rapidly exchange heat and pressurize the containment building, i.e., direct containment heating. Such predictions can be compared with the various direct containment heating experiments.

Consider an example with system properties like those used previously with the additional features of a Zion-like reactor cavity as shown in Figure 3, i.e., a debris characteristic length of $L = 12$ m, a path length of $L_p = 21$ m, and a horizontal surface area of 50 m^2 . For these conditions the extent of debris which could be entrained by the gas is about 23,400 kg. It should be noted that this analysis only

considers the reactor cavity and instrument tunnel. No consideration is given in these calculations for separation of the debris from the gas stream by structures in the lower containment compartment.

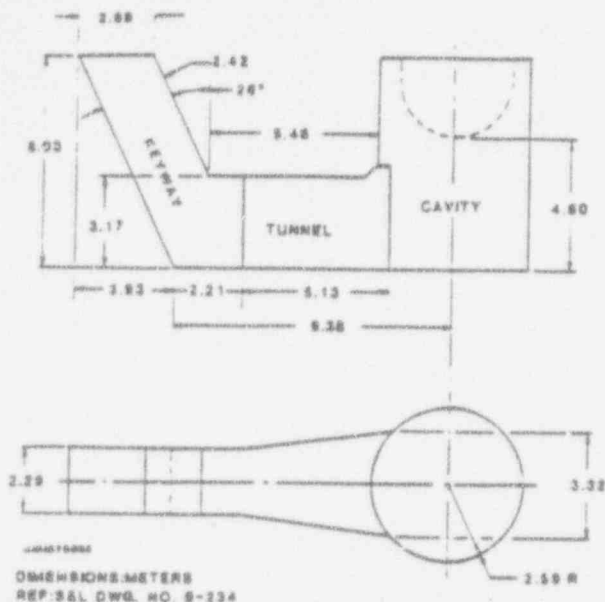


FIGURE 3 ZION-LIKE REACTOR CAVITY AND INSTRUMENT TUNNEL DIMENSIONS

The potential for breaking up molten globules once they are entrained can be related to a critical Weber number (We).

$$We = \frac{\rho U^2 d}{\sigma} \quad (21)$$

For this order of magnitude assessment, it may be assumed that the entrainment occurs immediately as the gas is released from the reactor vessel such that the initial gas velocity in the cavity is the most appropriate value. Using Equation (1) and assuming the gas in the cavity behaves as an ideal gas, this velocity is given by

$$U_c = \frac{0.6 P}{P_{co}} \left(\frac{A_y}{A_c} \right) \left(\frac{RT}{M_w} \right)^{0.5} \quad (22)$$

Using the values considered in the previous examples, the initial gas velocity would be about 100 m/sec. An initial cavity pressure of 0.3 MPa is assumed. The particle size, from Equation (21), associated with this velocity is about 110 μ m. The maximum velocity which could be developed in the cavity would be the velocity of sound. Hence, U should be limited to $(RT/M_w)^{0.5}$. If the sonic velocity at the initial cavity conditions is not sufficient to vent the incoming gas flow, the reactor cavity pressure would increase over its initial pressure to a value sufficient to allow the cavity exit flow to equal the flow from the vessel. For the assumed isothermal expansion, this would occur when

$$P_c = P_v \left(\frac{A_y}{A_c} \right) \quad (23)$$

At this pressure, the gas density in the reactor cavity and instrument tunnel would be

$$\rho_{gs} = \frac{P M_w}{RT} \left(\frac{A_y}{A_c} \right) \quad (24)$$

Using this density in the Weber number relationship, Equation (21), with the velocity of sound, the stable particulate size can be expressed as

$$d = \frac{We \sigma}{P_v \left(\frac{A_y}{A_c} \right)} \quad (25)$$

The extent of direct heating represented by the mass of debris calculated to be finely distributed can be evaluated by assuming that this debris achieves thermal equilibrium with the gas in the simulated containment volume. Under such conditions, the final temperature (T_f) achieved by the debris and gas is given by

$$T_f = \frac{m_D c_D T_D + m_G c_v T_i + Q_R}{(m_G c_v + m_D c_D)} \quad (26)$$

Assuming perfect gas behavior, the final pressure achieved by the direct heat exchange from the debris to the gas phase can be estimated by

$$P_f = P_i \frac{T_f}{T_i} \quad (27)$$

This relationship ignores the gas added to the simulated containment as a result of the blow-down process, the oxygen removed from the atmosphere by oxidation, energy transfer from the remainder of the debris, and also energy liberated by further debris oxidation. However, Equation (27) does provide a convenient check on the model with respect to its first order evaluation of peak pressures as a result of the dispersal process. In particular, the relationship developed for the mass dispersed is substantially less than the total mass injected in many experiments and therefore provides a convenient check on the capability of this model to represent the experiments performed to date.

For actual containment configurations of a more complex nature than that illustrated in Figure 1, the above model overestimates the debris entrainment since the shape of the reactor cavity has not been addressed. One would anticipate that the action of flowing through directional changes would cause entrained debris to re-deposit on the channel walls. This process has however not been included in this model. Hence, the resulting calculation for the reactor core should be expected to somewhat overstate the mass of material which could be finely particulated. Thus, the fission product release resulting from such entrainment would be overestimated by the model.

Fission product release involves diffusion of the various materials to the melt surface and convective removal of those materials from the surface. In this analysis, it is assumed that

WESTINGHOUSE CLASS 3

the release is limited by diffusion through the molten material such that the molar flux of species i is given by

$$\frac{\dot{N}_i}{A} = -D_i \left. \frac{dc_i}{dr} \right|_{r=R} \quad (28)$$

For diffusion in a static droplet, the release can be related to an effective boundary layer of $1/3$ the radius. Consequently, Equation (28) can be approximated by

$$\frac{\dot{N}_i}{4\pi R^2} = -D_i \frac{9 N_i}{4\pi R^3 \cdot R} \quad (29)$$

which reduces to

$$\dot{N}_i = -\frac{9 D_i N_i}{R^2} \quad (30)$$

or

$$\ln \frac{N}{N_0} = -\frac{9 D_i t}{R^2} \quad (31)$$

The time during which debris may exist in the entrained state can be represented by the time

TABLE 1 DCH-1 INITIAL CONDITIONS

Melt Mass	20.0 kg
Thermite Composition	Iron Oxide ^a (Fe_3O_4) 76.2 Mass % Plus Aluminum (Al) 23.8 Mass %
Melt Composition (Fully Reacted)	Iron (Fe) 55.2 Mass % Plus Alumina (Al_2O_3) 44.8 Mass %
Dopants	Lanthanum Oxide (La_2O_3) - 118 g, Barium Molybdate ($BaMoO_4$) - 313 g, Niobium Pentoxide (Nb_2O_5) - 143 g, Nickel (Ni) - 100 g
Ambient Temperature	26°C
Ambient Pressure	0.08 MPa (12.0 psia)
Driving Gas	Dry Bottled Nitrogen (N_2)
Melt Generator Gas Volume	0.109 m ³ (41.1 cm Diameter by 136.7 cm Long)
Initial Gas Pressure	1.86 MPa (270 psig)
Fusible Plug Diameter	4.8 cm

- a. Chemalloy MS-30 (100% minus 30 mesh).
b. ALCOA Atomized Powder (flake form).

of flight. This period can be estimated as the sum of the debris removal time from the cavity and the transit time through the region above the cavity (such as the lower compartment in a reactor configuration) which will be represented as L_0/U . The parameter L_0 is the effective height of the compartment. This results in an expression for the dissolved species remaining in the melt as

$$\ln \left(\frac{N}{N_0} \right) = -\frac{9 D_i}{R^2} \left\{ \left[\frac{10.4 L_0 L A_c}{F_v A_s} \right]^{0.5} + \left(\rho_D \rho_E \right)^{0.25} + \frac{L_0}{U_c} \right\} \quad (32)$$

If the diffusion coefficient is specified, the fractional releases, as dictated by diffusion to the surface, can be evaluated.

COMPARISON WITH EXPERIMENTS

SURTSEY TESTS

DCH-1. The DCH-1 test used 20 kg of molten iron thermite in the melt generator with approximately 11.6 kg being dispersed out of the reactor cavity into the large test vessel. The melt was doped with lanthanum oxide, barium molybdate, niobium pentoxide, and nickel to simulate dissolved fission products. Table 1 (from Reference 7) delineates the experimental initial conditions and the masses of fission product simulants. The test configuration, which includes a chute installed on the end of the instrument tunnel, is shown in Figure 4. The important dimensions for model application were taken from Reference 7.

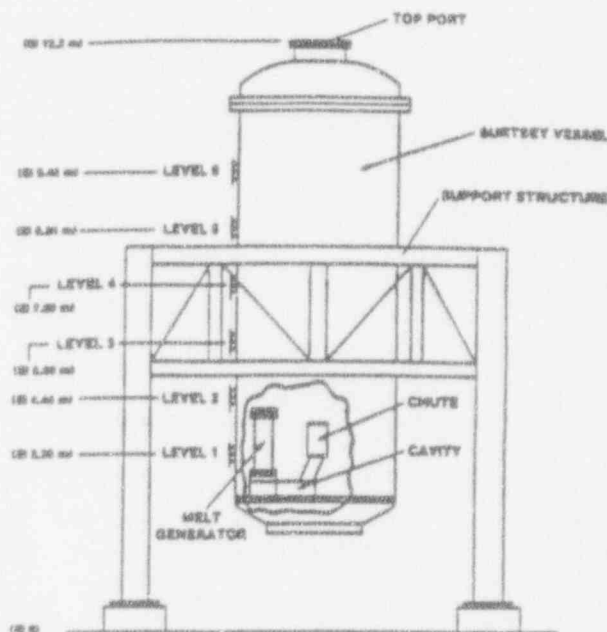


FIGURE 4 SCHEMATIC OF THE DCH-1 APPARATUS IN THE SURTSEY DIRECT HEATING TEST FACILITY

As a result of heating during the thermite reaction, the crucible pressure increased to a maximum of about 2.4 MPa, which would correspond to an average gas temperature of 386K. With the geometrical parameters given in Table 2, the debris particulation can be evaluated through the Weber number criteria. As shown in Table 2, this results in a predicted size which is somewhat smaller than the measured mass mean. This small predicted debris size may be due to the use of the minimum cross-sectional area in the model, which usually occurs at the exit of the instrument tunnel. If a value typical of the horizontal segment of the tunnel (where the entrainment initially occurs) had been used, a larger debris size would have been predicted.

Table 2 also lists the predicted peak pressure and temperature in the SURTSEY vessel along with the measured values. As shown, the model predicts that the total mass used in the melt generation could be dispersed as fine scale debris. Reference 7 lists the locations where debris was deposited and a significant fraction (~ 0.5) was found to be frozen in the melt generator and the reactor cavity. This potential for freezing debris on the reactor cavity and instrument tunnel walls was not included in the thermal-hydraulic model. As a result, the driving potential is sufficient to disperse essentially all of the melt in the generator. Thus, there was sufficient potential to particulate and disperse the available molten

materials. This condition of having the potential to entrain and disperse more material than is available in a molten state is only observed for the DCH-1 test, in which only 20 kg of thermite was used. For all subsequent experiments (DCH-2, -3 and -4), 60 kg of thermite was used, and the melt mass exceeds the potential for entrainment and dispersal.

As applied to the DCH-1 test, the model results is a prediction consistent with the observation, i.e., all the available melt would be dispersed. Since the rapidly frozen material was not dispersed, the maximum temperature and pressure calculations are compared to measure conditions by using the measured mass dispersed from the cavity. By using the measured mass, the applicability of the modeling approach to represent the energy transferred to the gas space can be tested. As observed by the comparisons shown in Table 2 for peak pressure and temperature, the model is consistent with the DCH-1 test results.

For the maximum pressure and temperature predictions, the reaction heat was assumed to be negligible. Measurements of oxygen depletion from the atmosphere following the DCH-1 test were not sufficiently accurate to determine the extent of reaction. However, the DCH-4 test, was performed in an inert atmosphere, and the pressure rise and peak pressure were not greatly

TABLE 2 MODEL COMPARISONS FOR DCH TEST

Test Parameters/ Predictions/ Measurements	DCH-1	DCH-2	DCH-3	DCH-4
1. Geometrical Parameters and Vessel Pressure				
A (m ²)	0.002	0.002	0.002	0.002
A _v (m ²)	0.5	0.5	0.5	0.5
L (m)	2.8	2.3	2.8	2.8
L _v (m)	1.45	1.45	1.45	1.45
A _v (m ²)	0.04	0.04	0.04	0.04
P _v (MPa)	2.3	6.8	6.8	6.9
2. Debris Size				
Predicted (μm)	266	65	66	38
Measured Mass Mean (μm)	550	Not Available	Not Available	Not Available
3. Mass Dispersed as Fine Particulate				
Predicted (kg)	26	27	31	33
Measured (kg)	11.6	33	18.6	18
		(Mass Deposited on the Lower Head)	(Mass Deposited on the Lower Head)	(Mass Deposited on the Lower Head)
4. Peak Temperature				
Predicted (K)	681	1032	1104	1138
	(Using Measured Mass Dispersed)			
Measured (K)	581	1150	1193	1193
5. Peak Pressure				
Predicted (MPa)	0.19	0.38	0.32	0.33
	(Using Measured Mass Dispersed)			
Measured (MPa)	0.18	0.33	0.28	0.27

different from those in the DCH-3 test which had an air atmosphere in the vessel. Consequently, the oxidation must occur over an interval in which the vessel heat sinks are also very important. Therefore in all of the adiabatic representations of peak pressure and temperature, the reaction heat has been neglected.

DCH-2. This experiment provides a more meaningful test of the model since it used a larger melt inventory (80 kg) and higher nitrogen driving pressure (4.03 MPa). The reactor cavity/instrument tunnel configuration was similar to DCH-1 but did not use a chute at the end of the instrument tunnel.

The driving pressure increased to a maximum of 6.8 MPa during the reaction which corresponds to an increase in the average gas temperature to 491K. Using these values with the geometrical parameters listed in Table 2 results in a predicted mass of finely particulated debris of 27 kg at the diameter of 65 μ m - the remainder of the debris being dispersed without fine particulation.

The DCH-2 debris characterization is greatly different from that in DCH-1. Large quantities of debris were found frozen on the vertical walls and the upper head of the SURTSEY vessel. Such observations are consistent with the modeling approach in that 27 kg is predicted to be fine particulated, entrained and dispersed while the remainder of the material would be dispersed as a relatively coherent mass. Molten debris dispersed as a comparatively continuous mass could impact the vessel vertical wall, freeze as a crust, the thickness of which would be dictated by the heat transfer into the steel, and the remainder could continue to flow upward to the head. Finely particulated material would rapidly exchange heat with the vessel atmosphere, freeze and fall to the lower head. Thus, mass recovered from the lower head (33 kg) can be compared to, and is in agreement with, the predicted value of 27 kg.

The predicted peak pressures and temperatures are in agreement with the observed values but somewhat understate the results. This may be due to either limited oxidation during the expulsion process or some heat transfer to the atmosphere from the fraction of debris which was not fine particulated but nonetheless was expelled from the instrument tunnel, impinged on the SURTSEY vessel wall, and froze. Neither of these are currently included in the model. The DCH-4 test with an inert atmosphere, which is discussed later, shows the same general behavior as DCH-2. This indicates oxidation of the fragmented material in these tests is not a first-order process in terms of heating the gas atmosphere. Hence, it is reasonable that the model ignore oxidation.

DCH-3. This test has not been fully reported and the extent of experimental observations is limited.⁹ Conditions used for the model benchmark are an initial melt inventory of 80 kg and a configuration like DCH-1 with a

chute added to the exit of the instrument tunnel. Table 2 lists the geometrical parameters and the predicted values for debris size, mass dispersed, peak temperature, and peak pressure. As shown, the model predictions are in agreement with the observed peak pressure and temperature. Since the extent of particulated debris is not presently available, the predicted value is compared with that accumulated on the lower head of the SURTSEY vessel as it was with the DCH-2 test. As discussed previously, this represents the finely divided material which froze during transit through the containment atmosphere while also being decelerated quickly after being discharged from the instrument tunnel. Both of these would tend to keep this material in the vessel atmosphere such that it would eventually settle on horizontal surfaces, i.e., the vessel lower head. The comparison shows the model somewhat overpredicts the experimental result.

DCH-4. This test was virtually identical to DCH-3 (including 80 kg of thorite and use of a chute) except the SURTSEY vessel atmosphere was inerted. The model does not use rapid oxidation to assess the peak pressure. Hence, the predictions for this test are very close to those of DCH-3. Table 2 lists the parameters for the DCH-4 comparison. The predicted and measured values of the vessel pressure and temperature are in agreement with the test results. Also, the mass of debris removed from the vessel lower head agrees with the material mass predicted to be finely particulated. Comparison of these results with those of DCH-3 may indicate the level of resolution for the data. In particular, the measured peak temperatures are in agreement, yet the final disposition of debris on the lower head differs by 40%. Hence, this is likely the resolution of the experimental information at this time, subject to more detailed reporting of the experimental results of tests DCH-3 and DCH-4.

In summary, these comparisons with the four DCH tests run in the SURTSEY facility show the proposed model to be consistent with the test observations. These comparisons include the mass which could be finely particulated, the peak vessel pressure, and the peak vessel temperature.

Comparison With Fission Product Release Data

The DCH-1 test used fission product simulants to represent the dissolved low volatile species in the debris. If the time for fission product release is the time of flight, the appropriate time for the DCH-1 test would be the time the material is resident in the cavity (~ 0.04 seconds) plus the time of flight between the cavity mouth and the upper head (~ 0.07 seconds). The results in a flight time of about 0.1 seconds. If the diffusivities are considered to be about 10^{-8} m²/sec, about 10% of the fission product would be released from the fine particulated material. Since the finely fragmented and dispersed mass was about 50% of the debris in DCH-1, this corresponds to approximately 5% of the inventory. Table 3 lists the measured release fractions for the various

materials in this test. The estimated release value characteristic of the overall inventory of approximately 5% is in general agreement with these data. Such variations are well within the uncertainty bounds of the limited data base for diffusivities in the melt.

TABLE 3 MEASURED ELEMENTAL AEROSOL RELEASE FRACTIONS IN DCH-1

Element	Mass in Relocated Debris ^a (g)	Mass in Aerosol ^b (g)	Release Fraction ^c (%)
Fe	5610	353	6.3
Al	2430	44	1.81
Mo	51.5	9.8	19.0
Ni	51.0	4.8	9.4
Nb	51.0	0.98	1.92
Ba	73.7	1.11	1.51
La	51.3	0.35	0.68

a. Uncertainty in relocated mass = $\pm 10\%$.

b. Uncertainty in aerosol mass = $\pm 53\%$.

c. Resulting uncertainty in release fraction = $\pm 54\%$.

SUMMARY OF RESULTS AND CONCLUSIONS

The issue of fission product release during the primary system blowdown following meltthrough of the reactor vessel lower head has been addressed by developing a model for the extent of fine scale debris particulation and the resultant diffusion of low volatility fission products in the melt fragments. This model also relates to the issue of direct containment heating. The model has been benchmarked with the results of the DCH tests performed at SNL. Such comparisons have demonstrated that the model predictions agree with the observed peak pressures and temperatures, especially the tests using a larger melt mass. The current model addresses only the reactor cavity and instrument tunnel configuration and ignores the lower compartment structures. Consequently, the model represents a conservative assessment of the potential influence of direct containment heating on current containment configurations.

The model also predicts the scale of debris particulation and the diffusion of fission products to the surface of this finely divided debris. This model was compared with the results of the SNL DCH-1 test. A comparison of the model predictions to the data show agreement with the test results with the major uncertainty being the diffusivity of the fission products (or their simulants) in the finely particulated debris.

REFERENCES

1. "Zion Probabilistic Safety Study", Commonwealth Edison Company, (September, 1981).
2. "Indian Point Probabilistic Safety Study", Prepared for Power Authority of the State of New York and Consolidated Edison Company of New York, Inc., (March, 1982).
3. "Technical Support for Issue Resolution", IDCOR Technical Report 85.2, Atomic Industrial Forum, (July, 1985).
4. U.S. NUCLEAR REGULATORY COMMISSION (USNRC), "Reactor Risk Reference Document", Draft, NUREG-1150, (February, 1987).
5. NORTHEAST UTILITIES, "Millstone-3 Probabilistic Safety Study", (August, 1983).
6. PICKARD, LOWE AND GARRICK, INC., "Seabrook Station Probabilistic Safety Assessment", Prepared for Public Service Company of New Hampshire and Yankee Atomic Electric Company, PLC-0300, (December, 1983).
7. W.W. TARBELL, ET AL., "Results From the DCH-1 Experiment", Sandia National Laboratory Report, NUREG/CR-4871, (June, 1987).
8. W.W. TARBELL, ET AL., "DCH-2: Results From the Second Experiment Performed in the SURTSEY Direct Heating Test Facility", Sandia National Laboratory Report, NUREG/CR-4917, (January, 1988).
9. W.W. TARBELL, ET AL., "DCH Experiments and Analyses at Sandia National Laboratories", Presentation to the NUREG-1150 Containment Loads and Molten Core Containment Expert Opinion Meeting, (December 15-18, 1987), Albuquerque, New Mexico.
10. B.W. SPENCER, ET AL., "Corium/Water Dispersal Phenomena in Ex-Vessel Cavity Interactions", Proc. Intl. Mtg. on Light Water Reactor Severe Accident Evaluation, Cambridge, Massachusetts, (August 28 - September 1, 1983), American Nuclear Society Publication, Vol. 2, pp. 15.5-1 through 15.5-7.
11. B.W. SPENCER, ET AL., "Hydrodynamics and Heat Transfer Aspects of Corium-Water Interactions", EPRI NP-5127, Electric Power Research Institute, Palo Alto, California, (March, 1987).
12. S.S. KUTATELADZE, "Elements of the Hydrodynamics of Gas-Liquid Systems", Fluid Mechanics/Soviet Research, 4, 1, (1972), p. 29.
13. H.K. FAUSKE and M. EPSTEIN, "Source Term Considerations in Connection With Chemical Accidents and Vapour Cloud Modeling", Journal of Loss Prevention Process Industry, 1, (April, 1988), pp. 75-83.
14. F.B. RICO and D.B. SPALDING, "Measurements of Entrainment by Axisymmetrical Turbulent Jets", Journal of Fluid Mechanics, 11, (1961), pp. 21-32.

WESTINGHOUSE CLASS 3

NOMENCLATURE

A	surface area of a droplet of radius R
A_c	minimum cavity flow area
A_s	horizontal surface area of the reactor cavity and instrument tunnel
A_v	RPV failure area
b	width of the cavity
c_i	concentration
c_v	gas specific heat at constant volume
c_D	debris specific heat
D_i	diffusivity (or diffusion coefficient) of fission product i in the melt
E_o	entrainment coefficient
g	acceleration of gravity
L	effective length of the debris
M_w	gas molecular weight
m_g	mass of gas in the volume
\dot{m}_g	gas mass flow rate
P_c	pressure in the reactor cavity
P_{co}	pressure in the cavity at the start of the blowdown
P_v	RPV pressure
Q_R	heat of reaction
R	universal gas constant
r	droplet radius
T	absolute temperature
T_i	initial temperature of the gas
T_D	initial temperature of the debris
U	homogeneous mixture velocity of the gas and the entrained debris in the reactor cavity
U_c	gas velocity over the molten material
U_r	relative velocity
U_1	gas velocity after the expansion
ρ	density of the two-phase flowing stream
ρ_D	debris density
ρ_g	gas density
σ	liquid (debris) to gas surface tension
δ	debris depth

APPENDIX B

Calculations of DCH Temperature and Pressure Rise

An important consequence of vessel failure is an increase in containment pressure. Direct containment heating by core debris expelled at vessel failure may be a significant contributor to the total containment pressure increase. This appendix provides a method for estimating the energy released to the containment atmosphere by the core debris released due to high pressure melt ejection following vessel failure.

Although the level of DCH is determined from the amount of energy that is transferred to the containment atmosphere, there are many factors that can affect the actual amount of energy transfer. Overall, the physico-chemical and thermo-fluidodynamical processes leading to DCH are highly complex. These individual factors and processes can be summarized as follows:

- 1) The mode of reactor failure which determines
 - 1.1) reactor vessel pressure at the time of vessel failure,
 - 1.2) failure size,
 - 1.3) fraction of core mass that would be ejected into the cavity.
- 2) The amount, temperature and size of the ejected mass that would be dispersed into the containment atmosphere by the follow-on high velocity steam/gas flow which are affected by
 - 2.1) quenching of debris by water possibly present in the cavity prior to vessel failure,
 - 2.2) enhanced dispersal of debris by water possibly present in the cavity prior to vessel failure due to vigorous steam generation,
 - 2.3) dispersal process including displacement and entrainment of molten debris.

- 3) Redirection and subsequent de-entrainment of debris particle due to structural impediment (such as a 90° turn, grating and stairway).
- 4) Shortening of particle flight time due to redirection of debris onto floor at the tunnel exit and due to structural barriers in the loop compartment.
- 5) Deposition of debris on structures.
- 6) Extent of chemical reactions which include oxidation of metallic constituents with steam and oxygen and hydrogen combustion.

The method to be used to estimate the core debris energy release that could contribute to direct containment heating is based on the assumption that the debris mass successfully entrained into the containment atmosphere equilibrates thermally with the containment atmosphere. The evaluation includes the debris superheat, the debris latent heat, the debris sensible heat, as well as the energy produced by oxidation of corium constituents (Zr, Fe, UO₂) and by combustion of hydrogen.

The final atmospheric temperature (T_f) is the solution of the following energy balance based on thermal equilibration:

$$\begin{aligned}
 & \text{debris super heat} \qquad \qquad \text{latent heat of fusion} \\
 & f_e m_D \sum C_{c,j} w_j (T_c - T_{c,m,j}) + f_e m_D \sum H_{f,j} w_j \\
 & \text{sensible heat} \qquad \qquad \text{heat of reaction with steam} \\
 & + f_e m_D \sum C_{c,j} w_j (T_{c,m,j} - T_f) + f_e m_D \sum_{H_2O} f_j w_j \Delta E_j
 \end{aligned}$$

*heat of reaction with oxygen**heat of reaction with steam*

$$+ f_e m_D \sum_{O_2} f_j' w_j \Delta E_j' + \left(m_H + 2 m_D f_e \sum_{H_2O} \frac{f_j w_j}{M_j} \ell_j \right) \Delta E_H$$

gas and steam sensible heat

$$= (m_s C_{vs} + m_g C_{vg})(T_f - T_g) - m_{sp} C_{vs} (T_{ps} - T_f) + \text{HEAT LOSS (assumed zero)} \quad (\text{B-1})$$

where

- C_{sj} = specific heat of corium species j [kJ/kg · K],
 C_{vg} = specific heat at constant volume of air [kJ/kg · K],
 C_{vs} = specific heat at constant volume of steam [kJ/kg · K],
 ΔE_j = heat of reaction of corium species j with steam [MJ/kg species j],
 $\Delta E_j'$ = heat of reaction of corium species j with oxygen [MJ/kg species j],
 ΔE_H = heat of combustion of hydrogen [MJ/kg] (set ΔE_H to zero if no H_2 burn is assumed),
 f_e = fraction of corium entrained to containment atmosphere,
 = $1 - \alpha$ (α = de-entrainment fraction due to structural impediment obtained from Equation (2-1)),
 f_j = fraction of corium species j reacted with steam,
 f_j' = fraction of corium species j reacted with oxygen,
 H_{fj} = latent heat of fusion of corium species j [MJ/kg],
 ℓ_j = molar ratio of hydrogen produced to reactant corium species j consumed during steam oxidation (see Table B-1),

- m_D = total debris mass entrained from cavity [kg] (determined by Equation 20 of Appendix A),
 m_{cj} = mass of corium species j in the pressure vessel [kg],
 m_g = initial mass of air in the containment,
 m_H = mass of hydrogen expelled from RPV during high pressure melt ejection,
 m_s = total mass of steam in the containment prior to high pressure melt ejection [kg],
 m_{sp} = steam mass expelled from RPV at vessel failure [kg],
 $\quad = P_{ps} V_{ps} / RT_{ps}$,
 M_j = atomic mass of corium species j [kg/kmol],
 P_{ps} = primary system pressure at vessel failure [Pa],
 T_c = temperature of corium prior to vessel failure [K],
 T_{cmj} = melting temperature of corium species j [K],
 T_f = final containment air temperature [K],
 T_{ps} = primary system temperature at vessel failure [K],
 T_g = temperature of air in the containment prior to high pressure melt ejection [K],
 R = universal gas constant = 8 314 [kJ/kmole . K],
 V_{ps} = primary system volume [m³],
 w_j = mass fraction of corium species j.

Subscript

- j = refers to corium species such as ZrO_2 , UO_2 , Zr and stainless steel (Fe, Ni, Cr).

Summation

- \sum_{H_2O} = sum over species reacting with steam,

$$\sum_{O_2} = \text{sum over species reacting with oxygen.}$$

Solving Equation (B-1) for T_f yields

$$T_f = \frac{1}{C_{vg} + \gamma C_{vs} + \epsilon \sum C_{c,j} w_j} (\epsilon S_1 + \epsilon S_2 + \beta \Delta E_H + C_{vg} T_g + \gamma C_{vs} T_{ps}) \quad (B-2)$$

where:

$$S_1 = \sum C_{c,j} w_j T_c + \sum H_{f,j} w_j + \sum_{H_2O} f_j w_j \Delta E_j + \sum_{O_2} f'_j w_j \Delta E'_j$$

$$S_2 = 2 \sum_{H_2O} \frac{f_j w_j}{M_j} \ell_j \Delta E_H$$

$$\epsilon = \text{entrained mass ratio} = f_e m_D / \left(m_g + m_s \frac{C_{vs}}{C_{vg}} \right),$$

$$\beta = \text{primary system hydrogen mass ratio} = m_H / \left(m_g + m_s \frac{C_{vs}}{C_{vg}} \right),$$

$$\gamma = \text{primary system steam mass ratio} = m_{sp} / \left(m_g + m_s \frac{C_{vs}}{C_{vg}} \right).$$

Information necessary for calculating terms in Equation (B-2) is provided in Tables B-1, B-2, and B-3. Note that S_1 in Equation (B-2) represents a collection of properties of corium such as heat capacity, heat of fusion, heat and extent of reactions, corium composition, and corium superheat. S_2 represents heat of combustion of hydrogen (per unit mass of corium) produced by steam oxidation of metallic contents of debris during high pressure melt ejection.

The containment final pressure (P_f), assuming the applicability of the ideal gas laws, is determined from the knowledge of T_f of Equation (B-2) by

$$P_f = \frac{T_f R}{V_c} \left[\frac{m_g}{M_g} + \frac{m_s}{M_s} + \frac{m_{sps}}{M_s} \right] \quad (\text{B-3})$$

containment air containment steam blowdown mass

where:

- M_g = average molecular weight of dry air,
- M_s = molecular weight of steam,
- P_f = containment final pressure [Pa],
- V_c = containment total free volume [m^3],

Table B-1

HEAT OF OXIDATION

(Adapted from [Pilch, et al., 1986] and [Spencer, et al., 1988])

OXIDATION OF DEBRIS CONSTITUENTS IN AN OXYGEN ENVIRONMENT

Reaction	Heat of Reaction Per Unit Mass of Reactant [MJ/kg]
$\text{Zr} + \text{O}_2 \rightarrow \text{ZrO}_2$	11.8
$\text{Fe} + 1/2 \text{O}_2 \rightarrow \text{FeO}$	4.78
$3\text{UO}_2 + \text{O}_2 \rightarrow \text{U}_3\text{O}_8$	0.483

OXIDATION OF DEBRIS CONSTITUENTS
IN A STEAM ENVIRONMENT

Reaction	Heat of Reaction Per Unit Mass of Reactant [MJ/kg]
$\text{Zr} + 2\text{H}_2\text{O} \rightarrow \text{ZrO}_2 + 2\text{H}_2$	6.74
$\text{Fe} + \text{H}_2\text{O} \rightarrow \text{FeO} + \text{H}_2$	0.43
$3\text{Fe} + 4\text{H}_2\text{O} \rightarrow 4\text{H}_2 + \text{Fe}_3\text{O}_4$	0.98
$2\text{Cr} + 3\text{H}_2\text{O} \rightarrow 3\text{H}_2 + \text{Cr}_2\text{O}_3$	4.2
$\text{Ni} + \text{H}_2\text{O} \rightarrow \text{NiO} + \text{H}_2$	0.04

HYDROGEN COMBUSTION

Reaction	Heat of Reaction Per Unit Mass of Reactant [MJ/kg]
$\text{H}_2 + 1/2 \text{O}_2 \rightarrow \text{H}_2\text{O}$	121

Table B-2

PROPERTIES OF CORE DEBRIS CONSTITUENTS

Material	Solid Density ρ (kg/m ³)	Thermal Conductivity k (W/m K)	Specific Heat Capacity* (J/kg K)	Melting Point (K)	Latent Heat of Fusion (MJ/kg)
Carbon Steel	8,000.	50.0	797 ¹ 864 ²	1,800.	0.250
Zircaloy	6,500.	18.0	356	2,098.	0.225
Zircaloy Oxide	5,600.	3.0	645	3,000.	1.196
Uranium Oxide	10,100.	3.3	491 ¹ 698 ²	3,113.	0.274

¹At temperature of 2501 K.²At temperature of 3001 K.

Table B-3

PRIMARY SYSTEM AND CORE DEBRIS CONDITIONS FOR DCH ASSESSMENT
(In Accordance with NUREG-1150, Vol. 3, Appendix J.5)

Reactor Coolant System Pressure (P_{ps})	600-2400 psig
Reactor Coolant System Temperature (T_{ps})	Corresponding Saturation Temperature
Melt Temperature (T_c)	1800-2500 K
Fraction of Core Melted and Ejected	20-80 %
Hydrogen Generated in Core (m_H)	20-70 %
Hydrogen Generated in Core (m_H)	Proportional to Fraction of Oxidized Metal (30-80 %)
Completeness of Chemical Reactions*	50-95 %

*Large uncertainty remains in estimating the extent of oxidation reactions with steam and oxygen which depend strongly on the debris temperature. As ballpark figures, the analyses of CWTI-DCH experiments suggest the following:

$$f_j = \begin{array}{l} 0.75 \text{ for fully wet cavity regardless of water in the lower compartment} \\ 0.5 \text{ for dry cavity and wet lower compartment} \end{array}$$

and

$$f'_j = \begin{array}{l} 0 \text{ for fully wet cavity with Zion-type impediment at tunnel exit} \\ 0.05 \text{ for fully wet cavity without impediment at tunnel exit} \\ 0.31 \text{ for dry cavity with Zion type impediment at tunnel exit} \\ 0.67 \text{ for dry cavity without impediment at tunnel exit} \end{array}$$

These values represent the conditions for the small scale ($3 \frac{1}{3}\%$) mockup, and should be considered as the lower bound for a reactor scale. The effects of presence of water are made clear in the values of f_j and f'_j .

APPENDIX C

Hydrogen Combustion Limits

Numerous experiments have been performed to establish the combustion limits of hydrogen as a function of hydrogen concentration and inert gases. One such study [Benedick, 1984] provided a demonstration of the inerted capabilities of carbon dioxide. The results for these experiments performed in the VGES test vessel at Sandia are illustrated in Figure C-1, which is taken from Reference [Benedick, 1984]. This also shows the results of other experiments at Lawrence Livermore and Sandia using steam as the inerting material. As shown, the atmosphere becomes inerted at a CO₂ concentration of 52%.

A substantial experimental program was performed in the FTIS vessel at Sandia to clearly define the combustion boundaries for a hydrogen-air-steam mixture both in quiescent conditions and in a turbulent environment (fans operational). This set of experiments is particularly meaningful to accident management evaluations because (1) steam is the inerting medium, (2) the boundary is clearly defined and (3) the experimental apparatus took great pains to attempt ignition of the mixture. Figure C-2 taken from Reference [Marshall, 1986] illustrates the test results for both the "fans off" and "fans operational" conditions. Those conditions which are represented as "no burn" represent the mixture state in which neither repeated spark initiators nor a glow plug was capable of initiating a burn.

The experimental information was subsequently formulated into a correlation to represent the combustion limits. This is given by

$$\% \text{ Steam} = 100 - \% H_2 - 37.3e^{0.007\% H_2} - 518e^{-0.488\% H_2} \quad (C-1)$$

and is compared to the experimental results in Figure C-2. This result is particularly meaningful to accident management guidance since it demonstrates that containment buildings could be absolutely inerted against hydrogen combustion with a steam concentration of approximately

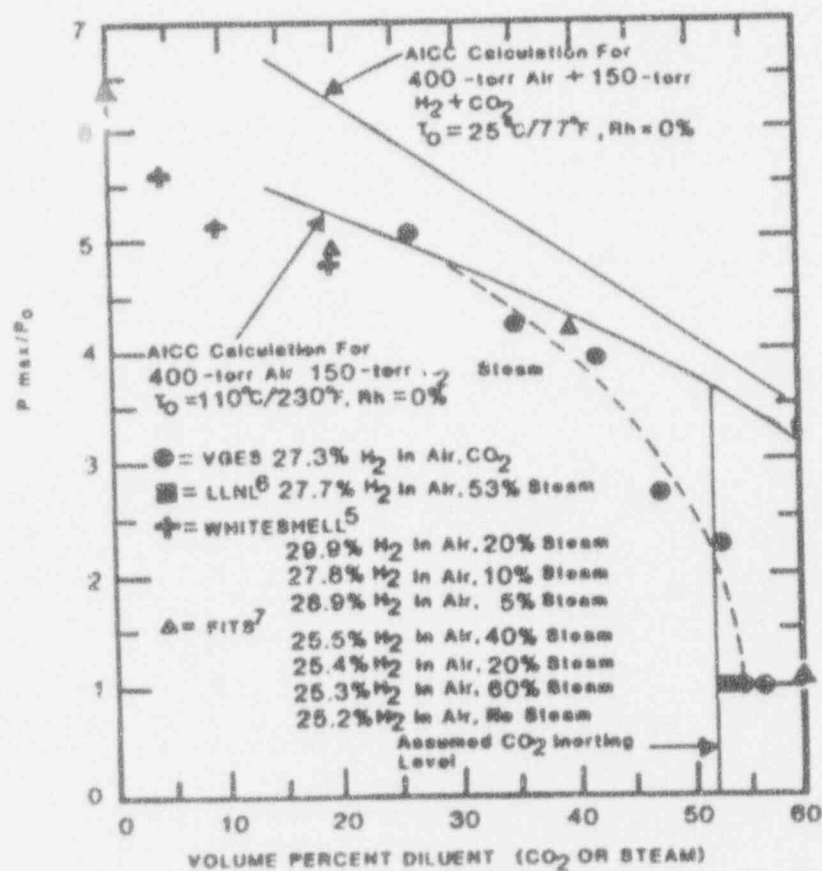


Figure C-1

Normalized peak pressure (P_{max}/P_0) for hydrogen:air:diluent mixtures, comparing CO_2 and steam (AICC = adiabatic isochoric complete combustion, R_h = relative humidity).

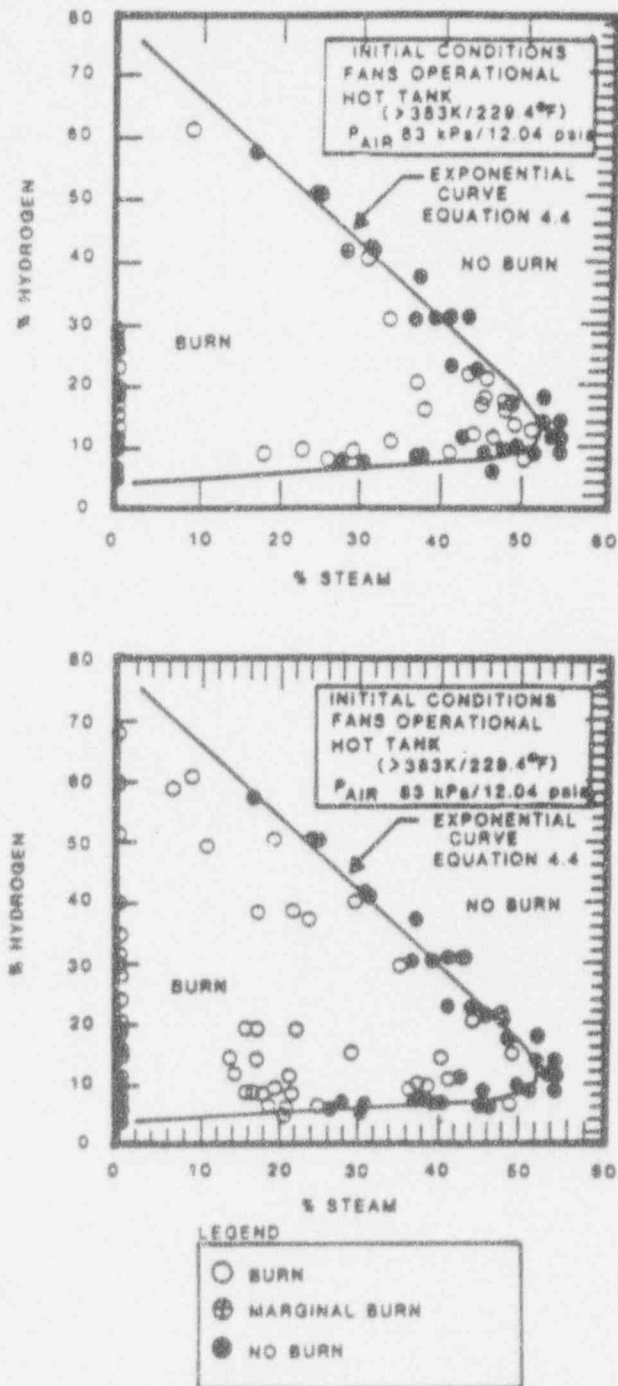


Figure C-2

Experimental data for combustion limits with fans on and off shown with the exponential curve fit.

53%. This means that if sufficient steam is released to a non-inerted containment building to produce a steam partial pressure of slightly over one atmosphere, hydrogen combustion would be precluded regardless of how much hydrogen was accumulated in containment. Since steam would be produced as a natural consequence of the accident condition the containment could be completely inerted prior to vessel failure. This should be assessed, where necessary, on a sequence specific basis.

APPENDIX D

Scaling of Entrainment and Displacement Rates

For scaled experiments to provide a meaningful representation of the reactor condition, the experiment should exhibit the same relative rates of debris entrainment and displacement, i.e., the ratio of the rates should be the same. As discussed in Appendix A, we can use the Ricou-Spalding correlation to represent the entrainment rates.

$$\dot{m}_e = C_1 A_s \sqrt{\rho_D \rho_g} U_c \quad (D-1)$$

where A_s is the cavity floor area available for entrainment. The displacement rate can be viewed as the mass of core debris over the displacement time.

$$\dot{m}_e = C_1 A_s \sqrt{\rho_D \rho_g} U_c \quad (D-2)$$

Assuming a constant acceleration (constant pressure differential), the displacement time is given by,

$$t_D = \sqrt{\frac{2L_p}{a}} = \sqrt{\frac{2 \rho_D L_p L}{\Delta P}} \quad (D-3)$$

where a is the acceleration ($a = \Delta P/(\rho_D L)$) and the terms L and L_p are defined in Figure 2-10.

The pressure differential can be related to the gas dynamic head,

$$\Delta P = \frac{\rho_g U_c^2}{2} \quad (D-4)$$

such that

$$\dot{m}_D = 0.5 \delta_b \sqrt{\frac{L_p}{L}} \sqrt{\rho_D \rho_g} U_c \quad (\text{D-5})$$

Formulating the ratio between the two rate dependent processes yields,

$$\frac{\dot{m}_e}{\dot{m}_D} = \frac{C_1}{0.5} \sqrt{\frac{L_p}{L}} \left(\frac{H}{\delta} \right) \quad (\text{D-6})$$

Where H is the height of the horizontal portion of the cavity/tunnel and δ is the height of the debris layer on the cavity floor. This shows that a linearly scaled model preserves the ratio of the relative rates for debris removal from the reactor cavity/instrument tunnel region.

1.0 PURPOSE

The Advanced Light Water Reactor (ALWR) design requirements as reported in [DOE, 1991] and [EPRI, 1990] call for passive plant design features and operating characteristics which limit the likelihood and magnitude of containment challenges resulting from severe accident sequences. One approach to minimizing containment challenges is to provide capabilities for intervention during the early phases of a severe accident which can return the plant to safe, stable shutdown conditions. In general, early termination of severe accident conditions can significantly reduce, or prevent altogether, challenges to containment integrity resulting from severe accident phenomena characteristic of the later stages of a severe accident progression.

The Westinghouse AP600 passive core cooling system (PXS) design features allow for substantial flooding of the lower containment regions in the vicinity of the reactor pressure vessel (RPV), thus there exists a high potential for significant heat removal through the vessel shell to the containment water pool. During a severe accident, this heat removal process could substantially influence the accident progression by removing,

- stored heat from the vessel steel,
- a significant fraction of the decay heat generated in the core, and
- all the energy transferred to RPV wall should molten core debris slump into the lower plenum.

All of these heat removal processes would be influential in preventing, limiting or mitigating the effects of the accident condition.

For severe accidents, the potential for sufficient heat removal through the vessel wall to prevent vessel failure and retain the core material in the RPV is of major importance. This would prevent ex-vessel phenomena such as,

- high pressure melt ejection and direct containment heating,
- core-concrete attack,

- ex-vessel debris coolability, and
- ex-vessel fission product release.

Given the considerable importance of this cooling mechanism, the objectives of this paper are to,

- outline the essential features of the phenomena associated with external vessel cooling;
- describe supportive experimental results to demonstrate that external cooling of the RPV shell is a viable mechanism for prevention of RPV failure; and
- examine the AP600-specific engineered design features to assess the capability of the AP600 plant design to accommodate the RPV external cooling mechanisms.

2.0 PHENOMENA

2.1 Description

2.1.1 Controlling Physical Processes

Submergence of the RPV lower head would result in substantial heat removal capability through the vessel wall. This is of major importance if a severe accident results in molten core debris slumping into the RPV lower plenum as occurred in the TMI-2 accident [Epstein, 1989]. As this melt would contact the cold carbon steel wall and as a thermal profile develops in the vessel wall, the melt would form a crust. When the thermal wave penetrates the wall, boiling would be initiated on the vessel outer surface. If boiling could remove the heat flux transferred through the vessel wall, the outer surface temperature would remain at essentially the saturation temperature corresponding to the containment pressure.

In the TMI-2 accident, the water level in containment was not sufficient to submerge the RPV lower head when molten core debris drained into the lower plenum. This occurred at about 22 minutes into the accident. Calculations [Thinnes, 1989] of the vessel wall thermal transient show that the wall temperatures likely reached values greater than 1200°F (~ 920K) and were eventually mitigated when the debris was quenched. Such elevated temperatures would not have occurred if the RPV could be cooled by nucleate boiling on the outer surface.

The crust formed by the melt as it freezes on the vessel wall would help protect the steel from the high temperature debris and would control the heat flux which could be transferred to the wall. In turn, this would determine the inner vessel wall temperature; the thermal profile in the steel wall being essentially linear as long as boiling on the outer surface could remove the imposed heat fluxes.

Natural convection currents like those shown in Figure 2-1 would be established inside of the molten debris. These would dictate the heat flux to the crust, and under steady-state conditions to the RPV lower head. This will be considered in Section 2.3.

2.1.2 Relationship to Containment Failure Mechanisms and Modes

The issue of external cooling of the RPV lower head and retention of the debris within the RPV is perhaps the most important phenomenological issue associated with the core meltdown process. In particular, all ex-vessel phenomena, with the exception of hydrogen combustion, and deposition of volatile fission products, would only occur if debris is discharged from the reactor vessel. The phenomena that could challenge containment integrity that result from debris in containment include:

- high pressure melt ejection and direct containment heating,
- core-concrete attack,
- ex-vessel debris coolability,
- ex-vessel fission product release,
- ex-vessel steam explosions,
- ex-vessel hydrogen generation, and
- containment performance under severe accident conditions.

As illustrated by this list, the phenomena precluded by retaining the debris in the RPV are all of those that have been subscribed to early containment failure and substantial releases of the non-volatile fission products. Hence, prevention of the lower head failure once severe core damage has been detected, would (1) limit the amount of fission products released from the reactor fuel, (2) limit the challenges to the containment integrity, (3) slow the accident progression, and (4) begin recovery from the accident state by removing some of the decay heat through the RPV wall.

In addition to the prevention of the RPV lower head failure, the accumulation of water in the containment could submerge substantially more of the RPV than just its lower head. As a result, the combination of radiation and convection off the debris upper surface, as illustrated in Figure 2-1, could provide for substantially more heat removal than that which is conducted through the crust on the vessel wall. In fact, it is possible for all of the decay heat to be

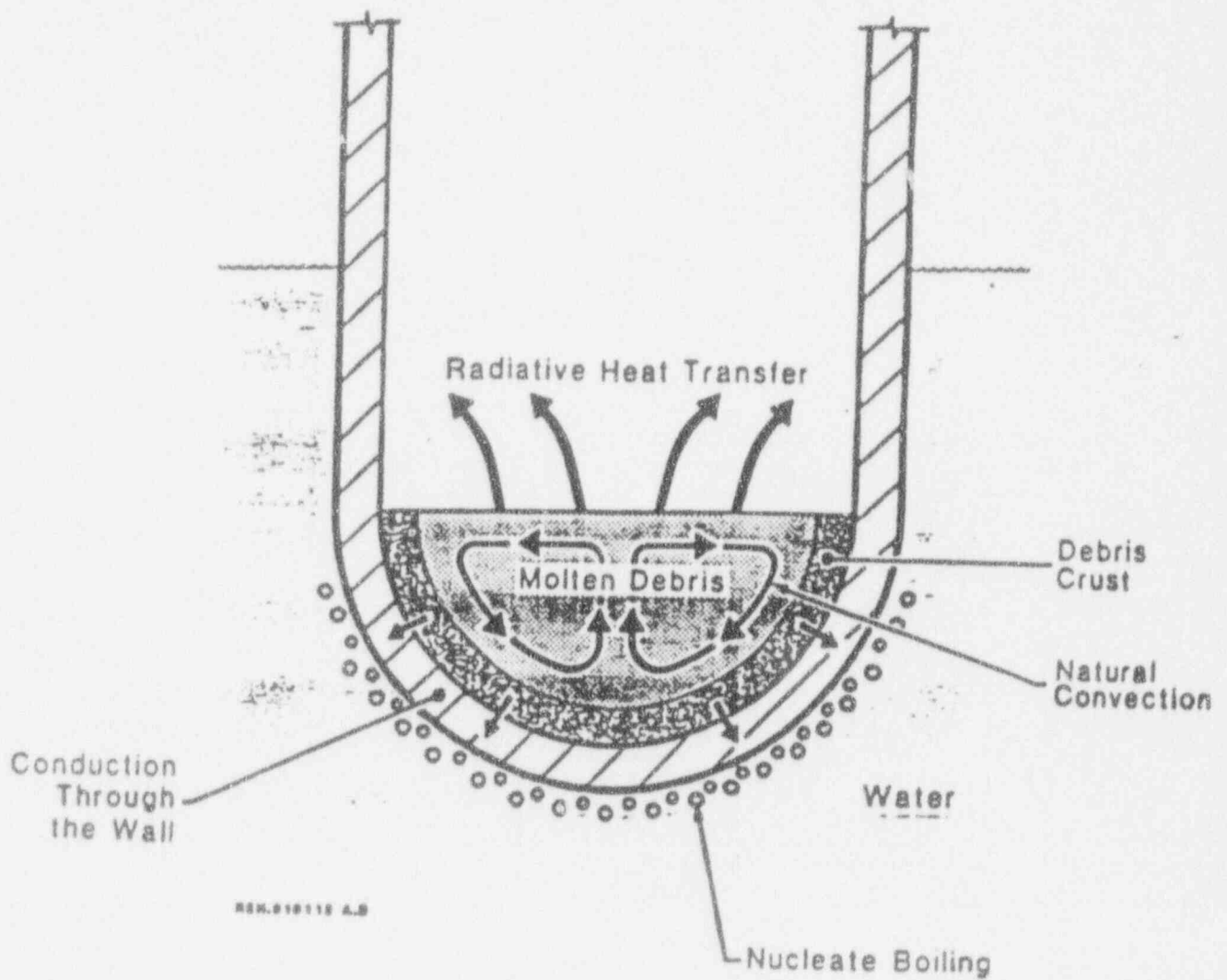


Figure 2-1 Heat transfer from the molten debris to the RPV wall.

transferred to the reactor vessel wall if the water level is flooded well above the lower head. In these cases, the accident progression would be terminated and the debris would achieve a safe stable configuration in which the energy would be transferred through the wall with nucleate boiling on the vessel outer surface. Steam would be released to the containment and operation of the AP600 passive containment cooling system (PCCS) would provide heat removal sufficient to prevent containment overpressurization.

As illustrated by the above discussion, the potential for mitigating, slowing and terminating the accident progression by external vessel cooling is extremely influential. Also, since this phenomenon has a global influence on the accident behavior, the Commonwealth Edison Company (CECo) has sponsored fundamental experiments on the potential for heat removal from the outer surface of an insulated RPV [Henry, et al, 1991]. Of particular interest is whether there is a limitation to nucleate boiling processes within the limits of the heat fluxes that could be delivered from the debris to the reactor vessel wall. Section 2.2 summarizes the experiments.

2.1.3 Relationship to Source Term

As discussed above, prevention of the vessel lower head failure would retain the debris within the reactor vessel and prevent core-concrete attack and the associated gas sparging mechanisms for release of non-volatile fission products from the debris. This has a first order influence on limiting the source term to the containment atmosphere, and for those sequences where the containment integrity would be jeopardized, thereby limiting the radiological source term which could be released to the environment. In addition, the prevention of core-concrete attack removes two mechanisms for threatening the containment integrity: overpressurization by noncondensable gases and overpressurization by hydrogen combustion with the added contribution of ex-vessel hydrogen generation. Finally, the prevention of lower head failure would eliminate considerations of high pressure melt ejection and direct containment heating in accident sequences where the automatic depressurization system does not work, thereby removing one mechanism which has been postulated to result in early containment failure and direct releases of large quantities of radionuclides to the environment. Therefore, prevention of the

lower head failure by external RPV cooling would have a first order influence on reducing the source term and challenges to the containment integrity.

2.2 Relevant Experiments

Because of the extremely important influence of external vessel cooling on the accident progression, CECO has sponsored experiments at a significant scale to investigate the nucleate boiling heat removal process. In particular, these tests were directed at evaluating whether the vessel insulation provided any significant limitation for water cooling on the vessel outer surface. These experiments were performed by pouring a high temperature iron thermite melt (3900°F/2400K) into a dry, submerged simulated vessel 12" pipe with pipe cap. Heat fluxes through the vessel wall were measured by thermocouple pairs in the vessel wall while other thermocouples measured the outer surface temperature. These latter measurements provided direct insight into whether the outer wall remained in nucleate boiling or experienced transition into another regime, such as film boiling. Tests were performed both with the vessel uninsulated and insulated by reactor grade reflective insulation purchased from Diamond Power. Figure 2-2 is a schematic of the experimental apparatus showing:

- the thermite mixture (powder),
- the thermite crucible,
- the simulated RPV lower head,
- reflective insulation,
- the thermocouples used for instrumentation, and
- the water level surrounding the insulation.

Figure 2-3 illustrates the insulation used in the experiment. The test matrix for these experiments is given in Table 2-1 and as illustrated, includes shakedown tests, uninsulated experiments and insulated tests. All of these experiments demonstrated that the heat fluxes through the vessel wall, even in the insulated case, always resulted in nucleate boiling on the outer surface of the vessel. This was true even though heat fluxes in excess of 700,000 W/m² were measured for typically 100 seconds. These heat fluxes are well above those which would

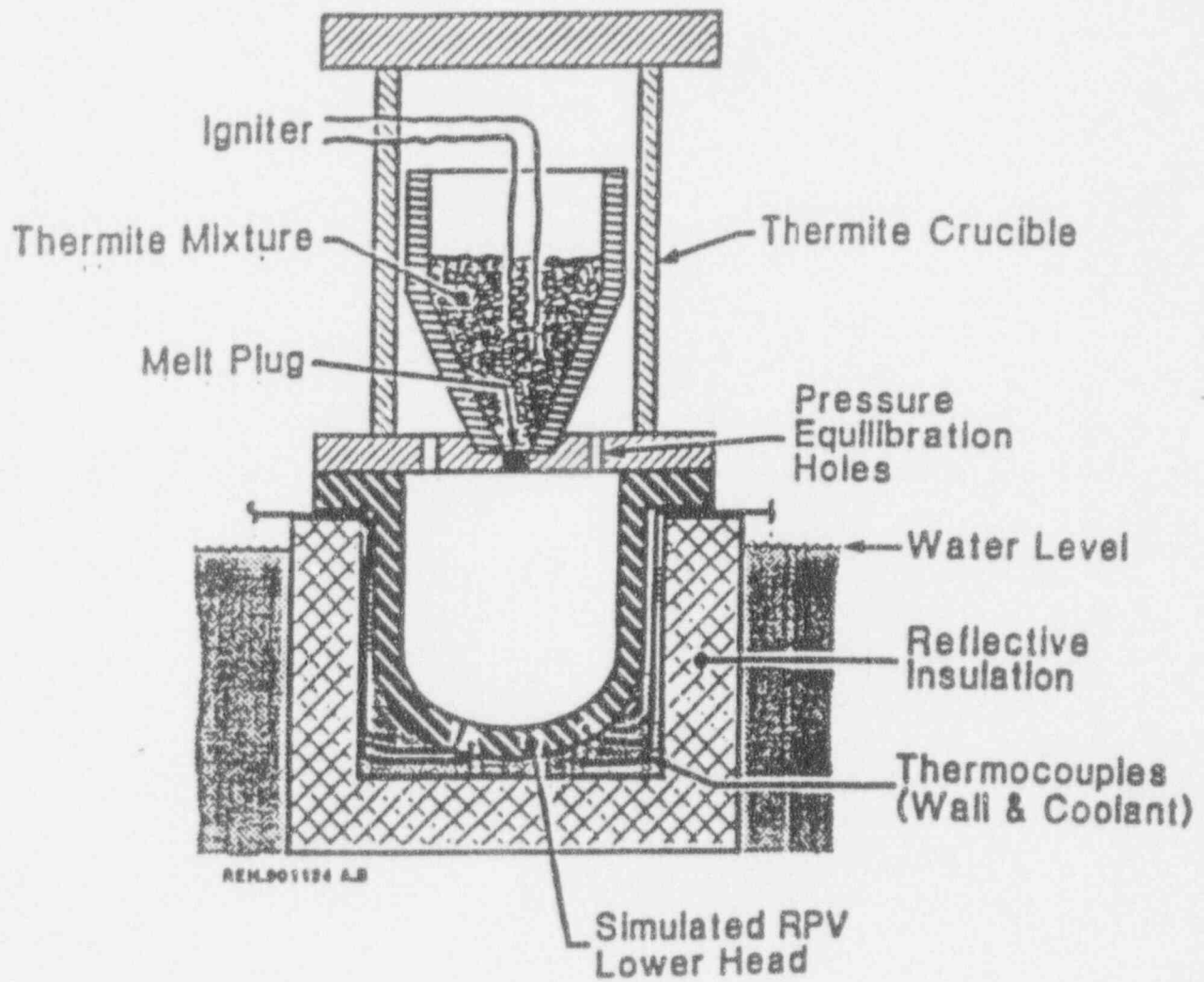


Figure 2-2 Schematic of the CECO experimental apparatus.

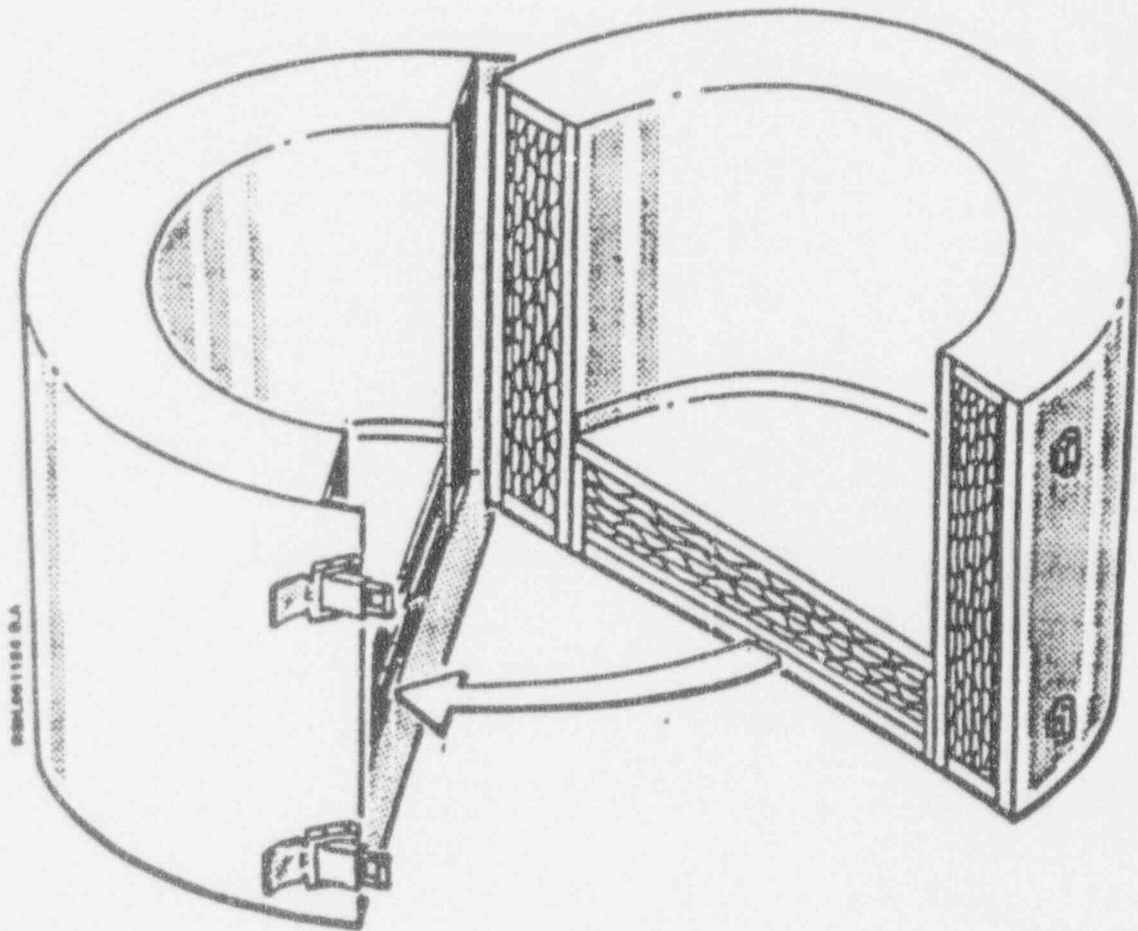


Figure 2-3 Description of the reflective insulation used in CECo tests.

Table 2-1

CEC₀ LOWER HEAD COOLING EXPERIMENTAL MATRIX

Test	Thermite Mass (kg)	Vessel Wall Thickness (cm)	Insulated
1	10	- - - Shakedown - - -	
2	10	- - - Shakedown - - -	
3	10	3.3	No
4	10	1.75	No
5	10	3.3	Yes
6	20	3.3	Yes

be anticipated to be transferred through a reactor vessel wall. The details of the experiment and the measurements are given in [Henry, 1991].

The experimental measurements were typical of the insulation in which water would ingress through a single joint at the base of the simulated reactor vessel. For actual commercial light water reactor systems, there are numerous joints available in the insulation, both in the base of the insulation as well as on the sides of the insulation cylinder surrounding the RPV. The leak rate for the single joint in the insulation provided for the experiments was measured to be 0.25 lbm/sec (0.115 kg/sec) for a pressure differential of 0.5 psi (3400 Pa). If this limited potential is translated into a reactor system, with the numerous joints between panels available only in the base of the insulation (about 300 ft/100 m), the water flow rate would be sufficient to remove all of the decay heat. This is substantially more than would be transferred to the reactor vessel wall. Hence, scaling the observations to those which would be representative for a commercial nuclear power plant results in no limitation for water cooling on the RPV outside surface.

Although the insulation incorporated into the AP600 design provides a minimum [(a,c) around the reactor vessel cylindrical section, water flowing into the cavity region must pass through the insulation to come in contact with the vessel. [

(a,c)

] Thus, experiments with insulation on the simulated RPV are the ones most relevant to the AP600 design.

With the above experiments and the application to the reactor plant, evaluations were performed for the AP600 system to determine the net results of external cooling for the reactor system. This methodology is described in Section 3.0 of this paper.

(a,c)

Figure 2-4 AP600 design reactor vessel insulation.

2.3 Relevant Analyses

The effectiveness of external cooling of an RPV during a core melt accident has been assessed analytically. Several of these assessments are briefly summarized in this section. They all demonstrate the effectiveness of submerging the RPV in water for removing large decay heat fractions and preventing RPV melt-through.

Heat Transfer in Core Meltdown

[Tong, 1968] assessed the heat transfer through the RPV walls given a molten core pool in the lower plenum. His assessment only dealt with the steady state configuration and did not include any transient states which would occur while the steady state configuration was being established. Below the molten pool's surface, heat transfer was modeled by conduction through the bottom of the reactor vessel to water outside the reactor vessel. Above the molten pool's surface, heat transfer was modeled by thermal radiation and boiling of a molten steel layer on top of the UO_2 layer. The model included a crust of frozen UO_2 between the vessel wall and the pool, as well as a crust on the top of the molten UO_2 pool.

The external surface of the RPV lower head was modeled as being submerged in water and a DNB heat flux for a slightly inclined surface was assumed, i.e., 0.945 Mw/m^2 ($300,000 \text{ BTU/hr-ft}^2$). A minimum wall thickness was calculated which showed some wall thinning per the sample calculation.

The heat transferred by thermal radiation and steel evaporation was modeled as being absorbed by the vertical reactor vessel wall and conduction through the wall to an external heat sink. The lowest section ($\sim 10 \text{ ft.}$) of the cylindrical portion of the RPV wall receives most of the radiated heat. The outside surface of this portion of the wall is assumed to be submerged in water and capable of dissipating heat at a rate up to 1.58 Mw/m^2 ($500,000 \text{ BTU/hr-ft}^2$). The middle portion of the RPV (next $10'$ of cylindrical section) is assumed to be immediately above the external water pool. This portion of the RFV is modeled as being externally cooled by a mist flow in which liquid droplets are entrained in the stream from the pool boiling outside of the

RPV. Heat transfer to the mist as well as by radiation from the external vessel wall is credited with a heat flux of 0.32 Mw/m^2 ($100,000 \text{ BTU/hr-ft}^2$). The top portion of the RPV is modeled to absorb the thermal radiation and partially melt.

This paper estimates that the heat dissipation rate from these several mechanisms is greater than the decay heat rate of the molten core. It concludes that a complete core meltdown will not melt through the bottom of the reactor vessel.

SBLOCA Outside of Containment

[Condon, 1982] assessed the effectiveness of cooling the outer wall of a RPV that contained relocated core material. This assessment was for a specific severe accident initiator for a given BWR plant. The principal of vessel protection by outside flooding considered for this plant design is the same as that considered for other reactor designs.

In this study the pool containing molten core material in the lower plenum was assumed to be in the form of stratified layers of UO_2 and steel. The study showed that for realistic decay heat generation rates, the flooding of the reactor cavity such that the RPV was submerged would prevent vessel melt-through. It was also concluded for the given BWR plant assessed, that the pumping capacity available for flooding the reactor cavity would have to be upgraded to flood that region of the plant within thirty minutes. The thirty minute interval was the calculated elapsed time between the beginning of core melting and major core relocation into the lower plenum. Another plant specific issue was identified with respect to the potential for containment overpressurization due to containment flooding in the absence of containment venting.

The assessment presented in this reference included one dimensional steady state calculations with a specified temperature for the vessel outer wall. The molten debris in the lower plenum was modeled as a layer of UO_2 and an upper layer of stainless steel. A UO_2 crust at the vessel interface was included in the model and two submodels that included and excluded a crust of UO_2 on the top of the pool were also assessed. Radiation heat transfer was modeled off the top pool's surface. However, the response of the balance of the RPV and its internal

structures were not assessed in this calculation. Decay heat was held constant throughout each analysis and it was used as a parameter in the parametric study conducted in this paper. The calculation demonstrated that if the RPV lower head is submerged in water then vessel melting would occur only for very high decay heat (approximately 4 W/cm^2 or greater). However, a debris decay heat power as large as 4 W/cm^2 could only exist if core slumping occurred within approximately 150 seconds after reactor scram, which is an unrealistically short time interval. Therefore, the paper concluded that a flooded RPV external surface would prevent vessel melt-through under the assumptions of its steady state models.

Outside Cooling of PWR Vessel Lower Head

[Park, 1991] assessed the effect of external cooling on the thermal behavior of a PWR vessel lower head containing molten core material. Two dimensional finite difference numerical analyses were performed for both transient and steady state cases. The purpose of these assessments was to investigate the effectiveness of flooding the cavity of a PWR in preventing vessel melt through for a severe accident.

Analytical results were obtained for the vessel shell temperatures, pool temperatures and the crust thicknesses for both unsteady state and steady state conditions. For both conditions, calculations were made for various values of the emissivity of the molten pool surface, the vessel wall and the upper structure, and the temperature of the upper structure. For a certain set of parameters, nucleate boiling occurs on the outside surface of the submerged vessel wall, which was found by these analyses to be effective in lowering the temperature of the inner wall. A parametric analyses found that if the vessel wall emissivity was greater than 0.2 then some melting of the unwetted portion of the vessel wall was calculated to occur. However, the melting was calculated to not propagate further than one fifth of the vessel thickness.

The analyses showed that it may take several hours before quasi-steady state conditions would be established. During the transient period crust thickness and the pool temperature would increase. However, in some cases crust growth would be followed by remelting of the crust. The parametric study suggested that emissivities of the pool surface, the structures, and the vessel

wall play an important role. However, the structure temperature (800°K used in this study) has a small effect on the temperature distribution around the vessel in the wall. The thermal analysis showed that for the range of parameters studied, flooding of the reactor cavity may provide an effective means of retaining the core in-vessel. The authors note that for this analysis between 70 and 80% of the decay heat is absorbed in the structures within the RPV that do not relocate with the core melt and its relocation. This fraction of the decay heat energy must get redistributed in the remainder of the reactor coolant system (RCS) by convection. As such this raises the possibility of the failure of the hot leg nozzle or the steam generator tubes in the absence of any effective heat sinks for these components. This paper did not analyze the time for a break to develop in the RCS due to such convective heat transfer nor the potential of failure of the reactor vessel due to excessive thermal stresses or due to creep rupture.

Thermal Analysis of Reactor Lower Head

[O'Brien, 1991] performed a thermal analysis to assess the viability of external water flooding as a cooling strategy to prevent reactor vessel thermal failure in the case of a severe accident with partial core melting and core relocation to the reactor vessel lower head. Vessel wall temperatures and heat fluxes were predicted over a range of decay heating values using a one-dimensional heat conduction model in conjunction with literature correlations for the local heat flux distributions associated with natural convection inside the molten debris pool. A finite-element prediction of flow and heat transfer inside the internally heated molten pool was also obtained. Vessel wall temperature results were highly dependent on the distribution chosen to represent heat transfer along the lower surface of the melt region. The literature correlations which were obtained for low Rayleigh number natural convection in two-dimensional rather than asymmetric geometries predicted much higher heat fluxes for the upper melt surface compared to the lower surface. The finite-element computational fluid dynamic predictions obtained for turbulent natural convection indicated similar heat flux levels for the upper and lower surfaces. Vessel wall temperature predictions were satisfactory when the literature heat flux correlations were used, i.e., the predicted wall temperatures were less than the steel melting temperature. However, inside vessel wall temperatures in excess of the melting point of steel were indicated when the finite-element heat flux distribution was applied to the model. In both cases the model

included the corium crust between the molten pool and the vessel wall and on top of the molten pool.

The finite-element turbulent natural convection simulation (κ - ϵ) turbulence model predicted the presence of a single large convection cell in the molten region, with upflow near the center line and downflow along the hemispherical boundary of the lower plenum. The predicted heat flux distributions indicated similar average heat flux values for the upper and lower surfaces, whereas at the same volumetric heating level, literature correlations (Mayinger) predicted an average upper-surface heat flux that is larger by a factor of four than the lower surface heat flux. Correspondingly higher peak vessel wall temperatures (> 2400 K) were therefore predicted for a volumetric heating level of 1 MW/m^3 . In fact, a large portion of the inner surface of the vessel wall was predicted to be above the steel melting temperature at this heat generation rate by the turbulence based model. Therefore, if the turbulent natural convection heat transfer distribution predicted from the turbulent natural convection simulation were correct, the thinning of the vessel wall could occur per this calculation. It should be noted that for the AP600 analysis performed in Section 3.0 the correlations of [Mayinger, 1976] are used rather than the (k, ϵ) turbulence model.

Counter Current Flooding Limit

Another aspect of the steam generated by external cooling that should be considered is the potential for flooding in the annular region surrounding the reactor vessel. The rising steam and the "falling" water would constitute a vapor-liquid countercurrent flow configuration in the annulus between the vessel and cavity insulation. An assessment has been performed to determine whether a countercurrent flow limitation would occur due to the upflow of vapor around the annular outer periphery of the AP600 reactor vessel during a severe accident scenario [O'Brien, 1992]. This assessment concludes that the anticipated steam generation rates would be sufficiently small that flooding would not be expected for the AP600 plant configuration.

3.0 METHODOLOGY

3.1 Analysis

To investigate the thermal and mechanical response of the bottom head to this mass of molten UO_2 , it is assumed that the pool is in steady-state heat balance. That is the heat loss to the bottom head is equal to the heat produced by the decay heat within the interior of the pool minus that which is transferred from the debris upper surface by convection and radiation. The model for the molten pool is illustrated in Figure 3-1.

The problem of predicting the heatup rate of the bottom head is somewhat complicated by the presence of a growing and, perhaps, remelting debris crust on the inner surface of the bottom head. If it is assumed that the temperature profile through the crust is linear, then the convective flux from the internally heated pool is transmitted directly to the inner surface of the bottom head and the problem is simplified. Owing to the presence of the crust, the steady-state pool supplies a constant heat flux, namely

$$q'' = h \Delta T \quad (3-1)$$

to the bottom head at all times, where h is the heat transfer coefficient and ΔT is the pool temperature relative to its melting temperature. While q'' is considered constant for each element of the RPV bottom head, it may vary with vertical distance along the head.

A debris pool is assumed to fill the lower head and therefore is regarded as a hemisphere of radius R and the heat transfer correlations obtained with water pools are assumed applicable to the molten core materials. Accordingly, the upward heat flux, q_u , to the pools crust cover is given by the analysis of Epstein [Epstein, 1989] that incorporates the correlations of Mayinger, et al [Mayinger, 1976] as

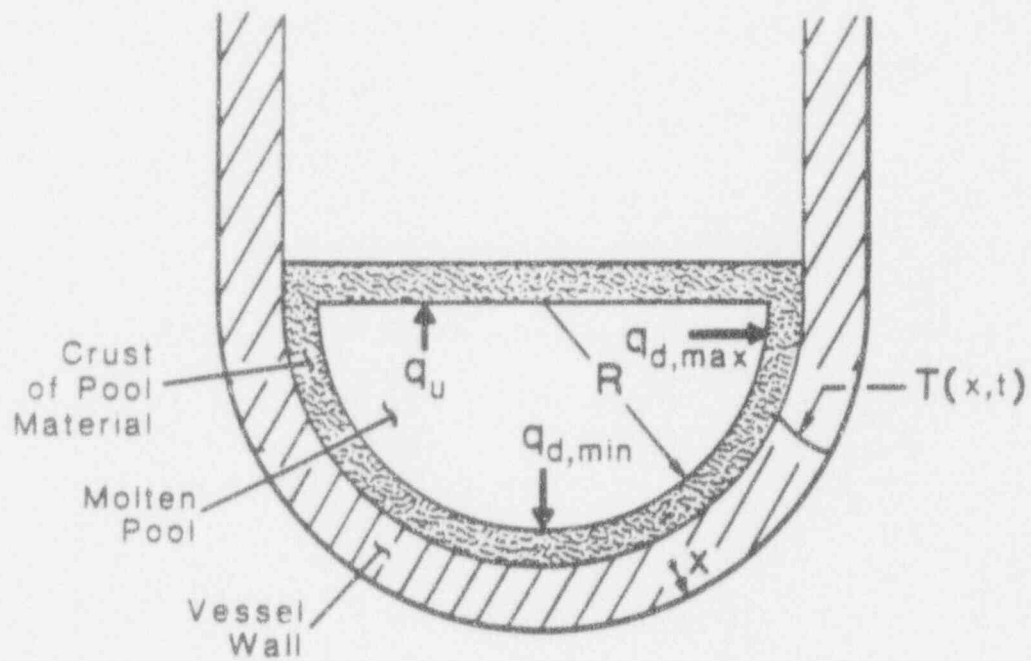


Figure 3-1 Heat transfer from the molten debris to the RPV wall.

$$\frac{q_u R}{k \Delta T} = 0.36 Ra^{0.23} \quad (3-2)$$

and the average downward (and horizontal) heat flux, q_d , to the hemispherical bottom head is given by

$$\frac{q_d R}{k \Delta T} = 0.54 Ra^{0.18} \left(\frac{\ell}{R} \right)^{0.26} \quad (3-3)$$

where the $\left(\frac{\ell}{R} \right)^{0.26}$ term accounts for debris pool depth that only partially fills the hemispherical lower head. Under steady-state conditions, the volumetric heat generation rate Q is equal to the sum

$$\frac{2}{3} \pi R^3 Q = \pi R^2 q_u + 2\pi R^2 q_d \quad (3-4)$$

Substituting Equations (3-2) and (3-3) into (3-4) to eliminate q_u and q_d , we arrive at the expression,

$$1 = \frac{3}{2} \left(\frac{k \Delta T}{R^2 Q} \right) \left[0.36 Ra^{0.23} + 1.08 Ra^{0.18} \left(\frac{\ell}{R} \right)^{0.26} \right] \quad (3-5)$$

This expression may then be solved for the pool superheat (ΔT),

$$\Delta T = \frac{2}{3} \cdot \frac{R^2 Q}{k} \left[0.36 Ra^{0.23} + 1.08 Ra^{0.18} \left(\frac{\ell}{R} \right)^{0.26} \right]^{-1} \quad (3-6)$$

where Ra is the Rayleigh number for a heat generating fluid:

$$Ra = \frac{g \beta Q R^5}{\alpha \nu k} \quad (3-7)$$

The experimental studies of Gabor [Gabor, 1980] and Jahn and Reineke [Jahn, 1987] have shown that the maximum local heat flux would occur at the extreme edges of the pool (where the pool surface contacts the vessel wall) and is approximately twice the average downward flux. The minimum heat flux is at the very bottom of the vessel and is about one-half the average flux.

3.2 Approach

The approach in this paper assumes that 100% of the core material is molten and accumulated in the RPV lower plenum and assesses whether the external cooling mechanisms are sufficient to remove the imposed heat fluxes from the molten pool for the AP600.

This assessment is accomplished by first examining the AP600 passive core cooling system (PXS) attributes and the containment geometry to determine the conditions under which the RPV can become submerged by containment water pools. Next, with the assumption of 100% of the core material accumulated in the lower plenum, the heat fluxes to the reactor vessel wall are evaluated based upon the analysis presented in this section for internal circulation within the molten debris pool. Calculations of the wall heat fluxes will be based on the AP600-specific RPV and containment geometry. Typical values for the physical properties of the core debris are given in Section 4 and these are used to calculate the average, maximum and minimum heat fluxes to the reactor vessel wall. Once the wall heat fluxes are determined, these are compared to those measured in the CECo sponsored experiments. If the heat fluxes are well below those measured in the experiments, there will be no limitation to heat removal off of the vessel outer surface. It should be noted that those CECo experimental configurations which placed reflective insulation around the simulated RPV lower head are similar to the actual AP600 lower head geometry which employs standoff insulation. Thus, the CECo experiments run with reflective insulation on the simulated RPV most directly represent the AP600 configuration.

4.0 PLANT SPECIFIC APPLICATION

4.1 AP600 Design Considerations

The many engineered design features of the AP600 promote flooding of the containment cavity region and submergence of the RPV lower head and cylindrical section during the very early stages of postulated design basis accidents. The enhanced flooding capability of the AP600 is a result of containment geometry considerations as well as the large, passively injected, safety grade water reservoirs. The absence of penetrations in the RPV's lower head eliminates that potential failure location and failure mechanism which has been given significant attention in safety analyses of traditional vintage LWR's.

The AP600 Passive Core Cooling System (PXS) is designed to assure uninterrupted core heat removal capabilities following postulated events in accordance with NRC and ANSI safety criteria. To satisfy this function the PXS consists of several safety-grade systems capable of supplying water in the quantities indicated in Table 4-1. Water from the various PXS reservoirs serves to maintain water levels above the top of active fuel by injecting directly into the vessel in the short term and by flooding the containment to a level above the top of the hot legs for long term cooling.

During accident conditions, the AP600 containment design directs all primary system liquid effluent, which may include the initial RCS inventory plus that of the various PXS reservoirs, into the IRWST compartment or the reactor cavity. [

[

] (a,c)

Table 4-1

AP600 PASSIVE CORE COOLING SYSTEM WATER INVENTORIES

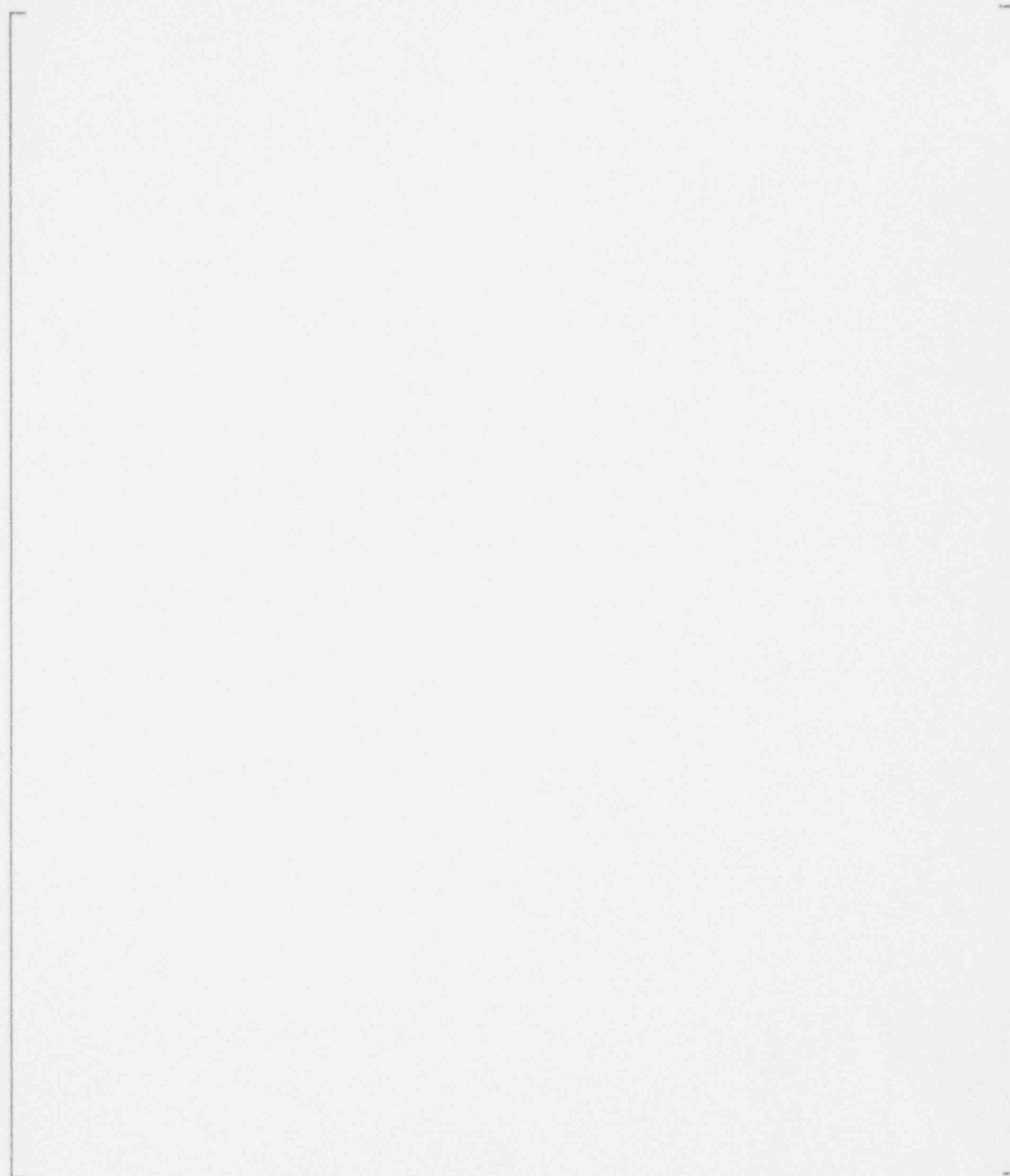
(a,c)

(a,c)

Figure 4-1a AP600 containment isometric view.

(a,c)

Figure 4-1b AP600 containment isometric view.



(a,c)

Figure 4-1c AP600 containment isometric view.

For non-LOCA accident sequences, water drains into the cavity region along a different flow path. For these types of sequences, assuming loss of residual heat removal systems, core decay heat is removed primarily by the discharge of high energy primary system fluid to the IRWST through the reactor coolant system depressurization spargers. [

(a,c)

] Thus, in either scenario depicted above (LOCA or non-LOCA) the AP600 configuration promotes rapid flooding of the reactor cavity region including submerging of the RPV, itself.

(a,c)

(a,c)

Figure 4-2 AP600 reactor cavity flooding from refueling canal.
(Note: IRWST drain lines not shown; Ref. Westinghouse 1992d)

The full range of cavity flood heights as a function of water volume discharged into the steam generator and reactor cavity compartments is provided in Figure 4-3 for LOCA-type sequences. These flood heights are based on the containment geometry as specified in [Westinghouse, 1991]. Cavity flooding during non-LOCA sequences with failure to inject the IRWST contents is discussed below.

Postulated accident sequences leading to core damage in the AP600 preclude the successful operation of all PXS systems. Thus, it is instructive to examine the minimum set of PXS components which must deliver their water inventories to the containment to submerge the reactor vessel and achieve sufficient ex-vessel cooling so as to prevent RPV failure. As mentioned previously, the maximum heat flux to the RPV shell occurs at the top of the debris bed. So, to achieve adequate external heat removal at this point, the RPV shell must be submerged to at least the level of the top of the debris pool. [

For non-LOCA sequences with failure to inject the IRWST, two possible cavity flood heights can be calculated depending on the status of the ADS system. A best estimate success criteria calculation provided in [Westinghouse, 1992d] assumes partial operation of the ADS system which allows approximately half of the RCS inventory to be sparged through the IRWST. The resulting thermal expansion of the IRWST pool is [(a,c) The most conservative assumption is complete failure of the ADS system and no thermal expansion of the IRWST pool. Thus, the conservative non-LOCA calculation has more hold up in the IRWST and a lower cavity flood level. Table 4-2 contains non-LOCA results for the conservative case only since this would bound the best estimate, non-LOCA case. As shown, cavity flooding

(a,c)

Figure 4-3 AP600 containment flooding.

Table 4-2
AP600 NON-LOCA CAVITY FLOOD HEIGHT WITHOUT
IRWST THERMAL EXPANSION

(a,c)

sufficient to prevent downward vessel failure cannot be achieved even with the injection of both accumulators and both CMT's due to the holdup in the IRWST and refueling canal.

Although the above calculations assume failure of the IRWST to inject into the vessel, operator actions could be performed to drain the IRWST contents directly into the containment. The motor operated valves isolating this flow path would be opened by the operators when they receive indication that core damage was imminent or had occurred. These actions would result in submerging of the RV lower head if such a configuration had not yet been achieved and would provide a long term recirculation path between the IRWST and cavity region to ensure continued ex-vessel cooling. So, under almost any circumstances sufficient water could be delivered to the AP600 containment to provide adequate external cooling of the RPV.

The final aspect of the AP600 design to consider for external vessel cooling purposes is the time required to achieve a flooded cavity configuration. For LOCA-type sequences or sequences where early PXS injection (i.e., prior to core uncover) occurs, a substantial portion of the RPV lower head and cylindrical section would become submerged by the cavity water pool well before slumping of molten core debris into the lower head. This would provide the maximum benefit to the vessel from external cooling mechanisms and timing of cavity flooding relative to the timing of core melt and relocation would not be an issue. In other instances, such as non-LOCA sequences with PXS injection failure, cavity flooding would not be initiated until the IRWST drain lines could be opened by operator actions. For these cases, the timing of cavity flood up and submergence of the RPV lower head relative to the timing for core damage and relocation requires further consideration. The plant parameter (indication) to be used to initiate IRWST injection by operator action still remains to be selected. It should be selected such that the expected time before debris relocation into the lower plenum is less than the cavity flood up time to submerge the lower head.

Direct flooding of the reactor cavity region by IRWST injection (i.e., without first injecting into the RPV or spilling into the refueling canal) can be achieved by [

](a,c) Once these lines are opened, the static head of the IRWST pool will drive flow through the drain lines and discharge into the steam generator compartments at the [(a,c) elevation. The discharge can then

flow along the steam generator compartment floors and into the cavity region via the cavity manway.

Figure 4-4 summarizes calculations presented in [Westinghouse, 1992a and 1992b] for cavity flooding due to IRWST discharge through various combinations of the [

](a,c) lines. The data is presented in Figure 4-4 by conservatively assuming dry cavity conditions prior to the opening of the MOV's on the [](a,c). This data is also presented without accounting for void effects which could substantially increase the submerged length of the vessel. As expected, discharge only through the [](a,c) only requires the longest time to sufficiently submerge the reactor vessel while simultaneous discharge through both lines results in the most rapid flooding situation. Depending on which combinations of drain lines are open, the vessel can be submerged up to the expected maximum debris depth in as little as approximately [](a,c) or as long as approximately [](a,c) given an initial cavity water level of zero.

The timing of the manual actuation of the IRWST drain lines will depend upon the plant parameter selected for the initiation signal and the specific accident sequence. The accident sequence will depend upon the degree of successful operation of the several PXS injection sources. These variables will establish the timing and amount of debris that may be relocated to the lower plenum. The initiation signal parameter should be selected to cause external flooding of the lower head prior to relocation of a significant mass of debris. For some LOCA cases (see Appendix A) as little as approximately [](a,c) may pass between core uncover and the on-set of relocation of debris to the lower plenum. If another initiation parameter, such as core exit temperature or hot leg gas temperature, were selected then debris relocation could occur in even less time [](a,c). Hence, if only the [

](a,c) were used, the water level in the cavity would only increase a foot or two before debris entered the lower plenum. However, for the LOCA case, a significant water level would already exist in reactor cavity when the IRWST drain was manually initiated. Hence, even for such an extreme condition, it is expected that the AP600 design would cause the lower plenum to be submerged prior to significant quantities of debris entering the lower plenum. Clearly, if the [

](a,c) line or both operate, the cavity flood rate will be much larger and assure lower plenum submergence.

(a,c)

Figure 4-4 AP600 cavity flooding based on IRWST discharge through 10" and 4" drain lines.

For non-LOCA sequences (such as blackouts, loss of feedwater, etc.) a longer interval exists between core uncover and debris relocation to the lower plenum. Thus, although the cavity water level may be essentially zero at the time of manual initiation of the IRWST drain, the lower plenum can be submerged prior to debris relocation.

In addition to submerging the lower portions of the vessel lower head, continued feed from the IRWST directly into the containment will result in flooding of the cavity up to and beyond the cold leg nozzles at the 102'8" elevation. [

(a,c)

] Although submerging the vessel up to the cold leg nozzles could remove significantly more energy from the vessel than submerging just the lower head (possibly 100% of the debris decay heat generation would be removed in this extended flooding situation), this will not impact the potential of the ex-vessel cooling mechanisms to prevent lower head failure for the cases discussed previously.

4.2 AP600 RPV Cooling Analysis

The methodology described in Section 3 is applied to the AP600 specific geometry in this section. In particular, the melt superheat in the pool is calculated which can then be used to determine the average and peak downward heat fluxes to the RPV wall. These are then compared with the boiling heat transfer heat fluxes in the CEC sponsored experiments. [

(a,c)

[

(a,c)

Hence, the total calculated downward energy transfer is about [

](a,c) Since this value is much less than those observed in the experiments, there is no limitation to the heat removal capabilities on the vessel outer surface.

[

(a,c)

Of course, the minimum heat flux, $q_{d,min}$, is directed at the very bottom of the vessel and the experimental results [Gabor, 1980b] and [Jahn, 1987] indicate that it is approximately one-half the average heat flux. Thus, we infer

All of these are well within the values which could be removed by nucleate boiling on the vessel's outside surface. Hence, the vessel lower head, once submerged in a water pool, would not be anticipated to experience a lack of heat removal capability.

Given that the external surface of the RPV is submerged and provides the desired cooling and decay heat removal, the ability of the reactor cavity configuration to release steam generated in the external water pool must be assured. This has been recognized in other assessments of the feasibility of in-vessel melt rejection by external flooding. For example, such an approach is the cornerstone of the accident management program being employed at the Loviisa plant [Tuomisto, 1991]. For that given plant's decay power level and plant configuration the lower head requires a significant vapor venting capacity around the vessel-cavity annulus. Hence, in order to assure the effectiveness of in-vessel melt retention by external cooling, specific actions have been identified and provided for in the Loviisa plant design to ensure an adequate vent path for the steam such that the stability of the natural circulation cooling path can confidently be expected. An assessment of the steam generation rate and implied venting requirement for the AP600 plant is provided below.

(a,c)

(a,c)

Applying the methodology of Section 3.0 to the AP600 design results in heat fluxes to the vessel wall which would readily be removed by nucleate boiling on the outer RPV surface. Consequently, those sequences with a submerged RPV lower head at the time of debris relocation to the lower plenum would be expected to retain the debris within the vessel.

5.0 UNCERTAINTIES

Since the AP600 design incorporates only top entry reactor vessel penetrations, the single largest uncertainty in the external cooling assessment has been removed. Questions pertaining to the performance of in-vessel penetrations in direct contact with molten core debris are no longer an issue of concern. There are, however, lesser uncertainties in the assessment which should be considered. These are, namely, the timing and degree of reactor vessel submergence relative to the onset of core melt and the possibility of creep-induced failures in the reactor coolant loop piping.

Non-LOCA sequences with ADS failure would require operator actions to open motor operated valves on the IRWST drain lines in order to initiate flow from the IRWST into the containment. Based on operator instructions, these actions would not occur until some time after core uncover, resulting in a delayed flooding of the cavity and submerging of the vessel. This is in contrast to the majority of postulated core melt sequences where primary system break flow (for LOCA type sequences) or successful injection of PXS components result in early cavity flooding.

For some cases where only the [](a,c) is opened to allow IRWST flow into the cavity, the reactor vessel may not be submerged until after core uncover. Best estimate calculations presented in Section 4.1 for this limiting case indicate that sufficient flooding to prevent vessel failure would exist. However, the portion of the vessel which would be submerged at the time of debris relocation to the lower head would be affected by the timing of operator actions and the debris relocation rate. Depending on the exact configuration for such a delayed flooding scenario, the sequence progression could be impacted by:

1. increased thermal stress on the reactor vessel shell;
2. the development of a film boiling regime as the rising cavity water level comes in contact with portions of the reactor vessel shell at elevated temperatures;

3. debris attack on portions of the vessel wall not submerged in the cavity water pool leading to a localized, creep-induced vessel failure.

Possible impacts on the source term analysis can be envisioned for the extreme case of vessel failure as well as for the cases of elevated shell temperatures. Vessel failure would remove a key fission product barrier and necessitate the consideration of a spectrum of ex-vessel phenomena resulting from high pressure melt ejections. As for elevated shell temperatures, the in-vessel airborne fission product concentration would likely increase due to increased volatilization of deposited fission products.

For sequences with adequate, external cooling of the vessel lower head, but limited cooling around the upper regions of the vessel, heating of the RCS piping may occur from radiation off the debris pool, convection from circulating gases, and conduction from heat generating fission products deposited on these surfaces. Creep-induced failures resulting from this added heat load on localized surfaces would only be a concern, however, for sequences with elevated primary system pressures (i.e., non-LOCA sequences with ADS failures), and even then only if wall temperatures exceeded about 1340°F (1000 K).

The degree to which the vessel is submerged following core relocation and the timing of vessel submergence will dictate the maximum vessel wall and RCS piping temperatures. Thus, high pressure core melt sequences considered in the AP600 risk analysis with delayed or limited cavity flooding should be examined individually to determine the potential for creep failures of the RCS boundary away from the lower head region.

Since any induced failures of the RCS boundary would allow fission products to bypass the IRWST, these failures would have a significant impact on the AP600 source term analysis. Furthermore, the combined effects of high primary system heat sink temperatures coincident with the onset of creep failures and the reduced primary system pressure following failure would result in significant fission product revaporization rates. This consequence of creep rupture failures would also impact the AP600 source term analysis.

Both uncertainties discussed above (timing and degree of vessel submergence, and creep rupture failures at the RCS boundary) could be favorably influenced by considering the effects of steam voids on the cavity water level and steam cooling of the reactor vessel at elevations above the water line. Although not included in the current external cooling assessment, consideration of these two additional cooling mechanisms could further reduce the already small influence of the aforementioned uncertainties on the AP600 risk analysis.

6.0 ACCIDENT MANAGEMENT IMPLICATIONS

For severe core damage events, external cooling of the RPV lower head has more impact on accident management considerations than any other individual phenomena except for direct water addition to the debris. This is particularly important for the AP600 risk analysis since many accident sequences considered would result in PXS injection and water accumulation in the reactor cavity. With this water accumulation, the lower RPV head and a substantial fraction of the vessel cylindrical section would be submerged. Experimental and analytical information presented in this paper demonstrate that debris could be retained in the lower head should it slump into the lower plenum as was the case in the TMI-2 accident. Hence, the best estimate evaluation of such accident scenarios is that debris would be retained within the lower plenum.

This insight is directly relevant to accident management strategies. In particular, should an accident condition progress to the point of significant core damage, the submergence of the lower head would provide an additional method for protecting the containment and for removing heat from the core debris. Flooding the reactor cavity would be tremendously influential, since cooling of the core debris would be accomplished in all cases. However, the facet of major importance for accident management would be to terminate the debris progression and retain the material in a stable configuration within the RPV lower plenum. This would minimize the threat to the existing fission product boundaries (particularly the containment). It would also remove the ex-vessel phenomena from consideration, minimize the fission products released from the core material and extend the accident progression (thus providing additional time for recovery actions to be implemented). Steam generated by boiling off the vessel outer surface would be easily condensed by the passive containment cooling systems incorporated into the AP600 design.

As mentioned earlier, the TMI-2 vessel wall heat up was considerable. This could be prevented by external cooling. Thus, if severe core damage conditions are detected, water should be added both to the RPV and the containment to submerge the RPV lower head. The first would directly cool the debris and the second would maintain the vessel wall integrity should molten debris drain into the lower plenum.

In summary, this action of submerging the lower head and a substantial fraction of the RPV cylinder could result in complete termination of the accident progression, the development of a safe stable state and the preservation of the remaining (containment) fission product boundary. These are the fundamental goals of accident management strategies.

7.0 SUMMARY

An analysis to determine the potential for external cooling of a reactor vessel during core melt conditions has been performed based on the proposed Westinghouse AP600 advanced light water reactor design. This analysis concludes that the AP600 design features a high likelihood, during any credible accident sequence, of submerging the reactor vessel in a containment water pool to a sufficient depth so as to remove decay heat transferred to the vessel lower head. This is a significant attribute of the AP600 design since maintaining lower head integrity mitigates consequences resulting from the phenomenological process associated with ex-vessel debris distribution and core concrete attack -- a major step in terminating the accident progression.

8.0 REFERENCES

- Bates, J. L., McNeilly, C. E. and Rasmussen, J. J., 1971, "Properties of Molten Ceramics," in Materials Science Research, Vol. 5 - Ceramics in Severe Environments, (W. W. Kriegel and H. Palmoun, Eds.), Proc. 6th Univ. Conf. Ceramic Sci., N. Carolina State University, Raleigh, NC, (December 7-9, 1970), Plenum Press, New York.
- Condon, W. A., Greene, S. R., Herrington, R.M., Hodge, S. A., 1982, "SBLOCA Outside Containment at Browns Ferry Unit One - Accident Sequence Analysis," NUREG/CR-2672, ORNL/TM-8119.
- DOE, 1991, "Passive ALWR Requirements to Prevent Containment Failure," DE-ACO7-76ID01570.
- EPRI, 1990, Advanced Light Water Reactor Requirements Document, Volume III Utility Requirements for Passive Plants, Palo Alto, California.
- Epstein, M. and Fauske, H. K., 1989, "The Three Mile Island Unit 2 Core Relocation - Heat Transfer and Mechanism," Nuclear Technology, Vol. 87, pp. 1021-1035.
- Gabor, J. D., Baker, Jr., L., Cassulo, J. C., Erskine, D. J. and Warner, J. G., 1991, "Heat Transfer to Curved Surfaces from Heat Generating Pools," J. Heat Transfer, Vol. 102, pp. 519-524.
- Henry, R. E., Burelbach, J. P., Hammersley, R. J., Henry, C. E. and Klopp, G. T., 1991, "Cooling of Debris Within the Reactor Vessel Lower Head," to be presented at the ANS Topical Meeting, June, 1991.
- Jahn, M. and Reineke, H. H., 1987, "Free Convection Heat Transfer with Internal Heat Sources, Calculations and Measurements," Proc. of the 5th Intl. Heat Transfer Conf., Tokyo, Paper NC 2.8.
- Mayinger, F., et al., 1976, "Examination of Thermalhydraulic Processes and Heat Transfer in a Core Melt," BMFT RS 48/1, Institute fur Verfahrenstechnik der T. U. Hanover.
- O'Brien, J. E., Hawkes, G. L., 1992, "ARSAP AP600 in-Vessel Coolability Thermal Analysis Final Report," EG&G-NE-XXXX.
- Park, H., Dhir, V. K., 1991, "Effect of Outside Cooling on the Thermal Behavior of a Pressurized Water Reactor Lower Head," 27th ASME/AIChE/ANS National Heat Transfer Conference, Minneapolis, Minnesota.
- Thinnes, G. L. and Moore, R. L., 1989, "Comparison of Thermal and Mechanical Responses of the Three Mile Island Unit 2 Reactor Vessel," Nuclear Technology, Vol. 87, pp. 1036-1049.

- Tong, S. L., 1968, "Core Cooling in a Hypothetical Loss of Coolant Accident Estimate of Heat Transfer in Core Meltdown," Nuclear Engineering and Design 8, North-Holland Publishing Company, Amsterdam.
- Tuomisto, H., Theofanous, T. G., 1991, "A Consistent Approach to Severe Accident Management," Specialist Meeting on Severe Accident Management, Rome, Italy.
- Westinghouse, 1991, John Spaargaren, "AP600 Plant: 11 Node Parameter File for MAAP4", Rev. 3 (December 20, 1991).
- Westinghouse, 1992a, V. Srinivas letter to R. Hammersley (February 7, 1992).
- Westinghouse, 1992b, V. Srinivas letter to R. Hammersley (February 10, 1992).
- Westinghouse, 1992c, V. Srinivas transmittal to R. Hammersley, AP600 Reactor Vessel Sectional and Plan Views (April 1, 1992).
- Westinghouse, 1992d, "Success Criteria for External Cooling and Debris Coolability for AP600 Level II PRA", Calcnote CN-PRRA-92-161-R0.
- Westinghouse, 1992e, R. Hammersley, "Summary of Phone Conversation on AP600", with V. Srinivas (April 7, 1992).

APPENDIX A

MAAP 4 Analysis of External Cooling
of the RPV for the AP600 Design

AP600 MAAP ANALYSIS SUMMARY

Sequences

L1_COOL - large LOCA
 S2_COOL - small LOCA
 T0_COOL - transient with medium LOCA

Parameter Files

John Spaargaren, "AP600 Plant: 11 Node Parameter File of MAAP4," Rev 3
 (December 20, 1991).

Note: Input decks contain local parameter file changes to core the UO_2 and Zr initial

(a,c)

Plot Files

L1_COOL_78.PLT - PS & CNTMT T/H Response

MCMTPS - Mass of corium in lower head
 MWPS - Mass of water in PS
 ZWRB(i) - Water level in CTMT Node i
 PRB(i) - Pressure in CTMT Node i

L1_COOL_76.PLT - Primary System Heat Sinks

TBH(i,j) - Broken hot leg temp (K) in axial node i, radial node j
 TBHT - Broken loop hot side S/G tubes
 TRV - Reactor vessel temps from bottom of lower head
 (TRV(1,1)-TRV(1,5) to RV flange (TRV(5,1)-TRV(5,5))

AP600 MAAP ANALYSIS SUMMARY

<u>Node</u>	<u>Description</u>
1	SG Room 1 (Broken Loop)
2	SG Room 2 (Unbroken Loop)
3	Lower Compartment (CMT areas, ACC, CVCS, PRZ Rooms)
4	Cavity
5	IRWST Room
6	Upper Compartment Cylinder
7	Upper Compartment Annulus
8	Upper Compartment Dome
9	PCCS Dome
10	PCCE Annulus
11	Electrical Penetration Area (Auxiliary Building)

(a,c)

FAI/92-11

PHENOMENOLOGICAL EVALUATION SUMMARY
ON
MOLTEN CORE-CONCRETE INTERACTION
IN SUPPORT OF
AP600 PLANT RISK ANALYSIS

Submitted To:

Westinghouse Electric Company
Pittsburgh, Pennsylvania

Prepared By:

Fauske & Associates, Inc.
16W070 West 83rd Street
Burr Ridge, Illinois 60521

May 1992

ABSTRACT

Phenomenological issues on molten core-concrete interaction (MCCI) have been examined in support of the AP600 Risk Analysis. The approaches taken were (1) to synthesize MCCI knowledge from experimental data, computer codes and analytical tools, and (2) to develop a failure criterion to determine if such a postulated phenomena could challenge containment integrity of the AP600 design.

For the AP600, basemat penetration due to molten corium-concrete interaction is a postulated containment failure mechanism. The likelihood of this containment failure mechanism occurring is extremely remote for the AP600 design. For all credible accident scenarios, the core debris will be retained within the vessel, or a sufficient water inventory will be available in the reactor cavity to quench debris released after vessel failure. If molten core debris breaches the reactor vessel and contacts concrete surfaces, molten corium-concrete interaction can occur. For the AP600 design, MCCI would most likely occur (if it occurs at all) in the cavity region of the containment. MCCI will erode concrete in both the sideward and downward directions, but a failure criterion is based on the downward direction because the downward erosion speed is faster than the sideward erosion speed. The containment is considered failed when the depth of concrete erosion is equal to the combined depth of the cavity floor and the containment basemat.

To estimate the extent of concrete erosion with time, a technique suitable for hand-calculations is presented along with experimental and analytical results relevant to MCCI. This technique expresses conservation of mass and energy for MCCI and proceeds in a piecewise fashion to account for changes in core debris and chemical phenomena in time. The technique is used to find the following: the time interval during which the zirconium in the debris pool is being oxidized, the depth of erosion during the zirconium oxidation phase, and the time to containment failure by MCCI. Inputs to the calculation technique stem from the analytical and experimental results presented herein. Appropriate physical properties required for MCCI

calculations (densities, specific heat, etc.) are tabulated herein. Other parameters, most notably the sideward erosion rate to downward erosion rate ratio, are assigned values based upon the BETA and SWISS test series described here. The AP600 parameter file is used to provide values for the geometry of the cavity and the corium debris itself. Calculations were performed with this technique for the "dry" case where the debris cannot be covered permanently by an overlying pool.

Based on these calculations, MCCI can be excluded as a containment failure mechanism, relative to other containment failure mechanisms. For the case where the debris is permanently covered, MCCI would be halted by water ingress into the debris bed. For dry cases, the predicted failure times are so long that sufficient recovery actions will be taken to establish an overlying pool in the cavity and halt concrete ablation.

TABLE OF CONTENTS

	<u>Page</u>
ABSTRACT	i
1.0 PURPOSE	1-1
2.0 PHENOMENA	2-1
2.1 Description	2-1
2.1.1 Physical Processes	2-2
2.1.2 Relationship to Containment Failure Mechanisms and Modes	2-4
2.1.3 Relationship to Source Term	2-4
2.2 Experimental Results	2-5
2.2.1 SWISS: Sustained Heated Metallic Melt/ Concrete Interaction With Overlying Pool	2-6
2.2.2 BETA: Large Scale Metal/Oxide Interaction Experiments	2-6
2.2.3 SURC: Sustained-Urania Concrete Interaction Experiments	2-14
2.2.4 Summary of Experimental Results	2-18
2.3 Analytical Approaches	2-18
2.3.1 CORCON	2-18
2.3.2 WECHSL	2-22
2.3.3 DECOMP	2-23
2.3.4 VANESA	2-24
2.3.5 METOXA	2-24

TABLE OF CONTENTS

(Continued)

	<u>Page</u>
3.0 METHODOLOGY	3-1
3.1 Step 1: Define Failure Criteria	3-2
3.2 Step 2: Determine Overall Time Interval to Exceed Mode Limiting Failure Criterion	3-3
4.0 APPLICATION OF METHODOLOGY TO AP600 POWER PLANT	4-1
4.1 Debris Coolability	4-1
4.2 MCCI Failure Criterion (Step 1)	4-4
4.3 Time Interval to Exceed the Failure Criterion (Step 2)	4-5
5.0 UNCERTAINTY CONSIDERATIONS	5-1
6.0 ACCIDENT MANAGEMENT INSIGHTS AND CONSIDERATIONS	6-1
7.0 CONCLUSIONS	7-1
8.0 REFERENCES	8-1
APPENDIX A: Derivation of Concrete Erosion Calculations	A-1
APPENDIX B: Code Input and Calculations	B-1
APPENDIX C: MCCI Calculation Source Code	C-1

LIST OF FIGURES

<u>Figure No.</u>		<u>Page</u>
2-1	The SWISS experimental apparatus	2-7
2-2	BETA experimental apparatus	2-9
2-3	Results of the BETA V1.8 experiment	2-12
2-4	Results from the BETA V2 experiments series	2-13
2-5	SURC-4 experimental apparatus	2-16
2-6	SURC-3 experimental apparatus	2-17
4-1	AP600 cavity elevation drawing	4-2
4-2	AP600 containment isometric view of cavity and loop compartment	4-3

LIST OF TABLES

<u>Table No.</u>		<u>Page</u>
2-1	BETA Experimental Matrix	2-10
2-2	SURC Test Matrix	2-15
2-3	Summary of Selected Core-Concrete Interaction Experiment Initial Conditions	2-19
2-4	Observed Eroded Concrete Depth and Mass	2-20
3-1	Molten Core-Concrete Interaction Calculation Data	3-4

1.0 PURPOSE

The potential failure of a containment building due to molten core debris attack on its concrete floor has been a subject of concern for the Nuclear Regulatory Commission (NRC) Staff since the Reactor Safety Study [NRC, 1975] identified it as the mechanism for two possible containment failure modes. One concern is that molten core debris ejected from a failed reactor vessel would come into contact with the containment floor and eventually erode a large enough volume of concrete that either the reactor cavity walls would lose their load-carrying capability or the basemat would be penetrated and core debris would exit the containment. Also, debris attack would generate steam and noncondensable gases that would contribute to the potential for containment failure by over-pressurization.

Advanced light water reactor (ALWR) requirements [DOE, 1991] provide directives for addressing these concerns and mitigating the effects of MCCI during AP600 severe accident scenarios. The objective of this paper is to demonstrate how the AP600 design meets the ALWR requirements with respect to MCCI. In this paper, only containment failure due to concrete ablation during MCCI is considered. Overpressurization caused by noncondensable gases generated during MCCI is not considered here.

2.0 PHENOMENA

2.1 Description

Thermal attack of structural concrete in a containment building can occur during a core melt sequence if the molten core debris breaches the reactor vessel and contacts the concrete surfaces in the containment building. In a PWR plant, the concrete surface that experiences the most severe thermal attack typically is the cavity floor. The interfacial heat transfer between the core debris and concrete drives the thermal decomposition and erosion of the concrete. The thermal attack on the concrete can be broken up into three different phases: a short-term, localized attack as debris leaves the reactor pressure vessel; an aggressive attack by high-temperature debris immediately after the core material is released from the primary system; and a long-term attack in which the debris temperature would remain essentially constant and the rate of attack is determined by the internal heat generation.

Immediately after vessel failure, debris is discharged from the vessel into the reactor cavity. This material, which may be molten, induces an aggressive localized jet attack upon the concrete surface, given the absence of water in the cavity. A pool in the cavity could greatly mitigate this attack, depending upon its depth. The thermal attack is localized to the area below the failure. Estimates of this attack based on analyses in [IDCOR, 1985] show the depth to be 4 to 8 inches (10 to 20 centimeters), depending upon the primary system conditions at vessel failure.

After the jet attack, the reactor cavity floor region may be covered by high-temperature debris which aggressively attacks the concrete substrate. Free water, bound water, and gases generated by concrete decomposition are then released. The gases stir the melted material and promote convective heat transfer between this material and the concrete. The combination of the sensible heat added to the concrete, the endothermic chemical reactions involved in releasing water vapor and decomposing the concrete, and the latent heat of fusion for melting the substrate extracts a considerable amount of energy from the high-temperature melted material. In fact, the

aggressive attack generally requires more energy than is generated by the decay power. Such additional internal heat generation can result from the oxidation of metallic constituents within the melted material by the steam and possibly by carbon dioxide released from the concrete substrate. Typically, the high-temperature, aggressive attack is driven by internal heat generation and secondly, to a lesser extent, by the initial stored energy.

During the long-term attack, the debris remains at an essentially constant temperature, and the rate of attack is determined by the difference between the internal heat generation and the heat losses to the containment environment. Without water, these heat losses are principally due to convection and radiation, and are somewhat influenced by the natural convection of high-temperature gases throughout the containment. The resulting concrete attack rate is much reduced from that typical of the high-temperature attack phase and occurs over a much longer interval. The noncondensable gases generated during this period contribute to long-term overpressurization of the containment.

2.1.1 Controlling Physical Processes

The major physical phenomena affecting the extent of concrete erosion by core debris are closely interrelated and therefore difficult to separate. For the purpose of this discussion, these phenomena are identified as follows: rate and amount of core debris expulsion from the reactor vessel; melt-water dynamic interaction and melt spreading; configuration of the debris mass on the concrete; depth of the melt bed; and the quenching effect of water. The following are brief discussions of how the controlling phenomena influence this issue.

The core debris flow rate from a failure in the bottom of the reactor vessel determines the initial velocity with which the melt spreads. As the initial spreading rate decreases, there is an increase in the time for heat transfer from the melt to the concrete floor and, if present, overlying water pool. Thus, the initial spreading rate and the energy losses from the melt influence the extent of initial melt spreading.

The initial extent of melt spreading is also very dependent on the effects of the water/debris dynamic interaction on the heat transfer from the molten debris. If the interactions between the melt and water cause the debris to disperse, or cause violent oscillations at the melt-water interface, these interactions might lead to heat transfer rate far in excess of heat transfer rates associated with critical heat flux boiling. If not, the melt-water interface would undergo film boiling rather than nucleate boiling.

After the molten debris has initially spread out, two types of debris configurations are possible: a discontinuous porous debris bed composed of discrete particles; or a continuous slab of partially molten pool. The debris bed configuration has been shown to occur when sufficient water is available to quench the debris as it leaves the reactor vessel. Otherwise, a continuous slab configuration typically occurs because there is less water available than would be necessary to ensure debris fragmentation. It is possible that a debris bed can evolve into a continuous debris slab. If the porosity in the bed limits the bed dryout heat flux below decay power heat removal requirements, the debris bed would heat up and eventually melt into a continuous debris configuration. The debris configuration strongly affects the quenching capability of overlying water.

The depth of the debris also affects how effectively energy is removed from the debris. If it is postulated that the initial debris layer is so thick that the rate of heat removal from the debris is exceeded by the internal heat generation rate, then the debris would reheat and ultimately remelt. Further spreading of molten or partially molten debris would then occur, aided by gas agitation from concrete erosion if the concrete were sufficiently heated. The debris would spread until the heat removal rate was sufficient to freeze it, or was constrained by the cavity. In [NRC, 1988], the NRC has stated that a debris layer less than 10 in (25 cm) in depth may be considered to be coolable.

The last phenomena to discuss is the quenching effect of water. For a debris bed, the physical mechanism of cooling is water ingression into the bed with overflow of steam from the bed. The coolability limit for debris beds is a hydrodynamic limitation within the bed itself that

strongly depends on the porosity, and is fairly independent of the debris bed depth. For a thin debris slab or shallow pool, conduction is an effective heat transfer mechanism and the slab can cool quickly with little or no cracking. However, for a thicker slab or deeper pool, coolability requires cracking of the slab or overlying crust and ingress of water into the debris. Such cracking would be expected to occur as a result of the volume reduction associated with debris cooling and phase change, as well as sparging of offgases produced by any thermal attack of concrete.

2.1.2 Relationship to Containment Failure Mechanisms and Modes

Extensive erosion of concrete by high-temperature core debris is a potential late containment failure mechanism that would be expected to occur many hours after reactor vessel failure and debris release into the containment. Three actual failure mechanisms are considered possible as a result of concrete erosion: penetration of the containment base mat, sufficient deterioration of the load-carrying capability of the cavity walls that the reactor vessel moves and causes gross mechanical failures of penetrations for piping connected to the reactor vessel, and failure by pressurization due to the production of non-condensable and condensable gases during concrete ablation. The first two of these containment failure mechanisms would be expected to result in large containment failure areas (on the order of several square feet).

2.1.3 Relationship to Source Term

Long-term molten core-concrete attack leading to containment failure influences the expected fission product release for a sequence by providing a large gas and/or corium flow path out of the containment long after vessel failure. The effect on the source term, however, depends on the presence of water in the cavity during a sequence prior to containment failure. For a dry sequence, since the airborne fission product concentration in a closed containment tends to decay with time due to naturally-occurring fission product retention mechanisms, a late containment failure due to MCCI generally results in modest source terms, relative to early failures. For gross mechanical failures of containment penetrations, however, the relatively large expected failure

size assures a rapid blowdown of the initially available airborne fission products to the environment. Fission products entering the containment atmosphere after the blowdown would experience little driving force from the containment. Thus, fission products evolved by long-term revaporization within the reactor vessel would be subject to the naturally-occurring deposition mechanisms in the containment. Fission products released ex-vessel during MCCI would also be subject to the same deposition mechanism.

Basemat penetration by MCCI is a late containment failure mode that leads to a large failure area. A rapid blowdown is not assured because the soil underneath the basemat provides an obstructed release path. This also results in a very different offsite consequences, relative to other containment failure modes, because the release is to underlying soil rather than the atmosphere. Soil provides a very effective fission product scrubbing, although a basemat failure could potentially contaminate the local water table.

For a wet sequence, the expected fission product source term would be reduced relative to a dry sequence due to the capture of fission product aerosols by the overlying pool.

2.2 Experimental Results

A wide variety of molten debris-concrete interaction experiments have been performed at Sandia National Laboratory (SNL) and Kernforschungszentrum Karlsruhe (KfK). In general, these experiments were undertaken to validate models and understanding of MCCI phenomenon. The SNL experiments considered either initially metallic or oxidic melts. Metallic experiments at SNL were usually performed with a stainless steel melt charge, while oxidic experiments were performed with a uranium dioxide and zirconium dioxide melt charge. Two SNL tests have employed both oxides and zirconium metal. The KfK BETA series of experiments featured stainless steel and concrete oxide melt charges.

2.2.1 SWISS: Sustained Heated Metallic Melt/Concrete Interaction with Overlying Pool

A schematic representation of the SWISS experimental apparatus is shown in Figure 2-1. The SWISS experiments performed at SNL consisted of two test runs designed to observe the effect of an overlying pool on MCCI. The SWISS-1 test involved 99.2 lb (45 kg) of stainless steel initially at 3005.6 F (1925 K) inductively heated over a period of about 40 minutes with one power interruption [Bloese, 1987]. An average of about 0.205×10^5 Btu/h (60 kW) net power was input to the melt charge by the induction source. About 32 minutes after the melt was teemed into the crucible, water was poured over the melt. Erosion was essentially one-dimensional, downward into a 8.5 in (21.6 cm) diameter limestone-common sand concrete plug, because a non-ablating MgO sidewall was used. A value of 95099 Btu/h-ft² (300,000 W/m²) was suggested as an average sideward heat flux lost to the MgO crucible walls. The concrete was a limestone-common sand variety essentially identical to a default type used on the CORCON code [Muir, 1981] and typical of many U.S. plants.

Test SWISS-2 was similar to test SWISS-1 except that water was continuously poured onto the debris immediately after the melt teem and two power interruptions occurred. A value of 63400 Btu/h-ft² (200,000 W/m²) heat flux to the MgO sidewall was suggested on the sideward heat losses.

2.2.2 BETA: Large Scale Metal/Oxide Interaction Experiments

The BETA test series consisted of a series of large-scale metallic melt experiments conducted at KfK research center [Alsmeyer, 1986]. These experiments were originally conceived and designed to provide reliable experimental data for verification of severe accident programs, such as the WECHSL code [Reimann, 1981].

The BETA tests typically consisted of large, high temperature metallic melts, initially at 3632°F (2000°C) or higher, produced by thermite reaction. These melts were usually poured

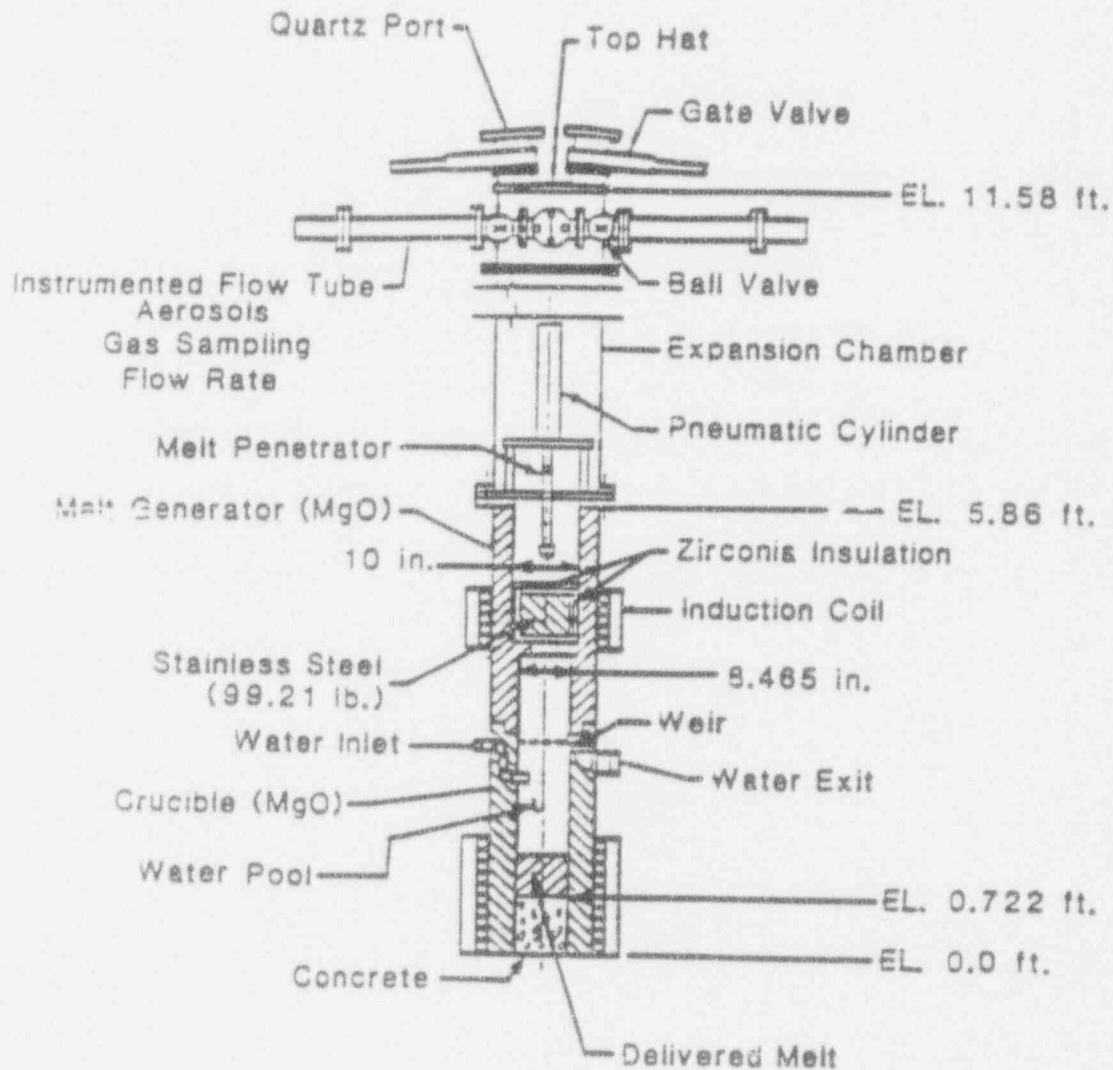


Figure 2-1 The SWISS Experimental Apparatus.

into an instrumented siliceous concrete crucible of 15 in (0.38-m) inside diameter (see Figure 2-2). The interactions were sustained by inductive heating. The BETA experimental facility has the capability to supply up to 6.48×10^6 Btu/h (1.9 MW) of inductive heating power, which allowed observations of the various physical and chemical processes occurring during molten melt-concrete interactions for an extended period of time under quasi-steady state conditions. Typical melt charges in the BETA tests were composed of 661.4 lbm (300 kg) of steel and 330.7 lbm (150 kg) of oxides. The steel components typically included Fe, Cr, and Ni. The oxides used were aluminum oxide (Al_2O_3), silicon oxide (SiO_2), and in some cases calcium oxide (CaO). Table 2-1 summarizes the BETA experiments conducted over the span of two years, from 1984 to 1986. The composition of the silicate concrete utilized in the experiments is somewhat similar to the basaltic concrete variety used in the United States. BETA V3 series was an exception as it employed limestone-common sand and concrete. No fission product stimulants were employed in any BETA tests.

Major results of BETA tests are [Alsmeyer, 1987]:

1. The temperature of the melt pool dropped rapidly from an initial temperature close to 3320.6 F (2100 K) to a temperature slightly above the mixture melting temperature, even when the inductive heating power was very high.
2. The experiments are characterized by the dominance of downward erosion in high power tests, and to a lesser extent in lower power tests.
3. Dispersion or entrainment of the metal layer into an overlying oxide layer was observed in the high power tests. It appears that the process of dispersion is driven by the high gas fluxes evolving from the concrete.
4. When CaO was added to the melt pool, no entrainment of metal into the oxide layer was observed. Apparently, CaO serves to lower the viscosity of the oxide layer, and thus, the metal-oxide layers remained stratified. It is noted

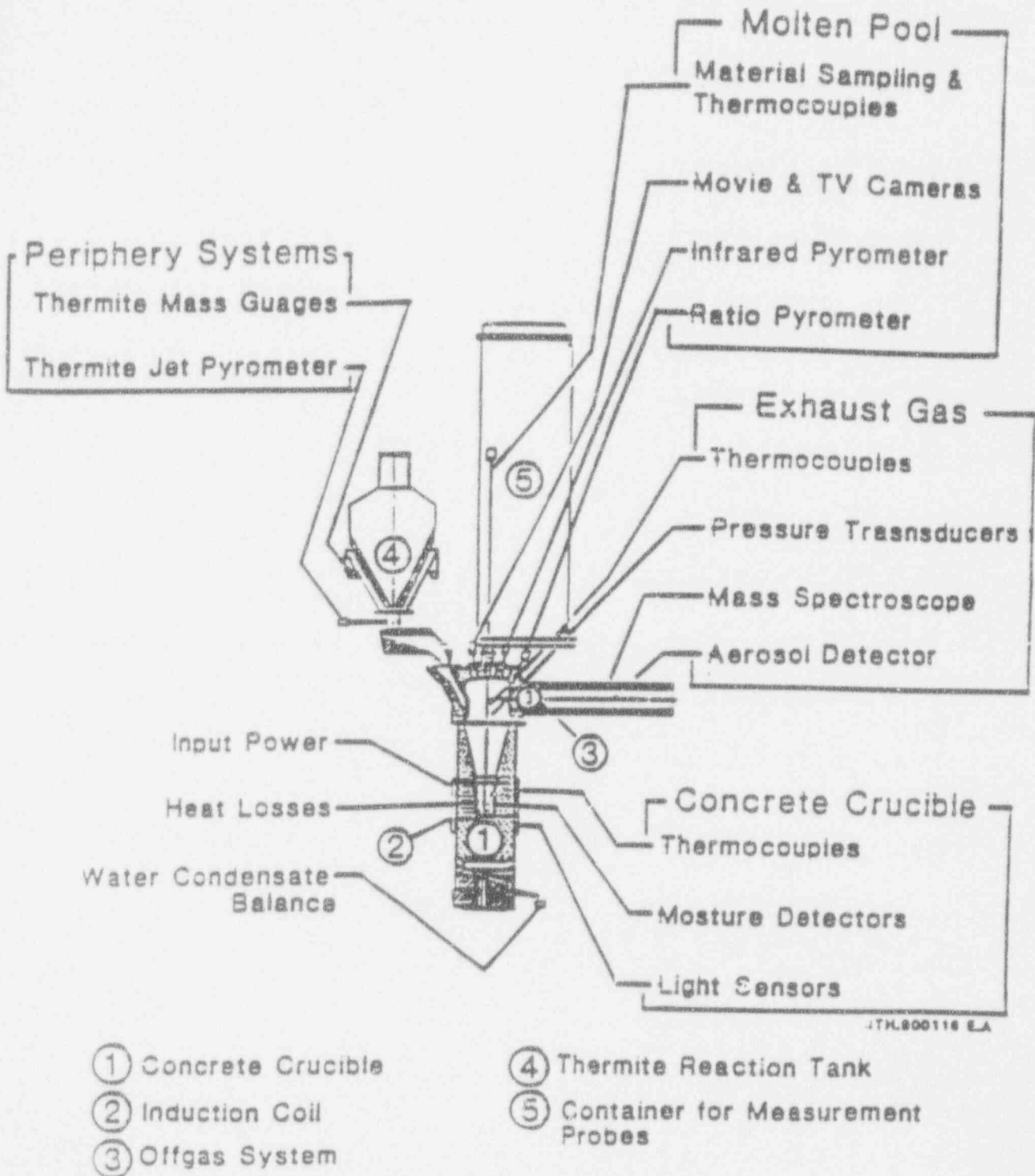


Figure 2-2 BETA Experimental Apparatus.

Table 2-1

BETA EXPERIMENTAL MATRIX

Text	Melt	Power/ (Btu/hr)	Power/kW	Remarks
V0.1	Iron	0	0	Test of Facility
V0.2	Iron	1.36	400	
V0.3	Iron + Oxide	5.80	1700	
V1.1	Iron	Pulsed	Pulsed	Pour failed
V1.2	Iron + Oxide	Pulsed	Pulsed	Lorentz-force excluded
V1.3	Steel + Oxide	3.41	1000	Transient
V1.4	Steel	0	0	
V1.5	Steel	1.54	450	
V1.6	Steel + Oxide	3.41	1000	No dispersion (CaO) CaO added
V1.7	Steel + Oxide	5.80	1700	
V1.8	Steel + Oxide	6.48	1900	
V1.9	Steel + Oxide	1.36-0.68	400-200	CaO added
V2.1	Steel + Oxide	0.41-0.51	120-150	
V2.2	Steel + Oxide	0.17-0.31	50-90	
V2.3	Steel + Oxide	0.82	240	US Lime/Comm Sand, Heating from 0-66 s only
V3.1	Steel + Oxide	5.80-8.53	1700-2500	
V3.2	Steel + Oxide	1.36->3.41 2.05-0.68	400->1000 600-200	
V3.3	Steel + Oxide			US Limestone, 30 min heating US Lime/Comm Sand, 60 min heating
V4.1	Steel + Oxide	3.41-1.02	1000-300	19.685 ft dia crucible

that all low power experiments resulted in separated metal and oxide layers.

In the BETA V1.8 experiment, 6.48×10^6 Btu/h (2900 kW), the highest net inductive heating power of the series was used, corresponding to an internal power density more than a factor of ten higher than that of decay power. A melt charge composed of 771.6 lbm (350 kg) of steel (82% Fe, 10% Cr, 8% Ni) and 286.6 lbm (130 kg) of oxides (70% Al_2O_3 , 30% CaO), produced by a thermite reaction, was poured into the interaction cavity at an initial temperature of 3266.6 F (2070 K). The observed downward erosion rate was approximately 0.04 in/s (1 mm/s), resulting in a total eroded depth of about 15.75 in (40 cm) in 7 minutes. Sideward erosion was stated as only a few centimeters (see Figure 2-3).

Experimental results showed that the chromium metal had oxidized completely in about one minute, and hand calculations indicate that gas evolving only from the concrete floor was insufficient for complete oxidation of the chromium. Thus, gases released from decomposition of the sidewall must have entered the debris pool and contributed to chromium oxidation.

The oxide layer was observed to be clearly separated from the metal layer and well mixed with concrete slag, thus entrainment of metal into the oxide layer was not observed. In a similar high-powered ($\sim 5.8 \times 10^6$ Btu/h) test V1.7 in which no CaO was added, complete entrainment of metal into the oxide resulted.

The BETA V2 series are low power experiments designed to investigate crust formation and its influence on the melt-concrete interaction. The V2.1 test consisted of the melt charge composed of 661.4 lb (300 kg) steel (90% Fe, 10% Ni) and 330.7 lb (150 kg) oxides (70% Al_2O_3 , 30% SiO_2) initially at 3632°F (2000°C). The melt pool was sustained at an induced power of approximately 4.09×10^5 to 5.12×10^5 Btu/h (120 to 150 kW) for more than 100 minutes. This power level is representative of long-term decay power. A total of about 13.78 in (0.35 m) downward and 3.94 in (0.10 m) sideward erosion was observed, with an average 0.0024 in/s (0.06 mm/s) downward erosion rate (see Figure 2-4). In the experiment, sideward erosion stopped at about 1000 seconds after a depth of 3.94 in (10 cm) was attained.

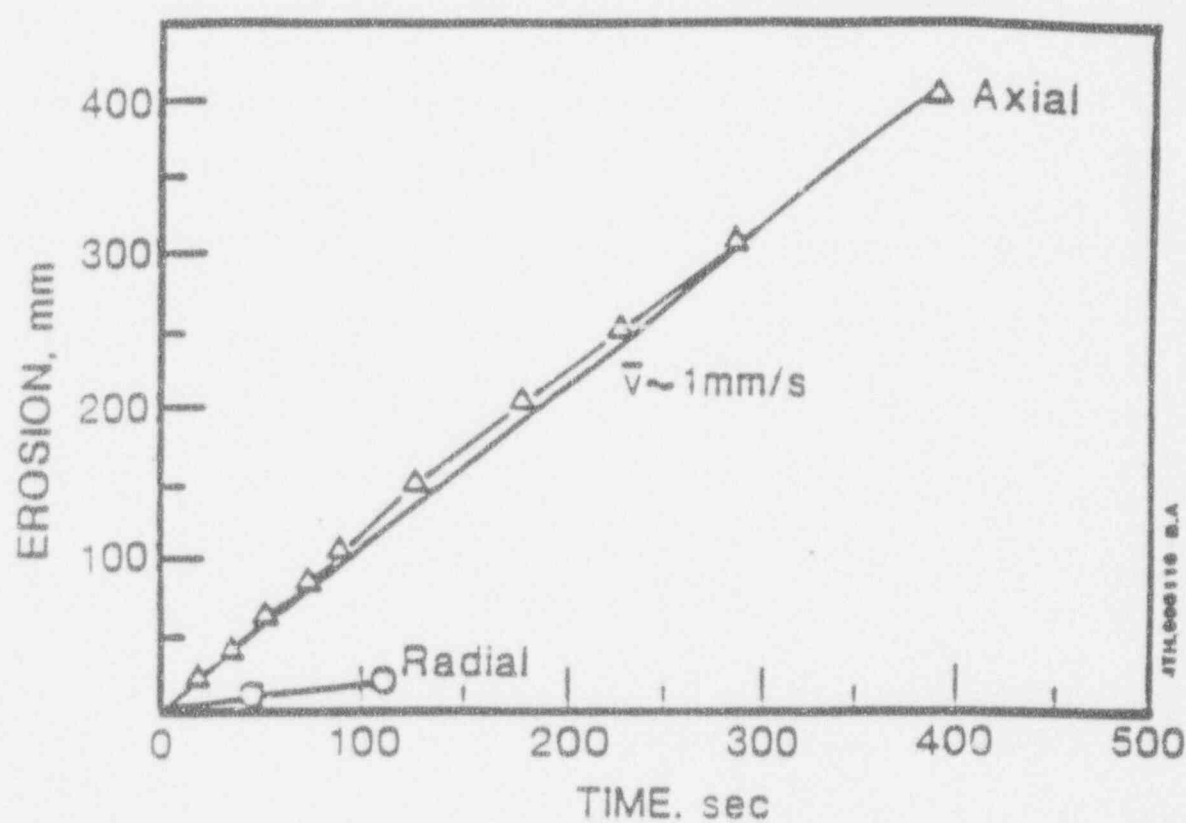


Figure 2-3 Results of the BETA V1.8 Experiment.

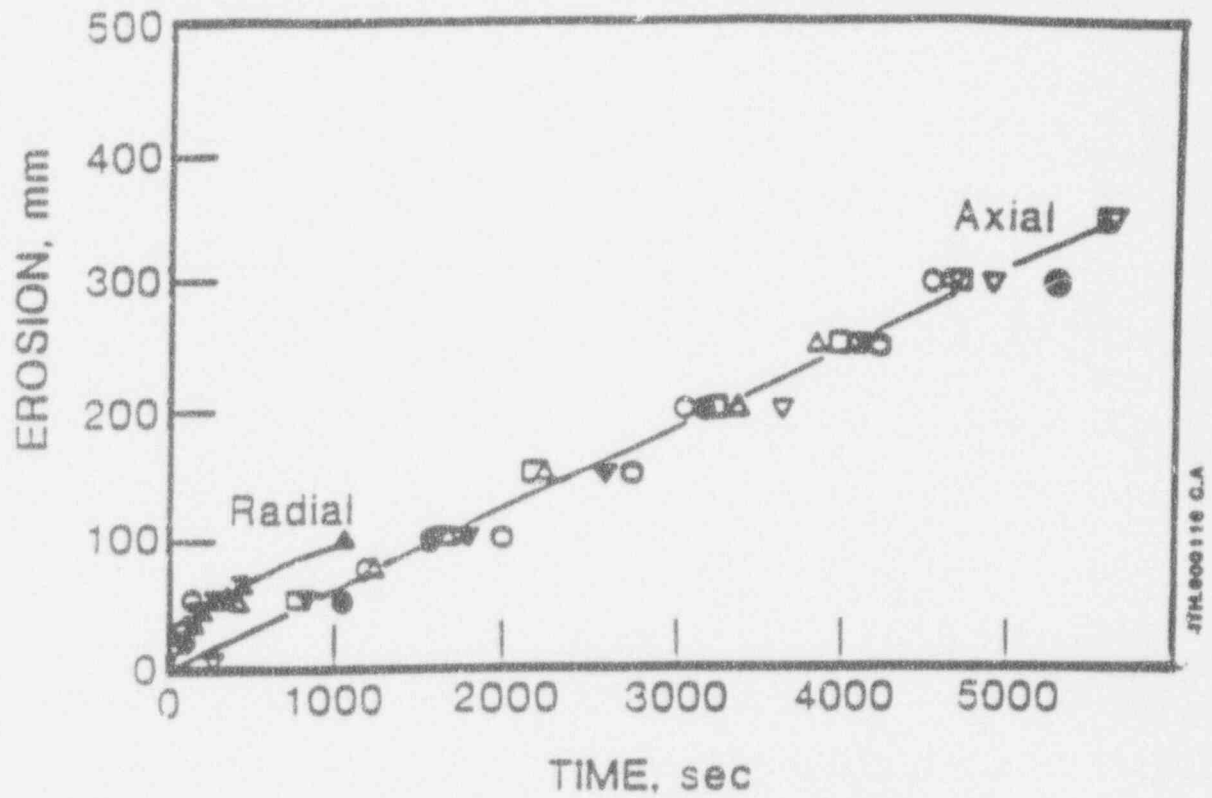


Figure 2-4 Results from the BETA V2 Experiment Series.

2.2.3 SURC: Sustained-Urania Interaction Experiments

Sandia National Laboratories is conducting an ongoing series of Sustained Urania-Concrete (SURC) tests. Table 2-2 identifies the SURC experiment matrix. Experiments SURC-3, SURC-3A, and SURC-4 are considered here.

The interaction crucible for the SURC-4 experiment [CSNI, 1989] consisted of an MgO annulus of 15.75 in (40-cm) inside diameter with a basaltic concrete plug at its base. A schematic of the SURC-4 experimental apparatus is illustrated in Figure 2-5. The test charge for SURC-4 consisted of 440.9 lb (200 kg) SS-304 (approximately 73% Fe, 19% Cr, 8% Ni) inductively heated in the interaction crucible to approximately 2690.6 F (1750 K) prior to the onset of erosion. Fission product stimulants were employed to simulate fission product release, consisting of 1.1 lb (0.5 kg) Te, 2.58 lb (1.17 kg) of La_2O_3 , 2.71 lb (1.23 kg) CeO_2 , and 2.43 lb (1.1 kg) BaO.

A net 2.05×10^5 Btu/h (60 kW) inductive heating power was applied to the test charge for the duration of the test and a value of 31700 Btu/h-ft² (100,000 W/m²) was suggested as representative of the heat loss through the MgO wall. Because of the relatively inert nature of the MgO annulus sidewall to the molten debris, only one-dimensional downward erosion was possible. After quasi-steady concrete erosion was initiated, 44.1 lb (20 kg) of zirconium were instantaneously added to the molten debris to observe the effect of oxidation. Observed erosion was between 9.65 in to 10.83 in (24.5 to 27.5 cm) of concrete.

The melt charge for SURC-3 [Bradley, 1987], composed of 110.2 lb (50 kg) of SS-304 (73% Fe, 19% Cr, 8% Ni), was inductively heated to approximately 3050.6 F (1950 K) prior to being teemed into the interaction crucible. The interaction crucible consisted of an MgO annulus of 7.87 in (20-cm) inside diameter and a limestone-common sand concrete plug base. A schematic of the SURC-3 experiment apparatus is shown in Figure 2-6. A net of 1.024×10^5 Btu/hr (30 kW) inductive heating power was applied to the melt charge for the duration of the experiment. A value of 31700 Btu/h-ft² (100,000 W/m²) was suggested as representative of heat

Table 2-2

SURC TEST MATRIX

Test	Melt Charge	Mass (lb)	Mass (kg)	Concrete	Water
1	UO ₂ -ZRO ₂ -ZR	551	250	LIMESTONE	NO
2	UO ₂ -ZRO ₂ -ZR	551	250	BASALTIC	NO
3	STEEL-ZR	110.2	50	LIMESTONE	NO
3A	STEEL-ZR	110.2	50	LIMESTONE	NO
4	STEEL-ZR	441	200	BASALTIC	NO
5	UO ₂ -ZRO ₂ -ZR	551	250	LIMESTONE	YES
6	UO ₂ -ZRO ₂ -ZR	551	250	BASALTIC	YES
7	STEEL-B ₄ C	441	200	LIMESTONE	NO
8	STEEL-B ₄ C	441	200	BASALTIC	NO

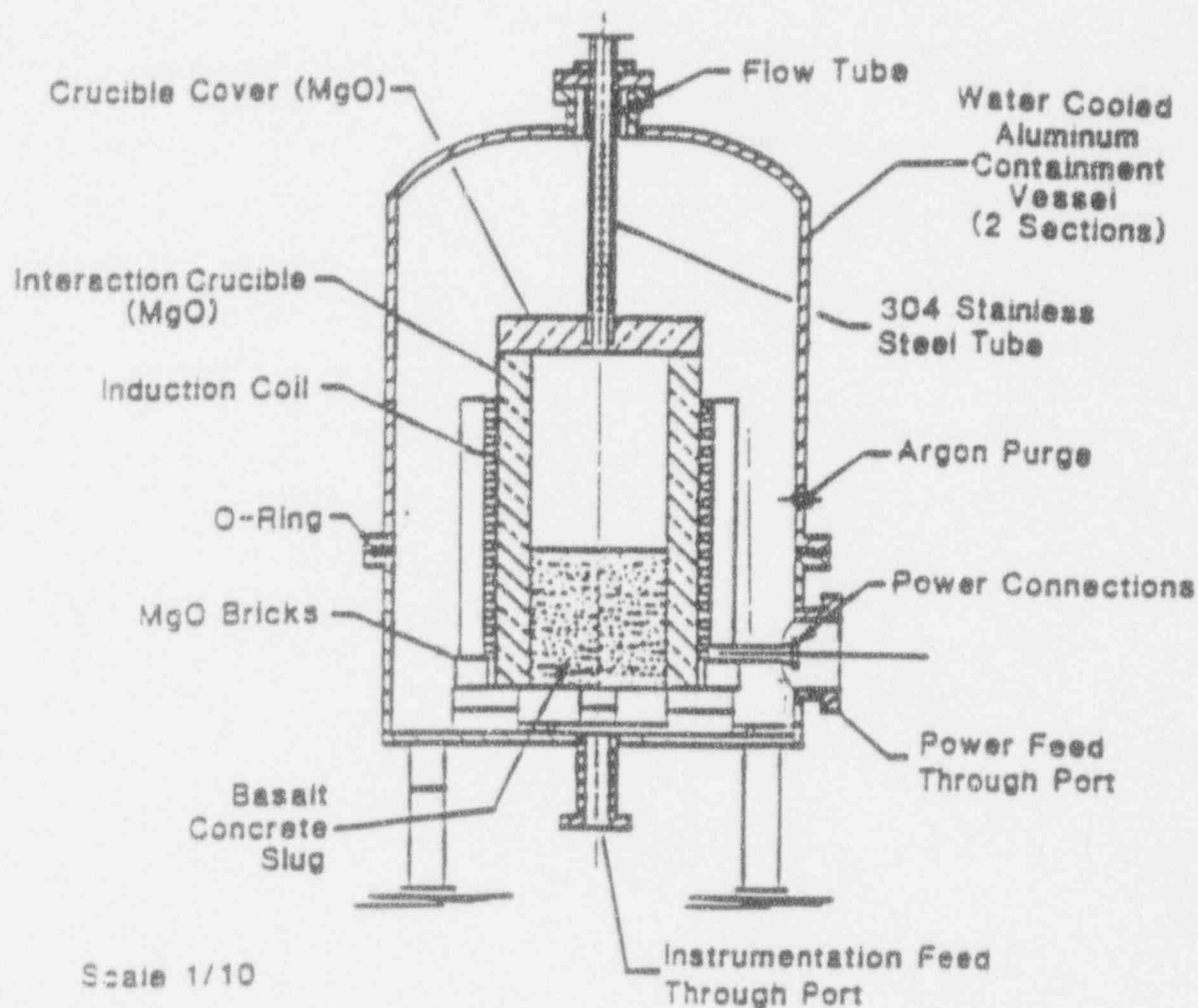


Figure 2-5 SURC-4 Experimental Apparatus.

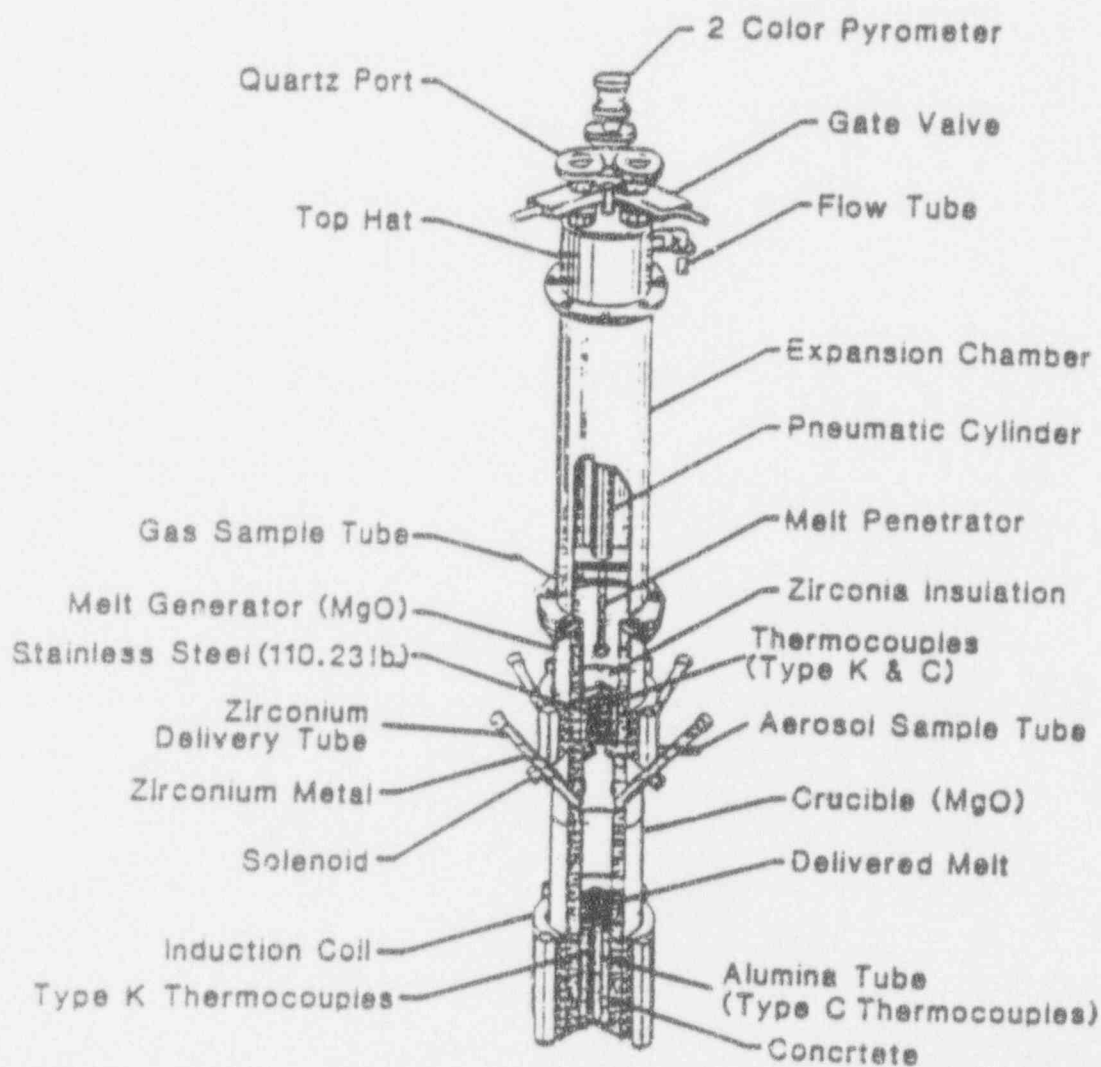


Figure 2-6 SURC-3 Experimental Apparatus.

loss through the MgO wall. Because of the relatively inert nature of the MgO annulus sidewall to the molten debris, only one-dimensional erosion was possible. After quasi-steady concrete erosion was initiated, 3.09 lb (1.4 kg) of zirconium were instantaneously added to the molten debris. Observed erosion was about 13.8 in (35 cm) of concrete.

2.2.4 Summary of Experimental Results

In summary, we can compile the results from several experiments with different scales, different debris material masses and composition, and different power levels to develop a basis on which to provide a method for assessing MCCI and potential failure times (see Tables 2-3 and 2-4). This data has been used to benchmark the core-concrete interactions models used here and in the MAAP code (DECOMP). This data also provide a basis for estimating the fraction of the debris' downward heat flux to be 0.5 and for estimating the ratio of sideward and downward erosion to be 0.2.

2.3 Analytical Approaches

Results of numerous predictions for the experiments described above have been reported in the literature. However, rather than discuss the results of all of these calculations, the principal computer codes used to obtain the results will be discussed. The principal computer codes used for thermal-hydraulic calculations related to core-concrete interactions are CORCON, WECHSL, and DECOMP; the principal computer codes used for aerosol release calculations related to core-concrete interactions are VANESA and METOXA.

2.3.1 CORCON

Sandia National Laboratory's CORCON [Muir, 1981] is incorporated in the NRC's MELCOR code [Summers, 1990] and the Source Term Code Package (STCP) [Fieseke, 1986]. CORCON models the two-dimensional attack of concrete by core debris during severe accidents

Table 2-3

**SUMMARY OF SELECTED CORE-CONCRETE
INTERACTION EXPERIMENT INITIAL CONDITIONS**

Test	Diameter (m/in)	Debris Height* (m/in)	Metal Mass (Kg/lb)	Oxide Mass (Kg/lb)	Temperature ^b (K/F)	Input Power (kW/Btu-h)
SWISS-1	0.216/8.5	0.16/6.3	45/99.2	-/-	1925/3005.6	55/187660
SWISS-2	0.216/8.5	0.16/6.3	44/97	-/-	1925/3005.6	60/204720
SURC-3	0.216/8.5	0.18/7.09	50/110.2	-/-	1970/3086.6	30/102360
SURC-4	0.40/15.75	0.20/7.87	200/440.9	-/-	1746/2683.4	60/204720
BETA V1.8	0.38/15.0	0.78/30.7	350/771.6	130/286.6	1970/3086.6	1900/6482800
BETA V2.1	0.38/15.0	0.72/28.3	300/661.4	130/286.6	2173/3452	120/409440

*Approximate initial collapsed height.

^bEither at melt time or at start of erosion.

Table 2-4

OBSERVED ERODED CONCRETE DEPTH AND MASS

Experiment	Eroded Concrete Depth in (cm)	Eroded Concrete Mass lbm (kg)
SWISS-1	6.7 (17)	31.5 (14.3)
SWISS-2	6.8 (17)	31.5 (14.3)
BETA V1.8		
side	0.78 (2)	229.5 (104.3) ^b
down	16 (40)	942.9 (429.6) ^c
BETA V2.1		
side	3.9 (10)	200.9 (92.3)
down	14 (35)	2223 (1010.4)
SURC-4	10 (26)	165 (75.1)
SURC-3	14 (35)	55.7 (25.3)

^aMass derived from concrete density ($\rho = 2260 \text{ kg/m}^3$) multiplied by estimated volume of concrete eroded.

^bLow estimate based on 1-D eroded only.

^cHigh estimate based on 2-D eroded depth and with assuming cylindrical shape of molten corium.

in light water reactors. It assumes an immediate separation of the molten core into immiscible layers; namely, a metallic and an oxidic layer. As the MCCI proceeds, the decomposed concrete forms a second oxide layer. The orientation of layers depends on their relative density. During the early stage of concrete attack, a configuration of heavy oxide-metal-light oxide is possible. As the MCCI proceeds, the heavy oxide layer is diluted by the molten concrete (slag) and eventually reaches a point where the density of the heavy oxide layer is less than that of the metallic. At this time, the heavy oxidic and metallic layers are assumed to flip instantaneously, and the heavy oxidic layer combines with the light oxidic layer. CORCON also assumed a gas film exists at the molten core/concrete interface. Heat transfer from the molten core pool to concrete is governed by the convective and radiative processes across the film. In CORCON, the concrete ablation is calculated based on steady-state one-dimensional energy balance at the molten core/concrete interface. The decomposition heat of concrete is calculated based on the user specified concrete decomposition temperature. Transient heat conduction into the concrete is not modeled.

CORCON also assumes that, upon solidification, crusts will form at one or more interfaces with the interior of the layer remaining liquid. If part or all of a layer becomes frozen, energy can only be transferred by heat conduction through crusts, which is ordinarily far less effective than convection. Because of internal heating of debris and the fact that cooling cannot continue unless heat losses exceed sources, freezing is largely self-limiting. A simple quasi-steady-state crust formation model was included in the CORCON code to calculate the thickness of the crust and the rate of heat transfer from the partially solidified core debris to concrete. In order to model the crust formation process, some assumptions were made in CORCON to calculate the liquidus and solidus temperatures of the metallic and oxidic mixtures. For the metallic mixture, a simple fit to the iron-chromium-nickel ternary phase diagram was used. The presence of metals other than Fe, Cr and Ni was ignored. CORCON treats the oxidic mixture as a pseudo-binary system in which the fuel oxides ($\text{UO}_2 + \text{ZrO}_2$) form one "component" and concrete and steel oxides form the other; the two components are assumed to form an ideal solution in both the liquid and solid phases.

In CORCON, the oxidation reactions between the metallic constituents and the concrete decomposition gases are assumed to proceed to equilibrium concentrations defined by minimization of the Gibbs free energy for 38 chemical species composed of 11 elements. Carbon is among the 38 species considered in the chemical reactions calculation of CORCON and therefore, the coking reactions are modeled by CORCON.

2.3.2 WECHSL

WECHSL, KfK's stand-alone code [Riemann, 1981], models the two-dimensional concrete attack of the core debris during severe accidents in light water reactors. It assumes the existence of an underlying metallic layer covered by an oxidic layer of fuel, metal oxides, and/or the concrete decomposition products. Heat transfer from melt to concrete is modeled in analogy to boiling phenomena. A film model, discrete bubble model, or transition boiling model for heat transfer are used according to the existing gas flow and inclination of the interface.

When freezing processes become important due to cool-down of the melt, crust formation is modeled starting from the melt/concrete interface and possibly resulting in a fully frozen layer. Crusts are assumed to be permeable to the gases. Transient heat conduction into the concrete is not considered in the WECHSL code. The solidus and liquidus temperatures of the metallic mixture in the WECHSL code are calculated by a simple fit to the chromium-nickel-iron ternary phase diagram. The same set of equations is used in the CORCON and WECHSL codes to predict solidus and liquidus temperatures of the metallic mixture. In WECHSL, the liquidus and solidus temperatures of the oxidic mixture are determined either by a "binary" phase diagram or by a user input table.

In WECHSL, the gases released from the decomposing concrete may oxidize the constituents of the metal layer. The metal oxidation reactions take place in the order zirconium, chromium, and then iron. This means that no chromium-oxidation is considered as long as zirconium is present in the melt, etc. The rate of oxidation for chromium and zirconium is

limited by the gas supplied from the concrete. A temperature dependent equilibrium constant is used to determine the oxidation rate of iron.

2.3.3 DECOMP

DECOMP is a subroutine from the MAAP code [Fauske & Associates, 1990]. It considers the debris to be either a solid cylinder or a molten pool surrounded by a crust, depending upon its energy. Crust growth/shrinkage based on energy balance describes the solidification process occurring within the molten debris, and temperatures are determined from phase diagrams based on the composition of the debris. Transient conduction calculations are carried out in the concrete floor, sidewall in contact with debris, and upper wall (surroundings), and concrete ablation is allowed in all heat slabs. For the case that the debris is partially molten, the heat transfer coefficient at the molten pool/crust interface is a user-defined constant.

The liquidus and solidus temperatures of the metallic phase of the mixture are determined as follows:

- (i) The CORCON fit to the iron-chromium-nickel ternary phase diagram is used to determine the liquid and solidus of the steel mixture containing iron, chromium, and nickel.
- (ii) The Fe-Zr binary phase diagram with iron replaced by stainless steel is used to obtain the liquid and solidus temperatures of Zr-steel mixture.

In DECOMP the treatment of liquid and solidus temperatures of the oxidic phase is similar to the CORCON treatment of oxides.

The chemical reaction model of DECOMP considers chemical equilibrium by a Gibbs free energy minimization technique. Chemical equilibrium is calculated in METOXA, another subroutine from the MAAP code, by solving the algebraic relations for mass action and element

balances. An ideal solution model is used with three phases: liquid metal, liquid oxides and gases. Non-ideality is allowed for some compounds through user-input activity coefficients. A Newton-Raphson technique is employed with a reduced set of algebraic relations, known as basis equations. The equations are solved to yield the molar abundances of particular species important to a stable, efficient solution. Reactions and element balances for the basis set are given in [Fauske & Associates, 1990].

2.3.4 VANESA

The VANESA code calculates the release of fission products and structural material during MCCI. VANESA models the vaporization of melt species into gases which are produced from concrete decomposition. The thermochemistry and kinetics of this process are modeled mechanistically. As the gases exit the melt, aerosol formation from bubbles breaking the melt surface and from the condensation/nucleation of vapors is modeled empirically.

The corium is modeled as a layered two-phase system: an oxidic layer above a dense metallic layer which is in contact with the concrete basemat. The reaction of CO_2 and H_2O with the major metallic constituents are evaluated to determine the equilibrium oxygen potential. This oxygen potential is assumed to hold for the oxide phase and is used to calculate the equilibrium vapor pressures of species in the M-O-H ternary phase diagram where M is the element of interest. The chemical species considered in the VANESA code are given in [Lee, 1985]. A kinetic analysis, which considers condensed phase transport, transport across the gas/melt interface and gas phase transport, is then performed to estimate the amount of material transferred from the melt to gas bubbles.

2.3.5 METOKA

The fission product chemistry of METOKA, a MAAP subroutine, is described above in Section 2.3.3. In METOKA, aerosol generation occurs only through chemical reactions. Mechanical aerosol generation is not modeled.

These codes are all capable of producing MCCI simulations that agree with experiments given they are used by people experienced in the respective code. In particular, the heat balance on the debris that apportions the distribution upward, sideward, and downward is a key modeling consideration and must be properly described via the code model inputs and boundary conditions. This was demonstrated in an international standard problem that employed the SURC-4 data [CSNI, 1989]. The predicted erosion depths for the various codes were shown to be in good agreement with the experimental results.

3.0 METHODOLOGY

The aggressive attack on concrete by molten core debris may lead to a late containment failure if actions are not taken to cover the debris with water and thereby arrest the attack. This attack could occur for certain low probability core melt sequences that lack water in the reactor cavity at the time of vessel failure. Also, in some sequences, a sufficient water inventory might be present in the cavity initially, but the inventory might not be replenished because condensate from the containment shell may become trapped in the refuel canal holdup volume. The debris could reheat and attack the concrete. Even with the appropriate response, deep core debris beds may not be coolable. In [NRC, 1988], the NRC states that experimental evidence exists that suggests core debris beds with depths greater than 10 in (25 cm) may not be coolable.

A simple, stand-alone calculation procedure is included in the method to estimate containment failure time due to MCCI. Although MAAP, or a comparable integral code, should be used to address all aspects of MCCI for a sequence (including non-condensable gas generation, ex-vessel fission product release, etc.), the method provided here can be used to estimate containment failure time due to concrete erosion for a basic sequence. The procedure outlined here has three advantages: (1) it obviates lengthy MAAP runs, (2) it provides a convenient means of investigating ablation phenomena, and (3) it is scrutable to independent reviewers.

In the event the debris is not coolable, the calculation method to be used to determine the possibility of containment failures caused by molten core-concrete interaction is based on the following simplifying assumptions:

- Erosion of the upper portion of the cavity wall by radiative heat transfer is negligible compared to the direct attack of the core debris.
- Erosion proceeds equally at all locations covered by debris.
- Zirconium is the only important source of chemical energy in the core debris.

- The ratio of the rates of advance of sideward and downward concrete attack is constant.

The evaluation method consists of the following steps:

- Step 1: Define failure criteria for basemat and reactor cavity walls.
- Step 2: Determine the time required for the concrete attack by core debris released from reactor vessel to exceed the most limiting failure criterion identified in Step 1.
- Step 3: Based on extent of concrete attack, select the appropriate treatment of containment failure caused by molten core concrete interaction.

3.1 Step 1: Define Failure Criteria

Core debris-concrete interaction is hypothesized to be able to cause containment failure either by penetrating the cavity floor, containment vessel lower head, and basemat or, by weakening the reactor vessel supports sufficiently that the reactor vessel and attached piping move and tear out associated penetrations through the containment. For the latter failure type, the failure criterion must account for the weakening of the cavity wall as this wall's thickness decreases due to erosion, as well as the associated weakening of the wall due to the dehydration of the concrete that occurs ahead of the erosion front. The criterion for failure of the cavity wall may be stated functionally as follows:

$$x_{e,s} \geq (1 - f_1) x_p \quad (3-1)$$

where:

$x_{e,s}$ = total concrete erosion in the sideward direction, ft (m),

x_p = width of the cavity wall, ft (m),

f_1 = minimum fraction of cavity wall required for reactor vessel support.

Note that for a large, dry PWR such as the AP600, the width of the cavity wall is large. Values for f_1 must be in the range $0 < f_1 \leq 1$; a value of 0.5 for f_1 would increase stresses in the containment wall by about a factor of two and would represent removal of design margin corresponding to a safety factor less than two in the original design (since the dehydration front slightly decreases the load-bearing fraction of the wall cross-sectional area).

For basemat penetration, the failure criterion is simply:

$$x_{e,d} \geq x_f + x_b \quad (3-2)$$

where:

$x_{e,d}$ = total concrete erosion in the downward direction, ft (m),

x_f = thickness of the cavity floor, ft (m),

x_b = thickness of the basemat, ft (m).

3.2 Step 2: Determining Overall Time Interval to Exceed Most Limiting Failure Criterion

The calculation method presented below is based on [Plys, 1987]. Typical values for data required by the calculation are provided in Table 3-1. The calculation proceeds in a piecewise continuous fashion to account for changes in the governing phenomena as time passes. The first phase of the erosion process is considered to be an interval during which unoxidized zirconium in the core debris is assumed to react with steam and carbon dioxide liberated by the concrete erosion. During the second phase of the erosion process, the chemical reaction energy is considered negligible and the concrete decomposition enthalpy reduced to reflect the assumed lack of chemical reactions. The calculation method proceeds by determining whether

Table 3-1**MOLTEN CORE-CONCRETE INTERACTION CALCULATION DATA**

Molar Weights: $A_v = 91.22$ lb/lb-mole

$A_{CO_2} = 44$ lb/lb-mole

$A_{H_2O} = 18$ lb/lb-mole

Heats of Reaction: $Q_{H_2O} = 1.2898 \times 10^5$ Btu/lbm (3×10^8 J/Kg)
[Plys, 1987]

$Q_{CO_2} = 1.1608 \times 10^5$ Btu/lbm (2.7×10^8 J/Kg)
(no coking assumed) [Plys, 1987]

<u>Concrete Properties</u>	<u>Limestone/ Common Sand</u>	<u>Basaltic</u>	<u>Limestone</u>
ρ_{cn} (lbm/ft ³)	143.59	143.59	143.59
λ' (Btu/lbm) [Lee and Kazimi, 1985]	1539	1242.5	1780
f_{H_2O} [Lee and Kazimi, 1985]	.047	.049	.041
f_{CO_2} [Lee and Kazimi, 1985]	.22	.015	.357

Miscellaneous [Plys, 1987]

$$\lambda_{cn} = \lambda'_{cn} + c_{p,slag} \Delta T$$

$$c_{p,slag} = 0.23885 \text{ Btu/lbm-F}$$

$\Delta T = 932^\circ\text{F}$ during zirconium reaction
= 392°F during iron reaction

containment failure would be predicted to occur before the zirconium in the core debris bed is depleted. If containment failure occurs first, then the time at which containment failure would occur is obtained by a straightforward calculation. If zirconium depletion would occur first, then the calculation procedure becomes more complicated. First, the time interval to reach zirconium depletion is determined. Then, an iterative calculation is required to determine the predicted depth of concrete erosion corresponding to zirconium depletion. Finally, the additional concrete mass that must be eroded to cause containment failure and its corresponding time interval must be determined.

To determine whether containment failure would be predicted to occur before zirconium depletion occurs, the masses of concrete that would be eroded at these times are calculated and compared. To estimate the mass of concrete that has been eroded when the zirconium is complete oxidized, the number of moles of zirconium available for reaction (N_{Zr}) must be determined:

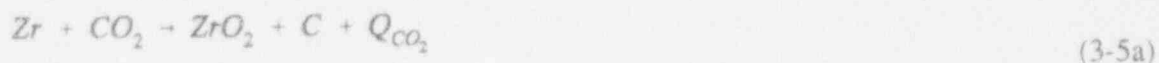
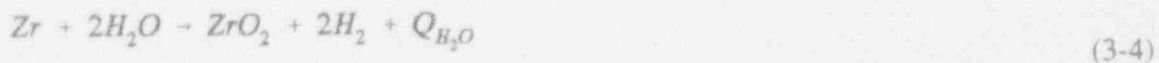
$$N_{Zr} = m_{Zr}/A_{Zr}$$

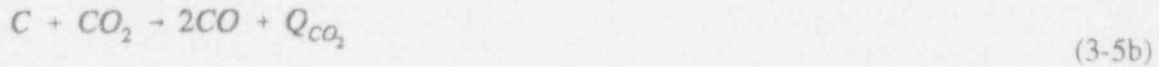
where

m_{Zr} = mass of unoxidized zirconium in the core debris contained in the cavity, lbm (kg),

A_{Zr} = molecular weight of zirconium, lb/lb-mole (kg/kg-mole).

The governing chemical reactions are taken to be:





where:

Q_{H_2O}, Q_{CO_2} = heat of reaction per mole of gas produced, Btu/lb-mole
(J/kg-mole).

Thus, by Equation (3-4) two moles of gas are produced for each mole of zirconium reacted:

$$N_g = 2N_z \quad (3-6)$$

The number of gas moles produced per unit mass of concrete eroded (n_g) is given by:

$$n_g = \frac{f_{H_2O}}{A_{H_2O}} + \frac{f_{CO_2}}{A_{CO_2}} \quad (3-7)$$

where:

f_{H_2O}, f_{CO_2} = concrete gas mass fractions for steam and carbon dioxide,

A_{H_2O}, A_{CO_2} = molecular weights of steam and carbon dioxide, lb/lb-mole
kg/kg-mole.

The total concrete mass that would be eroded during phase 1 ($m_{cn,zf}$) may then be estimated as:

$$m_{cn,zf} = N_g / n_g \quad (3-8)$$

The mass of concrete that would be eroded at the time either of the failure criteria area satisfied (see Equations (3-1) and (3-2)), may be estimated using Equation (A-6b) from Appendix A:

$$m_{CN,S} = \rho_{CN} f_s \bar{A}_d x_{e,s} / r_s \quad \text{lbm (kg)} \quad (3-9a)$$

$$m_{CN,d} = \rho_{CN} f_s \bar{A}_d x_{e,d} \quad \text{lbm (kg)} \quad (3-9b)$$

where:

ρ_{CN} = concrete density, lbm/ft³ (kg/m³),

$f_s = 1 + r_s A_s/A_d$ rate, of total to downward volumetric erosion rate,

\bar{A}_d = average area subjected to downward erosion over the erosion time interval of interest, ft² (m²),

r_s = ratio of sideward rate of erosion to downward rate of erosion.

If either $m_{CN,S}$ or $m_{CN,d}$ are less than $m_{CN,Zr}$, then containment failure would be predicted to occur before the zirconium in the core debris mass was fully oxidized. The time interval of interest may be estimated using Equation (A-8) and the following expression for the integrated core decay power [El-Wakil, 1978]:

$$\int_{t_1}^{t_2} Q_{DK} dt = 0.128 Q_o (t_2^{0.74} - t_1^{0.74}) \quad (3-10)$$

where:

Q_{DK} = core decay power, Btu/h (or Watts),

Q_o = core full power, Btu/h (or Watts),

t_1 = start of time interval of interest after core shutdown, second,

t_2 = end of time interval of interest after core shutdown, second.

For this case, the time at which the uncoolable core debris bed was formed corresponds to the start of the time interval, while the time that the containment fails is the end of the time interval. Substituting Equation (3-10) into Equation (A-8) and rearranging yields the desired end time:

$$t_2 = (t_1^{0.74} + 7.8 m_{cn} (1 - f_q Q_o / (f_s \lambda_{cn})) / (Q_o f_q \lambda_{cn}))^{1.35} \quad (3-11)$$

where

$m_{cn} = m_{cn,s}$ or $m_{cn,d}$, whichever corresponds to the containment failure condition,

f_q = fraction of core debris bed power assumed to enter concrete,

λ_{cn} = total erosion enthalpy, Btu/lbm (J/kg), including sensible heat to concrete melting, sensible heat to corium temperature, slag heat of fusion, and chemical reaction energy addition,

Q_o = total heat of reaction to oxidize zirconium, Btu/lbm (J/kg), see Equation (A-4).

If containment failure will be predicted to occur after zirconium depletion, then the length of time required to fully oxidize the zirconium in the core debris must be determined, before the containment failure time can be estimated. This requires that the depth of erosion corresponding to $m_{cn,zr}$ be determined. This is done using the following equations in an iterative fashion:

$$x_{d,zr} = m_{cn,zr} / (\rho_{cn} f_s \overline{A_d}) \quad (3-12a)$$

$$x_{s,zr} = r_s x_{d,zr} \quad (3-12b)$$

where:

$x_{d,zr}$ = depth of eroded concrete when zirconium is depleted, ft (m),

$x_{s,zr}$ = sideward erosion distance when zirconium is depleted, ft (m).

The factor f_s is determined by:

$$f_s = 1 + r_s (\overline{A_s/A_d}) \quad (3-13)$$

where:

A_s = area subjected to sideward erosion, ft² (m²),

$\overline{A_s/A_d}$ = average value of A_s/A_d over time interval of interest.

The averaged values used in Equations (3-12a) and (3-13) are defined as following for this time interval of interest:

$$\overline{A_s/A_d} = \frac{1}{2} \left(\frac{A_{s0}}{A_{d0}} + \frac{A_{s,zr}}{A_{d,zr}} \right) \quad (3-14)$$

(3-15)

$$\overline{A_d} = \frac{1}{2} (A_{do} + A_{d,2r})$$

If a rectangular geometry is used to approximate a cavity, for example, the initial values for sideward and downward erosion areas, A_{so} and A_{do} , respectively, are:

$$A_{so} = (2L_o + 2W_o) h_o \quad (3-16a)$$

where

L_o, W_o = original cross-sectional dimensions of the cavity, ft (m),

h_o = original depth of the debris on the cavity floor, ft (m).

$$A_{do} = L_o W_o \quad (3-16b)$$

The values of the sideward and downward erosion areas to be used in the second iteration cycle and all subsequent cycles may be expressed as:

$$A_{s,2r} = (2L_o + 2W_o + 8x_{s,2r})(h_o + x_{d,2r}) \quad (3-17a)$$

and

$$A_{d,zf} = (L_o + 2x_{s,zf})(W_o + 2x_{s,zf}) \quad (3-17b)$$

Similar expressions would be determined for other uncoolable debris bed configurations.

The steps in the iteration procedure involve estimating and updating \overline{A}_d and $\overline{A}/\overline{A}_d$ as the estimated values for $x_{d,zf}$ and $x_{s,zf}$ change. To start the iteration, use A_{d0} for A_d , and A_{s0} and A_{d0} in $\overline{A}/\overline{A}_d$. Next, calculate a value for f_s using Equation (3-13), and then obtain first estimates of $x_{d,zf}$ and $x_{s,zf}$ from Equations (3-12a) and (3-12b), respectively. The revised values for erosion distances then should be used to start the next iteration cycle. Update values for $\overline{A}/\overline{A}_d$, f_s , and \overline{A}_d using (in order) Equations (3-17a), (3-17b), (3-14), (3-15), and (3-13). Then, calculate new values for $x_{d,zf}$ and $x_{s,zf}$ using Equations (3-12a) and (3-12b). Satisfactory convergence is obtained when the value of $x_{d,zf}$ changes less than 0.1% from the previous iteration.

Once convergence is reached for the erosion distances, the end time of the interval required to deplete unreacted zirconium in the core debris bed should be estimated using Equation (3-11), with $m_{cn,zf}$ identified as the appropriate value for the factor m_{cn} .

To then determine the containment failure time, the additional mass of concrete that must be eroded after zirconium is fully oxidized to reach the containment failure conditions (Δm_{cn}) must be found. This value may be determined as follows:

$$\Delta m_{cn} = \Delta x \rho_{cn} f_s \overline{A}_d \quad (3-18)$$

where:

Δx = distance erosion front must advance to cause containment failure, m.

The value for Δx in Equation (3-18) should be selected as the minimum of $\Delta x_{e,s}$ and $\Delta x_{e,d}$:

$$\Delta x_{e,d} = x_{e,d} - x_{d,zf} \quad (3-19a)$$

$$\Delta x_{e,s} = (x_{e,s} - x_{s,zf})/r_s \quad (3-19b)$$

where:

$\Delta x_{e,d}$ = distance erosion front must advance in downward direction to reach containment failure criterion for downward direction, ft (m).

$\Delta x_{e,s}$ = distance erosion front must advance in downward direction to reach containment failure criterion for sideward direction, ft (m).

The values of $\overline{A/A_d}$ and $\overline{A_d}$ to be used in Equations (3-13) and (3-18) should be as follows:

$$\overline{A_d} = \frac{1}{2} (A_{d,zf} + A_{d,cf}) \quad (3-20)$$

$$\overline{A/A_d} = \frac{1}{2} \left(\frac{A_{s,zf}}{A_{d,zf}} + \frac{A_{s,cf}}{A_{d,cf}} \right) \quad (3-21)$$

where:

$A_{d,cf}$ = cross-sectional area of uncoolable core debris bed at time of containment failure, ft^2 (m^2),

$A_{s,cf}$ = sideward erosion area of uncoolable core debris bed at time of containment failure, ft^2 (m^2).

As an example, the values for $A_{s,cf}$ and $A_{d,cf}$ for containment sump geometry would be given by

$$A_{s,cf} = [2L_o + 2W_o + 8 (x_{s,zf} + r_s \Delta x)](h_o + x_{d,zf} + \Delta x) \quad (3-22a)$$

$$A_{d,cf} = [L_o + 2 (x_{s,zf} + r_s \Delta x)][W_o + 2 (x_{s,zf} + r_s \Delta x)] \quad (3-22b)$$

Once Δm_{cn} has been determined, the predicted time of containment failure may be found from Equation (3-11), using the time at which zirconium was depleted as t_1 , Δm_{cn} as m_{cn} , Q_r set equal to zero, and the appropriate value of λ_{cn} from Table 3-1.

The result of the preceding calculation is an estimate of the least time required for molten core-concrete interaction to exceed a containment failure criterion. If the criterion stated by Equation (3-1) is the most limiting condition, then containment failure is assumed to be at a penetration as a result of vessel movement; fission products then would be released from the containment building to the environment. If the criterion stated by Equation (3-2) is the most limiting condition, then containment failure is assumed to be caused by basemat penetration; fission products and/or core debris would be released from the containment building to the soil underneath the containment basemat.

4.0 APPLICATION OF THE METHODOLOGY TO THE AP600 PLANT DESIGN

4.1 Debris Coolability

(a,c)

Figure 4-1 AP600 Cavity Elevation Drawing

(a,c)

Figure 4-2 AP600 Containment Isometric View of Cavity and Loop Compartment

(a,c)

These sequences are given no further consideration here. Only sequences where the debris is not quenched throughout the accident duration create any potential for significant MCCI. For these sequences, as unlikely as they may be, the methodology of Section 3.0 can be applied to investigate the response of the AP600 design in relation to the ALWR requirements and the AP600 design goals. This is carried out in the following section by determining a MCCI failure criterion and the time required to exceed it.

4.2 MCCI Failure Criterion (Step 1)

4.3 Time Interval to Exceed the Failure Criterion (Step 2)

The time to exceed the failure criterion is determined by the procedure outlined above, subject to a key assumption - the entire core, with its full initial inventory of zirconium and fission products, is expelled instantaneously at the start of the time interval. Although some fraction of the core could remain cooled in-vessel while the bulk of the core is expelled, it is much easier to make the conservative assumption that the entire core is expelled with its full initial inventory of fission products and zirconium. In many accident sequences, a substantial fraction, as much as, say, 50%, of the zirconium can be oxidized in-vessel, as opposed to being oxidized during corium-concrete attack. This potentially decreases the duration of the zirconium oxidation phase and slows corium-concrete attack overall, since the chemical energy of the corium is decreased. This possibility is not considered. Moreover, a substantial fraction of the core's initial fission product inventory will not reside in the corium attacking the basemat. Fission products are distributed throughout the primary system and containment compartments in a manner that depends upon the severe accident progression. Volatile fission products initially present in the corium can be vaporized or entrained to form aerosols which are transported throughout the containment. The net effect of these mechanisms reduces the mass of fission products and decay heat in the corium as it attacks the cavity floor.

For an initial debris pool depth, the condensed debris depth in the cavity is given by:

$$h_o = \frac{\left(\frac{M_u}{\rho_u} + \frac{M_{ZR}}{\rho_{ZR}} + \frac{M_{CSP}}{\rho_{SS}} \right) + V_{LH}}{A_c} \quad (4-1)$$

where:

The data required were taken from Table 3-1, the AP600 MAAP 4.0 parameter file, [Westinghouse, 1991a] and [Westinghouse, 1991b]. [

The cavity floor is modeled as a rectangle without the complexities of the actual geometry.

Other parameters required for the procedure, such as the ratio of sideward rate of erosion to downward rate of erosion (r_s) and the fraction of core debris power to concrete (f_q), are derived from the experimental evidence cited above. A ratio of the sideward rate of erosion to the downward rate of erosion must be specified based on the BETA experiments and engineering judgement. Clearly, the lower bound for f_s of zero will result in the maximum downward erosion rate. Also, the downward erosion area will remain constant during the attack for an r_s of zero, resulting in very simple expressions for Δm_{cn} . However, even small values of r_s greatly increase containment failure time relative to the $r_s = 0$ assumption because f_s is made larger than 1. The assumption that $r_s = 0$ is quite convenient, but it results in unrealistically conservative answers. Experimental evidence suggests that the ratio of erosion rates is non-zero, but much less than one. From Table 2-4, the BETA experiments indicate an r_s of 0.05 for the V1.8 test and 0.29 for the V2.1 test. The V2.1 test was scaled to reflect long-term decay heat, in contrast to the V1.8 test which reflect a heat generation rate an order of magnitude larger than decay heat. As a result, 0.2 will be used as a best-estimate value for r_s .

A fraction of core debris bed power assumed to enter the concrete (f_q) must also be specified. A value of 1 is overly conservative because it neglects radiation and/or convection heat transfer from the top surface of the debris, while a value of 0, on the other extreme, denotes no concrete attack. The value of f_q would actually vary from sequence to sequence as a function of accident progression and operator actions. Similarly, for a given severe accident sequence, f_q would be a function of time due to operator actions, accident progression, fission product transport, etc. A constant value of 0.5 is used here as a best-estimate for the completely dry case

to be consistent with [Fauske & Associates, 1985]. This value was established based on mechanistic results of DECOMP (see Section 2.0), which show that by and large, about half the decay heat is transferred to the concrete, and about half is transferred to cavity gases or cavity walls.

And finally, an initial time for MCCI (t_i) must be specified to calculate the time to exceed the failure criterion. In those accident sequences where an overlying pool cannot be maintained to quench the debris, MCCI will begin once the debris has dried out. This timing is highly sequence dependent, of course, but no effort will be made to consider t_i for the various AP600 accident sequences. A conservative lower bound of $t_i = 2$ hours is selected based on experience with MAAP runs for large, dry Westinghouse PWRs. For the AP600, it is assumed that the minimum duration between the accident initiator and MCCI initiation is only 2 hours.

5.0 UNCERTAINTY CONSIDERATIONS

The results presented above are subject to uncertainties due to a lack of complete experimental data. In particular, the fraction of core decay heat power (f_q) is subject to large uncertainty as a result of two considerations: (1) the heat transfer mechanisms from the debris by radiation and convection to overlying water or gas, and (2) the transport of volatile fission products from the debris by vaporization and/or entrainment to other parts of the containment. The decay heat power fraction to the concrete was taken from [Fauske & Associates, 1985], but no effort was made to account for fission product release from the debris. Fission product release is now accounted for in a simple manner to scope out its potential impact and demonstrate the conservatism of the aforementioned results. This phenomenon essentially decreases the fraction of decay heat power to the concrete, so fission product release in the cavity can be addressed by varying the parameter f_q .

Fission product release and transport is dependent upon severe accident progression, timing, operator actions, etc. A few MAAP runs can be examined to find a range for the fraction of decay heat energy removed from the debris by transport of volatile fission products, and improve the accuracy of f_q . The MAAP User's Manual [Fauske & Associates, 1990] contains input decks and tabular output for three runs made with the "Zion-like" parameter file: a station blackout with no operator actions, a small LOCA without the recirculation mode, and a large LOCA without the recirculation mode. Tabular output for each of these runs gives the fraction of core decay heat in the cavity at various times. For the blackout case, 39% is in the lower compartment, and 29% is in the form of released fission products. For the large LOCA, 72% of the decay heat is in the cavity at 30 hours into the accident and 28% is in the form of released fission products. And finally, for the small LOCA, 71% of the decay heat is in the cavity at 44 hours and 29% is in the form of released fission products. Based upon these examples, it seems reasonable to assume that in the long term, 70%, rather than 100%, of the decay heat is in the cavity. [

](a.c)

Additional uncertainty considered here is the impact of the assumed constant erosion rate ratio (r_e). To simplify the calculation, r_e was assumed constant. Furthermore, the average value of r_e which was taken from experimental data ranges from 0.05 (in V1.8 test) to 0.29 (in V2.1 test) depending on the heat supply rate in the experiments. It is, therefore, important to take into account the sensitivity of r_e on the containment failure time. In general, the smaller value of r_e means more heat rate will be available to erode downward, thereby reducing the failure time in the downward direction. When $r_e = 0.1$ is assumed in the calculation, the containment failure time decreases to [](a,c) provided that all other parameters remain the same.

These uncertainty calculations demonstrate that the assumptions for the base case, as well as the model itself are robust and perhaps quite conservative. Even for pessimistic assumptions for r_e , the containment failure time on basemat melt-through is about [](a,c) With more realistic assumptions about fission product transport, the final failure timing is greatly increased from the base case.

6.0 ACCIDENT MANAGEMENT INSIGHTS AND CONSIDERATIONS

Many of the design features of the AP600 support the conclusion that MCCI will not be a relevant containment failure mechanism. The AP600 design ensures that the cavity will be flooded before any other compartment in the containment [Fauske & Associates, 1992], and provides redundant, passive means of supplying the necessary water inventory. In accordance with ALWR design requirements, the cavity configuration prevents local accumulation of uncoolable debris. This discussion presupposes vessel failure, when in reality, the ability to flood the cavity also means that vessel failure can be averted by cooling the RPV externally.

Even in the dry scenario, the AP600 response is very favorable, for several reasons. As with existing large, dry PWRs the massive amount of concrete in the shield walls and basemat floor make the shield wall failure scenario incredible. In the downward direction, the thickness of the basemat helps make the time to failure criterion very large. [

With respect to accident management insights and recovery actions, the important points are that the AP600 is configured so that the cavity will flood, and that the amount of time available to halt or mitigate ablation once it begins is very great. Unabated concrete ablation

would have to continue for days before the basemat would be breached, so operators would have ample time to establish injection into the failed vessel. At this point, the relevant question is whether the debris would be in a coolable configuration at the time injection is established. Even in the initially dry case, the debris should be coolable at the time the injection is established.

] The thickness of debris layer would increase as ablated concrete is incorporated, but the heat transfer surface area from the debris to overlying water would also increase, while the total volumetric heat generation rate (decay heat) decreased. Although a deep (~ 1 m) debris bed could not be quenched as rapidly as an initial debris depth of 25 cm, the large inventory of water available in the AP600 cavity would eventually lower the debris temperature below the melting point of concrete and halt ablation. Upward conduction of heat to the debris-water interface, aided by the convective process of ingression of water into fissures, blow-holes, etc., would eventually cool the debris and lead to a safe, stable state.

7.0 CONCLUSIONS

The results of the paper demonstrate that the concrete ablation resulting from MCCI is not a relevant containment failure mechanism for the AP600. The AP600 design is such that erosion of cavity walls supporting the reactor vessel is not a possible failure mechanism because basemat melt-through would occur first. For basemat melt-through, the developing experimental data base and the AP600 design considerations lead to the conclusion that significant MCCI will not occur if an overlying pool can be maintained in the cavity. This will be the case in almost all foreseeable AP600 severe accident sequence, and basemat melt-through will be averted in such sequences. Even given the extremely unlikely case where the cavity remains dry throughout the entire accident sequence, basemat melt-through is not a credible scenario. Calculations presented here indicate that basemat melt-through could occur only after several days of dry cavity conditions. Recovery actions will have taken place before then, however, to establish an overlying pool in the cavity and halt concrete ablation.

8.0 REFERENCES

Alsmeyer, H., 1986, Beta Experiments for Verifying the Weschl-Codes; Experimental Results for Melt-Concrete Interaction, English Translation.

Alsmeyer, H., et al., 1987, "Beta Experimental Results on Melt/Concrete Interactions: Silicate Concrete Behavior", Proceedings of the Committee on the Safety of Nuclear Installations (CSNI) Specialists' Meeting on Core Debris-Concrete Interactions, EPRI NP-5054-SR.

Blose, R. E., et al., 1987, SWISS: Sustained Heated Metallic Melt/Concrete Interactions with Overlying Water Pools, NUREG/CR-4727, SAND85-1546.

Bradley, D. R., and Copus, E. R., 1987, "Significant Results from SURC-3 and SURC-3A Experiments", Presented at 15th Water Reactor Safety Meeting, National Bureau of Standards, Gaithersburg.

CSNI, 1989, "SURC-4 Experiment on Core-Concrete Interactions", Committee on the Safety of Nuclear Installations, CSNI Report No. 155, Volume 2.

DOE, 1990, "Technical Support for the Debris Coolability Requirements for Advanced Light Water Reactors in the Utility/EPRI Light Water Reactor Requirements Document", ID-10278.

DOE, 1991, "Passive ALWR Requirements to Prevent Containment Failure".

El-Wakil, M. M., 1978, Nuclear Heat Transport, The American Nuclear Society, LaGrange Park, Illinois.

Fauske & Associates, Inc., 1985, "Approximate Source Term Methodology for Pressurized Water Reactors", FAI/85-58.

Fauske & Associates, Inc., 1990, MAAP 3.0B User's Manual.

Fauske & Associates, 1992, "Westinghouse AP600 Phenomenological Evaluation Summary on External Cooling of the RPV - Support of the ALWR Risk Analysis".

Gieseke, J. A., et al., 1986, "Source Term Code Package, A User's Guide (Mod. 1)", Battelle Columbus Division, NUREG/CR-4587, BMI-2138.

IDCOR, 1985, Grand Gulf Nuclear Station - Integrated Containment Analysis, IDCOR Technical Report 23.1GG, Mississippi Power and Light Co.

Lee, M., and Kazimi, M. A., 1985, Modeling of Corium/Concrete Interaction, MITNE-267.

Malinovic, B., Henry, R. E., and Sehgal, B. R., 1989, "Experiments Relating to Drywell Shell-Core Debris Interactions", National Heat Transfer Conference, Philadelphia, PA, AIChE Symposium Series, Vol. 85, No. 269, pg. 217-222.

Muir, J. G., et al., 1981, "CORCON/Mod 1: An Improved Model for Molten Core/Concrete Interactions", NUREG/CR-2142, SAND80-2415.

NRC, 1975, WASH-1400, Reactor Safety Study, NUREG/75-0114.

NRC, 1988, letter to All Licensees Holding Operating Licenses and Construction Permits for Nuclear Power Facilities, "Individual Plant Examination for Severe Accident Vulnerabilities - 10CFR 50.54(f)", Generic Letter No. 88-20.

Plys, M. G., 1987, "Hand Calculations for Core-Concrete Attack and Containment Failure Timing With Applications to LaSalle and Grand Gulf", Presentation to NUREG-1150 Molten Core-Containment Expert Review Group, Albuquerque, NM.

Reimann, M., and Murfin, W. B., 1981, "The WECHSL Code: A Computer Program for the Interaction of Core Melt with Concrete", KfK-2890.

Summers, R. M., et al., 1991, "MELCOR 1.8.0: A Computer Code for Nuclear Reactor Severe Accident Source Term and Risk Assessment Analyses", Sandia National Laboratories, Albuquerque, NM.

Westinghouse Electric Company, 1991a, AP600 MAAP 4.0 Parameter File, November, 1991.

Westinghouse Electric Company, 1991b, Letter from J. V. Miller to J. H. Scobel dated January 29, 1991, NSE-91-0033.

APPENDIX A

Derivation of Concrete Erosion Calculation

The calculation presented below is based on the method presented by [Plys, 1987]. The calculation is based on the following assumptions:

- The mass erosion rate is linearly proportional to the decay heat rate plus heat of chemical reactions.
- Only reaction heats from the downward attack are accounted.
- Sideward erosion speed is assumed a constant fraction of downward erosion speed (i.e., $r_s = U_s/U_d = \text{constant}$).

The energy balance for the eroded concrete according to the first assumption may be written as:

$$\rho_{cn} \lambda_{cn} (U_d A_d + U_s A_s) = Q \quad (\text{A-1})$$

where:

ρ_{cn} = concrete density, lbm/ft³ (kg/m³),

λ_{cn} = total erosion enthalpy, Btu/lbm (J/kg), including sensible heat to concrete melting, sensible heat to corium temperature, slag heat of fusion, and decomposition reactions.

U = erosion speed, ft/s (m/s),

A = area, ft², (m²),

Q = input power, w, including decay power and chemical reactions,

d = downward,

s = sideward.

The mass balance for the eroded concrete yields:

$$m_{cn} = \int_0^t \rho_{cn} (U_d A_d + U_s A_s) dt \quad (A-2a)$$

$$= \int_0^t (Q/\lambda_{cn}) dt \quad (A-2b)$$

where

m_{cn} = total eroded concrete mass, lbm (kg).

The input power in equation (A-1) may be written as:

$$Q = f_q (Q_{dk} + \rho_{cn} U_d A_d (\frac{f_{H_2O}}{18} Q_{H_2O} + \frac{f_{CO_2}}{44} Q_{CO_2})) \quad (A-3)$$

where

f_q = power fraction into concrete,

Q_{dk} = decay power, Btu/hr (J/s),

f_{H_2O}, f_{CO_2} = gas mass fraction in concrete,

Q_{H_2O}, Q_{CO_2} = heat of reaction per mole gas to liberate H_2 and CO , Btu/lb-mole,
(J/kg-mole).

Typical values for the latter quantities are:

$$Q_{H_2O} = 1.2898 \times 10^5 \text{ Btu/lb-mole } H_2O \text{ (} 3 \times 10^8 \text{ J/kg-mole } H_2O \text{)}$$

$$Q_{CO_2} = 1.1608 \times 10^5 \text{ Btu/lb-mole } CO_2 \text{ (} 2.7 \times 10^8 \text{ J/kg-mole } H_2O \text{)}$$

for overall reactions to H_2 and CO .

If we define:

$$Q_r = \left(\frac{f_{H_2O}}{18} Q_{H_2O} + \frac{f_{CO_2}}{44} Q_{CO_2} \right) \quad (A-4)$$

$$f_s = 1 + \frac{U_s A_s}{U_d A_d} = 1 + r_s \frac{A_s}{A_d} \quad (A-5)$$

Then, Equation (A-2a) may be rewritten as:

$$m_{cn} = \rho_{cn} f_s \int_0^t U_d A_d dt \quad (A-6a)$$

$$= \rho_{cn} f_s \bar{A}_d x_d \quad (A-6b)$$

where:

x_d = depth of eroded concrete, ft (m),

\bar{A}_d = average surface area of downward concrete erosion, ft² (m²).

Equation (A-2b) may be rewritten as:

$$\lambda_{cn} m_{cn} = f_q \int_0^t Q_{dk} dt + f_q \rho_{cn} Q_r \bar{A}_d x_d \quad (A-7)$$

Manipulating Equations (A-6b) and (A-7) then yields:

$$m_{cn} = \frac{(f_q / \lambda_{cn}) \int_0^t Q_{dk} dt}{1 - f_q Q_r / (f_s \lambda_{cn})} \quad (A-8)$$

$$x_d = m_{cn} / (\rho_{cn} f_s \overline{A_d})$$

(A-9)

$$x_s = r_s x_d$$

(A-10)

APPENDIX B

Code Input and Calculations

(a,c)

(a,c)

APPENDIX C

MCCI Calculation Source Code

(a,c)

(a,c)

(a,c)

(a,c)

(a,c)

WESTINGHOUSE CLASS 3

FAI/92-18

PHENOMENOLOGICAL EVALUATION SUMMARY ON
THE PROBABILITY AND CONSEQUENCES OF
DEFLAGRATION AND DETONATION OF HYDROGEN

IN SUPPORT OF THE
AP600 RISK ANALYSIS

Submitted To:

Westinghouse Electric Corporation

Prepared By:

Fauske & Associates, Inc.
16W070 West 83rd Street
Burr Ridge, Illinois 60521

May, 1992

ABSTRACT

This phenomenological evaluation summary assesses the susceptibility of the AP600 containment to failure due to hydrogen deflagrations and detonations that may occur during postulated severe accidents. The failure of the containment could provide a pathway for the release of fission products. In particular, the possibility of an early containment failure due to hydrogen deflagration or detonation is of key interest when assessing potential source terms.

The assessment concludes that the postulated containment loadings due to the deflagration of combustible gases in the AP600 containment will not cause failure of the containment structure. This conclusion is based on a bounding assessment of the containment pressurization potential assuming 100% oxidation of zirconium from the active fuel cladding. This bounding assessment conservatively ignores the hydrogen igniter system and the likely existence of inerting due to steam produced in the course of damaging the reactor core. The limiting calculation also ignores the possibility of incomplete combustion and the effectiveness of containment heat sinks including passive heat removal capability. The likelihood of detonations by either direct energy deposition or deflagration to detonation transition (DDT) has also been assessed. It is concluded that such detonations will not challenge the integrity of the AP600 containment. Thus, failure of the AP600 containment due to deflagrations and detonations will not be included as a separate node for either early or long term containment failure in the AP600 containment event trees.

Recommendations are provided regarding sensitivity studies that will be conducted as part of the AP600 risk analysis to address phenomenological uncertainties and the specifics of sequence-dependent timing of interacting phenomena. These sensitivity studies will be used to demonstrate the impact of phenomenological uncertainties and confirm this paper's conclusion regarding the capability of the AP600 containment to withstand potential deflagration and detonations. Additionally, it is recommended that the plant specific analyses (MAAP calculations) be reviewed to specifically summarize local effects of potential hydrogen deflagration in the various containment regions. The potential locations of hydrogen deflagrations

and detonations should be identified so that they may be used to assess any possible impact on the survivability of equipment, instrumentation and containment penetrations during a severe accident.

TABLE OF CONTENTS

	<u>Page</u>
ABSTRACT	ii
TABLE OF CONTENTS	iv
LIST OF FIGURES	vi
LIST OF TABLES	viii
1.0 PURPOSE	1-1
2.0 PHENOMENA	2-1
2.1 Description	2-1
2.1.1 Physical Processes	2-2
2.1.2 Relationship to Containment Failure Mechanisms and Modes	2-10
2.1.3 Relationship to Source Term	2-11
2.2 Relevant Experiments	2-11
2.2.1 Hydrogen Deflagration	2-11
2.2.2 Hydrogen Detonation	2-14
2.2.2.1 Intrinsic Detonability	2-14
2.2.2.2 Influence of Steam and Temperature	2-19
2.2.2.3 Initiation of Detonations	2-19
2.3 Analyses	2-22
2.3.1 Hydrogen Deflagration	2-22
2.3.2 Hydrogen Detonation	2-24
3.0 METHODOLOGY	3-1
3.1 Flammability	3-1
3.2 Combustion Completeness	3-2
3.3 Combustion Pressure Rise	3-2

TABLE OF CONTENTS
(Continued)

	<u>Page</u>
3.4 Evaluation of DDT Potential	3-2
4.0 PLANT SPECIFIC APPLICATION	4-1
4.1 Hydrogen Igniter System	4-1
4.2 Bounding Assessment of Hydrogen Deflagration	4-8
4.3 Assessment of Hydrogen Detonation Potential	4-13
4.4 Uncertainties	4-19
5.0 ACCIDENT MANAGEMENT IMPLICATIONS	5-1
6.0 CONCLUSIONS	6-1
7.0 REFERENCES	7-1
APPENDIX A: Calculation of H ₂ -Air-Steam Composition	A-1
APPENDIX B: Post-Combustion Pressure Rise Calculation	B-1
APPENDIX C: Summary of DDT Potential Evaluation From NUREG/CR-4803	C-1

LIST OF FIGURES

<u>Figure No.</u>		<u>Page</u>
2-1	Minimum ignition energy for hydrogen deflagrations (reproduced from Camp, 1983)	2-4
2-2	Comparison of ignition source energies (reproduced from Fauske & Associates, 1990a)	2-5
2-3	The flammability floor domain for upward flame propagation for H ₂ -Air-H ₂ -O (vapor) mixtures. The flammability limit curve is superimposed on the isobaric contours of calculated adiabatic explosion pressure (reproduced from Hertzberg, 1981)	2-6
2-4	Theoretical adiabatic, constant-volume combustion temperatures of hydrogen-air-mixtures (reproduced from Sherman, 1981)	2-7
2-5	AICC pressures for various containment initial conditions (reproduced from Sherman, 1984)	2-9
2-6	Degrees of combustion in hydrogen-air-steam mixtures (from Liu, 1981)	2-12
2-7	Combustion completeness for Nevada Test Site premixed combustion tests (reproduced from Ratzel, 1985)	2-13
2-8	The effect of steam addition at intermediate hydrogen concentration (reproduced from Kumar, 1984)	2-15
2-9	Comparative pressure profiles for three 8% (nominal) hydrogen combustion tests having different pre-combustion steam concentrations. Numbers in parentheses are the steam concentrations (reproduced from Ratzel, 1985)	2-16
2-10	Measured values (McGill, Sandia) of the detonation cell width (λ) as a function of hydrogen concentration (reproduced from Tieszen, 1987)	2-18

LIST OF FIGURES

(Continued)

<u>Figure No.</u>		<u>Page</u>
2-11	Detonation Cell width as a function of the equivalence ratio for various steam concentrations (reproduced from Tieszen, 1987)	2-20
2-12	Detonation cell width as a function of temperature (reproduced from Tieszen, 1987)	2-21
2-13	FLAME apparatus DDT results (reproduced from Sherman, Tieszen, Benedick, 1989)	2-23
4-1	Vertical section of AP600 containment (taken from Bechtel drawing 1000-P2-901)	4-2
4-2	Vertical section of AP600 containment (taken from Bechtel drawing 1000-P2-902)	4-3

LIST OF TABLES

<u>Table No.</u>		<u>Page</u>
4-1	Inputs for Bounding Assessment of Hydrogen Deflagration in the AP600 Containment	4-9
4-2	Results for Bounding Assessment of Hydrogen Deflagration in the AP600 Containment	4-11
4-3	DDT Scaling Assessment for AP600 Compartments With Transverse Venting	4-16
4-4	DDT Scaling Assessment for AP600 Compartments With No Transverse Venting	4-17
C-1	Classification of Hydrogen-Air Mixtures at 20°C and 1 atm Pressure	C-1
C-2	Geometric Classes for Flame Acceleration	C-2
C-3	Dependence of Result Class on Mixture and Geometric Class	C-3
C-4	Classification of the Probability of DDT	C-4

1.0 PURPOSE

The potential failure of a nuclear plant containment building due to an energetic hydrogen burn has been the subject of technical exchange between the Nuclear Regulatory Commission (NRC) Staff, NRC contractors, and the nuclear industry. Discussion has been motivated by the concern that hydrogen evolved during a core damage event could accumulate in the containment building and be ignited. Such an event occurred in containment during the TMI-2 accident. If the combustion was energetic enough to fail the containment, the timing (i.e., before or shortly after vessel failure) and uncertainties in location of the containment shell failure have potentially important ramifications regarding the radiological source term because natural fission product deposition mechanisms would not have sufficient time to significantly affect (reduce) the masses of fission products that could be released through the failure location.

The objective of this paper is to develop a strategy to account for postulated hydrogen combustion-induced failure of the containment when developing the source term portion of the ALWR Risk Analysis for the AP600. The occurrence of hydrogen combustion and/or detonation will be assessed to determine its potential for containment failure.

2.0 PHENOMENA

2.1 Description

Hydrogen combustion, or burning, is the result of a chemical reaction between gaseous hydrogen and gaseous oxygen. The products of such a reaction are steam and energy; the energy is liberated as light and heat. Necessary conditions for hydrogen combustion are the presence of the right amounts of hydrogen and oxygen, and the presence of an ignition source or a trigger.

Given a volume filled with only hydrogen and oxygen gases, minimum concentrations of hydrogen and oxygen are required for hydrogen combustion to occur. A mixture containing too little hydrogen to burn is called "lean", while a mixture containing too little oxygen to burn is called "rich". The presence of another gas that does not participate in the combustion reaction (such as steam or nitrogen) also acts to inhibit the occurrence of combustion. As the concentration of the inert gas increases, the threshold concentration of lean hydrogen combustion increases. Extensive research has been performed for numerous combinations of hydrogen, oxygen, and inert gases to map out the hydrogen and oxygen concentrations that are combustible. These maps are referred to as flammability limits.

Given a flammable hydrogen and oxygen mixture, a trigger is necessary to initiate burning. The AP600 design includes igniters which are designed to burn hydrogen as it evolves, so as to prevent the accumulation of large hydrogen concentrations. Typically a spark is sufficient to ignite a flammable mixture. The required trigger energy decreases as the hydrogen gas temperature increases, until a threshold temperature is reached. Above this threshold, the hydrogen is energetic enough to self-trigger (or auto-ignite) combustion of a flammable mixture.

Given a volume containing hydrogen and oxygen concentrations within the flammability limits, and a trigger that initiates combustion, the magnitude of energy release depends on the mass of hydrogen consumed by the chemical reaction. The combustion of one lb-mole of

hydrogen releases 1.04×10^5 BTUs of energy. Ignition of gas mixtures with hydrogen concentrations near the flammability limits have too little hydrogen or oxygen for the flame front to propagate throughout the entire volume and consume all of the available hydrogen; such burns are called "partial" burns. As the hydrogen concentration moves away from the flammability limits, more complete burning of the reactants occurs. Above threshold hydrogen and oxygen concentrations, ignition will cause complete consumption of the reactants or "global" burns. Global burns yield the maximum energy release that can be obtained from hydrogen combustion.

2.1.1 Physical Processes

Two types of hydrogen combustion reactions are pertinent to a PRA: deflagration and detonation. Deflagration is a combustion process in which the combustion front moves at subsonic velocity with respect to the unburned gas, while detonation is defined as sonic or supersonic propagation of the combustion front. This distinction is important because the pressure in the deflagration cannot exceed the adiabatic constant volume process value (adiabatic, isochoric, complete combustion, or AICC). In a detonation, transient overpressure can exceed this value by a factor of two or more, and pressure can vary significantly across the detonation front. Pressure is uniformly distributed during a deflagration because the flame moves slowly with respect to pressure waves. The transient overpressure associated with a detonation lasts only briefly, so structures may be able to withstand detonations when the impulsive load is not excessive.

Factors which determine the type of combustion reaction include the concentrations of fuel (hydrogen and carbon monoxide), oxidant (oxygen in air), and inertant (nitrogen, steam or carbon dioxide, in air), initial temperature and pressure, containment geometry, turbulence level, and combustible mixture ignition sources. Composition and the initial thermodynamic state impose limits to both flammability and detonation. Turbulence also enhances the burn completeness. In order for combustion to occur, the gas mixture must be flammable and there must be an ignition source. Relatively feeble sources such as static discharge and sparks can cause ignition. Figure 2-1 presents the minimum ignition energy for hydrogen deflagrations. For the case of

13% by volume of hydrogen in air, approximately 0.07 millijoules are sufficient to ignite a hydrogen burn. Figure 2-2 compares the energies of various potential ignition sources, including a match. A match burning for one second can release ten joules of energy, which is over three orders of magnitude more energy than that required to initiate a hydrogen burn.

High temperatures lead to slow volumetric oxidation, and very high hydrogen temperatures (about 1340 F (1000 K)) can cause autoignition. Autoignition is most likely to occur for sequences that release hydrogen rich and very high temperature gases from the reactor vessel into non-inerted compartments. It may also be possible that gas heating induced in the reactor cavity by dried-out core debris could result in very high temperature hydrogen mixtures being delivered to the lower compartment. Again, if the recipient compartment is not inerted, autoignition may occur. The well mixed average containment temperature is not hot enough during severe accident sequences to cause autoignition.

Classical limits for flammability and AICC maximum equilibrium final pressure are presented in Figure 2-3 [Hertzberg, 1981]. The region of concern generally lies below the line of stoichiometric mixtures, in which hydrogen is the limiting reactant. The minimum amount of hydrogen necessary for combustion is slightly over 4% in dry air. The minimum oxygen concentration necessary for combustion is about 5% in dry air, corresponding to about 75% hydrogen. Addition of steam to any mixture of hydrogen and air would reduce the hydrogen volumetric concentration and increase the required threshold concentration for combustion.

Figure 2-4 presents the AICC overpressure ratio resulting from combustion in air, and indicates classical deflagration and detonation limits [Sherman, 1981]. Figure 2-4 shows the lower limit corresponding to upward flame propagation (as indicated in Figure 2-3), and a higher limit corresponding to downward flame propagation (i.e., against the buoyancy forces acting on the flame). Also, the hydrogen concentration required for detonation is higher than the threshold for downward flame propagation. However, detonation limits shown in this figure are too

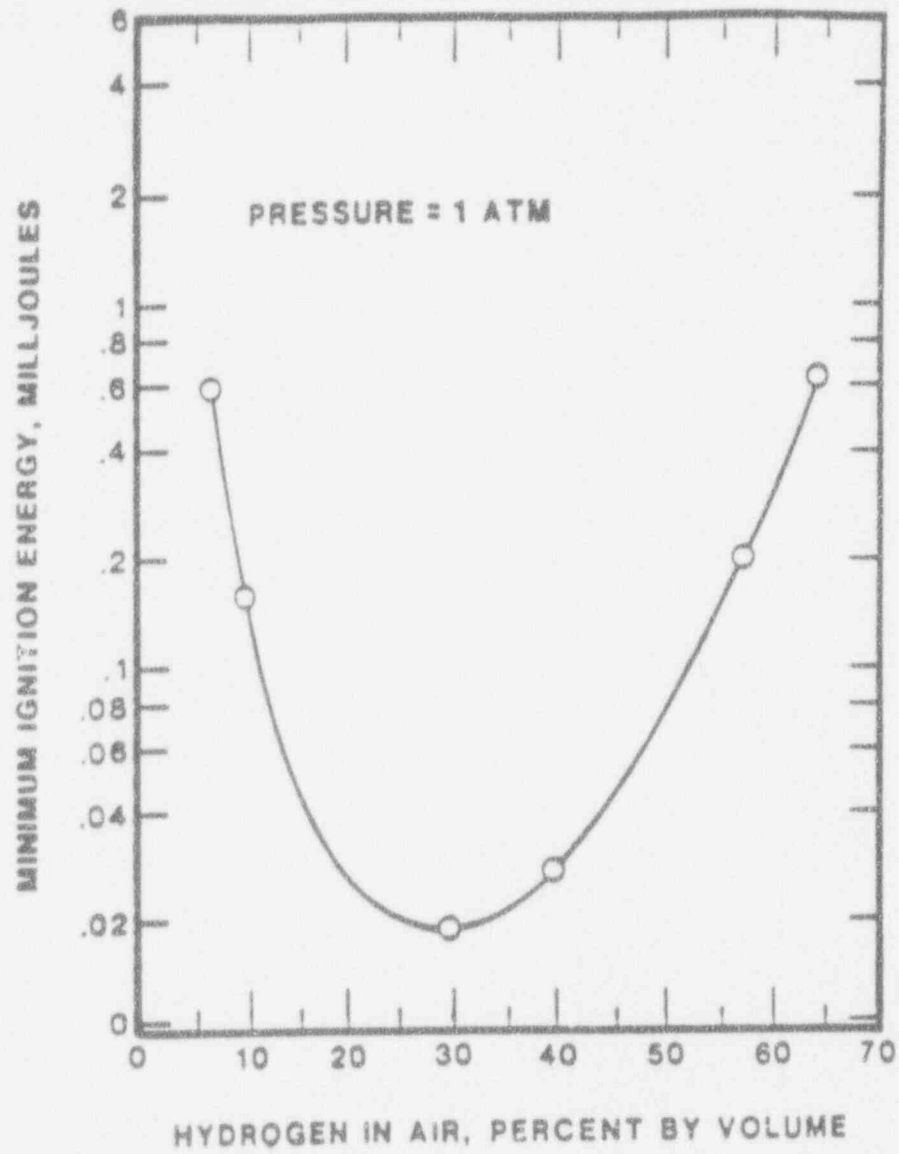


Figure 2-1 Minimum ignition energy for hydrogen deflagrations
(reproduced from Camp, 1983).

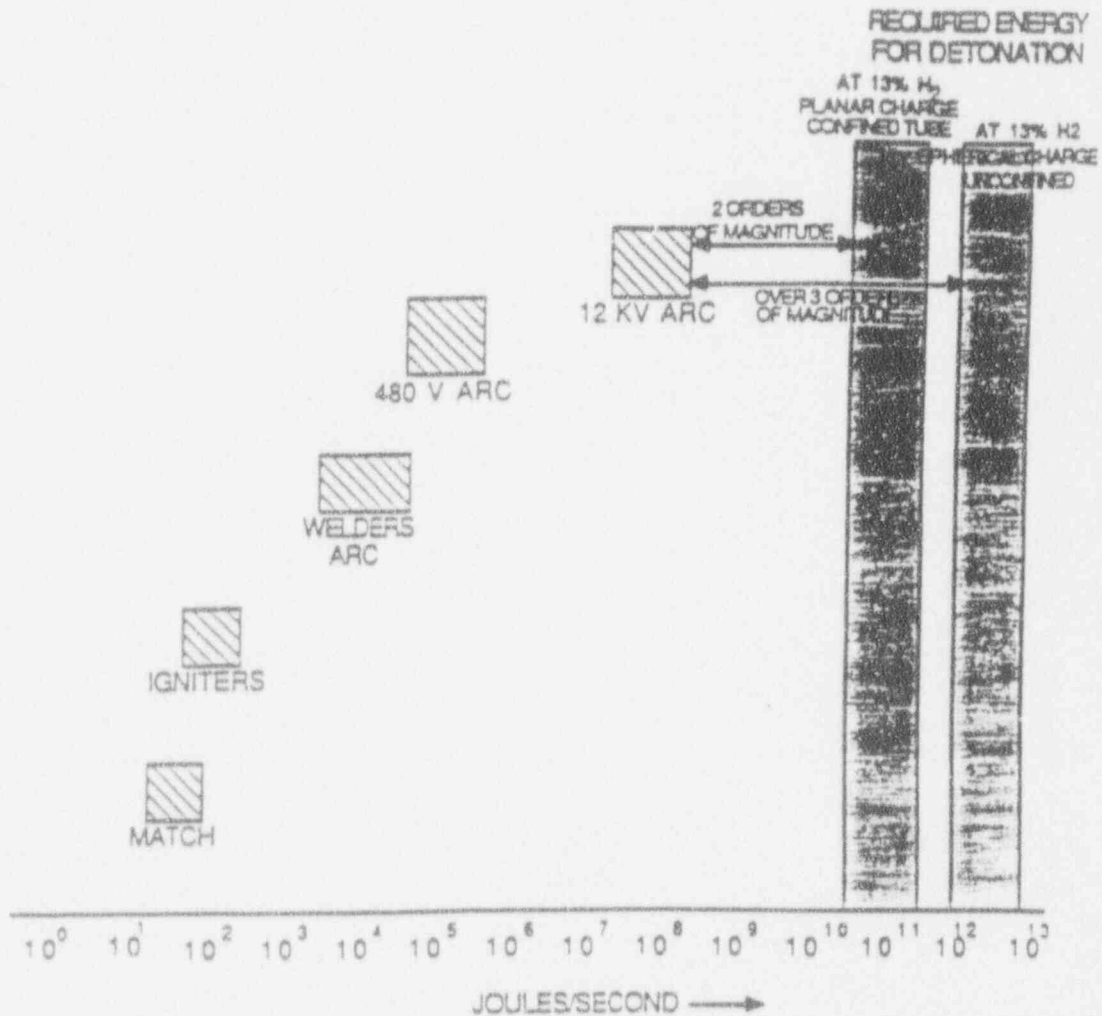


Figure 2-2 Comparison of ignition source energies (reproduced from Fauske & Associates, 1990a).

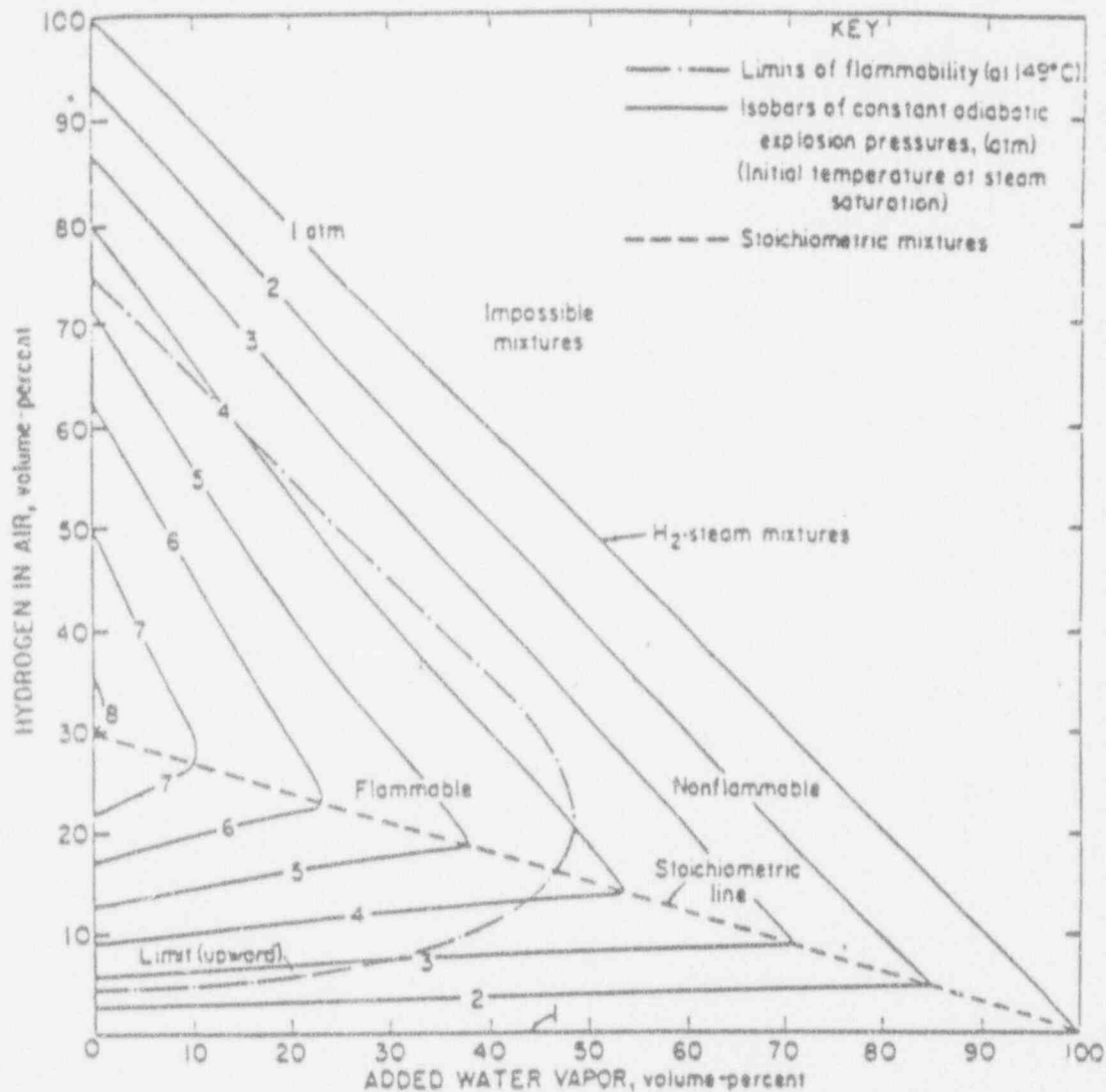


Figure 2-3 The flammability floor domain for upward flame propagation for H_2 -Air- H_2O (vapor) mixtures. The flammability limit curve is superimposed on the isobaric contours of calculated adiabatic explosion pressure (reproduced from Hertzberg, 1981).

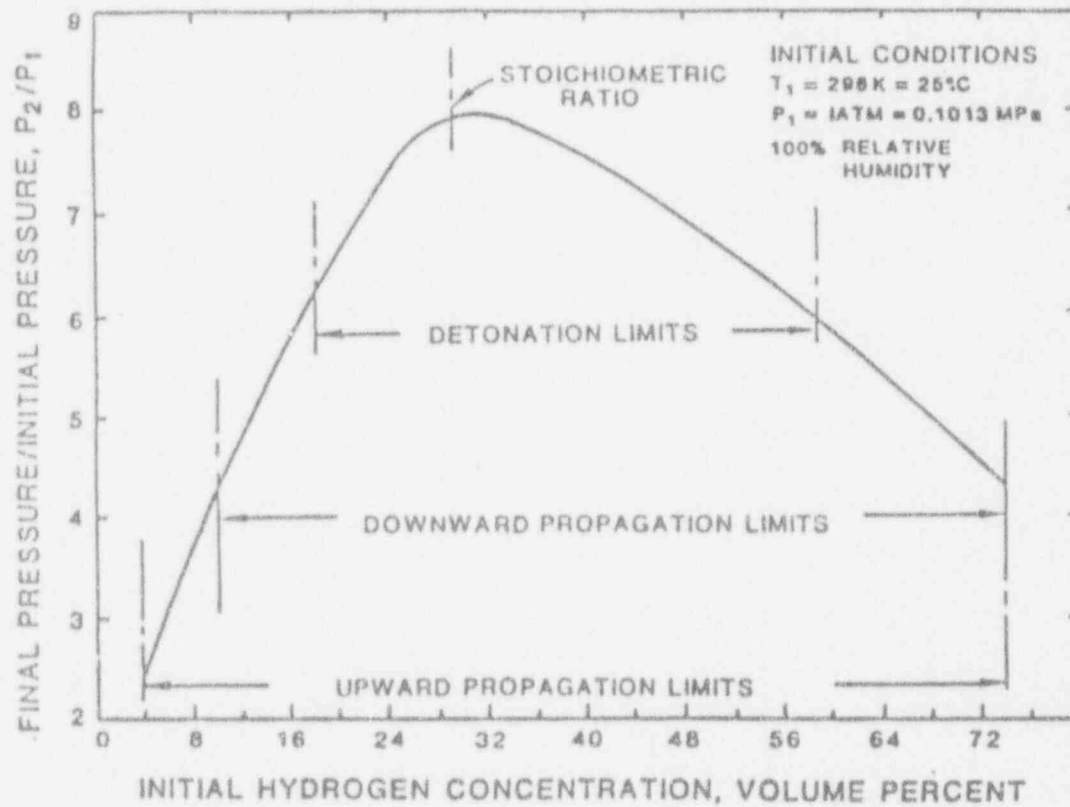


Figure 2-4 Theoretical adiabatic, constant-volume combustion pressures of hydrogen-air-mixtures (reproduced from Sherman, 1981).

simplistic for reactor applications because detonation limits have been shown to be dependent on scale and temperature in a systematic fashion.

The effect of steam on post-combustion pressure is quantified for various initial saturation conditions as a function of hydrogen concentration in Figure 2-5 [Sherman, 1984]. In this figure, the initial pressure is calculated by adding the partial pressure of hydrogen and steam to a humid air mixture originally at 14.7 psi (1.0 atm) total pressure at 80.6 F (300 K). A method for calculation of approximate pre-combustion conditions is shown in Appendix A. The post-combustion conditions for non-saturated conditions, or for mixtures containing carbon dioxide and/or carbon monoxide, can be easily found by iterative solution of the energy equation as shown in Appendix B.

Generally, combustion is incomplete for hydrogen concentrations in dry air less than 8% to 9% (the downward flammability limit). Also, the addition of steam reduces combustion completeness for lean mixtures. Therefore, the pressure calculations indicated in Figures 2-3 and 2-5 are upper bounds. Details are discussed in Section 2.2.

Detonations are more difficult to achieve than deflagrations. An initiation mechanism must exist, and the gas mixture must be intrinsically detonable (i.e., able to sustain a detonation once initiated). Initiation mechanisms include direct energy deposition and deflagration to detonation transition (DDT) during flame acceleration. Intrinsic detonability is a function of both thermodynamic variables (pressure, temperature, and gas composition) and geometry.

DDT is the most likely mechanism for initiation of detonations in a containment because known energy sources are not large enough for direct initiation to occur. Also, a hydrogen concentration of at least 15% in dry air is probably necessary for DDT in a containment. The required concentration for DDT increases with steam addition. Initiation of detonations is discussed in more detail in Section 2.2.

A mixture of 13% hydrogen in dry air at standard temperature and pressure (STP) is

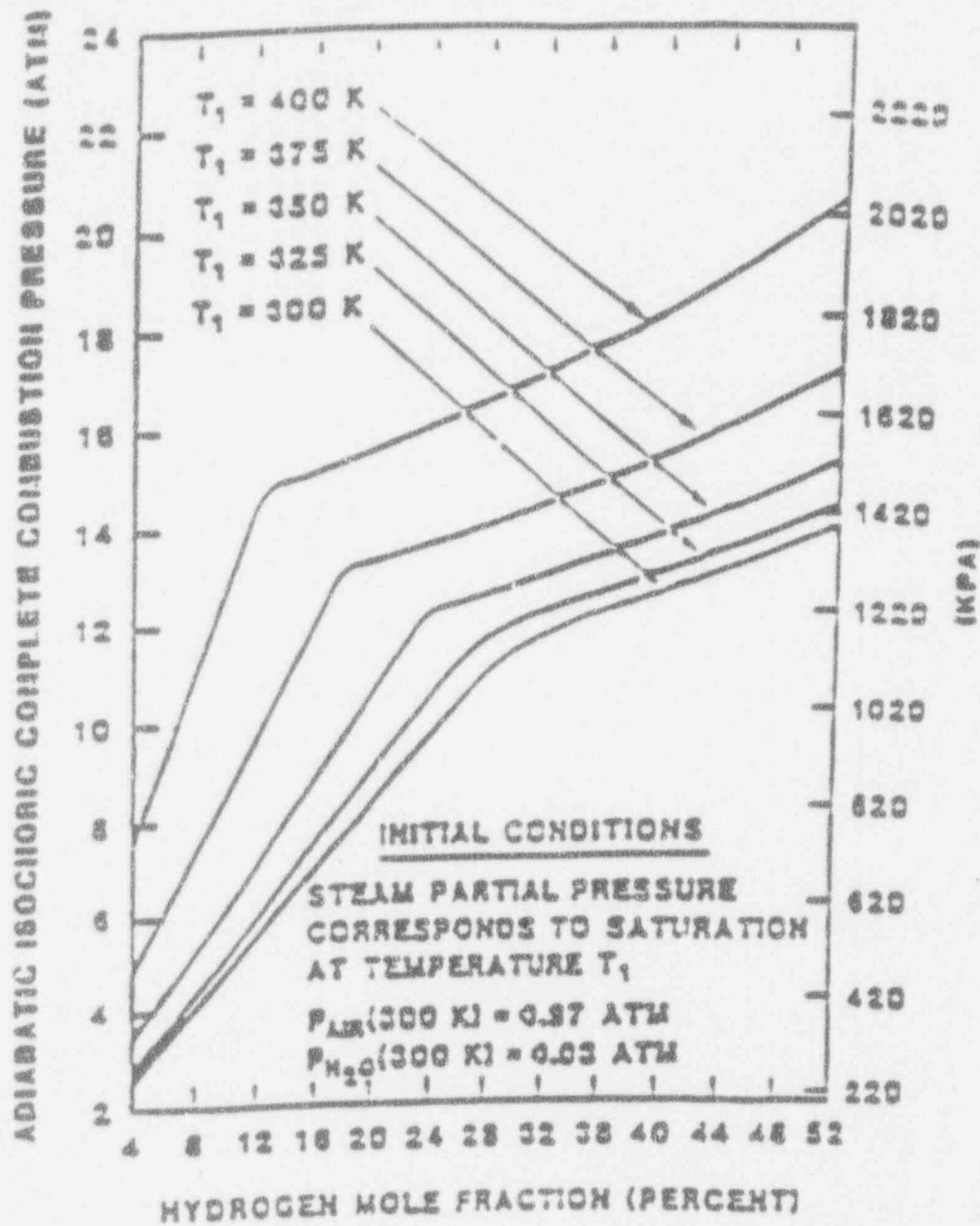


Figure 2-5 AICC pressures for various containment initial conditions (reproduced from Sherman, 1984).

intrinsically detonable. The required concentration decreases quickly with increasing temperature, but increases even more rapidly with steam addition. Mixtures with greater than 30% steam may be immune to detonations. Intrinsic detonability is also discussed in greater detail in Section 2.2.

2.1.2 Relationship to Containment Failure Mechanisms and Modes

Hydrogen combustion is a potential threat to containment integrity because of the increase in pressure and temperature during the event. During severe accidents, there are several potential sources of hydrogen. These sources include in-vessel oxidation of zirconium and stainless steel during core overheating and relocation. Ex-vessel sources include zirconium, chromium, and iron oxidation during core-concrete interactions or during high pressure debris dispersal (DCH) and long term relocation of degraded core materials following vessel failure. The quasi-static pressure load on the containment is limited to the AICC pressure, and is generally lower due to both incomplete combustion and heat transfer to structures during the event. The transient load during a detonation lasts only for a period of milliseconds and may be unable to cause containment failure, though equipment damage may still be possible. Because flames may accelerate during a deflagration, equipment damage may occur due to a local impulse loading. The temperature load only lasts from tens of seconds to a few minutes, with the peak being brief and decay being sharp.

From the phenomenological description in Section 2.1.1, it is clear that hydrogen combustion can only occur when both sufficient hydrogen and oxygen are present, when insufficient steam is present to prevent flammability, and when an ignition source exists. Therefore, hydrogen combustion is not a possible containment failure mechanism for inerted containments. This includes inerting due to steam which is often a direct and natural consequence of the postulated accident sequence and the progression to core overheating and damage. Also, the containment load is highly dependent upon initial conditions which influence combustion completeness and pressure rise. Therefore, the existence of a combustion event does not automatically imply containment failure. The maximum pressure must be compared against a containment failure criterion (see Section 4).

2.1.3 Relationship to Source Term

Combustion influences the source term primarily through containment failure. That is, if hydrogen combustion can result in containment failure, then the time of combustion becomes significant. In general, combustion can potentially increase the source term because containment failure can occur earlier through this mechanism than through slow pressurization due to loss of decay heat removal. Early containment failure generally increases the source term because the airborne fission product concentration tends to decay with time in an intact containment. In summary, the delay time between fission product release from fuel (either in-vessel or ex-vessel) and release to the environment (due to containment failure) may be decreased due to hydrogen combustion.

Because combustion influences containment gas and structure temperatures, a secondary influence on fission product revaporization occurs. This effect is usually minor in the containment, and is quantifiable with knowledge of the structure's temperature history.

2.2 Relevant Experiments

2.2.1 Hydrogen Deflagration

In the preceding section, a discussion of ideal adiabatic pressures resulting from hydrogen deflagrations was presented. In practice, at low hydrogen concentrations, this pressure limit is not achieved because combustion is incomplete. As illustrated in Figures 2-6 and 2-7, incomplete burning occurs for hydrogen concentrations below the downward flammability limit, but above that limit combustion is fairly complete. The effect of steam addition is also shown in these figures. There is close agreement between these sets of deflagration data despite a significant disparity in geometric scale of the vessel used in each experiment (i.e., 0.0763 ft³ (.002 m³) and 72,324 ft³ (2048 m³), respectively) [Liu, 1981; Ratzel, 1985]. In both cases, it

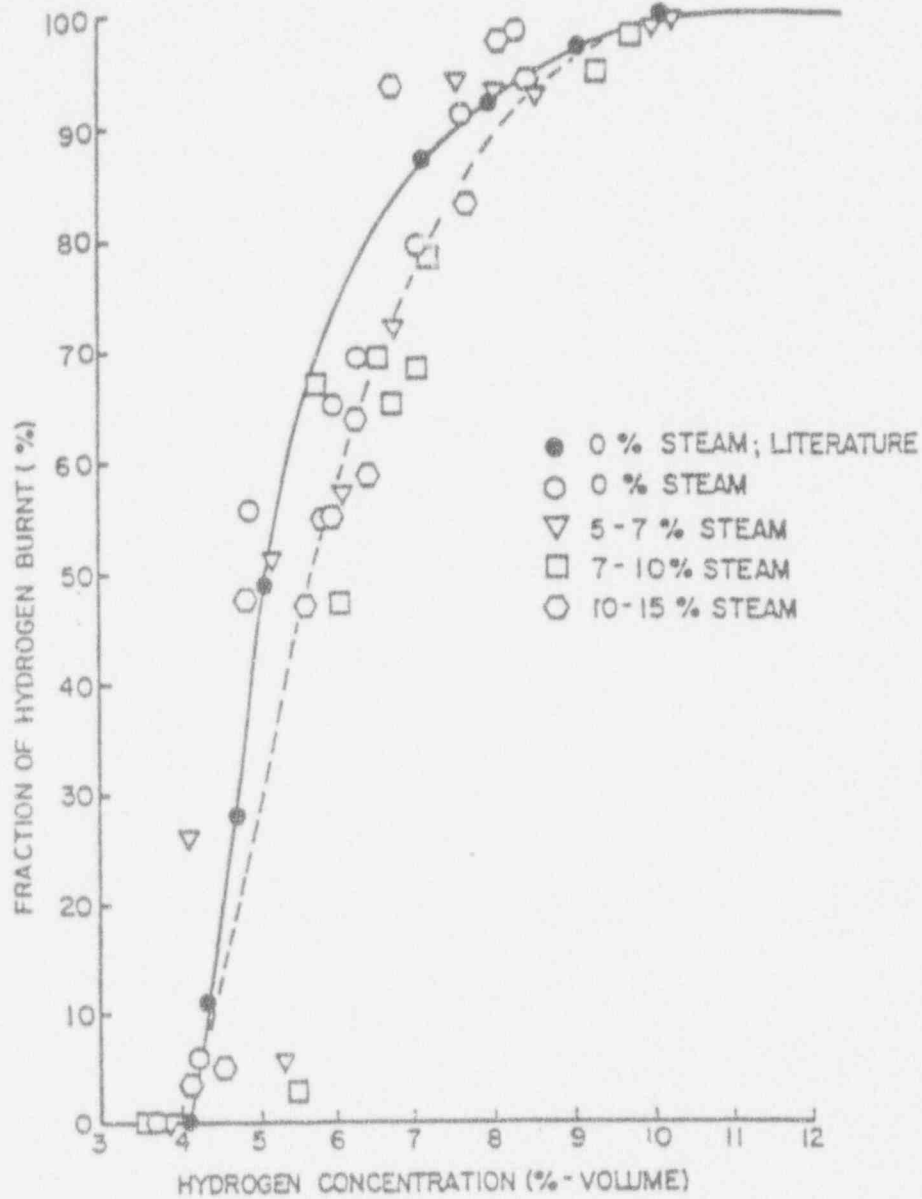


Figure 2-6 Degrees of combustion in hydrogen-air-steam mixtures
(from Liu, 1981).

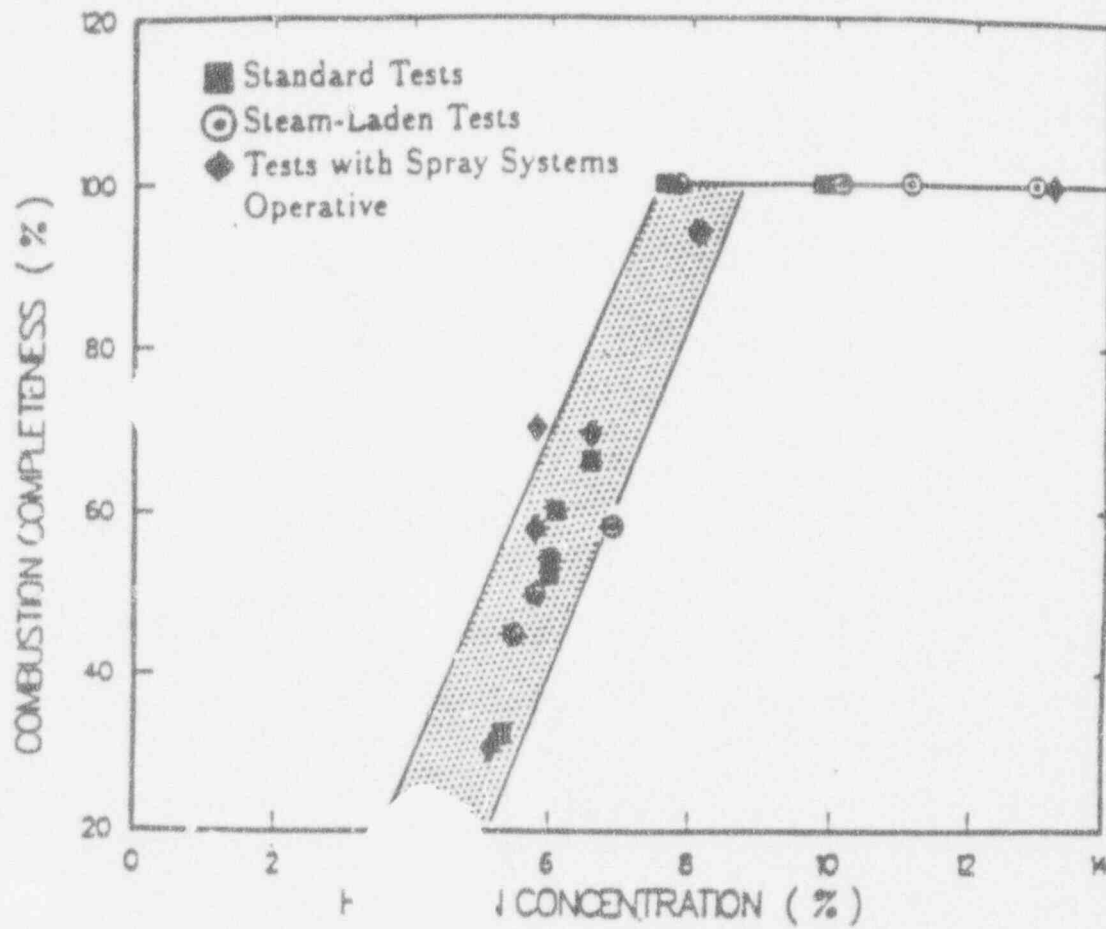


Figure 2-7 Combustion completeness for Nevada Test Site premixed combustion tests (reproduced from Katzel, 1985).

is evident that the addition of steam has an effect on the completeness of combustion, shifting the required hydrogen concentration to a higher value as more steam is added.

Steam affects the combustion completeness, flame velocity, heat capacity, and emissivity of the combustible gas mixture which, in turn, reduces the resultant system pressure rise. Figures 2-8 and 2-9 illustrate this reduction in combustion pressure as a result of increasing the relative concentration of steam for two different size systems: 222 ft³ (6.3 m³) and 72324 ft³ (2048 m³) spheres [Kumar, 1984; Ratzel, 1985]. Both sets of data were taken with initial hydrogen concentrations of 8%. The pressure rise ratio is reduced by about 50% in the large apparatus, and by an even greater factor in the smaller apparatus. In each case, combustion was only about 38% complete for the highest steam addition test.

2.2.2 Hydrogen Detonation

2.2.2.1 Intrinsic Detonability

The lowest value of hydrogen concentration for intrinsic detonability is now understood to be dependent upon geometric scale. Increasing scale allows the possibility of detonations at lower hydrogen concentrations. For example, the detonability limits shown in Figure 2-4 were based on observations in a small apparatus. Recently, detonability has been observed for mixtures of 13% hydrogen in dry air at 212°F (100°C) [Kumar, 1984] in a much larger apparatus (a 16.93 inch (43 cm) diameter tube). The National Research Council reached the conclusion that mixtures of 9 to 11% hydrogen might be detonable based upon these experiments with hot, dry mixtures driven by explosive charges. Of course, explosive charges do not exist in containment.

The ability for a detonation to be sustained or to propagate has been empirically found to be closely related to an intrinsic property of the mixture known as the detonation cell width, λ [Tieszen, 1987; National Research Council, 1987; Berman 1986]. The value of λ is lower for mixtures which are more easily detonable (hereafter termed more sensitive mixtures).

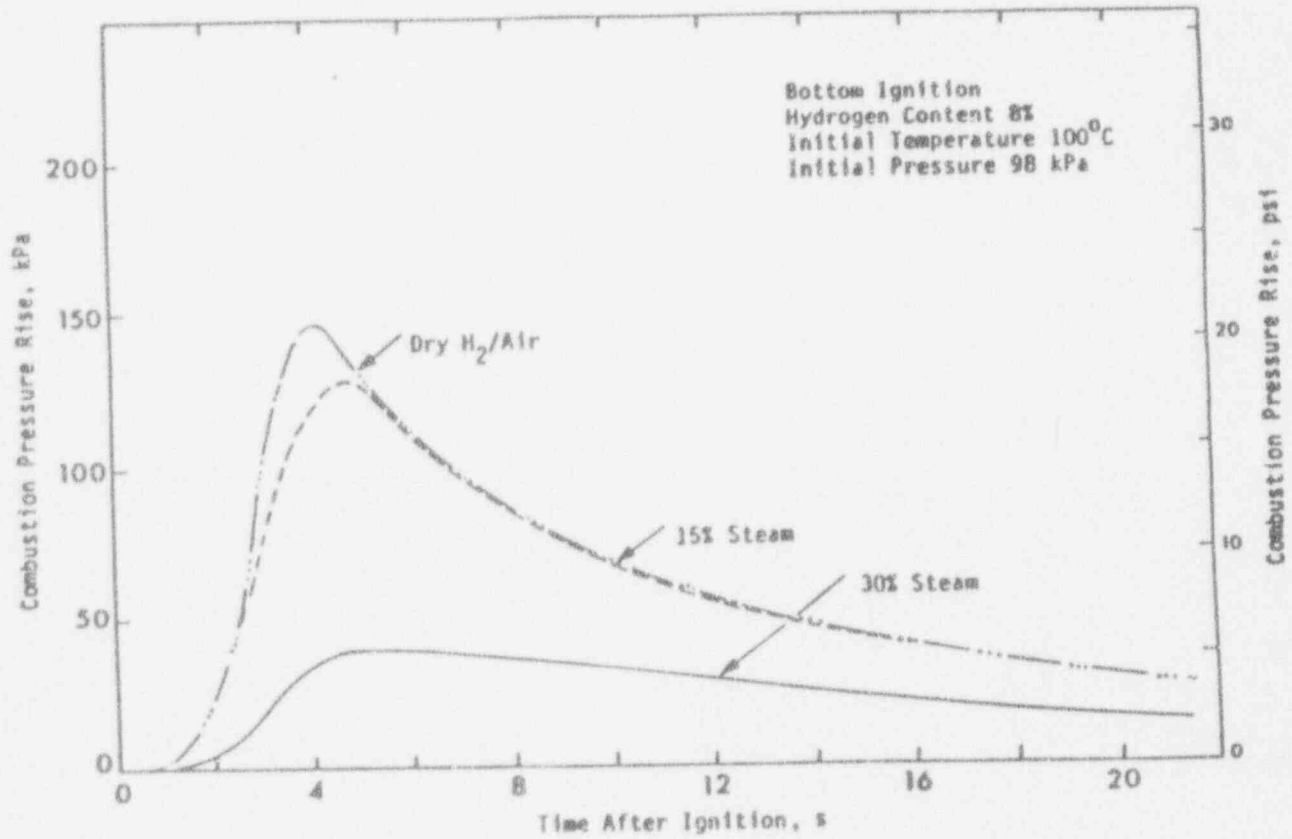


Figure 2-8 The effect of steam addition at intermediate hydrogen concentration (reproduced from Kumar, 1984).

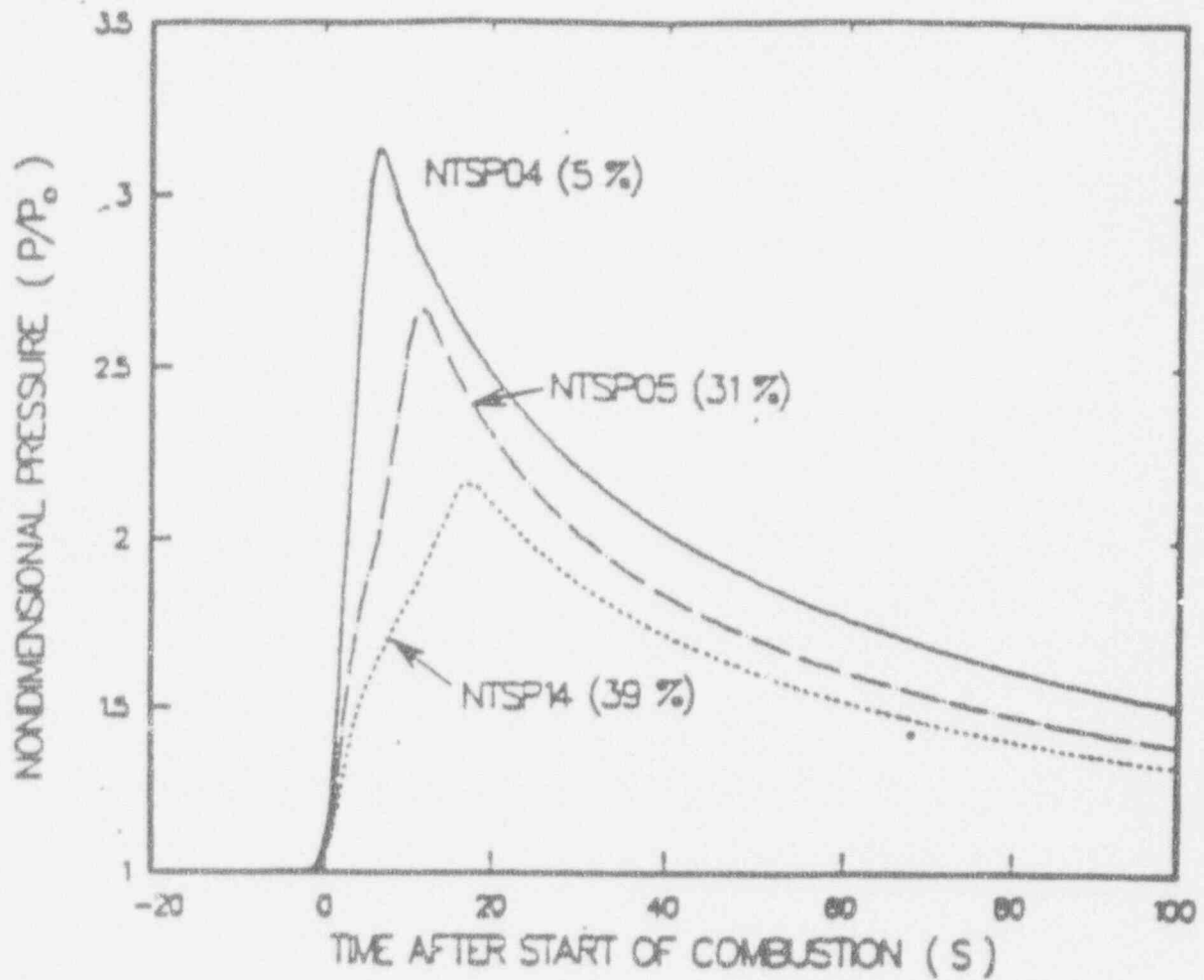


Figure 2-9 Comparative pressure profiles for three 8% (nominal) hydrogen combustion tests having different precombustion steam concentrations. Numbers in parentheses are the steam concentrations (reproduced from Ratzel, 1985).

Detonations have a three-dimensional cellular structure formed by multiple interactions of transverse waves and the main shock front. The structure is observable from the "fish-scale" pattern left on a smoked foil by shock wave intersections. The lowest stable detonation wave mode, called the singlehead spin mode, can be related to the tube diameter D through the relation $\lambda = \pi D$ [Tieszen, 1987]. For less sensitive mixtures, where λ is larger and $\lambda/\pi > D$, detonation is still possible given a sufficiently strong initiator. For an open, unconfined cloud, the detonation criterion is more strict than for tube geometry. The minimum cloud diameter d_c is related to the detonation cell width according to $\lambda = d_c/6.5$ [National Research council, 1987].

Measured cell widths for mixtures of hydrogen in dry air at 77°F (25°C) are shown in Figure 2-10. A minimum value of λ occurs near stoichiometry (29.7% hydrogen). For leaner mixtures λ increases rapidly, indicating a decrease in sensitivity. Detonation cell widths are uniformly lower at higher temperatures, indicating greater mixture sensitivity, that is, increased intrinsic detonability. These are plotted in terms of equivalence ratio, denoted by ϕ or ϵ , which is the molar ratio of hydrogen to air divided by the same quotient for dry air at stoichiometry. The equivalence ratio ϕ can be written as

$$\phi = \frac{SX_H}{1 - X_H - X_S} \quad (2-1)$$

where $S = 2.387$ and X_H and X_S are the hydrogen and steam mole fractions, respectively. The equivalence ratio for 13% hydrogen in dry air is 0.357. This value is unchanged by the addition of steam to the dry mixture because the overall H_2 and O_2 mole fractions decrease in the same proportion.

For the 16.93-in-diameter (43-cm-diameter) heated detonation tube (HDT) apparatus described in [Tieszen, 1987] the critical cell width is $\pi \times 16.93 = 53.16$ in., which corresponds to roughly 13% hydrogen from extrapolation of the curves in Figure 2-10. Thus, the



Figure 2-10 Measured values (McGill, Sandia) of the detonation cell width (λ) as a function of hydrogen concentration (reproduced from Tieszen, 1987).

observation of a detonation at 9.5% hydrogen [Stamps, 1987] demonstrates that high explosives can induce detonations in less sensitive mixtures. In that experiment 0.2337 lbm (106 grams) of high explosive, or about 474 Btu (0.5 MJ), provided the trigger.

2.2.2.2 Influence of Steam and Temperature

The detonation cell width increases dramatically with the addition of steam as shown in Figure 2-11 [Tieszen, 1987] for mixtures at 212°F (100°C). Thus, steam as a diluent makes detonation more difficult to achieve. As temperature increases, detonation becomes easier, as seen by the decrease in cell width in Figure 2-12 [Tieszen, 1987]. Comparing the two figures, one can clearly see that in this temperature range the steam inerting effect is far more pronounced than the heating effect on detonation cell size.

2.2.2.3 Initiation of Detonations

Detonations are much more likely to be initiated by deflagration to detonation transition (DDT) due to the size of ignition sources present in containment. The energy required for a detonation can be compared with energies of various ignition sources as shown in Figure 2-2 [Fauske & Associates, 1990a]. The largest possible ignition source in a containment, a 12 kv arc, results in a maximum arc energy of 37900 Btu (40 MJ) over four cycles. As shown in Figure 2-2, a 12 kv arc produces a peak rate of energy deposition that is about two orders of magnitude lower than the value for initiation of a planar detonation of 13% hydrogen in a confined tube (0.176 lbm (80 grams) of high explosive [Shepherd, 1985]). All the ignition sources indicated in Figure 2-2 are sufficient to cause a deflagration.

The lowest hydrogen concentration for which DDT has been observed is 15% [Sherman, et al., 1989]. The apparatus used was the FLAME facility at Sandia, which is a half-scale model of an ice condenser upper plenum, 8 ft (1.44 m) high, 6 ft (1.83 m) wide, and 100 ft (30.5 m) in length. To promote turbulence, obstacles were placed along the interior of this long straight rectangular channel. The 15% lower limit corresponds to a case with no top venting

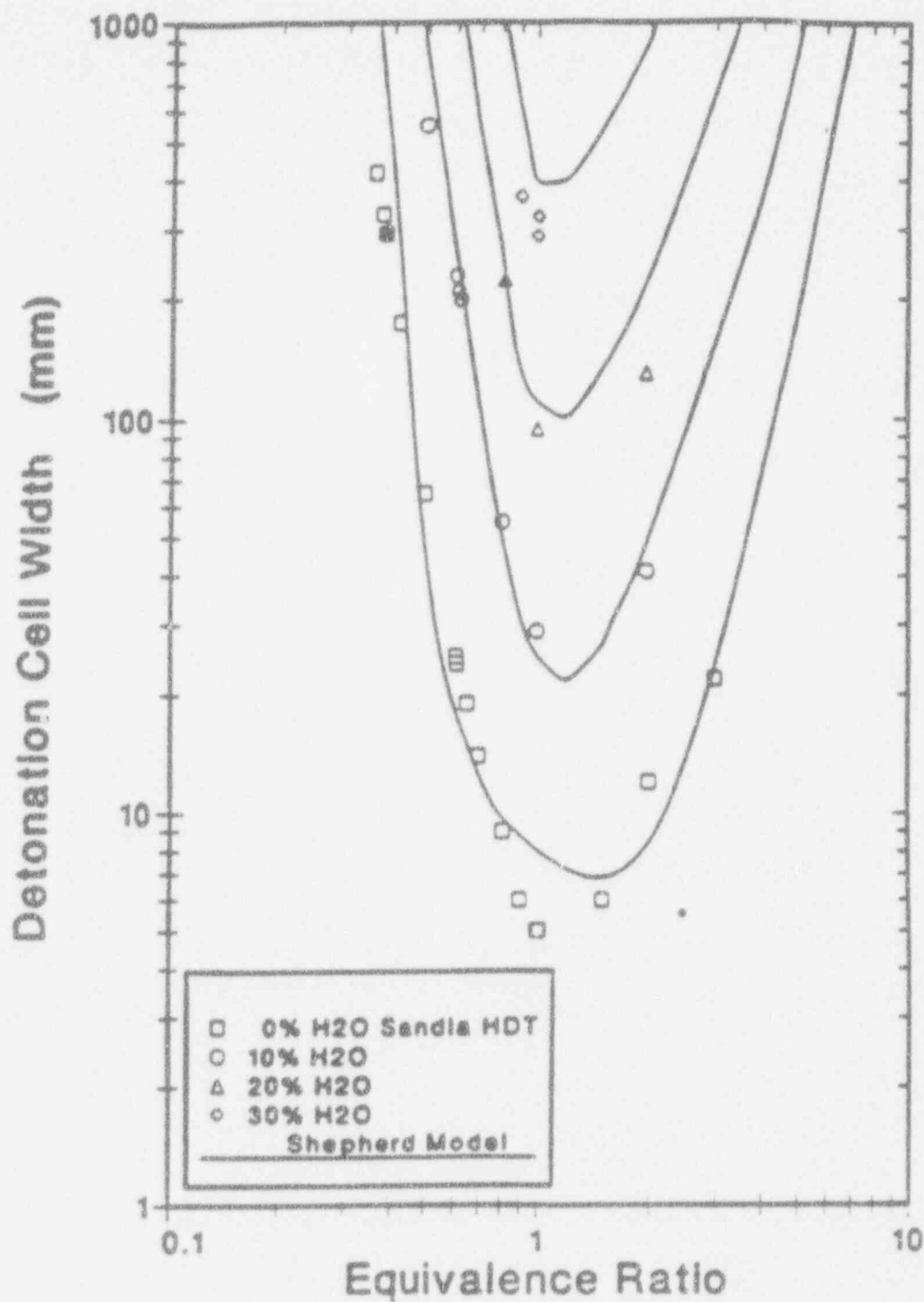


Figure 2-11 Detonation cell width as a function of the equivalence ratio for various steam concentrations (reproduced from Tieszen, 1987).

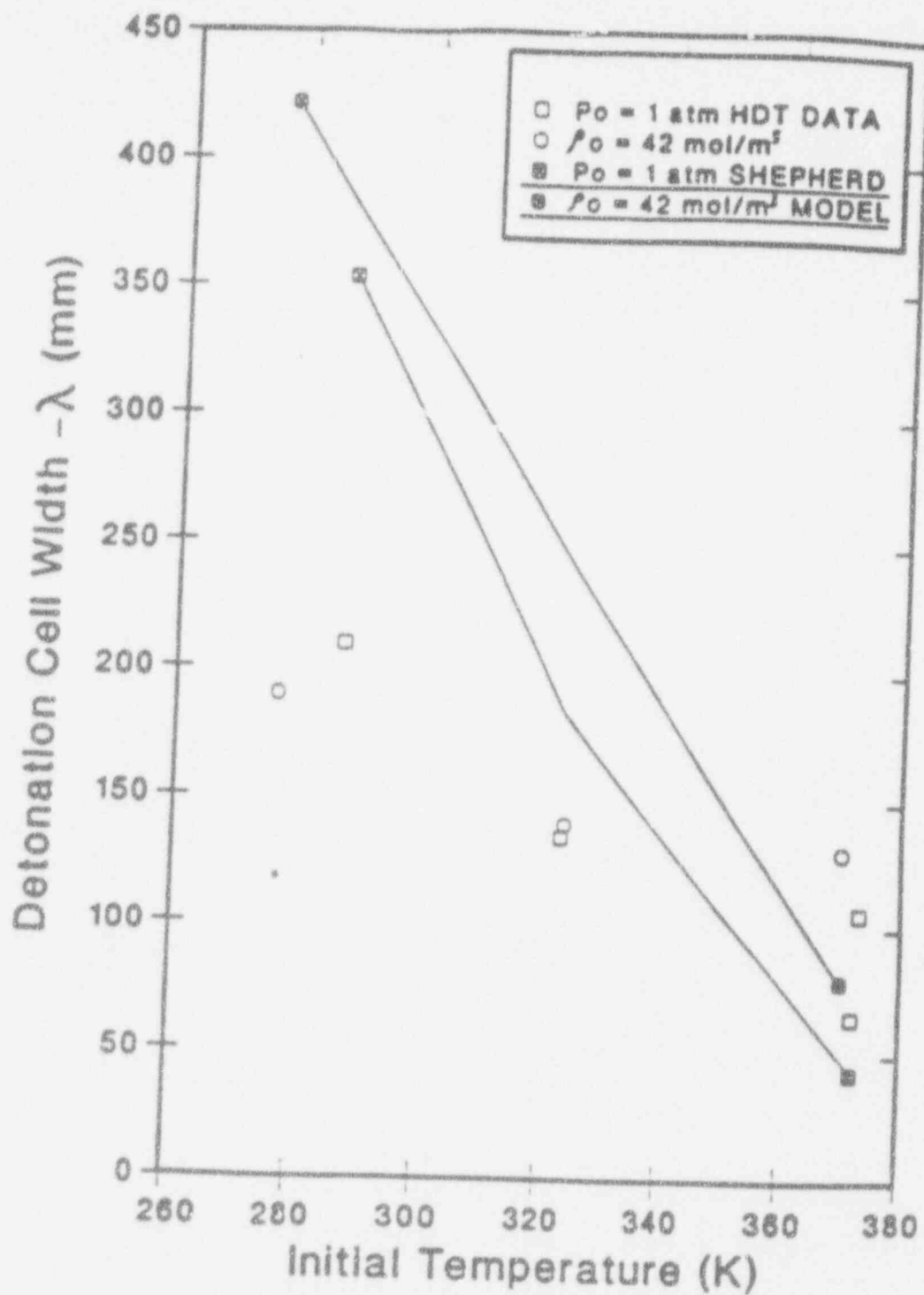


Figure 2-12 Detonation cell width as a function of temperature (reproduced from Tieszen, 1987).

and periodic obstacles every 6 ft (1.83 m). In a case with no obstacles, 25% hydrogen was required, as shown by Figure 2-13, and for a case with obstacles by 50% top venting, 20% hydrogen was required.

It is very difficult to relate the detonation cell width to a necessary or sufficient criterion for DDT because other characteristic lengths of the geometric configuration are influential. A case of attempted scaling of DDT by λ is reported by [Berman, 1986] who compares two sets of experiments [Stamps, 1987], one in a 3.28 ft by 3.28 ft (1 m by 1 m) channel and another in a 9.84 ft by 9.84 ft (3 m by 3 m) channel. The smaller experiments were performed at stoichiometry, and the larger experiments were performed at lower concentrations in the belief that scaling with λ could occur. At a concentration of 21% hydrogen ($\phi = 0.63$), for which $\lambda(\phi = 0.63)/\lambda(\phi = 1) = 3$, DDT occurred. This supports the hypothesis that in similar geometries DDT may occur for mixtures with similarly scaled cell widths. In both cases the apparatus included obstacles and was unvented.

2.3 Analyses

2.3.1 Hydrogen Deflagration

Two types of analyses are required for quantification of hydrogen deflagrations: flammability and pressure rise. The current state-of-the-art analytical tool for severe accident analysis is the combustion model developed by the DOE Advanced Reactor Severe Accident Program (ARSAP) [Fauske & Associates, 1990b] which has been incorporated into MAAP 4.0 as well as MAAP 3.0B.

In the absence of a more detailed model, the flammability limit diagram (Figure 2-3) can be used to estimate flammability. Mixture mole fractions can be estimated as shown in Appendix A. The combustion completeness can be estimated from Figure 2-7. The combustion pressure rise can be estimated through the methods discussed in Appendix B. Section 3.3 outlines an assessment methodology based on these appendices.

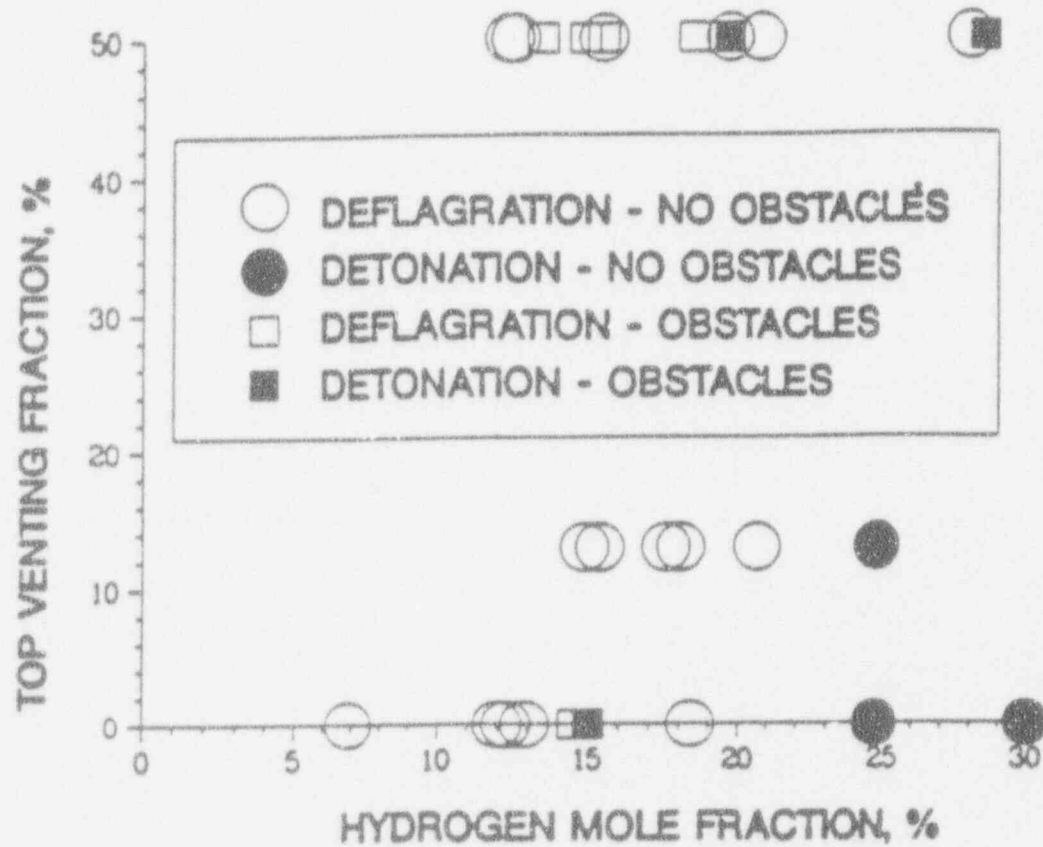


Figure 2-13 FLAME apparatus DDT results (reproduced from Sherman, Tieszen, Benedick, 1989).

2.3.2 Hydrogen Detonation

No publicly available computer programs exist which can predict the detonation cell width, the essential parameter for estimation of mixture detonability. Programs have been developed by the NRC for internal use [Shepherd, 1985] and agree fairly well with existing data, as shown in Figures 2-10 and 2-11. An empirical technique for judgement of detonability [Sherman and Berman, 1987] is described in Section 3.4.

3.0 METHODOLOGY

The methodology for determining the potential for hydrogen combustion consists of first identifying those sequences in which combustion might occur, and then estimating the combustion pressure rise. The potential for detonations is then considered. Finally, the load to containment must be compared with the containment failure criteria. The MAAP code can be used to study hydrogen combustion and the resulting containment load as an integral part of assessing severe accident sequences. Section 3.3 is applied in Section 4.1 in a simplified and conservative manner to assess the potential for containment overpressurization due to hydrogen burn for the AP600 containment.

3.1 Flammability

Identification of sequence in which combustion might occur requires calculation of the gas composition (mole fraction of all components), temperature, and pressure histories for all sequences. These states are then compared with a flammability limit diagram such as Figure 2-3. Fortunately, many sequences can be ruled out if one or more of the following conditions are met:

- less than 4% H_2 always,
- greater than 55% steam when H_2 present (steam inerting),
- less than 5% O_2 present.

The AP600 design includes a hydrogen igniter system. For sequences in which the igniters are operational, combustion is assured when the flammability condition is met. For sequences without igniters, combustion may never occur, although random ignition sources could ignite a flammable mixture at any time. Therefore, sequences for which flammable mixtures may form when the igniters are not operational should be evaluated both with and without combustion.

3.2 Combustion Completeness

A model can be used to quantify combustion completeness, or the data of Figure 2-7 will suffice for an estimate. An overestimate of combustion completeness will lead to an overprediction of final pressure, and therefore it may result in a conservative estimate of containment overpressure failure or conservatively early containment failure times.

3.3 Combustion Pressure Rise

Combustion pressure rise is determined through solution of the energy equation as shown in Appendix B. The steps to follow are:

1. Determine the initial gas composition (number of moles of each gas).
2. Determine the combustion completeness.
3. Determine the final gas composition.
4. Determine the heat of combustion.
5. Solve for the final temperature.
6. Solve for the final pressure.

3.4 Evaluation of DDT Potential

The potential for DDT in current commercial and advanced light water reactor containments has been evaluated using a procedure for engineering judgement by Sherman [Sherman and Berman, 1987]. The procedure assumes that the potential for DDT can be evaluated based on the mixture intrinsic flammability (detonation cell width) and type of geometry. Five classes of mixture sensitivity are defined ranging from Class 1, most detonable and near stoichiometry, to Class 5, least detonable, hydrogen mole fraction less than 13.5 in dry air. Five classes of geometry are defined, ranging from Class 1, which is most conducive to DDT and features large geometries with obstacles and partial containment, to Class 5, which is unfavorable to DDT and features large scale and complete confinement or small scale spherical

geometry with central ignition and no obstacles.

The mole fraction and equivalence ratios in Table C-1 are shown for dry hydrogen-air mixtures. For mixtures that include steam, experimental data and code calculations are used to calculate the corresponding cell widths. Figure 2-11 shows dependence of cell width on hydrogen and steam concentrations. Hence, the mixture class in Table C-1 corresponds to cell widths; the equivalence ratios/mole fractions shown are illustrations for the dry case.

Class 1 mixtures are extremely detonable. They are very likely to undergo DDT in most geometries of interest. Class 2 mixtures are slightly less likely to detonate. Class 3 mixtures have been observed to undergo transition in geometries which favor flame acceleration. Detonations have been propagated through Class 4 mixtures, but to date, DDT has not been observed for a hydrogen concentration less than 15%. Class 5 mixtures are unlikely to undergo DDT, although a detonation has been propagated in a 13.5% H_2 in air mixture at STP.

The procedure for estimating DDT potential is thus as follows:

1. Determine the mixture class from Table C-1 using Figures 2-10 and 2-11.
2. Determine the geometric class as guided by Table C-2.
3. Find the result class in Table C-3.
4. Assign a probability to this result from Table C-4.

4.0 PLANT SPECIFIC APPLICATION

Section 3 of this paper describes a method for assessing the effect of hydrogen deflagration or detonation within the containment during the course of a severe accident. The present section describes the application of that methodology to the risk analysis for the AP600 design. Containment pressurization due to hydrogen burns is assessed as a potential failure mode for the AP600 containment. Figures 4-1 and 4-2 illustrate the configuration of the AP600 containment.

The ultimate pressure capacity of the AP600 is about [(a,c) at 400°F, based upon expected actual material properties. The design philosophy of the AP600 emphasizes utilization of a hydrogen igniter system to prevent hydrogen accumulation and encourage a continuous burn, thereby minimizing the potential for a high-energy global burn. Specifically, the aim is to meet the requirements of 10CFR50.34, Appendix F, by limiting the hydrogen concentration to less than 10% by volume (dry conditions) and maintain containment integrity despite coincident combustion of all the hydrogen generated from 100% oxidation of the active fuel cladding. Note that these requirements are more stringent than those called for in the EPRI ALWR Requirements Document (13% H₂ and 75% oxidation).

4.1 Hydrogen Igniter System

The objective of the hydrogen igniter system is to promote hydrogen burning at as low a concentration as possible and to burn hydrogen more-or-less continuously so that the hydrogen does not accumulate in the containment. To achieve this goal, igniters are placed in all major regions of the containment where hydrogen may be released, through which it could flow, or where it may accumulate.

[(a,c)]

(a,c)

Figure 4-1 Vertical section of AP600 containment
(taken from Bechtel drawing 1000-P2-901).

(a,c)

Figure 4-2 Vertical section of AP600 containment
(taken from Bechtel drawing 1000-P2-902).

(a,c)

Igniters are placed in all major hydrogen transport paths so that it can be continuously burned close to the release point. This prevents hydrogen from accumulating preferentially in a certain region of the containment. Some igniters are positioned near the bottom of compartments so as to promote upward flame propagation at lean hydrogen concentrations. Where possible, they are placed away from walls and other large surfaces so that a fireball created by ignition at the bottom of a compartment can travel upward unimpeded.

One or more igniters are placed on or near the ceiling of compartments where the potential exists for hydrogen to rise and collect. Long, narrow compartments (corridors) are provided with sufficient igniters over their length so that the flame fronts created by the igniters need to travel only a limited distance before they merge, thereby limiting the potential for significant flame acceleration. Wherever possible, the igniters are located above the containment flood level.

(a,c)

(a,c)

Hydrogen released from the break during a LOCA is very likely to traverse through one of the steam generator compartments to reach the open space above the operating deck. It is preferable to burn the hydrogen in the steam generator compartment as it is likely to result in more or less continuous burning, which results in gradual addition of combustion energy to containment. Therefore, more time is available to dissipate this energy through the passive containment cooling system.

(a,c)

(a,c)

(a,c)

4.2 Bounding Assessment of Hydrogen Deflagration

As long as the igniters are operational, any hydrogen produced will be burned continuously and the associated containment pressurization will be insignificant. The only sequences of concern in terms of hydrogen deflagration are those where the igniters are not operable. The worst case scenario would then be a total station blackout, where all power to the igniters is lost, combined with a "single combustion event" in which all hydrogen generated from 100% oxidation of the zircaloy cladding is allowed to burn at once in the upper compartment. This is a very unlikely event for the AP600 design.

The initial conditions and inputs used for this limiting assessment are presented in Table 4-1. The values for the net containment volume and mass of zirconium cladding (active fuel) were taken from the AP600 MAAP parameter file. Since steam acts as an inertant, it is conservative to assume a completely dry atmosphere in the containment immediately prior to an accident (relative humidity = 0%). The actual initial relative humidity would be about 90%.

Step 1: Containment Hydrogen Composition

Following the method described in Appendix A, the moles of air (n_A) initially in the containment are calculated, using Equation (A-1) and Table 4-1, to be [

](a,c). This number represents the amount of dry air present under normal operating conditions, i.e., prior to a severe accident. The amount of nitrogen does not change during the severe accident, but the mass of steam does due to the initiating event and condensation on passive heat sinks. The mass of hydrogen is assumed to increase over time as a result of oxidation of zirconium with steam.

Additional hydrogen (and carbon dioxide) could potentially be produced due to molten core-concrete interaction (MCCI) over a long period of time starting from postulated debris dryout following reactor vessel failure. However, the availability of water from the AP600

Table 4-1

INPUTS FOR BOUNDING ASSESSMENT OF HYDROGEN DEFLAGRATION IN THE AP600 CONTAINMENT

CONTAINMENT

	(a,c)
--	-------

CORE

	(a,c)
--	-------

PHYSICAL PROPERTIES

<u>Gas</u>	<u>Constant Volume Heat Capacity (at 1160°F or 900 K)</u>
Nitrogen	0.195 BTU/lb _m -R (0.818 KJ/kg-K)
Oxygen	0.183 BTU/lb _m -R (0.767 KJ/kg-K)
Steam	0.43 BTU/lb _m -R (1.8 KJ/kg-K)
Hydrogen	2.53 BTU/lb _m -R (10.59 KJ/kg-K)

REACTIONS

	Heat of Reaction [Williams, et al., 1987] (BTU/lb _m -mol or MJ/kg-mol reactant)
$H_2 + \frac{1}{2} O_2 \rightarrow H_2O$	1.04 x 10 ⁵ or 242
$Zr + 2H_2O \rightarrow ZrO_2 + 2H_2$	2.57 x 10 ⁵ or 598
$Cr + \frac{3}{2} H_2O \rightarrow \frac{1}{2} Cr_2O_3 + \frac{3}{2} H_2$	0.86 x 10 ⁵ or 200
$Fe + H_2O \rightarrow FeO + H_2$	0.12 x 10 ⁵ or 28
$Ni + H_2O \rightarrow NiO + H_2$	0.01 x 10 ⁵ or 2.5

passive safety systems would prevent the debris from attacking the concrete and, thus, minimize hydrogen production during all but a few (very low probability) sequences.

(a,c)

Step 2: Combustion Completeness

Steam inerting can be anticipated in a majority of severe accident sequences, and it acts to inhibit or prevent hydrogen combustion. Igniters that burn hydrogen as it is released will maintain the hydrogen concentration at approximately the lean (upward propagation) flammability limit, i.e., approximately 4%. Hence, igniter system operation would prevent the accumulation of detonable concentrations of hydrogen but would not completely burn the hydrogen in containment. The bounding assessment provided in this section will conservatively assume complete combustion.

Step 3: Final Gas Composition

(a,c)

Table 4-2

**RESULTS FOR BOUNDING ASSESSMENT OF HYDROGEN
DEFLAGRATION IN THE AP600 CONTAINMENT**

<div data-bbox="185 519 413 559" data-label="Text"> <p><u>Before Accident</u></p> </div>	<div data-bbox="1296 619 1376 657" data-label="Text"> <p>(a,c)</p> </div>
<div data-bbox="185 734 498 776" data-label="Text"> <p><u>Before Hydrogen Burn</u></p> </div>	<div data-bbox="1296 1021 1376 1059" data-label="Text"> <p>(a,c)</p> </div>
<div data-bbox="185 1287 484 1330" data-label="Text"> <p><u>After Hydrogen Burn</u></p> </div>	<div data-bbox="1296 1464 1376 1502" data-label="Text"> <p>(a,c)</p> </div>

(a,c)

Step 4: Heat of Combustion

(a,c)

Step 5: Post-Burn Temperature

The pressure in containment is bounded by calculating the adiabatic isochoric complete combustion (AICC) of the hydrogen. This adiabatic calculation ignores the potential for containment heat removal. Thus, all the combustion energy is used to heat the containment atmosphere and produce the largest possible pressure increase. This calculation assumes that all the hydrogen produced during the severe accident accumulates in containment and burns all at once. This ignores the possibility of hydrogen burning as it is released, either by autoignition or ignition by igniters in localized regions should the flammability limits there be satisfied. If the hydrogen is burned as it is released, the passive containment cooling system would prevent significant pressurization.

(a,c)

Step 6: Post-Burn Pressure

(a,c)

Note that this bounding assessment has been based on conservative assumptions. The assumptions include a large source of hydrogen (oxidation of 100% of the active fuel cladding), no credit for containment heat sinks or the passive containment cooling system, no credit for the igniter system, and no credit for steam inerting. Nevertheless, the resulting post-burn pressure is still calculated to be within the AP600 containment's ultimate capacity.

It is concluded that hydrogen deflagration in the AP600 containment will not fail the containment boundary. Thus, the containment event trees do not need a separate node for hydrogen deflagrations.

4.3 Assessment of Hydrogen Detonation Potential

(a,c)

(a,c)

(a,c)

Table 4-3

DDT SCALING ASSESSMENT FOR AP600 COMPARTMENTS
WITH TRANSVERSE VENTING

(a,c)

Table 4-4

DDT SCALING ASSESSMENT FOR AP600 COMPARTMENTS
WITH TRANSVERSE VENTING

(a,c)

(a,c)

4.4 Uncertainties

The major uncertainties in assessing the potential for deflagration or detonation of combustible gases in the AP600 containment relate to the potential sources of hydrogen (and possibly carbon monoxide) and the flammability of the containment atmosphere. The flammability of the containment atmosphere depends upon the mole fractions of the combustible gases (hydrogen and carbon monoxide), of the oxygen, and of the inertants (nitrogen, steam and carbon dioxide). The mole fractions are influenced by the availability and effectiveness of the igniters and by the degree of mixing between regions.

The evolution of hydrogen, and possibly carbon monoxide and carbon dioxide given the unlikely occurrence of corium concrete attack, and the evolution of steam are all time dependent functions. The initiating event and subsequent sequence of key events including potential operator actions or recovery activities can influence the evolution of both combustible gases and inertant steam in the containment atmosphere. Thus it is prudent to utilize an integrated code (MAAP) to study the interactions between the several rate dependent processes. The MAAP code will be used to conduct sensitivity studies to address phenomenological uncertainties as part of the AP600 containment response and source term quantifications. The MAAP runs should be reviewed and insights derived regarding the likelihood of deflagrations within the several containment regions. Likewise, given the prediction of burns during severe accident sequences, the location and duration of the burns should be noted for use in other assessments regarding the performance of instrumentation within the containment and the performance of containment penetrations.

The key uncertainties associated with the sources of combustible gases during postulated severe accidents in the AP600 containment are discussed below.

The in-vessel generation of hydrogen due to the oxidation of zirconium during core overheating, degradation, and relocation represents a major source of uncertainties. Considerable research has been conducted both in the United States and abroad regarding core melt progression

and relocation processes. Additional research is in progress and is being planned. A means of addressing the unresolved issues associated with the complex process of core damage and relocation can be addressed using selected parameters available within the MAAP code. The degree of blockage of the fuel channels during core relocation is a major uncertainty. Likewise, the initiation of the relocation of core material impacts the degree of oxidation which may be assessed. This can be addressed by varying the eutectic temperature or core melt relocation temperature considered for such assessments. Lastly, the in-vessel hydrogen generation can be impacted by the duration of vessel failure, given that the time available for steam production and oxidation of zirconium while the debris is captured within the primary system affects the hydrogen production.

The potential ex-vessel sources of combustible gases also include some uncertainty. In the unlikely event of molten core concrete interactions, the amount of concrete attack depends upon the success in cooling the debris on the containment floor. (This subject is addressed in a separate phenomenological evaluation summary.) The coolability of core debris is an uncertainty which still remains in the technical community. Different rates of debris coolability can and should be assessed as part of the sensitivity studies performed for the AP600. If debris is rapidly cooled such that core concrete interactions are limited then the ex-vessel sources of hydrogen and carbon monoxide will essentially be precluded. It is therefore important to assure a supply of water for the long term maintenance of the debris coolability.

Ex-vessel contributions to hydrogen can also be postulated for high pressure melt ejection and subsequent direct containment heating sequences. The major uncertainty associated with high pressure melt ejection is the likelihood of the high pressure existing in the primary system at vessel failure. The Automatic Depressurization System (ADS) is expected to depressurize the primary system under most conditions while for other sequences the initiating event itself may depressurize the primary system. Given that some degree of pressurization is present in the primary system when the reactor pressure vessel is postulated to fail, the next uncertainties that need to be addressed are the mode of vessel failure, the degree of debris dispersal, and the amount of material available to be dispersed in a high pressure melt ejection event. (These issues

are also addressed in a separate paper.)

The containment failure pressure and mode is another uncertainty that impacts the consequences of potential hydrogen burns. If the containment undergoes strain before failure then its failure time will be delayed when compared to failure at a given fixed containment pressure. The uncertainty in the timing of the potential containment failure may impact the recovery action selected for the plant personnel's ability to perform it.

It is recommended that in order to ensure that the phenomenological uncertainties are completely addressed and documented that they be incorporated as part of the AP600 design sensitivity studies. However, the bounding assessment performed in this paper is sufficient to reach the conclusion that containment failure due to deflagrations and detonations is not expected for the AP600 design. Thus, the sensitivity studies should help confirm this conclusion and provide additional details and insights regarding the containment response to severe accidents for the AP600 containment design.

5.0 ACCIDENT MANAGEMENT IMPLICATIONS

The deflagration and detonation of combustible gases in the AP600 containment are dependent upon the amounts of combustible gases and inerting steam (flammability) and the presence of sources of ignition. The igniter system is activated upon detection of inadequate core cooling conditions. Other ignition sources, including static discharges, are widely distributed within the entire containment volume and are generally beyond the control of utility personnel. Thus, no other accident management strategy is recommended to address ignition sources. The amount of combustible gas present in the containment volume is dependent upon the duration and severity of the postulated severe accident sequences, while the degree of oxidation of zirconium within the reactor vessel depends upon the amount and duration of core overheating. The Emergency Operating Procedures (EOPs) address the need to maintain or restore adequate core cooling, and no additional accident management insights have been identified in this regard in this position paper.

The degree of ex-vessel oxidation of zirconium is influenced by the potential for debris dispersal during postulated high pressure melt ejection events and debris coolability during molten core-concrete interactions (MCCI). As discussed in the phenomenological evaluation summary on direct containment heating, no accident management actions should be taken to specifically address the DCH issue. (Note that the AP600 EOPs include actions to flood the reactor cavity and establish external cooling; these actions would prevent DCH.) MCCI, in addition to oxidizing zirconium, could also result in the oxidation of chromium from the structural steel as well as iron from the structural steel, RPV lower head, and rebar in the containment structures. These could be sources of both hydrogen and carbon monoxide.

The presence of water on the containment floor greatly inhibits or prevents MCCI and the containment production of the combustible gases. A natural result of the majority of postulated severe accident sequences is a large volume of water in the containment such that the reactor cavity and containment floor are flooded. This water provides a means of cooling core debris.

As discussed in the phenomenological evaluation summary on external cooling of the reactor pressure vessel (RPV), the submergence of the lower head and a substantial fraction of the RPV cylinder could result in complete termination of the accident progression. This would directly benefit the issue of deflagrations or detonations as it would obviate ex-vessel sources of combustible gases. Ex-vessel flooding is clearly an accident management strategy that precludes several ex-vessel phenomena and limits the potential combustible gas concentrations.

(a,c)

In summary, the accident management strategies that provide debris cooling (both in-vessel and ex-vessel) should be used as desired. They will also benefit the control of deflagrations or detonations by reducing the inventory of combustible gases. Recovery actions and accident management strategies should be selected to avoid containment overpressurization by steam production.

6.0 CONCLUSIONS

The assessment provided in this position paper for the susceptibility of the AP600 containment to postulated deflagrations and detonations of combustible gases during severe accidents concludes that the AP600 containment would not be failed by this postulated mechanism. This assessment takes no credit for the hydrogen igniter system. Potential sources of combustible gases are identified and discussed, and a bounding pressurization calculation is provided. Based on adiabatic isochoric complete combustion (AICC) of the selected hydrogen inventory (100% oxidation of active fuel cladding), the resulting containment pressure is calculated to be less than the ultimate capacity of the AP600 containment. It is therefore concluded that containment failure will not occur due to burns. This conclusion is based upon the existence of steam inerting and the bounding assessment. Clearly this is a very conservative assessment since postulated severe accident events in containment will most likely produce significant amounts of steam which will inert the containment against hydrogen burns or detonations. Furthermore, the hydrogen igniter system would burn hydrogen as it is produced and at relatively low concentrations, preventing hydrogen pocketing and minimizing the resultant containment loading.

It is concluded, based on the evidence presented in this summary paper, that detonation induced by direct deposition of energy in a detonable mixture of containment gases is not a possible containment failure mechanism. Detonation due to a transition from deflagration to detonation is also considered. Two methods are used (i.e., detonation cell width scaling and mixture/geometry classification) to assess the likelihood of the transition to detonation in the AP600 containment given the existence of a deflagration. Both of these methods result in a very low likelihood of a DDT. Due to the small size of ignition sources required to initiate a deflagration it is far more likely that combustible gases would be consumed within containment by deflagration rather than a detonation. Based on the lack of conditions that support DDT, the extensive, redundant system of igniters strategically placed throughout containment, and the open design and significant venting areas for the sub-compartments that help ensure a well mixed

atmosphere, it is concluded that detonations are not a credible challenge to the integrity of the AP600 containment.

Based upon the assessment provided in this paper and the conclusion that the likelihood of deflagrations or detonations in the AP600 containment is very low and improbable, it is concluded that the AP600 containment event trees need not incorporate a node for containment failure due to hydrogen deflagration or detonation.

7.0 REFERENCES

- Berman, M., 1986, "A Critical Review of Recent Large-Scale Experiments in Hydrogen-Air Detonation", Nuclear Science and Engineering, 93, 1986, pp. 321-437.
- Camp, A., et al., 1983, Light Water Reactor Hydrogen Manual, NUREG/CR-2726, SAND82-1137, Sandia National Laboratories, Albuquerque, NM.
- Fauske & Associates, 1990a, "Technical Support for the Hydrogen Control Requirements for the EPRI Advanced Light Water Reactor Requirements Document", DOE/ID-10290 U.S. Department of Energy.
- Fauske & Associates, 1990b, "Modifications for the Development of the MAAP-DOE Code - Volume III: A Mechanistic Model for Combustion in Integrated Accident Analysis".
- Hertzberg, Martin, 1981, "Flammability Limits and Pressure Development in Hydrogen-Air Mixtures", Proc. Workshop on the Impact of Hydrogen on Water Reactor Safety, Volume III, NUREG/CR-2017, SAND81-0661, Sandia National Laboratories.
- Kumar, R. K., et al., 1984, Intermediate Combustion Studies of Hydrogen-Air-Steam Mixtures, EPRI NP-2955, Electric Power Research Institute, Palo Alto, California.
- Liu, D. D., et al. 1981, "Some Results of WRNE Experiments on Hydrogen Combustion", Proc. Workshop on the Impact of Hydrogen on Water Reactor Safety, Volume III, NUREG/CR-2017, SAND81-0661, Sandia National Laboratories.
- National Research Council Report, 1987, Technical Aspects of Hydrogen Control and Combustion in Severe Light-Water Reactor Accidents, National Academy Press, Washington, D.C.
- Ratzel, A. C., 1985, Data Analysis for Nevada Test Site (NTS) Premixed Combustion Tests, NUREG/CR-4138, SAND85-0135, Sandia National Laboratories.
- Shepherd, J. E., 1985, "Chemical Kinetics and Hydrogen-Air-Diluent Detonations, Tenth International Colloquium on Dynamics of Explosions and Reactive Systems, Berkely, CA.
- Sherman, M. P., et al., 1981, "Deliberate Ignition and Water Fogs as H₂ Control Measures for Sequoyah", Proc. Workshop on the Impact of Hydrogen on Water Reactor Safety, Volume IV, NUREG/CR-2017, SAND81-0661, Sandia National Laboratories.
- Sherman, M. P., 1984, Hydrogen Combustion in Nuclear Plant Accidents and Associated Containment Loads", Nuclear Engineering and Design, 82, p. 13-24.

- Sherman, M. P., and Berman, M., 1987, The Possibility of Local Detonation During Degraded Core Accidents in the Bellefonte Nuclear Plant, NUREG/CR-4803, SAND86-1180, Sandia National Laboratories.
- Sherman, M. P., Tieszen, S. R., and Benedick, W. B., 1989, FLAME Facility, NUREG/CR-5275, SAND85-1264, Sandia National Laboratories.
- Stamps, D., 1987, Sandia National Laboratories, Handout at the Hydrogen Combustion Peer Review Committee Meeting, Washington, D. C., Called by M. Silberberg, Division of Reactor Accident Analysis, U.S. NRC.
- Stamps, D., Benedick, W. B., Tieszen, S. R., 1991, Hydrogen-Air Diluent Detonation Study for Nuclear Reactor Safety Analyses, NUREG/CR-5525, SAND89-2398, Sandia National Laboratories.
- Tieszen, S. R., et al., 1987, Detonability of H₂-Air-Diluent Mixtures, NUREG/CR-4905, SAND85-1263, Sandia National Laboratories.
- Williams, D. C., et al., 1987, Containment Loads Due to Direct Containment Heating and Associated Hydrogen Behavior: Analysis and Calculations with the CONTRAIN Code, NUREG/CR-4896, SAND87-0633, Sandia National Laboratories, Albuquerque, New Mexico.

APPENDIX A

Calculation of H₂-Air-Steam Composition

This appendix discusses the approximate method for evaluating the containment air mixture composition that is used to determine its flammability. An initially dry containment atmosphere is assumed. It is assumed that the moles of hydrogen in the dry atmosphere is known and that the pre-burn atmosphere (which includes steam) temperature and pressure are known.

Define

- n_A = initial dry air moles
- P_o = initial dry air pressure
- T_o = initial dry air temperature
- n_H = moles H₂ added
- P_{nc} = partial pressure of non-condensable gases after H₂ added
- $X_{H,d}$ = mole fraction H₂ in the dry mixture
- T_p = pre-burn temperature
- P_s = steam partial pressure at T_p
- P_p = total pressure at T_p
- n_s = moles of H₂O
- $X_{H,w}$ = wet H₂ mole fraction = $n_H / (n_H + n_s + n_A)$
- X_s = wet H₂O mole fraction = $n_s / (n_H + n_s + n_A)$
- ϕ = relative humidity
- V = containment free volume

The initial amount of air is given by

$$n_A = \frac{P_o V}{RT_o} \quad (A-1)$$

where

$$R = 8.314 \text{ J/mol-K}$$

Assuming that 21% of the (dry) atmosphere is oxygen, we have

$$\text{moles of oxygen} = 0.21 n_A, \text{ and}$$

$$\text{moles of nitrogen} = 0.79 n_A$$

The mole fraction of H_2 in a dry mixture is defined as

$$X_{H,d} = \frac{n_H}{n_A + n_H} \quad (A-2)$$

Next, the containment temperature and relative humidity, if known, are used to determine the partial pressure of steam:

$$P_s = \phi P_{sat}(T_p) \quad (A-3)$$

The partial pressure of the noncondensibles at this new temperature is found from the ideal gas law as

$$P_{nc} = P_o \frac{T_p}{T_o} \frac{n_A + n_H}{n_A} = \frac{T_p}{T_o} \frac{1}{1 - X_{H,d}} P_o \quad (A-4)$$

The sum of these two partial pressures yields the total containment pressure:

$$P_p = P_s + P_{nc} \quad (A-5)$$

It is likely that P_p is known instead of ϕ . In this case instead of using Eq. (A-3), Eq. (A-5) is solved for P_s from the known value of P_p and P_{nc} given by Eq. (A-4).

For cases of interest, the ideal gas law may be used for the steam mole fraction without significant error, if the steam inerting has high margin (i.e., the resulting mixture is far from the flammability limit). Therefore the steam mole fraction is

$$X_s = P_s / P_p \quad (A-6)$$

and the hydrogen mole fraction in the wet atmosphere is

$$X_{H,w} = X_{H,d} (1 - X_s) \quad (A-7)$$

Given the mole fractions, Figure 2-3 can be used to determine if the wet mixture is flammable.

The post-combustion pressure can be found directly from Figure 2-5 if the initial relative humidity is very close to one. Otherwise, the methods of Appendix B can be used.

Example (SI Units)

Suppose the containment volume is $10,000 \text{ m}^3$. It is initially at 300 K and not inerted. Assume that 100 kg of hydrogen are produced and put into the containment, and steam is generated such that the atmosphere is at 90% humidity at 330 K . Then the initial number of air moles is

$$n_A = \frac{P_o V}{RT_o} = \frac{(1.013 \times 10^5) (1 \times 10^4)}{(8314) (300)} = 400.9 \text{ kg-moles} \quad (\text{A-8})$$

and the dry hydrogen mole fraction is

$$X_{H,d} = \frac{n_H}{n_A + n_H} = \frac{(100/2)}{(401 + (100/2))} = 0.111 \quad (\text{A-9})$$

At 330 K (about 57°C) the vapor pressure of water is $0.172 \times 10^5 \text{ Pa}$, so that the steam partial pressure is

$$P_g = (0.9) (0.172 \times 10^5) = 1.548 \times 10^4 \text{ Pa} \quad (\text{A-10})$$

At this temperature the noncondensable partial pressure is

$$P_{nc} = (1.0 \times 10^5) \frac{330}{300} \frac{1}{0.889} = 1.237 \times 10^5 \text{ Pa} \quad (\text{A-11})$$

and the total pre-burn pressure is

$$P_p = 1.392 \times 10^5 \text{ Pa} \quad (\text{A-12})$$

The steam and hydrogen mole fractions are therefore

$$X_p = 1.548 \times 10^4 / 1.392 \times 10^5 = 0.111 \quad (\text{A-13})$$

$$X_{H_2O} = (0.111)(1 - 0.111) = 0.099 \quad (\text{A-14})$$

This mixture is flammable according to Figure 2-3. Since the relative humidity is near 1, Figure 2-5 may be used to find the post-combustion pressure.

APPENDIX B

Post-Combustion Pressure Rise Calculation

This appendix describes the calculation of the adiabatic isochoric complete combustion (AICC) temperature and/or flame temperature given initial gas masses, temperature, pressure and energy.

The AICC temperature is found by equating the end state energy to the sum of the pre-burn energy and the combustion energy release. A constant volume process (isochoric) is thus assumed.

$$\left(\sum_{i=1}^4 M_i c_{vi} \right)_{\text{postburn}} T_f = \left(\sum_{i=1}^4 M_i c_{vi} \right)_{\text{preburn}} T_p + Q_b \quad (\text{B-1})$$

where,

Q_b = heat of combustion,

M_i = mass of i-th component,

c_{vi} = specific heat at constant volume if i-th component,

T_p = preburn temperature,

T_f = post-burn (AICC) temperature,

$i = \text{H}_2, \text{O}_2, \text{N}_2, \text{H}_2\text{O}.$

The AICC pressure P_f is estimated by

$$P_f = \frac{n_f R T_f}{V} \quad (\text{B-2})$$

where,

V = containment free volume,

R = universal gas constant = 8.314 J/mol-K

n_f = final gas moles.

APPENDIX C

Summary of DDT Potential Evaluation from NUREG/CR-4803

Table C-1

Classification of Hydrogen-Air Mixtures
at 20°C and 1 atm Pressure

Mixture Class	Hydrogen Mole Fraction %	Equiv. Ratio	Cell Width		Hydrogen Mole Fraction %	Equiv. Ratio
			in	mm		
1	24-30	.75-1.0	0.787-0.59	20-15	38-30	1.5-1
2	21-24	.63-.75	1.575-0.787	40-20	48-38	2.2-1.5
3	15-21	.42-.63	12.60-1.575	320-40	63-48	4.1-2.2
4	13.5-15	.37-.42	47.24-12.60	1200-320	70-63	5.6-4.1
5	< 13.5	< .37	> 47.4	> 1200	no data	> 5.6

Table C-2

Geometric Classes for Flame Acceleration

Geometric Class 1. Large geometries with obstacles in the path of the expanding unburned gases. Partial confinement favors gas expansion past the obstacles. A large tube with numerous obstacles and with ignition going from a closed end to an open end is an example. Class 1 geometries are the most favorable to large flame acceleration.

Geometric Class 2. Geometries similar to Class 1 but with some feature which hinders flame acceleration. Examples would be a tube open on both ends or large amounts of transverse venting.

Geometric Class 3. Geometries that yield moderate flame acceleration but are neutral to DDT. Examples are large tubes without obstacles, small tubes (several inch diameter) with obstacles.

Geometric Class 4. Geometries unfavorable to flame acceleration. Examples are large volumes with hardly any obstacles and large amounts of venting transverse to the flame path, or small volumes without obstacles. DDT will not usually occur in a Class 4 geometry.

Geometric Class 5. Geometries so unfavorable to flame acceleration that not even large volumes of stoichiometric hydrogen-air mixtures are likely to detonate. The only examples are totally unconfined geometry at large scale, or a small spherical geometry without obstacles and central ignition.

Table C-3

Dependence of Result Class on
Mixture and Geometric Class

Geometric Classes		Mixture Classes				
		1	2	3	4	5
Very Favorable	1	1*	1	2	3	4
Favorable	2	1	2	3	4	5
Neutral	3	2	3	3	4	5
Unfavorable	4	3	4	4	5	5
Very Unfavorable	5	4	5	5	5	5

*Result classes are defined in Table C-4.

Table C-4

Classification of the Probability of DDT

Result Class 1	DDT is highly likely	P = .99
Result Class 2	DDT is likely	P = .90
Result Class 3	DDT may occur	P = .50
Result Class 4	DDT is possible but unlikely	P = .10
Result Class 5	DDT is highly unlikely to impossible	P = .01

FAI/92-31

A PHENOMENOLOGICAL EVALUATION SUMMARY
ON FISSION PRODUCT RETENTION CAPABILITY
IN SUPPORT OF THE AP600 RISK ANALYSIS

Submitted To:

Westinghouse Electric Corporation
Pittsburgh, Pennsylvania

Prepared By:

Fauske & Associates, Inc.
16W070 West 83rd Street
Burr Ridge, Illinois 60521
(708) 323-8750

March 1992

TABLE OF CONTENTS

	<u>Page</u>
TABLE OF CONTENTS	i
LIST OF FIGURES	iii
LIST OF TABLES	iv
1.0 INTRODUCTION	1-1
1.1 Purpose	1-1
1.2 Background	1-1
2.0 PHENOMENA	2-1
2.1 Description of Phenomena	2-1
2.1.1 Controlling Physical Processes for Fission Product Release	2-1
2.1.2 Controlling Physical Processes for Fission Product Transport and Deposition	2-5
2.1.3 Controlling Physical Processes for Fission Product Revaporization	2-15
2.1.4 Controlling Physical Processes for Aerosol Plugging	2-19
2.1.5 Passive ALWR Source Term	2-22
2.2 Experiments and Industry Experience	2-23
2.3 Analyses	2-25
2.3.1 Zion Probabilistic Safety Study	2-25
2.3.2 NUREG-1228, Source Term Estimation During Instant Response to Severe Nuclear Power Plant Accidents	2-26

TABLE OF CONTENTS
(Continued)

	<u>Page</u>
2.3.3 NUREG-1150, Reactor Risk Reference Document	2-27
2.3.4 IDCOR Approach (Individual Plant Examination Methodology)	2-28
3.0 METHODOLOGY	3-1
4.0 PLANT SPECIFIC APPLICATION	4-1
4.1 Aerosol Sedimentation Correlations	4-1
4.2 Comparison to MAAP4 Calculations	4-11
5.0 UNCERTAINTIES	5-1
5.1 Passive ALWR Source Term	5-1
5.2 Long Term Release From Molten Corium in the Lower Plenum	5-3
5.3 Revolatilization of Iodine From Water Pools	5-4
5.4 Methodology Sensitivities and Uncertainties	5-7
6.0 ACCIDENT MANAGEMENT IMPLICATIONS	6-1
7.0 SUMMARY	7-1
8.0 REFERENCES	8-1

LIST OF FIGURES

<u>Figure No.</u>		<u>Page</u>
2-1	Influence of steam mass fraction on the DF.	2-8
2-2	Influence of pool subcooling on the DF.	2-9
2-3	Influence of water depth on the DF.	2-11
2-4	Typical pathways for release of radionuclides to the atmosphere from a steam generator tube rupture.	2-12
2-5	Conditions in radionuclide release pathways following a "U" tube steam generator tube rupture to the environment.	2-14
2-6	Pathways for fission product release for AP600 design.	2-16
2-7	Experimental data for plugging of lines by aerosols.	2-21
3-1	Containment airborne aerosol mass density history.	3-4
3-2	Containment noble gas concentration history.	3-12
4-1	Aerosol mass density history for AP600 design.	4-5

LIST OF TABLES

<u>Table No.</u>		<u>Page</u>
2-1	Core Release Fraction Assumptions (1-Hour Release)	2-4
2-2	Melting Point and Boiling Point (°F) of Selected Materials	2-17
2-3	Fission Product Release Fractions to Primary Containment Atmosphere	2-24
3-1	Characterization of Source Term by Type of Severe Accident Sequence	3-2
3-2	Correlations for Aerosol Sedimentation	3-6
3-3	Integrated Aerosol Leakage Equations	3-10
3-4	Integrated Noble Gas Leakage Equations	3-13
3-5	Nomenclature and Input for Aerosol Sedimentation Correlations and Equations	3-14
4-1	AP600 Fission Product Inventory and RCS Aerosol Release Fractions	4-2
4-2	Calculated Release Fractions for AP600 Design	4-10
4-3	Comparison of Hand Calculations and MAAP4	4-12
5-1	Comparison of Release to Containment for Passive ALWR Source Term and Existing Regulatory Source Term	5-2
7-1	Comparison of AP600 Calculation and ARSAP Calculation	7-2

1.0 INTRODUCTION

1.1 Purpose

The purpose of this phenomenological evaluation summary is to assess the fission product retention capability of the AP600 design. The AP600 passive plant design implements EPRI's passive ALWR design requirements which make the likelihood of any core damage event extremely remote. Nonetheless, for defense-in-depth Volume 3 of the EPRI requirements document [EPRI, 1990] specifies that containment performance under severe accident conditions be evaluated. The Requirements Document were developed to meet the ALWR safety policy that states that, even in the event of a severe accident, containment integrity should be maintained and the fission product released to the environment should be very low. The potential challenges to the containment integrity of severe accident phenomena are addressed in other phenomenological evaluation papers. The nature of the fission product source term and the retention capabilities for the AP600 plant and passive containment are assessed in this summary.

1.2 Background

The design basis containment leakage rate limit for the AP600 is set at a low value, i.e., [](a,c) volume percent per day at the containment design pressure. Furthermore, the design does not incorporate a safety grade containment spray system. However, the set of passive safety systems that afford both core damage prevention and containment failure prevention also provide several means for mitigating the release of fission products to the environment. The several passive injection systems (core makeup tanks, accumulators, and IRWST) in addition to the primary systems water inventory collectively provide a significant volume of water which will accumulate within the containment during severe accidents. For loss of coolant (LOCA) related severe accidents a direct path from the primary system via the break exists that releases the primary system inventory as well as the injected water sources. For severe accident sequences

that do not include a LOCA event the primary system and injection inventories are discharged via the depressurization system through the IRWST and into the containment. In most cases a significant volume of water accumulates in the reactor cavity such that the RPV is externally submerged. There is a low probability therefore of not having water in the reactor cavity for the AP600 passive plant design. The successful cooling of the RPV by external vessel flooding has a profound benefit of reducing the potential for fission product release during severe accidents. If the core debris is successfully maintained within the RPV boundary then potential ex-vessel fission product release mechanisms are precluded.

During core damage the noble gas and volatile fission products will be released from the damaged fuel matrix. The noble gases may escape the primary system and accumulate within the containment gas space. Likewise a fraction of the volatile fission product species in the form of aerosols will accumulate within the containment gas space. The fraction of aerosol fission products which are transported to the containment gas space is influenced by the release path. For LOCA events, the break in the primary system may communicate directly with the containment gas space. Thus, the fraction of aerosols escaping the primary system could be released directly into the gas space. The fraction of aerosols that escape the primary system is influenced by the degree of fission product deposition and revaporization from the surfaces within the RCS. For non-LOCA sequences the release path includes the IRWST water inventory which would significantly reduce the aerosol fraction released to the containment gas space while not changing the noble gas release.

Low release rates in-vessel for the non-volatile fission product species will occur while the debris is maintained within the lower plenum. This would likely be the case given external vessel cooling. Following core damage and the accumulation of core debris in the lower plenum of the RPV the area available for fission product release will be significantly limited compared to the total surface area of the intact fuel rods. Hence, the release rate from the debris pool within the RPV when compared to that for the intact but overheated fuel rods is approximately one 200th of the release rate. The presence of a crust on the debris pool within the RPV lower

head indicates that the release of non-volatile fission products from the lower plenum is diffusion limited. The crust thickness represents a long diffusion length especially when compared to the radial dimension for fission product diffusion from an intact fuel rod. Lastly, the release of low volatility fission products would not be great since there will not be a sparging mechanism for the in-vessel debris pool configuration as would be the case for core-concrete attack. There will not be a net generation of significant volume of gases passing through the molten debris pool and carrying the non-volatile fission products out of the debris bed. Based on evaluations for pools with high gas through flow rates (as would be the case during molten core concrete interaction for an ex-vessel debris bed) it has been observed that the gas sparging mechanism is the dominant mechanism for non-volatile fission product release.

If it were postulated that vessel failure occurred even in the presence of an externally flooded RPV then the presence of water in the cavity would still have a major beneficial impact for reducing the fission product release. The presence of water during the discharge of debris from a failed reactor vessel provides significant cooling for the core debris. By quenching the core debris such that it changes from the molten to the solid state, the mechanism for fission product release from the debris again becomes solid state diffusion limited. Hence, the resulting debris configuration is one which severely inhibits the continued release of fission products. The accumulation of debris within a water pool provides a configuration that scrubs fission products and collects them within the overlying water pool. Thus, should the ex-vessel accumulation of core debris lead to core concrete interactions, the overlying water pool provides a mechanism for scrubbing the fission products. In a similar manner those fission products released in-vessel and directed through the IRWST water inventory would also be scrubbed. Thus, the inventory of water in the passive plant design is effective in reducing the fraction of fission product aerosols which could eventually be directed to the containment gas space.

[The AP600 design includes a passive containment heat removal system.]

(a,c)

] (a,c)

[] This design produces a containment atmosphere which contains large steam fractions. The presence of steam in the containment atmosphere enhances the removal of fission product aerosols from the containment gas space. The presence of a high steam fraction in the containment atmosphere accelerates the fission product deposition process for hygroscopic aerosols such as CsI and CsOH. The dripping or "rain" off of the inside surface of the containment dome also sweeps aerosol fission products from the containment airspace. Therefore, the passive aerosol removal mechanisms are effective in retaining fission products in the water pool that accumulate in the containment during a severe accident. Furthermore, the presence of steam environment causes the containment temperature to be relatively low for the saturated steam conditions. The low containment temperature during the functioning of the passive containment heat removal system precludes a significant revaporization of deposited fission products from surfaces in containment. If the long term failure of the containment is postulated due to overpressurization due to steaming off of a non-coolable core debris configuration then the fission product inventory is controlled by the presence of the overlying water pool.

The passive safety features of the AP600 design for both injection and containment heat removal provide significant capability for the retention of fission products within the containment or primary system. These capabilities in conjunction with the robust containment design (ultimate capacity of approximately [](a,c)) and the low design basis containment leakage rate ([](a,c) volume percent per day) result in a plant design that satisfies the ALWR safety policy and the EPRI requirements document goals of very low fission product releases to the environment.

2.0 PHENOMENA

2.1 Description of Phenomena

To describe the source term or release fraction of fission products to the environment one must estimate the behavior of the several fission product barriers and fission product removal mechanisms incorporated in the AP600 design. The AP600 basic design principle mimics that used in the LWR plants, namely, defense-in-depth by providing a series of barriers to the release of fission products. In particular the barriers for fission product release include the fuel pellets themselves, the fuel pin cladding, the primary system RPV and piping, the containment boundary, and secondary buildings. The following is a overview of the physical processes involved in fission product release, transport, and deposition.

2.1.1 Controlling Physical Processes for Fission Product Release

Several mechanisms should be considered to estimate the fraction of core fission products released following the failure of the fission product barriers provided by the fuel pellets and the fuel pin cladding. Fuel and cladding failures and subsequent release of fission products from the fuel to the primary system will primarily be a function of temperature. Four core damage temperature regimes may be considered:

1. Normal fuel pin leakage (normal operating temperature 600°F),
2. Fuel cladding rupture release (gap release, 1300°-2100°F),
3. Grain boundary release (> 3000°F),
4. Melt (in-vessel) release (> 4500°F).

Small quantities of fission products escape through small holes in the fuel pin cladding into the reactor system coolant during normal operation. The release of reactor coolant with the resulting levels of fission products from fuel pin leakage is considered in the design basis and

does not lead to unsafe conditions for the public. The release from the fuel cladding gap takes place during the heating of the fuel rods in the short time between vessel blowdown (core uncover) and reflooding. The overheated fuel causes some of the rod cladding to fail and the gases and volatile fission products in the gap are released into the RPV. The fission product gases produced and collected in the gaps in the fuel pins during normal plant operation are heated during temperature excursions from insufficiently cooled fuel. The cladding on the fuel pin may balloon due to an excess pressure differential during heating and oxidation may become extremely rapid between the temperature regimes of 1400 and 2000°F leading to rapid fuel pin failure. After a fuel pin cladding failure occurs, most of the fission gas and the fission gas plenum inventory will be released into the reactor coolant system. This release mechanism is often referred to as a burst release. Once the fuel pin plenum fission gas has been vented, the shallowly embedded gas atoms in the fuel pellet and interior cladding surface near the rupture area will diffuse into the reactor coolant system. This release mechanism is referred to as "gap release". The amount of radioactive fission products associated with the gap release will depend primarily on the number of failed fuel pins and the plenum fission gas inventory. It is important to realize that the variation in fuel temperature throughout the core could be considerable. This is evident from the different levels of core damage seen in the TMI core. Portions of the core were melted while other parts were not damaged. It is important also to realize that once the core is sufficiently uncovered, core temperature will increase rapidly (at about 1°F per second). Cladding failure could begin in about 15 minutes following core uncover and core melt in less than an hour. Therefore, if core conditions allow cladding failure, rapid failure of all the fuel pins and even fuel melt could result, if conditions are not improved quickly.

Following the gap release, the continued heating of the reactor fuel can lead to core damage and a meltdown release phase will occur. In the case of a core melt the aerosol source may be quite large because the melting fuel releases all volatile fission product and part of the low volatile fission products, fuel, and structural material. It must be emphasized that even though UO_2 is vaporized only to a small percentage, it and the cladding and steel support materials constitute the bulk of the mass of airborne solid material. Thus, the physical aerosol

behavior after a core melt is governed by the mass of UO_2 and steel aerosols. In the period before the RPV melt through (if it should occur), the aerosols have to travel through the primary system and may be retained to some extent as is the case for the gap release fraction. Once the clad fails, the release rate of various fission product increases rapidly with temperature. The release rate has been assumed to double approximately with every 180 degree of increase in temperature [McKenna, 1988]. By the time the fuel melts at about 4500°F, most of the volatile fission products may have been released from the fuel. However, these basic assumptions (as was shown at TMI) may not be correct. At TMI up to 20% of various fission products expected to be released by this rule of thumb were still retained in the melted core. As the fuel heats up bubbles form and expand causing the fuel grains to separate creating paths out of the overheated but unmelted fuel matrix. This is called the grain boundary release. As the heating continues and the fuel begins to melt and relocate, the remaining fission products are released from the fuel to the RPV. This last phase of the core damage process is referred to as in-vessel melting. Table 2-1 summarizes the core release fractions for each of these core conditions.

There is one additional potential fission product release mechanism that involves vessel melt-through. If the core melt continues and the core is not reflooded and cooled, it may eventually melt through the bottom of the reactor vessel and fall on the concrete containment floor. This would also imply that the vessel was not protected by external cooling either. If the floor is covered with water, it may provide adequate cooling, stopping further releases of fission products from the core debris. However, if the molten core contacts dry concrete, or if in some sequences the flooded conditions do not provide adequate debris cooling, the concrete will be attacked, decomposed, and thus yield steam and carbon dioxide. Such processes increase the access of the fission products to the surface of the molten debris mass leading to the formation of inert and radioactive aerosols. Thus, there is a potential for additional fission products to be released given the core debris was located in the containment.

Table 2-1

CORE RELEASE FRACTION ASSUMPTIONS (1-HOUR RELEASE)

Core Condition	Fuel Cladding Temperature	Fission Product	Assumed Release Fraction From Fuel
Fuel pin cladding intact - normal leakage	600°F	Design Basis Values	
Gas release (cladding failure)	1300°F-2100°F	Xe, Kr	0.03
		I	0.02
		Cs	0.05
		Te, Sb	1×10^{-4}
Grain boundary release	> 3000°F	Xe, Kr	0.5
		I, Cs	0.5
		Te	0.1
		Sb	0.02
		Ba	0.01
		Mo	0.01
		Sr	1×10^{-3}
		Ru	1×10^{-4}
Core melt (in-vessel) ⁽¹⁾⁽²⁾	> 4500°F	Xe, Kr	1.0
		Cs	1.0
		I	1.0
		Sb	0.02
		Te ⁽³⁾	0.3
		Bs	0.2
		Sr ⁽³⁾	0.07
		Mo	0.1
		Ru	7×10^{-3}
		La	1×10^{-4}
		Y	1×10^{-4}
		Ce	1×10^{-4}
		Np	1×10^{-4}

(1) Based on Tables 4-8 and 4-9 of NUREG-0956.

(2) For La, Y, Np, and Ce, the Zr release fraction was used, based on BMI-2104, Vol. VI, page 6-24 grouping, Battelle Columbus Laboratories, 1984.

(3) Ex-vessel (melt-through) melt release fractions may be much larger (0.4 to 0.8).

Reference: NUREG-1228.

2.1.2 Controlling Physical Processes for Fission Product Transport and Deposition

This section discusses the transport of fission products from the reactor fuel to the environment. The fraction of fission products released to the environment depends upon the pathway for the fission product transport and the effectiveness of the potential deposition mechanisms that the fission products may encounter during their transport. The current consensus [OECD, 1985] is that, during a severe core damage accident, most non-noble gas fission products will form particulates and aerosols. Therefore, it is often assumed that all non-noble gas fission products will form a homogeneous mass of aerosols and particulates. Noble gases are assumed not to be reduced by any of the potential removal mechanisms once released from the fuel. The primary way to reduce noble gas effects in the environment is to contain them within the RCS or containment to allow time for decay of the radioactive fission products.

As stated above, the release pathway will determine the removal media that the fission products will encounter on the way from the damaged fuel to the atmosphere. The basic removal media are gases and liquid. Undercooling events that lead to fission product release from the overheated and/or damaged fuel also lead to aerosol formation in the upper plenum of the reactor pressure vessel. The upper plenum contains structures such as the upper internals and control rod guide tubes. Aerosol and vapor deposition may occur on these structures. Flows from this region may carry fission products through the hot legs to the steam generators or to the pressurizer where they may be vented into the IRWST through the submerged quencher. All of these regions in the primary system (upper core plenum, hot and cold legs, pressurizer, and steam generators) provide large surface areas and small volumes that enhance fission product retention due to plateout on these surfaces. Transport of fission products throughout the primary system piping prior to vessel failure (should it occur) provides for significant deposition and retention of fission products within the reactor coolant system. Flows that pass through the pressurizer may encounter water in the pressurizer which would scrub fission products as the gases pass through the water. Likewise, those fission products remaining in the gas stream exiting the pressurizer would be discharged through the IRWST where additional scrubbing would occur.

prior to the gas escaping to the containment gas space. An alternate path of fission products to the containment would be from the upper plenum into the hot or cold leg through a break in the hot or cold leg into the containment gas space. If the hot or cold leg break location were submerged due to containment flooding then fission product scrubbing could occur in the water above the break location. The aerosols and particulates suspended in large volumes, such as the containment gas space and potentially the auxiliary building gas spaces, will be removed by natural processes from the gas space. The natural processes provide for aerosol agglomeration and deposition by several phenomena which include gravitational sedimentation, impaction, turbulence, diffusiophoresis, and thermophoresis. Furthermore, aerosol growth and deposition in the steam atmosphere rather than the dry mechanisms cited above can be a key removal mechanism for water soluble particulates in condensing steam such as cesium iodide and cesium hydroxide. The aerosols and particulates suspended in the containment gas space could also be removed by engineered safeguard features or other active systems such as sprays or by passage through filters. However, the AP600 design does not incorporate such active features and is therefore dependent on the natural removal processes. The passive containment cooling system design causes condensation to occur on the inside surfaces of the containment dome and walls. The dripping of condensate from these surfaces through the containment airspace would function in a manner similar to containment spray systems and it could be an effective yet passive means of impacting aerosol and removing it from the gas space. The principle deposition mechanisms of interest to the AP600 design are sedimentation and aerosol growth and deposition in a steam atmosphere. These mechanisms will be discussed in the Methodology (Section 3.0) and Uncertainty (Section 5.0) sections.

If the reactor pressure vessel should fail (which is not expected due to the effectiveness of external cooling of the RPV by water submergence) debris would exit the vessel and accumulate in the reactor cavity. Given the reactor cavity will be flooded with water, the debris would likely be quenched and thereby terminate additional release of fission products from the debris. Even if the debris was not quenched, it would be covered by an overlying layer of water which would provide a mechanism to scrub the fission products as they were released from the overheated and

unquenched debris. Those fission products and inert aerosols which pass through the overlying water pool would enter the containment gas space by passing through the series of connected containment volumes before reaching the containment dome. The several surface areas of the interconnected volumes as well as internal structures and equipment provide significant surface area for deposition of fission product aerosols.

Scrubbing of fission products in pools of water is possible as described by the several potential flow paths discussed above. Retention of fission products in water pools could occur for discharges that pass through a pressurizer water inventory, IRWST water inventory, for those LOCAs with the submerged discharge location and for those cases with vessel failure into a flooded reactor cavity. Furthermore, steam generator tube rupture events which are discussed separately below may provide a water pool in the discharge flow path which is effective in retaining the fission products by scrubbing. The effectiveness of scrubbing fission product aerosols and condensible vapors in water pools has received a great deal of analytical and experimental attention. The analyses and experiments demonstrate that there is a substantial variation in the decontamination factor for aerosol and fission product removal capability with:

- particle radius,
- steam mass fraction in the gas transporting the aerosols,
- subcooling of the water pool,
- means of injection (gas bubble size) of the gas transported into the water pool, and
- to some extent the depth of the water pool.

Other factors, such as the system pressure, the gas temperature, etc. have second order influences on the decontamination factor, but those given above are by far the dominant dependencies in pool scrubbing. Figures 2-1 and 2-2 illustrate the dependence of the decontamination factor with respect to aerosol particle size, steam mass fraction and pool subcooling. Also shown are the conditions with high steam mass fraction, which promotes extensive condensation (assuming the pool is subcooled), show very high decontamination factors

Sensitivity to Steam Mass Fraction

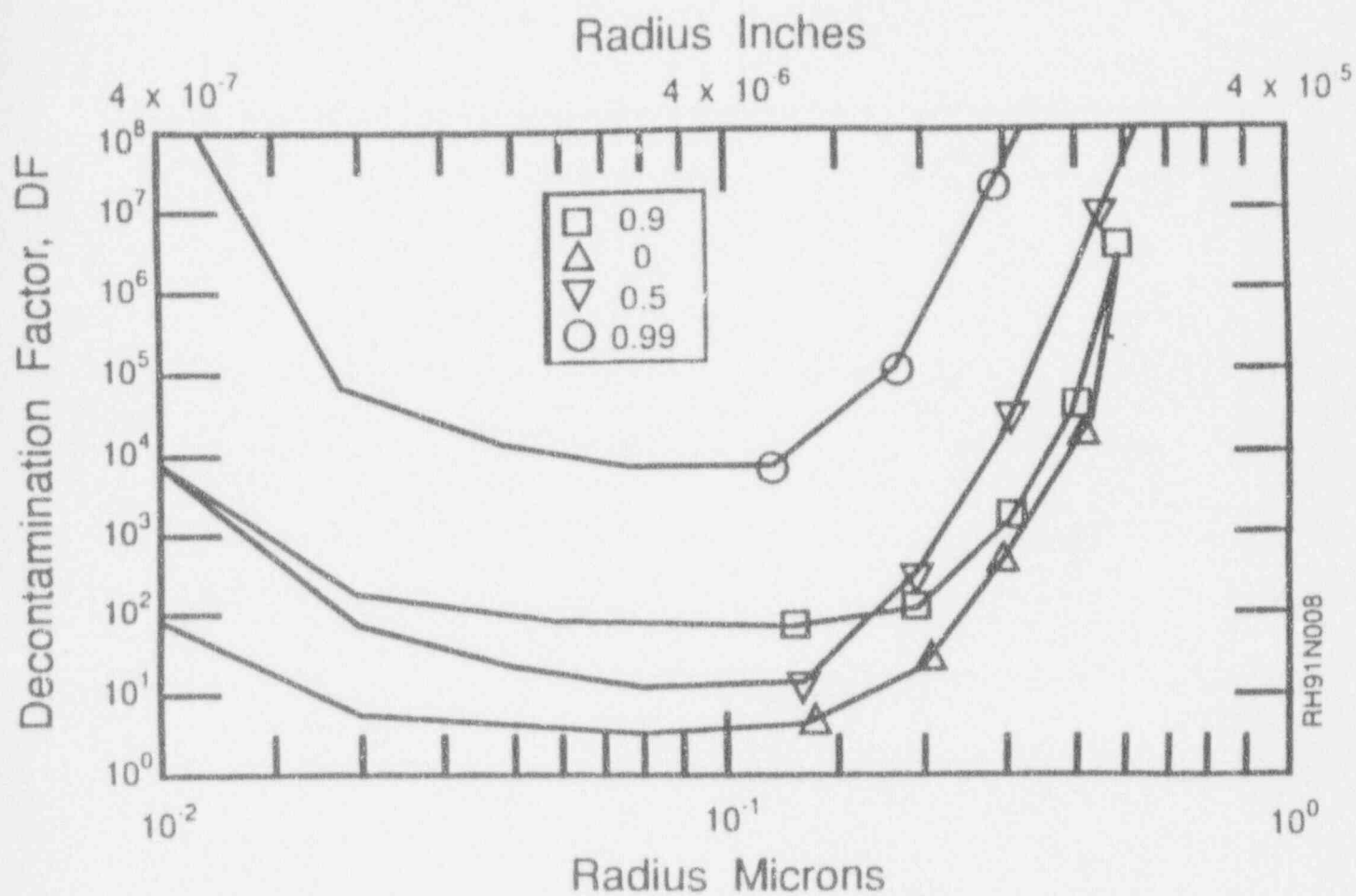


Figure 2-1 Influence of Steam Mass Fraction on the DF

Sensitivity to Amount of Subcooling

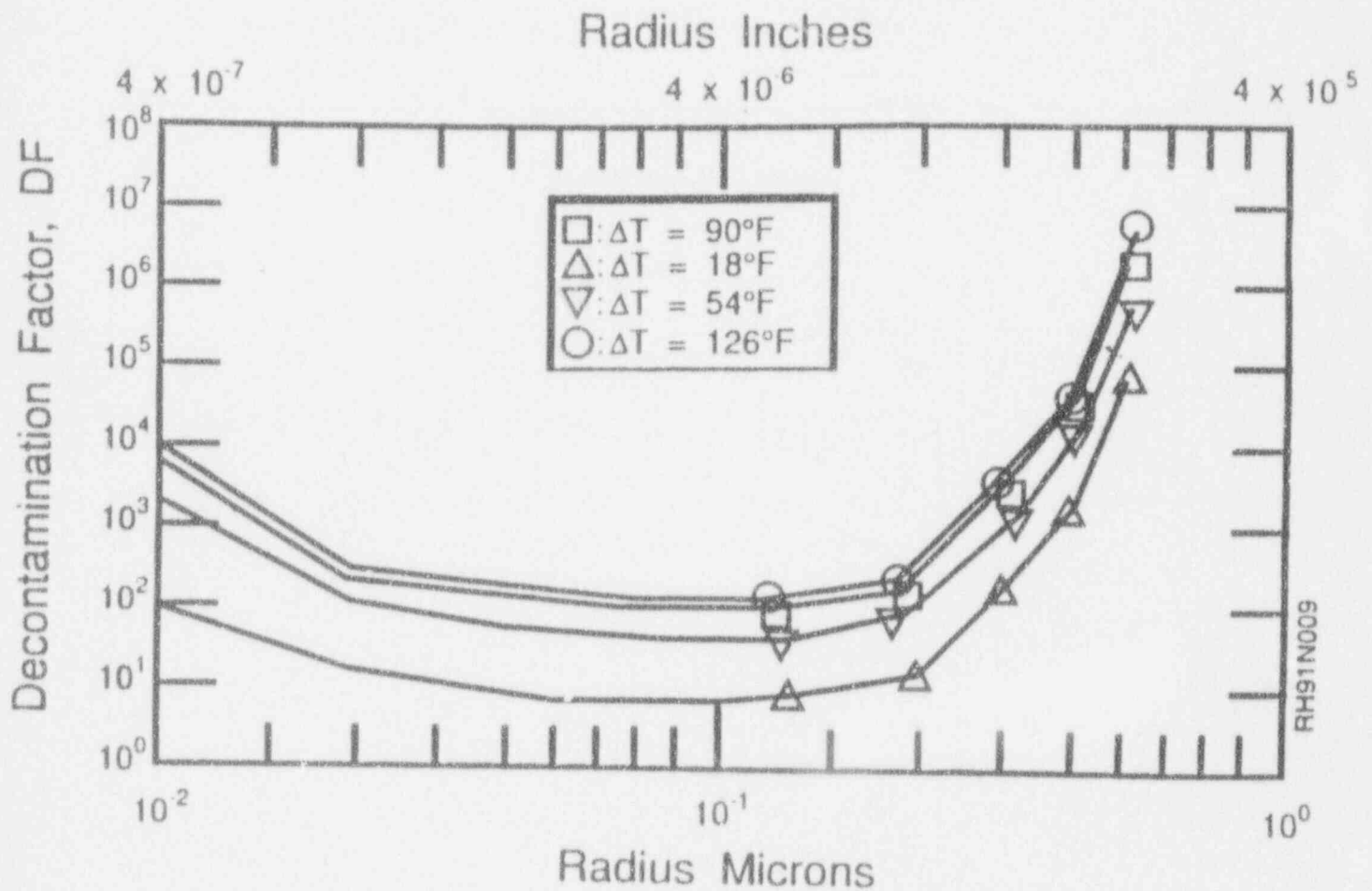


Figure 2-2 Influence of Pool Subcooling on the DF

as long as the pool can condense the steam flow. Figure 2-2 shows the influence of pool subcooling, which illustrates that higher subcoolings cause greater decontamination of the fission product aerosols and condensible vapors. Figure 2-3 depicts the influence of increased pool depth. As illustrated, increasing the depths from 13 feet to 20 feet (4 to 6 meters) does not substantially change the decontamination factor.

Several facets can be clearly stated for considering the effectiveness of pool scrubbing in the AP600 design which employs significant inventories of passively supplied water.

- Water is a very effective scrubbing media providing a decontamination factor of 10 or greater with limited water depths even when the water is essentially saturated.
- The more finely subdivided the gas flow (i.e. a sparged input) the greater the decontamination factor.
- The greater the steam mass fraction transporting the aerosols the higher the decontamination factor.
- The colder the water pool the more effective the decontamination (higher decontamination factor).
- The deeper the water depth over the release point into the pool the greater the decontamination factor, however, a pool depth of a few meters is essentially and infinite depth.

Hence, for the AP600 design with few exceptions the transport of fission product aerosols and vapors to the containment gas space will pass through a water pool which can provide an effective means of fission product removal.

Another category of potential severe accident sequences that provides a different path for fission product release is steam generator tube rupture events. Steam generator tube ruptures can provide three major release pathways to the environment as shown in Figure 2-4. If the main steam line does not isolate and the condenser is available, it would be preferred to direct the

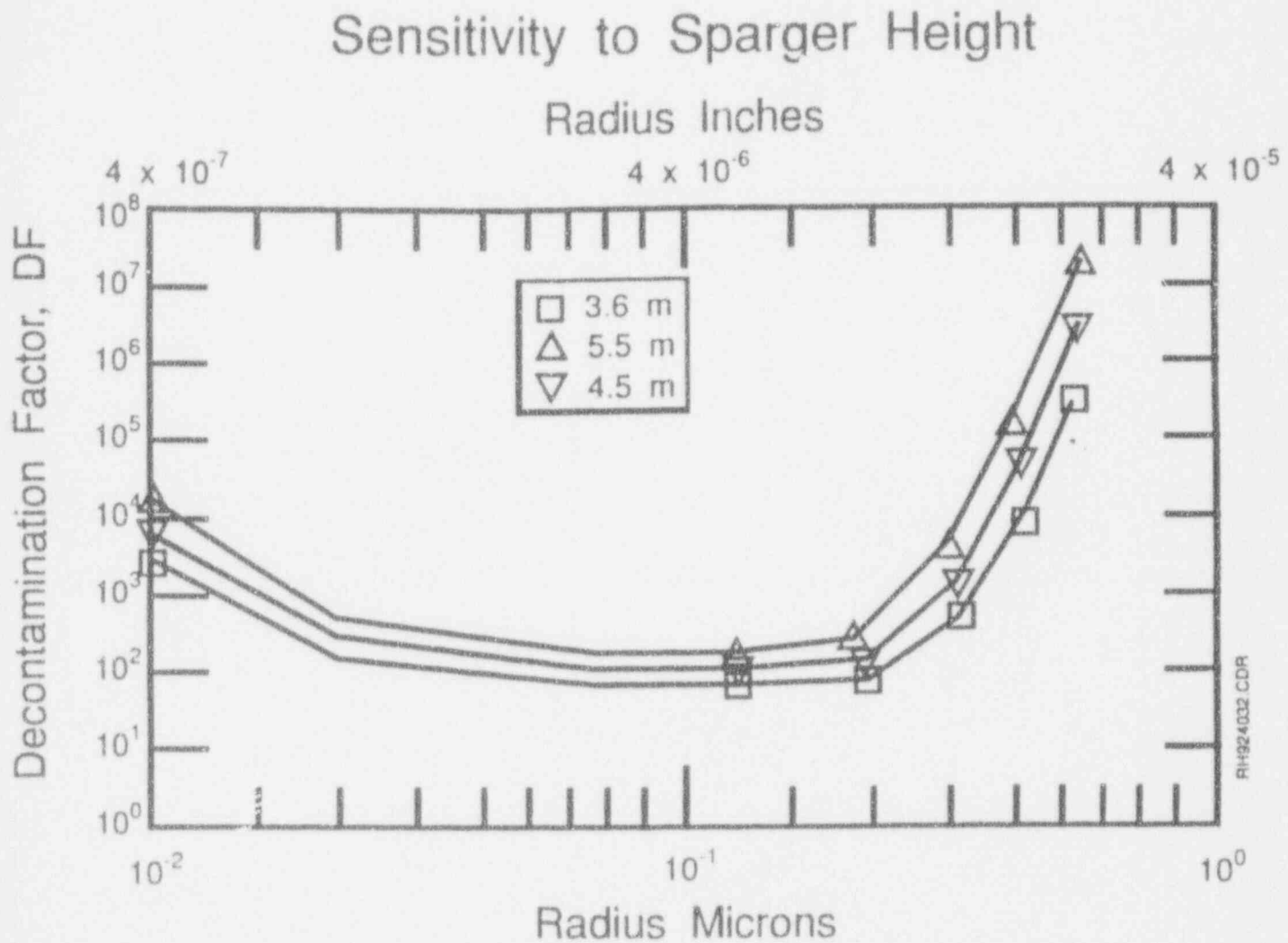


Figure 2-3 Influence of water depth on the DF.

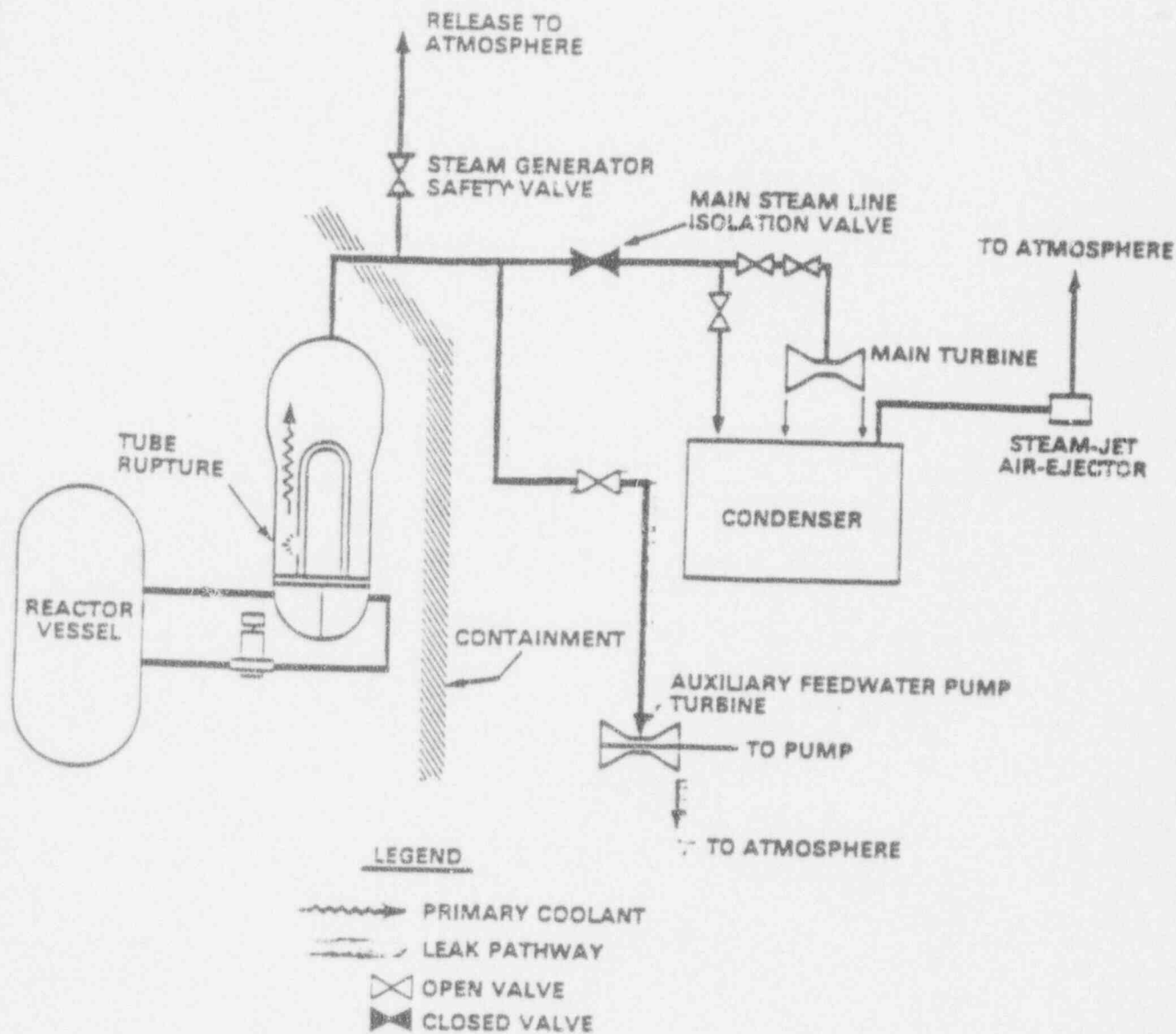


Figure 2-4 Typical Pathways for Release of Radionuclides to the Atmosphere from a Steam Generator Tube Rupture

reactor coolant system leakage to the condenser. Under these conditions it can be assumed that only the noble gas in the coolant will be released through the steam jet-air ejector to the environment. If the main steam isolation valve is closed (as shown in Figure 2-4) the safety valve provides a pathway to the environment. However, in most cases such releases will be greatly reduced as a result of fission product retention in the steam generator. The retention could be due to plateout on the steam generator internals as well as scrubbing if the steam generator tube rupture is submerged by the secondary side water inventory. In cases such as normal steam generator operation where a clear boundary exists between the boiling water on the secondary side and steam generated (see Figure 2-5, case A), a pool exists for scrubbing fission products. If the tube leak is massive, the secondary water could be boiling violently, and the secondary side steam would carry considerable contamination due to carry over. For steam generator tube ruptures where the secondary side water level is not properly controlled an overflow condition can occur which is shown in case B of Figure 2-5. Primary coolant can be ejected into the atmosphere through the safety valve. Therefore the iodine concentration in the release would be considerably above that which would be expected for case A. This transportation path for the fission products is an example of the contaminated water and all of its contaminants being injected into the atmosphere, the water flashing to steam and atomizing, carrying much of its contamination into the atmosphere. It is expected, however, that contaminated water will be diluted by the water in the secondary side of the steam generator.

Lastly, leakage of fission products through the containment is a possible release path to the environment. As stated in Section 1.0, the design basis leakage rate for the AP600 containment is set at a low value of [](a,c) volume percent per day. Leakage through penetrations goes into the middle annulus of the secondary building. From there it could go in three possible directions: 1) into the lower annulus through a pressure relief device, 2) into the upper annulus through the seal between the steel containment shell and the concrete deck, and 3) into the secondary building. Leakage that escaped to the secondary building would encounter a flow path through the secondary building that included significant area for fission product

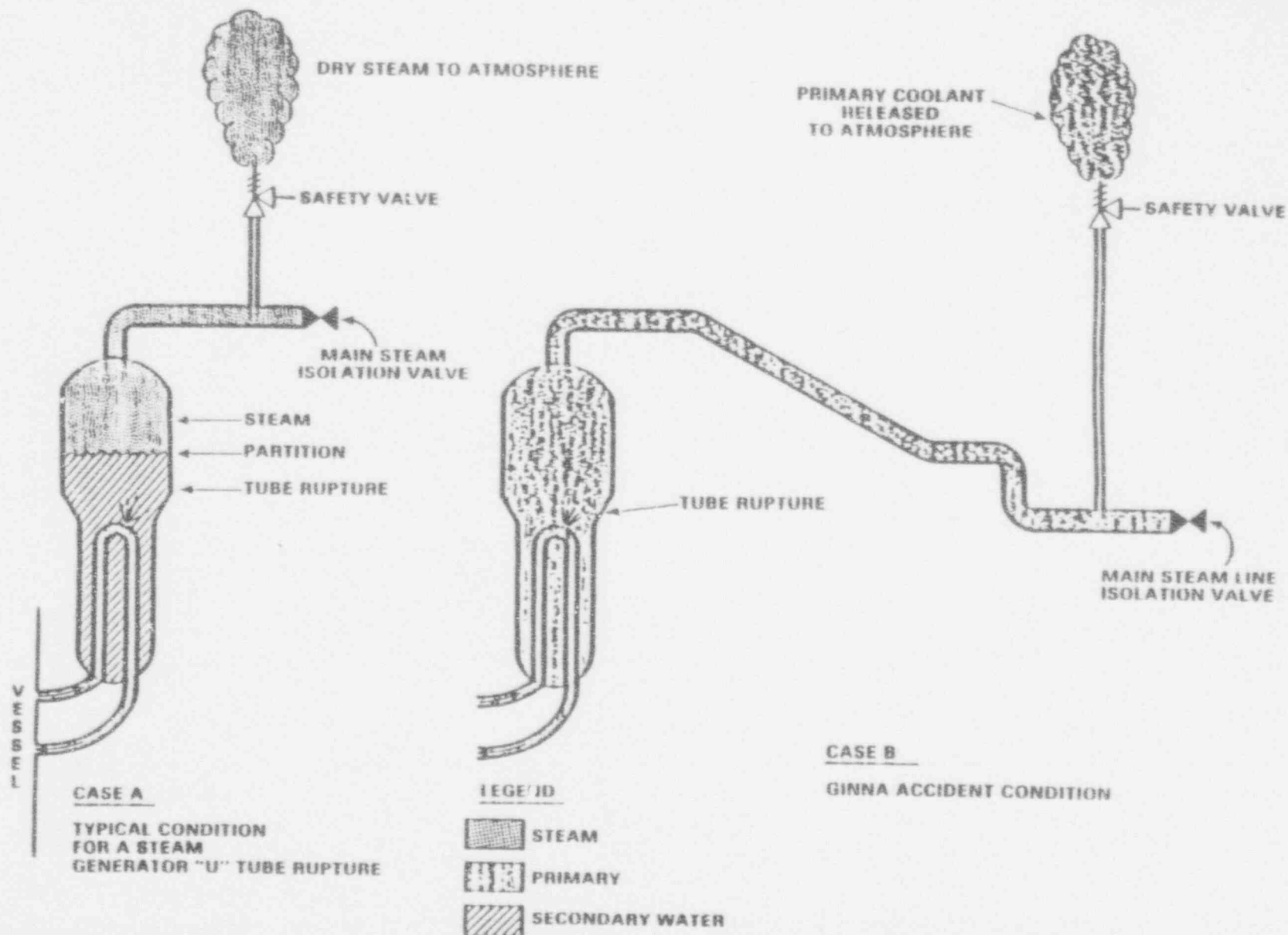


Figure 2-5 Conditions in radionuclide release pathways following "U" tube steam generator tube rupture to the environment.

plateout. Leakage that escaped through the upper annulus would encounter the external containment water spray and containment structures. The passage of aerosols through the leakage path which would be small cracks and not large openings could result in the deposition in those leakage paths of fission product aerosols. The potential for plugging of these flow paths by aerosol deposition is discussed below in Section 2.1.4.

(a,c)

2.1.3 Controlling Physical Processes for Fission Product Revaporization

The potential exists for revaporization of fission products that have been deposited (plated-out) on surfaces if the surface temperature increases to the point where the deposited material has a significant vapor pressure. Of particular interest are the more volatile fission products with cesium iodide, cesium hydroxide, and tellurium which could be deposited within the primary system, locally heat the structures to sufficient temperatures and revaporize. Table 2-2 provides the melting point and boiling point of selected materials which could be released as aerosols from a degraded core. The volatile fission products mentioned above are seen to have the lowest boiling point. The key process is the heatup of the structures on which the fission products have been deposited. The heat losses from those components with the deposited fission products therefore become of principle interest. Heat loss to external water sources, through insulation, or through gaps or leakage in the insulation have a major impact on assessing whether deposited fission products could be re-evolved. Likewise, the cooling of surfaces within the containment volume is important in assessing the potential for revaporization of fission products deposited on surfaces in the containment. For those conditions in which the deposited aerosol would be dry, heating of the deposited surface due to the energy generated by the deposited fission products and energy transferred to that surface by radiation and convection from the high temperature core debris, the surface and the deposited fission products could achieve a

(a,c)

Figure 2-6 Pathways for fission product release for AP600 design.

Table 2-2
MELTING POINT AND BOILING POINT (°F) OF SELECTED MATERIALS

Material	Melting Point	Boiling Point
<u>Volatile Fission Products</u>		
I ₂	237	365
CsI	1158	2336
CsOH	599	1814
Te	842	1810
<u>Refractory Fission Products</u>		
BaO	3493	5086
Ru	4082	7502
SrO	4406	5880
La ₂ O ₃	4199	>7232
<u>Control Rods</u>		
Ag	1761	3925
In	314	3763
Cd	609	1412
B ₄ C	4478	>6332
Hf	4031	8042
<u>Zircaloy</u>		
Zr	3365	7968
Sn	449	4717
<u>Stainless Steel</u>		
Fe	2795	5183
Cr	3434	4841
Ni	2647	5277
Mn	2271	3743
<u>Fuel</u>		
UO ₂	5144*	5959

*Oxidized Zr will form a liquefied two phase mixture with UO₂ at about 3484°F.
Reference: NUREG-1228.

temperature sufficient to produce a significant vapor pressure of the deposited materials. In this case the deposited fission products could be re-evolved (revaporized) due to the standard evaporative mechanism. Thus, the fission products deposited in the upper plenum of the RPV for example could be transported to the RCS loop. The rate of re-evolution of the deposited volatile fission products is determined by the difference between the vapor pressure of the fission products and the partial pressure of the material in the gas space as well as the strength of the circulation flow over the surface in question. When a large fraction of the volatile fission products are retained in the primary system, there is a potential for long term revolatilization. If sufficient heat removal is available from the primary system it may prevent significant revaporization releases from the primary system. Heat removal from the primary system is possible via the steam generators given cooling water is still available to the secondary side, the passive RHR used in the AP600 design, or due to losses from the primary system due to external flooding of the RPV and potentially even the hot and cold legs. For the AP600 design the maximum containment flood elevation for ex-vessel flooding of the RPV is approximately [](a,c) feet. The centerline elevation for the nozzles is approximately [](a,c) feet and therefore the nozzles and attached RCS piping could be completely submerged. The maximum containment flood height would not submerge the top head of the RPV which is also provided with insulation. The existence of water on the outside surface of the RPV and RCS piping provides a significant heat removal mechanism which could preclude or inhibit the revaporization of fission products. For those sequences that did not achieve the maximum containment flood height the surfaces may not be cooled sufficiently to prevent revaporization of the deposited fission products. However, as the deposited fission products were re-evolved and transported through the various pathways described in Section 2.1.2, they would likely encounter additional cool surfaces and thus be redeposited on them.

Those fission product aerosols that did escape to the containment airspace and get deposited on containment surfaces would provide a local heating source due to the radioactive fission products. The AP600 passive containment cooling system produces a containment environment of saturated steam. Saturated steam conditions produce temperatures that are well

below those presented in Table 2-2 and those that would be required for the re-evolution of the deposited volatile fission products. Thus, the AP600 design includes features which are desirable for providing significant heat removal mechanisms such that revaporization of deposited fission products would be inhibited.

2.1.4 Controlling Physical Processes for Aerosol Plugging

Airborne dry aerosols in the containment gas space could escape to the environment if the containment were not isolated. Aerosols could be deposited as the containment gas was discharged through the unisolated pathway. The long term influence of discharging gases with airborne aerosols was investigated by the IDCOR program [IDCOR, 1985a]. In particular, the Vaughan plugging model, as described by Morewitz [Morewitz, 1982], was integrated into the Modular Accident Analysis Program (MAAP) and used to analyze several sequences to examine the influence the model has on fission product releases. The Vaughan model states that m (grams), the suspended aerosol mass carried into the duct before plugging occurs, is proportional to the cube of the duct diameter, d (cm).

$$m = K d^3 \quad (2-1)$$

The proportionally coefficient, K , can be seen from the data to be in the range $K = 30 \pm 20$ g/cm³. Figure 2-7 shows the correlation and its uncertainty range as compared to several experiments.

This correlation was derived by Vaughan [Vaughan, 1979] and represents the modification of the flow geometry through a duct by accumulating deposits of principally dry aerosols. Vaughan first determined the mass of the plug at any time to be a function of the duct radius and the thickness of the deposit. A mass balance was derived equating the time derivatives of the mass to the deposition rate provided by assumptions about the flow and deposition mechanisms.

The deposition rate was then found to be a function of the suspended mass concentration; volumetric flow through the duct, and the ratio of the plug height to the duct radius. The product of the aerosol concentration and the volumetric flow can be eliminated by using the total mass transported up to the time of plugging as a variable. Integrating the mass transported as a function of time with appropriate boundary conditions for complete blockage of the duct leads to Equation (2-1).

Hilliard [Hilliard, et al, 1980] reported data that appears in Figure 2-7 for a range of duct diameters and pressure differentials. The duct diameters tested were from 0.87 to 10.43 in (2.2 cm to 26.5 cm) with plugging observed over a pressure difference range of 0.07 to 10.15 psia (0.5 to 70 KPa).

Experiments performed by Rockwell International [Vaughan, 1979] show plugging of a 12 in (30.5 cm) duct in approximately 8 hours. The aerosols was sodium carbonate at a concentration of about .0015 lbm/ft³ (23 g/m³), and was flowing through the duct at .20 standard ft³/min (7.2 standard m³/min).

Tests were performed to determine the plugging time and strength of the plug in several size capillaries [Rockwell International, 1977] using sodium oxide aerosol. Data from these tests indicate plugging consistent with Equation (2-1). The aerosol concentration for the different tests varied from 3.7×10^4 to 3.8×10^5 lbm/in² (2.6 to 27 $\mu\text{g}/\text{cm}^2$) with differential pressures across the plugs ranging from 2.5 to 10. psia (.17 to .68 atm). These test conditions are comparable with the 1.4×10^5 - 3.8×10^5 lbm/in² (10-26 $\mu\text{g}/\text{cm}^2$) aerosol concentrations for the reactor system. The pressure difference in the reactor system may range from 0-75 psia (0-5 atm).

The likelihood of complete blockage of an unisolated containment flow path would be sequence dependent as the containment pressure history is sequence dependent. If a mechanism exists for continued pressurization of the containment then the containment pressure may exceed

Leakage of Aerosols From Containment Buildings

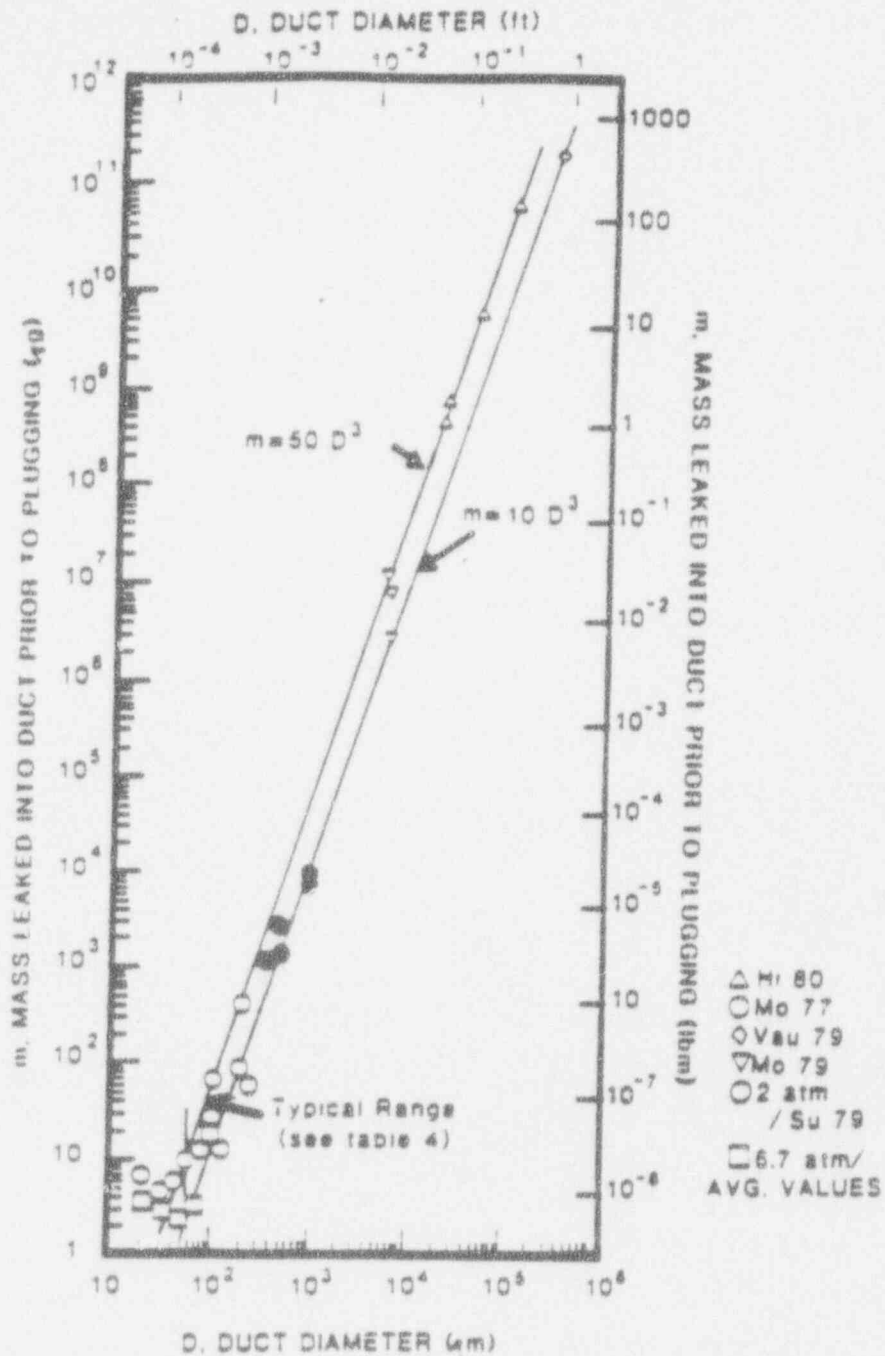


Figure 2-7 Experimental Data for Plugging of Lines by Aerosols

the strength of the plug of deposited aerosols. Nevertheless, the retention of aerosols within the unisolated flow path represents an additional fission product removal mechanism. When significant differential pressure exist, little if any credit may be taken for this removal mechanism.

Another situation that may involve aerosol plugging is leakage from an intact containment. Vaughan [Vaughan, 1979] has extended Equation (2-1) for predicting plugging in a crack with a characteristic length, ℓ , and a uniform width, w . The mass required to plug, m , in this configuration is calculated with an equation similar to that for a cylindrical duct,

$$m = K' \ell w^2 \quad (2-2)$$

where K' can be shown [Hilliard, et al., 1980] to be very close to the value of K in Equation (2-1). As for the unisolated flow path, the same limitation for those situations with a significant pressure differential also apply to leakage path.

2.1.5 Passive ALWR Source Term

The DOE's Advanced Reactor Severe Accident Program has produced a definition for the passive ALWR source term [Leaver, 1991]. As specified in the ALWR Requirements Document [EPRI, 1990], a physically-based source term shall be used as a design basis for passive plant accident mitigation systems. Since each standard plant design will be different, the associated physically-based source term will be specific to that design. [Leaver, 1991] describes the basis for the source term for the passive PWR designed to the ALWR requirements. The passive PWR ALWR source term is based on evaluation of a representative core damage event which results in a conservative, yet physically-based source term for the important sequence types. A physically-based source term (vs. the current non-mechanistic approach embodied in the regulations) is considered to be necessary to provide a more rationale basis for Passive ALWR

mitigation system design and to incorporate the body of source term knowledge gained in the thirty years since the TID 14844 [U.S. AEC, 1962] was issued. The representative core damage event selected for the passive PWR physically-based source term is a medium size loss of coolant accident with successful four stage depressurization with failure of the in-containment refueling water storage tank (IRWST) gravity drain. Reactor vessel failure is also postulated in the selected sequence.

The individual aspects of the physically-based source term include: reactor coolant gap activity release, early in-vessel release and late in-vessel release, RCS retention, revaporization release, and ex-vessel release. Table 2-3 presents the PWR ALWR release fractions to the primary containment atmosphere. The numbers presented in the table are the fraction of original core fission product inventory released to the primary containment atmosphere. These release fractions will be used in Section 4.0 of this evaluation summary.

2.2 Experiments and Industry Experience

[Leaver, 1991] discusses the individual aspects of the physically-based source term including a thorough survey of existing experiments and industry experience. Section 4.0 of [Leaver, 1991] provides detailed assessment of experiments and industry experience related to the coolant and gap activity source terms, early and late in-vessel release fractions, revaporization, RCS retention, and ex-vessel debris releases. This reference should be consulted if the experimental technical basis needs to be reviewed.

Table 2-3

**FISSION PRODUCT RELEASE FRACTIONS
TO PRIMARY CONTAINMENT ATMOSPHERE**

Nuclide	0-1 hr. Coolant Activity	1-5 hr. ^{(1),(4)} Early In- Vessel	5 hr. ⁽²⁾ Ex- Vessel	5-24 hr. ⁽³⁾ Late In- Vessel	Total
Nobles	See Note (5)	0.80	--	0.20	1.0
I		0.38	--	0.17	0.55
Cs		0.30	--	0.18	0.48
Te		0.08	--	0.03	0.11
Sr, Ba		0.004	--	--	0.004
Ru		0.004	--	--	0.004
Remainder		0.00004	--	--	0.00004

- (1) Assumes in-vessel releases and RCS retention of a part of the early releases.
- (2) All nobles released either early or late in-vessel. Remaining fission products retained in quenched debris or scrubbed through overlying water pool in reactor cavity.
- (3) Late in-vessel releases are sum of all late fuel releases and revaporization releases for wet cavity.
- (4) The gap activity is included in the 1-5 hr. release.
- (5) Coolant activity limits are assumed. Although important for steam generator tube rupture and steamline break, coolant activity makes negligible contribution to the source term from a core damage event and so is not included here.

2.3 Analyses

2.3.1 Zion Probabilistic Safety Study

The Zion Probabilistic Safety Study [CECo, 1981] included an estimate of the quantity of fission products released from the containment to the atmosphere for the various combinations of system and containment failure modes. In general the approach employed in the Reactor Safety Study [NRC, 1975] was generally followed in the Zion Probabilistic Safety Study.

As part of the Reactor Safety Study, the CORRAL code was developed for calculating the fraction of the core inventory of fission products released from the containment as a function of time. As input to the CORRAL analysis, relevant phenomenological information from the MARCH code was utilized for estimates of release of radioactivity from the core to the containment as a function of time. Four basic components of release from the core to the containment were considered: the gap-release component, the core melt release component, and vaporization release component, and the release component associated with steam explosions for those sequences where this phenomenon occurred. Release from the core to the containment and from the containment to the environment air pathway were calculated in terms of the fraction of core inventory. The models in the CORRAL code accounted for various processes which served to deplete the containment source term as a function of time such as plateout on the containment walls, washout by containment sprays, trapping by filter systems, and settling of aerosols. CORRAL then calculated the containment aerosol atmosphere source inventory as a function of time and used that information to estimate cumulative release fractions to the environment as time progressed. A similar approach was followed in the Zion Probabilistic Safety Study. In some instances the release categories employed in the Reactor Safety Study were used directly. There were, however, some additional release categories developed for the Zion Probabilistic Safety Study as a direct result of phenomenological investigations.

Core melt phenomenology, containment processes and containment failure modes were considered in developing the Zion Probabilistic Safety Study's source term categorization. In particular the phenomena of specific interest were early overpressure failure with limited time for spray interaction with the source and the incoherency of core melt progression. In addition, source terms were developed in the Zion Probabilistic Safety Study for core melt events where the containment did not fail and for an event where the containment was vented through a filter. Thus, the Zion Probabilistic Safety Study enhanced the approach used to describe fission product release fractions as done in the Reactor Safety Study.

Much of the basic technology and information assembled in the Reactor Safety Study was employed in the document described below in Section 2.3.2.

2.3.2 NUREG-1228, Source Term Estimation During Instant Response to Severe Nuclear Power Plant Accidents

This document presents a method of source term estimation that can be used during a severe accident event. The various methods of estimating radionuclide release to the environment (source terms) as a result of an accident at a nuclear power plant are discussed. The major factors affecting potential radionuclide releases offsite as a result of a nuclear power plant accident are described. The quantification of these factors based on plant instrumentation is also discussed. A range of accident conditions from those within the design basis to the most severe accidents possible are included in the text. A method of gross estimation of accident source terms and their consequences offsite are presented.

This document is a useful primer that provides an overview of the several aspects associated with fission product release and removal mechanisms including an assessment of consequences of the source term release. The document is dated 1988 and, hence, has not benefitted from additional research results which have been derived since it was produced.

2.3.3 NUREG-1150, Reactor Risk Reference Document

This study is the most current NRC study regarding the risk associated with severe accidents at reactor plants. Source term analysis is addressed in NUREG-1150 in order to predict the offsite consequences for the outcomes of the containment event tree analyses that define a set of containment failure conditions. The Source Term Code Package was used as a starting point for the assessment of the source terms in NUREG-1150. The package was used to model the physical processes occurring in a nuclear power plant from the initiating event to radioactive releases to the environment. The Source Term Code Package was viewed as having limited capability to examine some of the potentially important processes that were identified in NUREG-1150's containment event tree analysis. The potential effects of such phenomena, and the uncertainties in these phenomena, were assessed by additional analyses with detailed codes as well as by the use of expert judgement. These hard data and expert judgement were combined to yield ranges of source terms. The result of the source term uncertainty analysis was a large number of individual source terms, with characteristic information on the magnitude of release of a set of chemical species, the timing of the release (when it begins, how long it lasts, what radionuclides are present during each time period), and energy and elevation of the release. These data were used in offsite calculations as part of the NUREG-1150 study.

Ten source term issues were considered in the statistical sampling analyses for each of the four reference plants investigated. The issues included the following:

1. In-vessel release from fuel including details of melt progression.
2. Amount of cesium iodide decomposition.
3. Retention of volatile (iodine, cesium, and tellurium) within reactor coolant system.
4. Decontamination factor for V-sequences.
5. Magnitude of core-concrete interaction releases.

6. Decontamination factors for containment sprays.
7. Aerosol agglomeration uncertainties.
8. Late iodine release from containment due to evolution of iodine dissolved in water pools.
9. Late revolatilization from reactor coolant system.
10. Releases associated with high-pressure ejection and direct containment heating.

2.3.4 IDCOR Approach (Individual Plant Examination Methodology)

[IDCOR, 1987] provided an approximate source term methodology for pressurized water reactors. The methodology was developed as part of the IDCOR program to provide a specific methodology (the individual plant examination, IPE), for carrying out vulnerability studies. The IPE methodology was not a PRA but did make extensive use of the insights gained both in PRAs and the IDCOR program. The methodology was directed at the two key aspects of the vulnerability assessment: (1) the core melt prevention capability, and (2) the environmental releases from severe accidents. An approximate method for assessing the environmental releases from severe accidents was the subject of this document. As a result of the generic nature of the controlling processes for fission product deposition and retention, the analysis of thermal-hydraulic behavior and fission product release is somewhat easier than the assessment of core melt prevention capability. Specifically, for a given accident sequence, a few physical processes can be identified which control the release of fission products to the environment in all PWRs. Thus, relatively simple analyses suffice to estimate the release of fission products (the source term) and for many purposes, detailed computer studies may not be necessary. The IPEM source term calculation outlined simple procedures for estimating PWR environmental releases based on extended station blackout sequences. The applicability of these simple procedures for the interval preceding containment failure is directly useful for assessing the AP600 design with its passive containment cooling system. Thus, the containment integrity can be maintained and a closed volume with aerosol removal by natural processes is produced. Hence, the only

mechanism for releasing the fission products for the AP600 passive containment design is leakage through the containment boundary. Consequently, the airborne aerosol concentration in the containment decays either due to settling and deposition or leakage. The simplified procedure provided in this document provides a convenient mechanism for assessing sedimentation of dry aerosols in a closed volume. The technique described in Section 3.0 and applied in Section 4.0 of this evaluation summary closely parallels the IPEM approach.

3.0 METHODOLOGY

This section discusses a method for estimating the integrated mass of aerosol fission products and noble gases that could be released from a containment during a severe accident. The method employs correlations for aerosol sedimentation based on similitude rules. From these rules rational correlations have been developed [Epstein, 1986] for making engineering predictions of the instantaneous particle cloud density. The time dependent particle cloud densities are coupled with a knowledge of the containment leakage rate to determine the fission product inventory that escapes the containment.

In Section 2.1.2 of this document several postulated fission product pathways to the environment were discussed. Table 3-1 provides a characterization of the source term by the type of postulated sequence and the fission product release pathway. The majority of the sequence types have fission product release pathways that pass through one or more pools of water. These water pools may be in the pressurizer, the IRWST, the reactor cavity, or the loop compartments. As discussed in Section 2.0, water pools provide an effective means for scrubbing aerosol fission products. Hence, those sequence types that involve water pools will result in essentially only noble gases leaking from the containment. Some sequence types may provide a pathway directly from the reactor coolant system to the containment.

Due to the passive containment cooling system design and the presence of a large steam mass fraction within the containment, the wet conditions in the containment airspace greatly facilitate the removal of aerosol fission products. The simplified methodology will ignore the benefits of these wet conditions and assume dry aerosol sedimentation as the only active removal mechanism other than leakage from the containment. This assumption adds margin to this approach as discussed in Section 5.0.

The method assumes that all the fission products and inert aerosols that escape the primary system directly enter the containment gas space and completely mix throughout the

Table 3-1

**CHARACTERIZATION OF SOURCE TERM
BY TYPE OF SEVERE ACCIDENT SEQUENCE**

Sequence Type	Fission Product Release Pathway	Approximate Source Term
A. Non-LOCA ⁽¹⁾	Fuel to RCS to PZR to IRWST to containment	Noble gases
B. LOCA (break submerged) ⁽¹⁾	Fuel to RCS to water pool to containment	Noble gases
C. LOCA (break not submerged) ⁽¹⁾	Fuel to RCS to containment	Noble gases and volatiles
D. SGTR (MSIV open) ⁽²⁾	Fuel to RCS to S/G to condenser to air-ejector to environment	Noble gases
E. SGTR (MSIV closed) no overfill ⁽²⁾	Fuel to RCS to S/G water to environment	Noble gases
F. SGTR (MSIV closed) overfill ⁽²⁾⁽³⁾	Fuel to RCS to S/G to environment	Noble gases and volatiles

- (1) Includes sequences without or with vessel failure. Vessel failure will discharge debris into flooded cavity which will scrub aerosols and release noble gases to containment.
- (2) For sequences without vessel failure.
- (3) For sequences with vessel failure the approximate source term will include both noble gases and volatiles. Debris may be discharged into a dry reactor cavity unless the IRWST drains are manually opened. However, following vessel failure and debris discharge, the cavity would be flooded by the water that escapes from the failed vessel.

several compartments. Due to the very small design leakage rate, the airborne aerosol concentration can be assumed to be independent of leakage. This assumption means that the leakage does not impact the aerosol particle size distribution which influences the sedimentation rate. The method will be described by referring to Figure 3-1.

Four regions of aerosol behavior are considered to describe the airborne aerosol mass density in the containment gas space. In region 1 a steady aerosol source starts to deliver aerosols to the containment airspace at time t_{on} . The aerosol mass linearly builds up within the containment as a function of time to a steady state value where the source term of airborne aerosols equals the deposition rate. This interval (region 1) may be considered as the "buildup" region. The concentration is maintained as the steady state region during the presence of the steady aerosol source.

In region 2 the airborne aerosol mass concentration is constant once the steady state value is reached. The airborne aerosol mass concentration is maintained at this steady state value until the source is turned off at time, t_{off} .

Following the termination of the steady aerosol source, a third region may be considered. This region involves a "waiting" interval while the aerosol size distribution "ages". During the "aging" interval the aerosol size particle distribution adjusts itself by transitioning from the steady state particle distribution to a new particle size distribution. This transition involves the coagulation of the aerosol particles first due to brownian motion and then, as the particle mean size increases, by gravitational coagulation.

The final region, region number 4, involves a decay in the airborne aerosol mass concentration due to sedimentation within the containment. This interval can last until the end of the calculation or selected mission time.

In order to define these intervals one must be able to calculate the steady state airborne mass concentration, the buildup time to achieve this steady state concentration and the wait

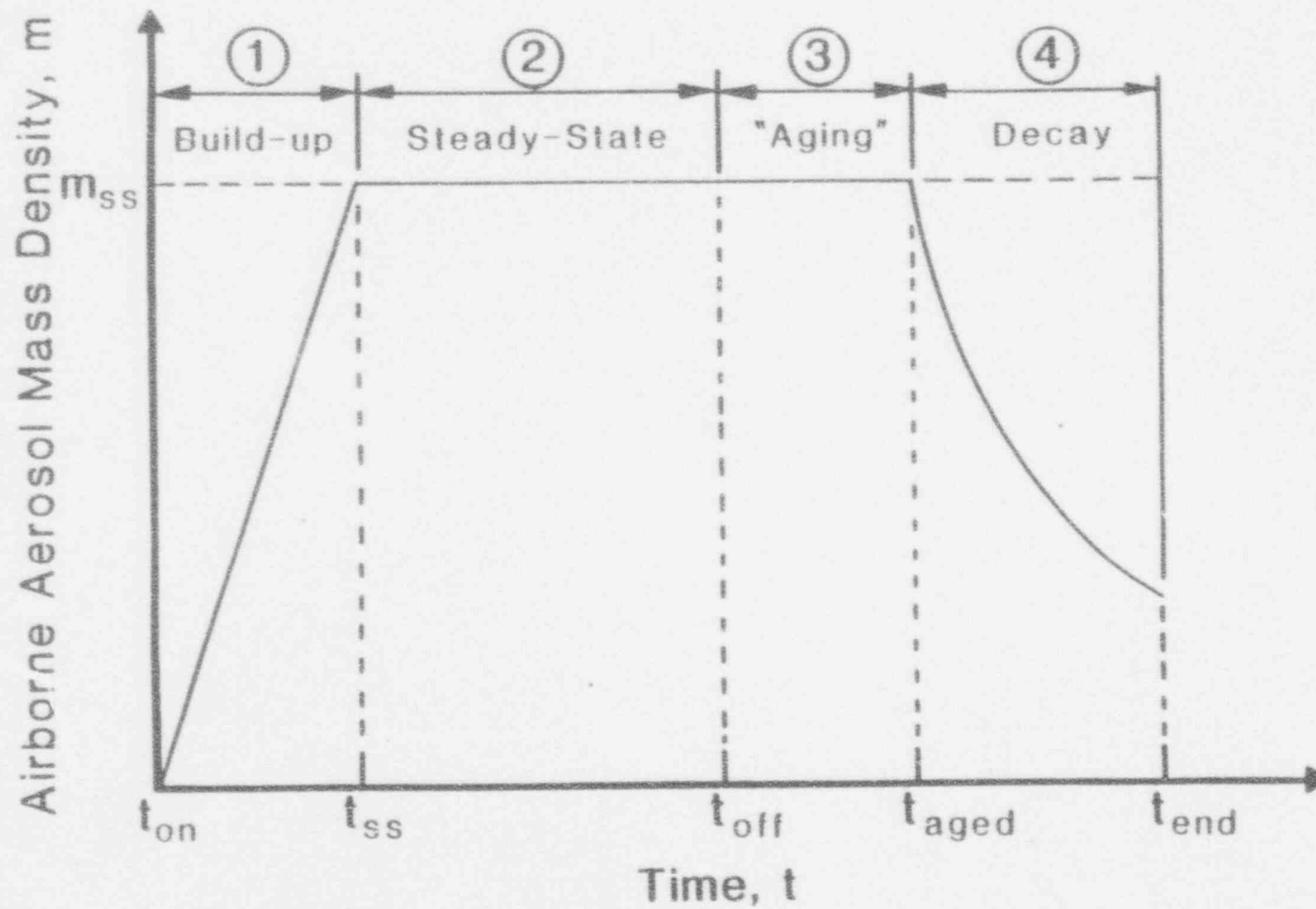


Figure 3-1 Containment airborne aerosol mass density history.

interval given the termination of the steady aerosol source. The correlations presented in [Epstein, 1986] can be used to quantify these parameters. The correlations used in this paper are summarized in Table 3-2.

Five steps are used to define the history of the containment's aerosol mass density. The aerosol mass density is combined with the containment volumetric leakage rate to determine the mass of fission products that leak from the containment. The first step is to define the aerosol source term. Aerosol source term is calculated by taking the core fission product inventory for the volatile aerosols and inert aerosols and multiplying by the release fraction that escapes to the primary containment. The resulting mass of aerosols is divided by the release duration and the containment total free volume. This results in the dimensional source term for aerosols, \dot{m}_p . Equation (3-1) is used to determine the dimensionless source term, \dot{M}_p .

The second step determines the steady state concentration of aerosols. The steady state concentration represents a balance between the source term of aerosols entering the containment and the removal (by sedimentation) of fission products from the containment gas space. Equation (3-4) can be used to solve directly for a steady state aerosol concentration based on the results from step 1. The second step is completed by calculating the dimensional volumetric steady state aerosol concentration, m_{ss} , by using Equation (3-2).

The third step is to calculate the time to reach the steady state aerosol mass density. The time, t_{ss} , is equal to the steady state aerosol mass density divided by the aerosol volumetric source term (m_{ss}/\dot{m}_p). Note that the special cases of a very low aerosol source such that the time to reach steady state exceeds the mission time or of a short release time such that the steady state aerosol mass density is not reached will be discussed later in this section. Additionally, the situation of an instantaneous release of aerosols is also addressed later in this section. Steps 1 through 3 allow region 1 of Figure 3-1 to be defined. Region 1, "buildup" of aerosol mass density, extends from the beginning of the problem (that is the initiation of the aerosol source) to the time to reach the steady state aerosol mass density.

Table 3-2

CORRELATIONS FOR AEROSOL SEDIMENTATION⁽¹⁾Dimensionless Quantities: \dot{M}_p = fixed dimensionless source strength

$$= \left(\frac{\gamma^{11} X^4 \mu h^8}{\alpha^5 K_o^3 g \rho^5} \right)^{1/4} \dot{m}_p \quad (3-1)$$

M = dimensionless aerosol mass density

$$= \left(\frac{\gamma^9 g h^4}{\alpha^3 K_o \rho^3 \mu} \right)^{1/4} m \quad (3-2)$$

 τ = dimensionless time

$$= \left(\frac{\alpha K_o g \rho}{X^2 \gamma \mu h^2} \right)^{1/2} t \quad (3-3)$$

Steady-State Aerosols (Fixed Source):

$$M_{ss} = M_{ss}(\dot{M}_p) = 3.19 \dot{M}_p^{0.78} (1 + 0.236 \dot{M}_p^{1.208})^{-0.1953} \quad (3-4)$$

⁽¹⁾See Table 3-5 for nomenclature.

Table 3-2 (Continued)

CORRELATIONS FOR AEROSOL SEDIMENTATION⁽¹⁾Decaying Aerosols (No Source):

$$M = M(\tau) = 7.87 \tau^{-1.15} ; \tau < 1 \quad (3-5)$$

$$M = M(\tau) = 74.2 \tau^{-3.05} ; \tau \geq 1 \quad (3-6)$$

$$M = M(\tau) = 74.2 \tau^{-3.05} (1 + 3.74 \tau^{-1.12})^{-1.7} \quad (3-7)$$

"Wait" Time (ϕ)

$$\phi = 4.11 M(0)^{-0.33} [1 + 0.623 M(0)^{0.66}]^{-0.82} \quad (3-8)$$

where $M(0)$ is the aerosol concentration at the beginning of the decay interval.⁽¹⁾See Table 3-5 for nomenclature.

Once the aerosol source is terminated, the aerosol will "age" while the aerosol particle size distribution changes. During the "aging" interval, the steady state aerosol mass density will continue to apply. Thus, region 2 of Figure 3-1 extends from t_{ss} to t_{off} . In step 4 the "wait" or "aging" interval is calculated by first determining the dimensionless aerosol mass density at the time that the source is turned off, t_{off} . This is done by using m_{ss} to calculate M_{ss} by applying Equation (3-1). Next the "aging" duration, ϕ , is calculated from Equation (3-8). ϕ is the "aging" duration in dimensionless time. To calculate the time interval of the aerosol aging period, Equation (3-3) is used to calculate t_{wait} based on the value of ϕ . Thus, region 3 extends from the time that the source of aerosols is terminated, t_{off} , to t_{aged} where t_{aged} equals t_{off} plus t_{wait} .

In step 5 the aerosol mass density for the final interval, the decay interval, is calculated. Once the aerosol "aging" is over, the aerosol mass density will decay due to sedimentation of the aerosol. The mass density for the decaying aerosol can be determined from Equation (3-5), (3-6), or both. In order to apply these equations one must first calculate the dimensionless time, τ , at the end of the "aging" period which is the start of the decay period. Equation (3-3) and t_{aged} are used to calculate this dimensionless time. If τ is greater than one, Equation (3-6) is used to represent the time dependent aerosol mass density during region 4 of Figure 3-1. If τ_{aged} is less than one, then Equation (3-5) is used for the intervals over which τ exceeds τ_{aged} but is less than one. Subsequently, Equation (3-6) is used once τ equals or exceeds one to the end of the mission time or calculational interval of interest.

These five steps will produce a history for the containment aerosol mass density during both the fixed (constant) source term interval and after the source of aerosols is terminated and the aerosol "ages" and decays by sedimentation. This calculational procedure assumes an average fixed (constant) rate of fission product release from the RCS to containment, homogeneous mixing in the containment, and a low leakage rate such that the particle size distribution is not effected by leakage. The time history of the aerosol density (as illustrated in Figure 3-1) will consist of a linear ramp to a steady state value followed by a constant steady state value until the source term is off and has "aged" and concluding in the decay to the end of the problem.

Given that the aerosol mass density history has now been determined, we can proceed to calculate the integrated leakage from the equations in Table 3-3. Equations (3-10), (3-12), (3-14), (3-16), and (3-18) are used to calculate the mass of aerosol leaked for each interval or region illustrated in Figure 3-1. The sum of these aerosol masses is the total mass of aerosols leaked. The fraction of the total mass of leaked aerosols that are volatile fission products is calculated by multiplying by a simple ratio of the initial volatile fission product mass to the total aerosol mass released from the RCS to containment. This result may also be expressed and reported as a fraction of the initial fission product inventory in the core.

The noble gas release from containment is simply calculated by integrating over the problem or mission time the product of the volumetric leakage rate and the containment's noble gas volumetric concentration. Figure 3-2 illustrates that only two regions apply for the noble gases which are not removed by sedimentation like the aerosols. The first region assumes a fixed (constant) release rate of noble gases from the RCS to the containment. The second region assumes a constant (no source) noble gas volumetric fraction in the containment gas space. This simplified formulation assumes uniform mixing and a small containment leakage rate. Equations (3-20) and (3-22) (see Table 3-4) are used to calculate the mass of noble gases that leak from containment. These two values are summed and cast as a fraction of the initial core inventory. Table 3-5 provides a nomenclature list for the equations used in this evaluation summary.

Several special cases could be addressed by the generalized approach presented above. For the aerosol leakage, if the aerosol release rate was very small or brief, a steady state condition may not be achieved before the source of aerosols was terminated. In such cases only the buildup, "aging", and decay regions would apply. Likewise, if an instantaneous release of aerosols were considered then only the "aging" and decay regions would apply. These cases could readily be addressed by the equations in Tables 3-2 and 3-3 subject to adjustment for the appropriate initial conditions and limits of integration. Furthermore, the fixed source term (aerosol or noble gases) could be treated as a series of intervals with different fixed release rates.

Table 3-3

INTEGRATED AEROSOL LEAKAGE EQUATIONS⁽¹⁾

REGION 1, BUILD-UP:

$$\frac{d m_{LA}}{dt} = Q_L m_{\text{build-up}} = Q_L \dot{m}_p t \quad (3-9)$$

$$m_{LA} = \int_0^{t_{SS}} Q_L \dot{m}_p t \, dt = \frac{Q_L \dot{m}_p}{2} t_{SS}^2 \quad (3-10)$$

REGION 2, STEADY-STATE:

$$\frac{d m_{LA}}{dt} = Q_L m_{SS} \quad (3-11)$$

$$m_{LA} = \int_{t_{SS}}^{t_{OFF}} Q_L m_{SS} \, dt = Q_L m_{SS} (t_{OFF} - t_{SS}) \quad (3-12)$$

REGION 3, AGING:

$$\frac{d m_{LA}}{dt} = Q_L m_{SS} \quad (3-13)$$

$$m_{LA} = \int_{t_{off}}^{t_{aged}} Q_L m_{SS} \, dt = Q_L m_{SS} (t_{aged} - t_{off}) \quad (3-14)$$

⁽¹⁾See Table 3-5 for nomenclature.

Table 3-3 (Continued)

INTEGRATED AEROSOL LEAKAGE EQUATIONS⁽¹⁾

REGION 4, DECAY:

If $\tau < 1$,

$$\frac{dm_{LA}}{dt} = Q_L m_{decay} = Q_L \frac{7.87 A^{-1.15}}{B} t^{-1.15} \quad (3-15)$$

$$m_{LA} = \frac{7.87 Q_L A^{-1.15}}{B} \int_{t_{aged}}^{t_{\tau+1}} t^{-1.15} dt = \frac{7.87 Q_L A^{-1.15}}{0.15 B} \left[\frac{1}{t_{aged}^{.15}} - \frac{1}{t_{\tau+1}^{.15}} \right] \quad (3-16)$$

If $\tau \geq 1$,

$$\frac{d m_{LA}}{dt} = Q_L m_{decay} = Q_L \frac{(74.2) A^{-3.05}}{B} t^{-3.05} \quad (3-17)$$

$$m_{LA} = \frac{74.2 Q_L A^{-3.05}}{B} \int_{t_{\tau+1}}^{t_{end}} t^{-3.05} dt = \frac{74.2 Q_L A^{-3.05}}{2.05 B} \left[\frac{1}{t_{\tau+1}^{2.05}} - \frac{1}{t_{end}^{2.05}} \right] \quad (3-18)$$

where

$$A = \left(\frac{\alpha K_o g \rho}{X^2 \gamma \mu h^2} \right)^{1/2} \quad B = \left(\frac{\gamma^9 g h^4}{\alpha^3 K_o \rho^3 \mu} \right)^{1/4}$$

⁽¹⁾See Table 3-5 for nomenclature.

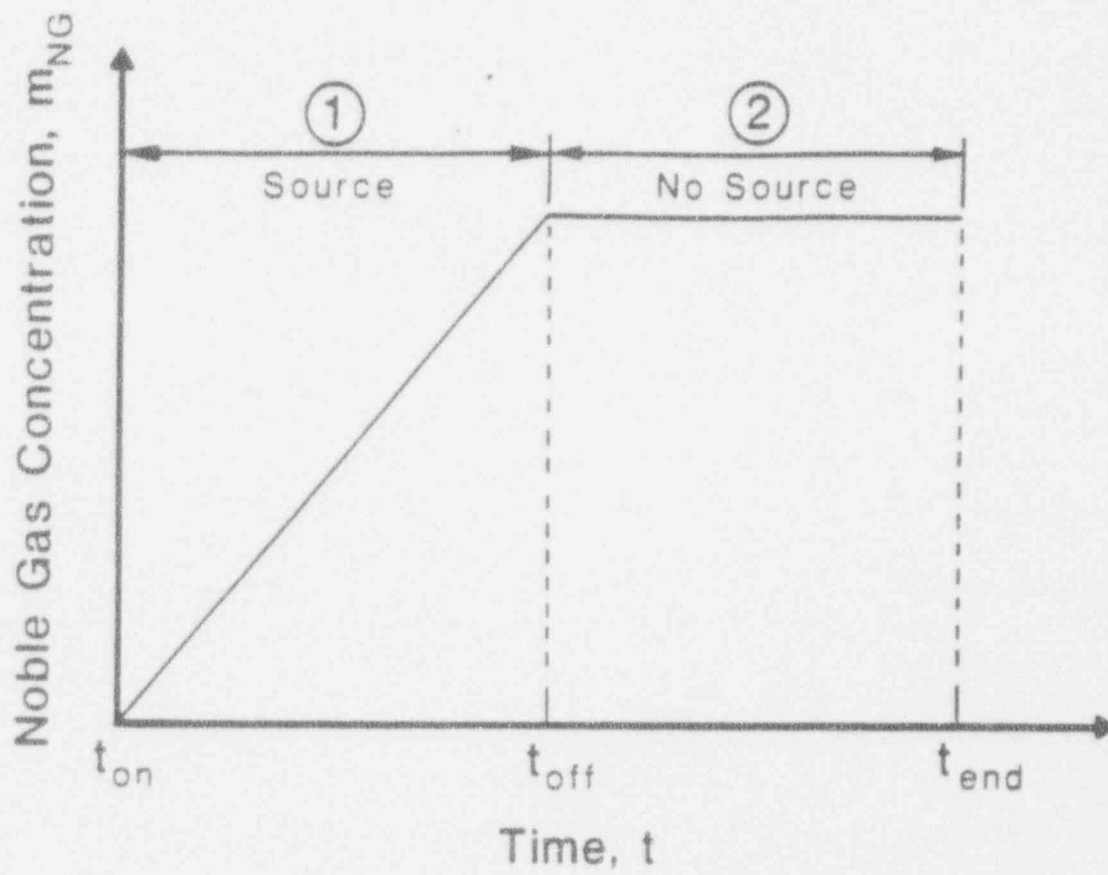


Figure 3-2 Containment Noble Gas Concentration History

Table 3-4

INTEGRATED NOBLE GAS LEAKAGE EQUATIONS⁽¹⁾

REGION A, FIXED SOURCE:

$$\frac{d m_{L,NG}}{dt} = Q_L \dot{m}_{NG} t \quad (3-19)$$

$$m_{L,NG} = \int_0^{t_{off,NG}} Q_L \dot{m}_{NG} t \, dt = \frac{Q_L \dot{m}_{NG}}{2} t_{off,NG}^2 \quad (3-20)$$

REGION B, NO SOURCE:

$$\frac{d m_{L,NG}}{dt} = Q_L m_{NG} \quad (3-21)$$

$$m_{L,NG} = \int_{t_{off,NG}}^{t_{end}} Q_L m_{NG} \, dt = Q_L m_{NG} (t_{end} - t_{off,NG}) \quad (3-22)$$

⁽¹⁾See Table 3-5 for nomenclature.

Table 3-5

NOMENCLATURE AND INPUT FOR AEROSOL SEDIMENTATION CORRELATIONS AND EQUATIONS

g	gravitational constant (9.8 m/s ²)
h	effective height of particle cloud; cloud volume divided by settling area (51,000 m ³ /5400 m ² = 9.4 m)
k	Boltzman constant (1.38 x 10 ⁻²³ J/°K)
K_o	normalized Brownian collision coefficient = $\frac{4kT}{3\mu}$ (5.03 x 10 ⁻¹⁶ m ³ /s)
m	airborne aerosol density (kg/m ³)
m_o	initial aerosol mass density (kg/m ³)
M	dimensionless airborne aerosol density
\dot{m}_p	mass rate of production of particles per unit volume of particle cloud (kg/m ³ -s)
M_a	molecular weight of aerosol material (133 kg/kg-mole)
\dot{M}_p	dimensionless mass rate of production of particles
M_w	molecular weight of water (18 kg/kg-mole)
Q_L	containment volumetric leakage rate (7.1 x 10 ⁻⁴ m ³ /s)
R_o	aerosol particle "seed" radius (0.3 x 10 ⁻⁶ m)
R_w	specific gas constant for water (462 J/kg-°K)
t	time (s)
T or T_w	gas temperature (450°K)

Table 3-5 (Continued)

Greek Letters

α	aerosol density correction factor (1)
γ	aerosol collision shape factor (1)
μ	gas viscosity (2.5×10^{-5} kg/m-s)
ρ	aerosol particle density (2.5×10^3 kg/m ³)
ρ_w	density of water (887 kg/m ³)
σ	surface tension of water (0.06 N/m)
τ	dimensionless time
ϕ	approximate dimensionless time where aging begins to decrease
χ	aerosol particle settling shape factor (1)

Subscript

A	aerosol
aged	aerosol particle size distribution aging complete
build-up	aerosol accumulation interval
decay	aerosol concentration decay interval
end	end of calculation period or mission time
L	leaked
N.G.	noble gas(es)
on	aerosol source on
off	aerosol source off
SS	steady state
wait	aerosol particle size distribution aging in progress

(aerosol or noble gases) could be treated as a series of intervals with different fixed release rates. Each interval would require a separate leakage integration. This would complicate the simplified approach but the method could be extended to such cases if such refinements were judged to be warranted.

Due to the low probability of steam generator tube rupture events leading to containment bypass and the release of fission products, no method for estimating the retention of fission products in the secondary side of the steam generator is provided in this paper. Failure to control steam generator level following a steam generator tube rupture is one mechanism that can lead to containment bypass. The AP600 design includes an automatic system to respond to steam generator overfill. The inclusion of an automatic protection system to avoid steam generator overfill further reduces the likelihood of a fission product release path being produced. Furthermore, the likelihood of primary system depressurization is very high due to ADS system incorporated in the AP600 design. Primary system depressurization reduces the driving potential for loss of reactor coolant through a failed steam generator tube.

4.0 PLANT SPECIFIC APPLICATION

In this section the methodology presented in Section 3.0 is applied to the AP600 design (Subsection 4.1). Furthermore, the results for an integrated calculation using MAAP4 is presented in Subsection 4.2 and compared to the conservative results derived from the hand calculations in Subsection 4.1.

4.1 Aerosol Sedimentation Correlations

In order to define the containment's aerosol mass density history the first step is to calculate the inventories of fission product and inert aerosols that will be released to the primary containment atmosphere. The EPRI physically-based source term (see Section 2.1.5) is used in this application. The containment's total aerosol mass is due to several major contributions [OECD, 1985], i.e.,

- control rod materials (As, In, Cd)
- structural materials (Fe, Cr, Ni, Mn)
- fuel (UO_2)
- single component of Zircalloy cladding (Sn)

in addition to the fission products. Per Table 2-2, the boiling points of many of these materials are low enough (of the order of 4500°F) such that they could vaporize during core damage. A release fraction from the RCS to containment for the inert (non-radioactive) aerosols of 0.5 is assumed in this calculation. The inert aerosols participate in the sedimentation process and help increase the removal of fission product aerosols from the containment airspace. Table 4-1 summarizes the aerosol and noble gas inventories used in this sample application.

The total aerosol mass is shown to be about [](a,c) in Table 4-1. The release interval defined by the EPRI source term is 24 hours. The AP600 containment's free volume

Table 4-1

AP600 FISSION PRODUCT INVENTORY AND
RCS AEROSOL RELEASE FRACTIONS

(a,c)

is approximately [](a,c). By assuming a uniform release rate over the 24 hour period, the fixed aerosol source term, \dot{m}_p , is calculated to be:

$$\left[\right] \text{ (a,c)}$$

Equation (3-1) in Table 3-2 is now used to calculate the fixed dimensionless source strength,

$$\left[\right] \text{ (a,c)}$$

The second step is to calculate the steady state aerosol density, m_{ss} , where the aerosol source term equals the aerosol removal due to sedimentation. Equation (3-4) is evaluated with $\dot{M}_p =$ [](a,c) $M_{ss} =$ [](a,c), and Equation (3-2) is used to calculate the dimensional value of the steady state aerosol density,

$$\left[\right] \text{ (a,c)}$$

The third step is to estimate the time it takes for the aerosol density in containment to reach this steady state value. This time, t_{ss} , is estimated by the quotient of m_{ss} and \dot{m}_p to be [](a,c). The aerosol density in containment grows linearly from the time the source starts (taken as $t=0$ in this calculation) to [](a,c) hours. The steady state aerosol density is maintained until the aerosol source is terminated which in this calculation is taken to be 24 hours.

The fourth step estimates the "aging" or "wait" interval that follows the aerosol source

termination and precedes the aerosol decay (due to sedimentation) interval. In this sample calculation the aerosol density is m_{ss} at the time of aerosol source termination and this does not change (significantly) until the "aging" interval is over. Equation (3-8) is evaluated with $M(0) = [\quad](a,c)$ to determine that ϕ equals $[\quad](a,c)$, i.e. the dimensionless time where decay is credited with starting. Equation (3-3) is used to convert the dimensionless time, $[\quad](a,c)$, into dimensional time,

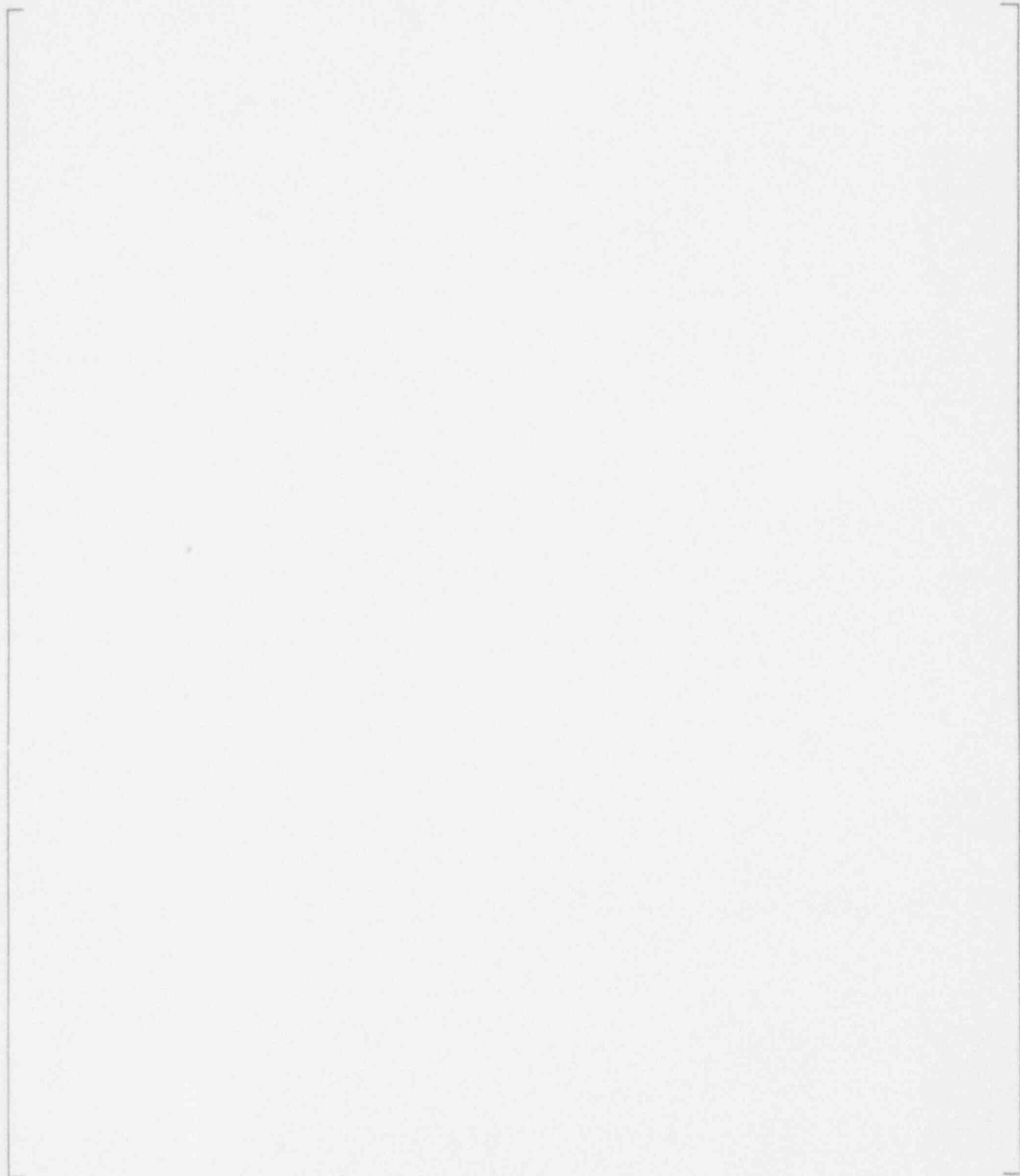
$$\left[\quad \right] (a,c)$$

The last step in determining the containment's aerosol density history, is to estimate the aerosol density during the decay interval. The decay interval starts at t_{aged} which equals $[\quad](a,c)$ and extends until the problem end time, t_{end} . In the leakage calculations that follow a 48 hr mission time for the source term will be assumed and the sensitivity to an infinite time for aerosol leakage will be presented. Since the decay interval starts at $\tau = [\quad]$, Equations (3-5) and (3-6) are used to describe the aerosol density, m , during the decay interval. Equations (3-5) and (3-6) are combined with Equations (3-2) and (3-3) to give

$$\left[\quad \right] (a,c)$$

$$\left[\quad \right] (a,c)$$

during the decay interval. These expressions are used in the calculation of the integrated leakage mass which follows. Figure 4-1 summarizes the containment's aerosol density history calculated in this sample application.



(a,c)

Figure 4-1 Aerosol Mass Density for AP600 Design

WESTINGHOUSE CLASS 3

The integrated mass of aerosol leaked from containment is now calculated for each of the four intervals (regions). The AP600 design basis leakage rate at the containment design pressure is [](a,c) containment volume per day. Hence, $Q_L = [](a,c)$ will be used in the leakage calculations.

Per Equation (3-10) for the aerosol build-up interval,

$$\left[\right] (a,c)$$

$$\left[\right] (a,c)$$

Per Equation (3-12) for the steady state interval,

$$\left[\right] (a,c)$$

$$\left[\right] (a,c)$$

Per Equation (3-14) for the "aging" interval,

WESTINGHOUSE CLASS 3

$$\left[\right] (a,c)$$

$$\left[\right] (a,c)$$

Per Equations (3-16) and (3-18) for the decay interval,

When $\tau < 1$,

$$\left[\right] (a,c)$$

$$\left[\right] (a,c)$$

When $\tau \geq 1$,

$$\left[\right] (a,c)$$

$$\left[\right] \quad (a,c)$$

NOTE: If t_{end} was taken to be very long (approaching infinite), then the second term would approach zero and m_{LA} during the decay interval would increase by about fifty percent. Thus, the leakage mass during the decay interval would still be small.]

Hence, the total integrated mass of leaked aerosols is 0.351 Kg. The volatile fission product mass is estimated by multiplying by the fraction that represents the volatile fission products $\left(\frac{42}{2100} = 0.02 \right)$, i.e., 0.0073 Kg of volatile fission products leaked. Table 4-1 indicates that the total AP600 core inventory for the volatile fission products (I, Cs, Te) is 95.6 Kg. Hence, the release fraction of the core inventory of volatile fission products from the containment is 7.5E-5 or 0.007 percent.

The noble gas release fraction can also be estimated per the methodology presented in Section 3.0. The fixed noble gases source, m_{NG} , for the one day RCS release interval is $3.1\text{E-}8 \frac{\text{Kg}}{\text{m}^3\text{-s}}$ based on 134.6 Kg of noble gases (see Table 4-1). The containment leakage rate, Q_L , is the same as for the aerosol calculation.

Per Equation (3-20) for the interval of fixed noble gas source,

$$\left[\right] \quad (a,c)$$

$$\left[\begin{array}{c} \text{ } \end{array} \right] \text{ (a,c)}$$

Per Equation (3-22) for the interval of no noble gas source,

$$\left[\begin{array}{c} \text{ } \end{array} \right] \text{ (a,c)}$$

$$\left[\begin{array}{c} \text{ } \end{array} \right] \text{ (a,c)}$$

Hence, the total integrated mass of leaked noble gases is [](a,c). Table 4-1 indicates that the total AP600 core inventory of noble gases is [](a,c). Hence, the release fraction of the core inventory of noble gases from the containment is [](a,c). summarizes the release fractions (to the environment) for all the aerosols species and the noble gases.

These calculated release fractions for the aerosol and noble gas fission products were based on a constant primary containment volumetric leakage rate equal to the design basis leakage of [](a,c) volume percent per day. The actual leakage rate will vary in proportion to the containment pressure. The passive containment heat removal system will limit the containment pressure to values smaller than the containment design pressure. Hence, a smaller (and time varying) volumetric leakage rate would be expected than conservatively assumed in these calculations. These calculated results can be directly scaled by the volumetric leakage rate, Q_L , to make estimates for different primary containment leakage rate histories.

Table 4-2

CALCULATED RELEASE FRACTIONS FOR AP600 DESIGN

(a,c)

(1) Fraction of core inventory released to environment in 48 hr interval.

4.2 Comparison to MAAP4 Calculations

To place the methodology applied in Section 4.1 in perspective, a sequence was run using the MAAP 4 computer with the AP600 design eleven node parameter file [Spaargaren, 1991]. The sequence that was run was a small break loss of coolant accident with failure of the ADS depressurization system, IRWST injection, passive RHR system, and the passive containment cooling system. Two accumulators and two core makeup tanks were injected during the sequence and ex-vessel cooling was modelled. The postulated sequence resulted in core uncover at approximately [](a,c). The peak containment pressure was approximately [](a,c) and steam mole fractions in excess of [](a,c) were observed in all the containment compartments except for the IRWST gas space. []

](a,c) The leakage flow path included in the MAAP4 calculation was in the area of the electrical penetrations and terminated in the auxiliary building. The design basis leakage rate was used to estimate the leakage area. A single node was included in the MAAP4 model for the auxiliary building which then discharged to the environment. For the purpose of this comparison leakage from containment was considered and no credit is given to any retention in the auxiliary building.

A 48 hour sequence was considered and the integrated release fractions to the environment are summarized in Table 4-3. The MAAP4 results provided in Table 4-3 estimate the integrated leakage for the design basis leakage area which is [](a,c) volume percent per day at design pressure. Table 4-3 also includes the calculated integrated leakage fractions as determined in Section 4.1 by the hand calculations.

Table 4-3

COMPARISON OF HAND CALCULATIONS AND MAAP4



(a,c)

WESTINGHOUSE CLASS 3

(a,c)

5.0 UNCERTAINTIES AND SENSITIVITIES

This section will address several of the key uncertainties that relate to the passive plant's source term definition and unique AP600 design features. This section will also discuss several key sensitivities related to the methodology presented in this paper.

5.1 Passive ALWR Source Term

The physically-based source term [Leaver, 1991] for the passive Advanced Light Water Reactors has been employed in this paper. Table 5-1 provides a comparison of the timing, magnitude and chemical form of the fission product release to the containment atmosphere for the passive ALWR physically-based source term versus the existing regulatory source term. The release rate and release duration are important source term attributes whose uncertainty is addressed in the physically-based source term definition. The ALWR release is over a period of 24 hours (although most of the release occurs in the first several hours of the accident) versus an instantaneous release for the existing regulatory source term. The magnitude for nobles is identical. The iodine release is 50% for the ALWR versus 25% for existing regulatory source terms, although the ALWR iodine release is spread out over a period of hours as noted above. The ALWR source term release is roughly half of the core inventory of cesium and lesser amounts of the remaining elements, whereas the existing regulatory guidance has no other release to the containment atmosphere. Another key uncertainty in source term definitions is the chemical forms for important fission products. The chemical forms require careful consideration of the chemical environment which a fission product experiences after being released from the fuel. The environment is determined by conditions existing in both the RCS and the containment region during accident sequences. The chemical forms have a strong influence on the fission product transport and deposition behavior and thus on the fission product inventory in the containment atmosphere that is available for leakage. The ALWR physically-based iodine chemical form is roughly a reversal of the elemental-particulate ratio for the existing regulatory source term. In general, the ALWR integrated release to containment is

Table 5-1

**COMPARISON OF RELEASE TO CONTAINMENT FOR PASSIVE
ALWR SOURCE TERM AND EXISTING REGULATORY SOURCE TERM**

	Passive PWR	Existing Regulatory Source Term
Release Timing	Release over a 24 hr period beginning 1 hr after initialing event	Instantaneous release at time of initiating event
Release Magnitude to Containment Atmosphere		
• Nobles	100%	100%
• Iodine	55%	25% ⁽¹⁾
• Cesium	48%	1% (to sump)
• Tellurium	11%	1% (to sump)
• Ba, Sr, Ru	0.4%	1% (to sump)
• Remainder	0.004%	1% (to sump)
Chemical Form in Containment		
• Iodine	2.85% elemental 97% particulate 0.15% organic	91% elemental 5% particulate 4% organic
• Cesium	100% particulate	Not specified
• Tellurium and remaining semi-and low volatiles	100% particulate	No specified

- (1) The 25% figure is arrived at by the Regulatory Guide 1.3, 1.4 assumptions that 50% of the iodine inventory is released to the containment and half of this 50% is instantaneously plated out.

significantly higher than the existing regulatory source term. This difference is due in part to the ALWR objective that the source term be based on a physically-based evaluation of a core damage event (hence, the release over a period of hours, the release of cesium and other elements, and the particulate form of iodine). It is also due to the desire that the ALWR physically-based source term incorporate margin beyond the source term expected from an actual ALWR core damage event. A detailed discussion of the considerations of these key uncertainties as well as other aspects of the physically-based source term is provided in [Leaver, 1991].

5.2 Long Term Releases From Molten Corium in the Lower Plenum

The design of the AP600 plant provides for external flooding of the RPV such that long term cooling is provided and the RPV integrity is maintained. Thus, during a severe accident sequence a configuration with core debris contained within the lower plenum of the RPV being cooled via heat losses through the intact RPV and radiation off the debris upper surface can result. This configuration could be maintained for an extended period of hours or perhaps days while the cooling of the retained core debris was completed. This configuration and its extended duration calls into question the uncertainty regarding the releases of low volatility (non-volatile) fission products during such events. Non-volatile fission product releases are dominated by temperatures in excess of 2700°K (4400°F). The release rates of the non-volatile fission products from melts should be controlled by the rate of vaporization from the surface of the crust surrounding the melt. There are no data for long term (greater than ten hours) releases of non-volatile fission products from molten pools such as may exist in the lower plenum of a reactor within a flooded cavity. To provide an upper bound estimate for long term release rates, experimental data had been modified [Hobbins, 1991] to account for differences in surface to volume ratio and system pressure between experiments and the conditions expected in the lower plenum of an advanced LWR. The automatic depressurization system for the AP600 will ensure a low pressure in the lower plenum. Analysis of the non-volatile fission product release from the molten pool in the TMI-2 accident [Petti, 1989] suggest that with natural convection in the pool, fission product transport to the pool surface is not limiting and long term releases are

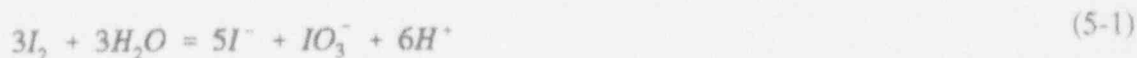
dominated by vaporization from the surface. Further, the melt is surrounded by self-healing ceramic crust. Fission products must diffuse through this crust before they can be released from the surface as vapor and aerosols. The thickness of a crust surrounding a melt in the lower plenum and radiating heat to the core region in the reactor vessel has been calculated to be on the order of four millimeters [O'Brien, 1991]. The analysis by [Reynolds, 1986] indicates that the fractional release rate of non-volatile fission products is directly proportional to vapor pressure and surface area and inversely proportional to system pressure. It should be noted that the surface to volume ratio for the debris pool contained in the lower plenum is approximately a factor of two hundred times smaller than that corresponding mass in rod geometry. The physically-based source term has accommodated the effects of reduced system pressure and surface to volume ratio by adjusting the measured release rates per the TMI-2 accident and the PBF-SFD experiments for these effects. Uncertainty remains in these estimates but these release rates should be bounding in that reductions because of diffusion through the crust and vaporization from the cooler temperatures on the surface of the crust have not been included in the physically-based source term evaluation. These two effects could easily amount for a further reduction of a factor of ten in release rates.

5.3 Revolatilization of Iodine From Water Pools

The consideration of volatile fission product species essentially reduces to an evaluation of iodine behavior. Other fission products have little or no tendency for forming volatile species at containment conditions and the radiological significance of possible exceptions to this generality are minor when compared against iodine. In the case of iodine and volatile species of concern historically the species of interest are elemental iodine and organic iodides (principally methyl iodide).

The iodine specie formed when either CsI or HI first dissolve in water is the iodide ion (I^-). However, even if a substantial fraction of the core iodine inventory should dissolve in available containment water reservoirs the resulting aqueous concentration would be quite low;

typically in the range of 10^{-5} molar. At such concentrations a variety of reactions with other substances in the water (i.e., dissolved gases or other minor impurities) can occur which will produce additional iodine species. The relationship between important aqueous iodine species at low concentration can be illustrated through use of the following equation [Clough, 1985]



This expresses a global equilibrium situation which involves numerous intermediate reactions and species that will have different rates and lifetimes depending on the specific thermochemical conditions. However, it also illustrates the observed fact that solution pH has an important influence on iodine speciation. High H^+ concentrations (low pH) tend to shift the equilibrium to the left (i.e., higher relative molecular iodine concentrations) while low H^+ concentrations (high pH) tend to increase the relative concentrations of the ionic species iodide and iodate.

A very important process that can affect iodine speciation in containment water reservoirs is radiolysis. At the radiation levels that would be expected in core damage accidents radiolysis generates appreciable aqueous concentrations of oxidizing entities such as hydroxyl free radicals, hydrogen peroxide, etc. These can readily oxidize I^- to I_2 and further through HIO to IO_3^- . The steady-state concentrations of the different iodine species depend upon ambient conditions, particularly pH. In general low pH conditions favor formation of I_2 while high pH tends to stabilize I^- . The production of I_2 in solution has two significant consequences. First, its limited solubility in water will cause some of it to volatilize (partition) into the overlying gas space where it can become available for leakage from containment. Second, I_2 in solution as well as I_2 in the gas phase can participate in reactions with a variety of organic materials (i.e., paints, oils, cable insulation, volatile solvents, methane, etc.) to generate low molecular weight organic iodides such as methyl iodide (CH_3I). Since these species are only slightly soluble in water and have relatively long airborne lifetimes in containment, they constitute another potential leakage form.

The importance of minimizing radiolytic I_2 formation by controlling pH is clear. Thus, the ALWR design requirements specify that the pH of containment water pools is to be maintained in an alkaline state for the accident duration. This may require addition of a relatively strong alkaline buffer to protect against long term acid sources such as nitric acid formation from radiolysis of moist air or perhaps carboxylic acid generation from radiolytic decomposition of oxygenated organic substances (paints, solvents, etc.) that might be in containment. Sodium hydroxide or any other similar alkaline salt could be used for this purpose.

In addition to radiolysis of aqueous iodide, which tends to produce a steady-state concentration of I_2 in the system, there are several other potential generators of I_2 that must be considered which are more transient in nature. These include possible oxidation of suspended CsI during hydrogen combustion events, I_2 formation during evaporation to dryness of shallow water puddles [Beahm, 1986], radiolysis of acidic droplets containing HI which may have been released from the RCS, and possible oxidation of iodide species that could be evolved should corium-concrete interactions occur in the reactor cavity following penetration of the reactor vessel lower head. Limited experimental data on the relevant phenomena combined with uncertainties in accident progression make precise quantification difficult, but I_2 yields from each of these processes are expected to be small.

With regard to the first process, any CsI that has dissolved in a water pool would not be affected by a hydrogen deflagration. To produce a significant effect, a large energetic hydrogen deflagration would have to occur early in an accident when most of the CsI aerosol is still suspended in the containment atmosphere. At early times steam partial pressures tend to be sufficiently high to preclude global combustion. Furthermore, recent experimental work shows that relatively low steam concentrations will act to protect airborne CsI from oxidation even if a hydrogen deflagration should occur.

Concerning the second process, experimental work has indicated that appreciable volatile iodine is produced when iodide solutions evaporate to dryness in a high radiation field. Alkaline

conditions reduce but do not eliminate liberation of volatile iodine which is presumably I_2 . However, the passive ALWR plant has such a large inventory of water in the containment that only an insignificant fraction would be expected to experience evaporation to dryness. It follows that I_2 generation from this process should also be insignificant.

The AP600 design includes the capability to maintain the desired post-accident pH conditions in the recirculation sump water after containment floodup. [

] Currently, there are no provisions for injecting sodium hydroxide into the IRWST water inventory nor the water which may overflow the IRWST and collect in the refueling canal during non-LOCA sequences. Since scrubbing of the fission products will occur in the IRWST for sequences which discharge through the ADS valves into the IRWST, uncertainty may exist in the source term given that the pH of the IRWST water inventory is not controlled and iodine may be re-evolved. However, the method applied in this paper ignored the fission product retention capability of scrubbing in water pools in the AP600 design. The method allowed the entire release fraction of volatile fission products to enter the containment airspace in the form of aerosols. Thus, the uncertainty regarding iodine re-evolution is incorporated within the conservatism of the methodology described in this paper.

5.4 Methodology Sensitivities and Uncertainties

The removal methodology employed in this paper treats the aerosol fission products as dry aerosols that have no affinity for water. If the aerosol material is water soluble, as for example, cesium hydroxide or cesium iodide, particle growth can occur as a result of gas-phase diffusion of steam to the particle surface. As a consequence, the particle size distribution of a water soluble aerosol is influenced by the condensation and coagulation. Coagulation is of minor

important compared to condensational growth in a saturated steam environment. Water soluble aerosols are described as being hygroscopic materials. The fact that the volatile fission product species are soluble in water would cause their removal rate from the containment space for the AP600 design to occur at a faster rate than that for dry aerosols. The AP600 design with a passive containment cooling system produces a containment environment of saturated steam which would be highly effective in removing soluble fission product aerosols. [IDCOR, 1985b] provides the following expression for the aerosol cloud density time history of an instantaneously generated aerosol in a saturated steam environment:

$$\left[\text{Equation (5-2)} \right] \quad (a,c)$$

where m is the time dependent aerosol mass density, m_0 is the initial aerosol mass density, t is time in seconds since the release of the aerosols to containment and the balance of the symbols are as defined in Table 3-5.

There is one significant analytical difficulty associated with water soluble particles that is not encountered with dry aerosols; that is the uncertainty about the size R_0 of the primary aerosols particle. A detailed treatment of combined coagulation and particle growth by steam condensation in the early stages of aerosol evolution may be necessary to avoid this difficulty. On the other hand, the simplicity of the technical basis for Equation (5-2) can be retained by determining R_0 from a comparison with experiment. Comparisons with existing experimental data [IDCOR, 1985a] suggest a range of R_0 of 0.3 to 0.5 microns. If one uses 0.3 microns as R_0 and applies Equation (5-2) to the AP600 design and conditions, then the following expression results

$$\left[\text{Equation (5-3)} \right] \quad (a,c)$$

The importance of the hygroscopic nature of the volatile fission products can be demonstrated by applying Equation (5-3) to demonstrate the effectiveness of the removal of water soluble fission products from a high relative humidity environment. If we compare the removal of a hygroscopic aerosol to just the decay region in Figure 4-1 which spans a [](a,c) hour interval, we see that Equation (5-3) yields a value of [](a,c) compared to a value of approximately [](a,c) ($m_{\text{end}}/m_{\text{SS}}$) for Figure 4-1. The results in Figure 4-1 were calculated for a dry aerosol. Furthermore, the hygroscopic behavior would be operable over the entire episode and not just during the decay interval considered in the methodology presented in Section 3.0. When Equation (5-3) is applied to a 48 hour interval, one calculates a remaining airborne fractions of [](a,c). Hence, acceptable margin is provided in the methodology in this report as was observed in the comparison presented and discussed in Section 4.2.

Another removal mechanism which is not incorporated in the dry aerosol sedimentation methodology is impaction of aerosol particles with water droplets produced by steam condensation on internal structures, the containment dome and walls, or in the steam filled gas space. The steam condensate would not contain sodium hydroxide as a "spray" additive as used in LWR designs but the droplet falling through the containment atmosphere would still be an additional and effective aerosol removal mechanism. A "wet" or high relative humidity containment atmosphere is the most likely condition that would exist for the AP600 design. The exclusion of this removal mechanism adds further margin to the methodology and conservatism to the results. Lastly, the application of the methodology provided in Section 4.0 employed a value of unity for the aerosol shape factors (γ, χ, α). The shape factors are defined and used to account for non-spherical aerosols. These factors are used to account for departures from spherical particles which are assumed in the application of Stoke's law. Liquid droplets will assume spherical shape and, hence, the correct values for the shape factors is one in such a case. If the aerosol is not in the form of water droplets but rather is dry particular material then the shapes may not be spherical and shape factors other than one would apply. However, currently there is insufficient experimental data to significantly improve these values for the dry aerosol shape factors. In the case of the AP600 design this is a negligible uncertainty in the methodology due to the steam environment and "wet" conditions within the containment.

6.0 ACCIDENT MANAGEMENT IMPLICATIONS

The AP600 design provides several passive means that ensure large inventories of water will be available in containment and that containment heat removal can be maintained. Such capabilities are central to accident management strategies and effectively reduce source term considerations for the AP600 design to only containment leakage. A low design value for the containment leakage rate of [](a,c) has been included in the AP600 design basis. This effectively addresses the issue of containment leakage. Therefore, the remaining potentially significant fission product release path would be associated with containment bypass. Several aspects of the EPRI requirements document for passive ALWRs address bypass issues. In particular steam generator tube rupture bypasses are addressed by the AP600 design features for automatically depressurizing the primary system and automatic overfill protection for the steam generators. The depressurization of the primary system by the ADS valves reduces the differential pressure between the primary and secondary systems and, thus, the potential driving mechanism for steam generator tube rupture leakage. The steam generator automatic overfill protection system trips the feedwater system and the chemical volume and control system and automatically starts the passive residual heat removal system. These capabilities provide significant protection for postulated steam generator tube rupture bypass events and assure a low probability of occurrence of such postulated sequences.

The safety valves that provide overpressure protection for the secondary side of the steam generators discharge directly to the environment. In the rare event of a steam generator tube rupture sequence which does not successfully avoid steam generator overfill or reduce the driving potential for that leakage path fission products could have a direct pathway to the environment as shown in Figure 2-6 and Table 3-1. A potential accident management implication for such an event would be to redirect the steam generator safety and relief valves discharges from the environment to the IRWST inside containment. This would provide a pool of water for scrubbing the fission products, a means of preventing a loss of coolant inventory outside of

containment, and a means of using the containment to control fission product releases to the environment.

Another rare event which probabilistically may not warrant additional attention would be a steam generator tube rupture that loses coolant inventory outside of containment and that included a failure of the passive water injection systems inside containment. This could lead to potential vessel failure with a dry reactor cavity. Should this occur subsequent interactions between the molten core debris and the concrete in the cavity could produce overpressure conditions that could challenge the containment's integrity as the passive containment heat removal system's effectiveness would be severely inhibited by the dry conditions inside containment. The accident management implication of such extremely rare sequences would be to direct the manual initiation of the IRWST drains. This would provide a means of flooding the reactor cavity and covering the core debris such that it could be cooled and terminate concrete attack as well as scrub fission products that were released during the quench interval. As operator guidance is already placed that directs the manual actuation of the IRWST drain prior to core damage, this situation would simply provide an additional reason for assuring the successful actuation of the IRWST drain. The accident management implication may simply be to assure that directions for manual actuation of IRWST are redundantly identified for such conditions as described here.

Lastly, the design and configuration of the auxiliary building regarding its capability to function as a fission product retention device should leakage occur into it is an additional accident management implication. Likewise, the ability to refill the water supply for the external containment water spray of the passive containment cooling system would provide a means of extending the ability to control leakage through the balance of the containment boundary.

7.0 SUMMARY

The EPRI Requirement Document dose requirements are stated as follows:

At site boundary: 25 Rem limit with a probability of 10^{-6} yr⁻¹ or less.

For emergency plaining zone (EPZ): 1 Rem limit at 0.5 mile for 24 hour exposure.

This evaluation summary addressed the retention capability of the AP600 design but did not include a consequence analysis for the calculated fission product releases. The consequence analysis performed for the probabilistic safety study was not yet completed at the time that this evaluation was performed. However, comparison of this summary's results to the dose calculations provided by ARSAP [Leaver, 1991] based on CRAC2 calculations are provided here via a comparison of the release fractions. [

(a,c)

As discussed in Section 4.2 and demonstrated in Section 5.0, the AP600 hand calculations provide conservative estimates for the volatile fission product release fractions. Iodine is the key volatile fission product that impacts the dose calculation. The AP600 design hand calculation is conservative by at least an order of magnitude. The dose results presented in [Leaver, 1991] for the ARSAP release fractions in Table 7-1 satisfy the whole body protective action guideline (PAG) for less than 1 Rem at a distance of 1/2 mile from the plant with margin. The thyroid dose at a distance of 1/2 mile depends on meteorology and the effectiveness of the auxiliary building for retaining fission products. These are site specific parameters. [Leaver, 1991] presents results for "typical" sites that show that median doses would be below the thyroid PAGs. Hence, assuming that the other assumptions used in the ARSAP dose calculations are held constant, similar or smaller doses would be expected for the AP600 design as assessed in this evaluation summary.

Table 7-1

COMPARISON OF AP600 CALCULATION AND ARSAP CALCULATION



(a,c)

Several notable conservatisms are incorporated in the method provided in this evaluation summary in addition to those discussed in Section 5.0. The ALWR dose requirement of 25 Rem is stated in probabilistic terms. The probability of the fission product release path including a water pool is sequence dependent and has not been addressed in this evaluation summary. A plant specific application of this methodology should assure that the probability of release is weighted by the probability of the appropriate release pathways. It is also significant to note that the containment leakage path was not explicitly quantified in this evaluation summary's methodology. The impact of the passive containment cooling system on fission product aerosol leakage was ignored. Water on the outside shell of the containment would capture aerosols as they exited via leakage paths. Furthermore, given that the water supply for the external containment spray was depleted the baffle and external containment shell would provide significant additional surface area for fission product deposition. Additionally, the impact of the auxiliary building as a fission product retention device have been ignored in this summary paper's simplified methodology. Leakage from the penetration area into the auxiliary building would not be impacted by water flow from the passive containment cooling system. However, the auxiliary building would provide significant surfaces for fission product deposition and retention. Furthermore, another conservatism relates to timing of the release. The protective action guidelines for the emergency procedures initiate evacuation and sheltering activities in the potentially impacted public. The methodology employed in this evaluation summary used time zero as the start of the release of fission products from the primary system. However, severe accident conditions would start several hours in advance of the beginning of the release of significant aerosol fission product inventories to the containment such that several additional hours could be available for initiating emergency actions should they be warranted compared to the timing presented in this summary.

It is concluded that the low design leakage rate and the design configuration with significant in-containment water sources assures the AP600 design's fission product retention capability will satisfy the appropriate dose requirements as established for the passive ALWR plants.

8.0 REFERENCES

Beahm, E. C., et. al., 1986, Chemistry and Transport of Iodine in Containment, NUREG/CR-4797.

CECo, 1981, "Zion Probabilistic Safety Study, ZPSS".

Clough, P. N., Starkie, H. C., 1985, "A Review of the Aqueous Chemistry and Partitioning of Inorganic Iodine Under LWR Severe Accident Conditions", European Applied Research Reports, 6, no. 4.

EPRI, 1990, Advanced Light Water Reactor Utility Requirements Document, ALWR Passive Plants, Volume III, Rev. 0.

Epstein, M., Elison, P. G., Henry, R. E., 1986, "Correlations of Aerosol Sedimentation", Journal of Colloid and Interface Science, Vol. 113, No. 2.

Hilliard, R. K., et al., 1980, "Venturi/Fibrous Scrubber System Performance During Containment Venting and Purging With Sodium Aerosols - CSTF Tests AC-5 and AC-6", Westinghouse Hanford Co., Hanford Engineering Development Laboratory Rep. HEDL-TME-80-47.

Hobbins, R. R., 1991, personal communication.

IDCOR, 1985a, "Integrated Containment Analysis for Grand Gulf Nuclear Station, IDCOR Task 23.1.

IDCOR, 1985b, "Technical Support for Issue Resolution", IDCOR Technical Report 85-2.

IDCOR, 1987, "IPE Source Term Methodology for PWRs", Technical Report 86.3A2.

Leaver, D. E., et. al., 1991, "Passive ALWR Source Term", DOE/ID-10321.

McKea, T. J., Flitter, J. G., 1988, "Source Term Estimation During Incident Response to Severe Nuclear Power Plant Accident", NUREG-1228.

Morewitz, H. K., 1982, "Leakage of Aerosols From Containment Buildings", Health Physics, Vol. 42, No. 2, pp. 195-207.

NRC, 1975, "Reactor Safety Study, An Assessment of Accident Risks in U.S. Commercial Nuclear Power Plants", WASH-1400.

O'Brien, J. E., 1991, personal communication.

WESTINGHOUSE CLASS 3

OECD, 1985, Nuclear Aerosols and Reactor Safety, Nuclear Energy Agency of Organization for Economic Co-operation and Development.

Petti, D. A., Adams, J. P., Anderson, J. L., Hobbins, R. R., 1989, "Analysis of Fission Product Release Behavior From the Three Mile Island Unit 2 Core", Nuclear Technology, 87, 243.

Reynolds, A. D., Kelly, J. L., Kim, S. T., 1986, "Role of Surface Vaporization in Low-Volatility Fission Product Release Experiments", Nuclear Technology, 74, 76.

Rockwell International, 1977, Quarterly Technical Progress Report, LMFBR Safety Program, AI-ERDA-13196.

Spaargaren, J., 1991, "AP600 Plant: 11 Node Parameter File for MAAP4", Rev. 3.

U.S. AEC, 1962, Calculation of Distance Factors for Power and Test Reactor Sites, TID 14844.

Vaughan, E. U., 1979, "HAA-3 Development", Quarterly Progress Report, LMFBR Safety Program, Rockwell International, Energy Systems Group Rep. ESG-DOE 13281 (Springfield, VA: NTIS).